Stockholm University

# Licenciate thesis

Marine Geology

# Arctic bottom water temperatures

## A benthic foraminiferal Mg/Ca–temperature field calibration and application

Natalia Barrientos Macho

Stockholm 2016

Department of Geological Sciences
Stockholm University
SE-106 91 Stockholm

Licentiate Thesis

**Marine Geology**

# Arctic bottom water temperatures

## A benthic foraminiferal Mg/Ca–temperature field calibration and application

**Natalia Barrientos**

**Stockholm 2016**

Natalia Barrientos, Stockholm University, 2016
Cover pictures by Natalia Barrientos

**Abstract**

The Arctic is more sensitive to modern global temperature rise than the rest of the planet, a phenomenon known as polar amplification. It is predicted that warming of Arctic bottom waters by only 1–2°C could mobilize vast stocks of fossil carbon on subsea shelves and margins. This could exacerbate global warming through release of greenhouse gases. To date, very little is known about the importance of these potential ocean-carbon system climate feedbacks, therefore records of past Arctic bottom water temperatures (BWT) and climate variability are of paramount importance for future climate modeling. This provides the motivation for this Ph.D. project/licentiate thesis as a component of the 2014 SWERUS-C3 program (Swedish- Russian-US Arctic Ocean investigation of Climate-Cryosphere-Carbon interactions), with the overarching aim to reconstruct Arctic Ocean bottom temperatures through glacial-interglacial cycles.

Reconstructing Arctic BWT in the Quaternary using palaeoceanographic proxies has proved challenging due to the unique physical and chemical environment of the Arctic Ocean. Mg/Ca palaeothermometry in calcitic microfossils has shown promise but a large amount of groundwork is still required to develop reliable Mg/Ca temperature calibrations. In this licentiate thesis, I present the results of two studies that investigate the applicability of Mg/Ca paleothermometry using Arctic benthic foraminifera. The first study explores the influence of temperature, salinity and carbonate ion concentration on Mg/Ca in six benthic species (*Elphidium clavatum*, *Nonionellina labradorica*, *Cassidulina neoteretis*, *Quinqueloculina arctica*, *Oridorsalis tener* and *Cibicidoides wuellerstorfi*) using material recovered from Arctic marine surface sediments and their complementary field oceanographic measurements. The applicability of Mg/Ca paleothermometry in Arctic shelves compared to the central Arctic is also explored. In the second study, I use benthic foraminifera Mg/Ca and stable isotope analyses in *E. clavatum* to infer late Holocene bottom water variability from the Herald Canyon (72 m water depth) in the Chukchi Sea. This area is characterized by exceptionally high sedimentation rates (~200 cm/kyr), which, with strong radiocarbon age control, provide unprecedented detail of Holocene Pacific-Arctic Ocean history. The obtained Mg/Ca values reveal bottom water variations over millennial time scales moving towards a cooling trend at ~1200 cal. yr BP. This signal is similarly recorded in Mount Logan (Yukon, Canada) $\delta^{18}O$ ice core record suggesting that Herald Canyon benthic Mg/Ca is recording BWT variability that is linked to Pacific atmosphere-climate oscillations. I conclude that benthic foraminiferal Mg/Ca proxy can be successfully applied in the Arctic Ocean, although using specific foraminifera taxa and preferentially in depositional environments associated with high sedimentation rates.

## Sammanfattning

Den globala temperaturökningen har varit större i Arktis på grund av ett fenomen som kallas för polar amplifikation. Temperaturökningen är inte bara begränsad till atmosfären, högre temperaturer har och även mätts i den Arktiska Ocean. En uppvärmning av bottenvattentemperaturer (BVT) i Arktiska Oceanen om endast ett par grader kan mobilisera stora mängder fossilt kol som finns upplåst i gashydrater i sediment längs kontinentalsluttningarna och i permafrost på de grunda kontinentalsocklarna. Även om det inte är utträtt till vilken utsträckning så kan det frigjorda kolet nå atmosfären i form av metangas, vilket är en kraftig växthusgas. Det är hittills inte klarlagt hur dessa återkopplingsmekanismer fungerar och det finns ett stort behov av en ökad förståelse av Arktiska Oceans BVT. Dessa ligger i sin tur till grund för modelleringar av gashydraters stabilitet i de marina sedimenten.

Denna licentiatavhandling utgör en del av SWERUS-C3 programmet (Swedish – Russian – US Arctic Ocean Investigation of Climate-Cryosphere-Carbon Interactions) som syftar till att undersöka kopplingar mellan klimatet, kryosfären, och kol. Licentiatavhandlingen är fokuserad på att rekonstruera BVT i Arktis Oceanen under ett tidsperspektiv omfattande glaciala-interglaciala cykler. Att rekonstruera BVT i Arktis Oceanen med hjälp av indikatorer över oceanografiska förändringar som ägt rum tillbaka i tiden, så kallade paleoceanografiska förändringar, är komplext. Flera av de vanligaste använda indikatorerna inom paleoceanografin bygger på analyser av kalkskaliga organismers skal vilka i Arktis har påverkats av kemiska förhållanden havsvattnet. Förhållandet Mg/Ca i mikrofossil med kalkskal har visat sig kunna användas för att rekonstruera temperaturer tillbaka i tiden, en så kallad ”paleotermometer”. En pålitlig kalibrering mellan Mg/Ca i kalkskaliga foraminiferer och bottenvattentemperatur har inte tagits fram för Arktiska Oceanen. I denna licentiatavhandling presenterar jag två studier som undersöker vilka faktorer som påverkar förhållandet Mg/Ca i bentiska foraminiferer. Den första studien undersöker hur temperatur, salthalt samt koncentration av karbonatjoner påverkar Mg/Ca i sex bentiska arter (*Elphidium clavatum*, *Nonionellina labradorica*, *Cassidulina neoteretis*, *Quinqueloculina arctica*, *Oridorsalis tener* och *Cibicidoides wuellerstorfi*). Användbarheten av Mg/Ca som paleotermometer i bentiska foraminiferer från den grunda Arktiska kontinentalsockeln jämfört med foraminiferer från centrala Arktis har också undersökts. Den andra studien, analyseras Mg/Ca samt stabila isotoper i den bentiska foraminiferen *E. clavatum* för att undersöka de senaste 4200 åren av bottenvatten-variabilitet i Herald Canyon (72 m vattendjup), som ligger i Tjuktjerhavet nära Wrangelön. Detta område karakteriseras av exceptionella höga sedimenteringshastigheter (~200 cm/1000 år) och studien bygger på en sedimentkärna med mycket bra ålderskontroll som togs under SWERUS-C3 expeditionen 2014. Resultaten ger en detaljerad inblick i historien över Stillahavets inflöde till Arktiska Oceanen via Beringssund. Mg/Ca-analyserna pekar på hundraåriga BVT variationer under ca 3000 år, vilka åtföljts av en betydligt kallare fas som startade för ca.1200 år sedan. Dessa Mg/Ca variationer är påfallande lika uppmätta förändringar av förhållanden mellan syreisotoper i en iskärna från Mount Logan, Yukon, Kanada. Detta tolkas i detta arbete som att Mg/Ca värden från bentiska formaninferer från Herald Canyon är kopplade till atmosfärförändringar i Stillahavs-regionen. Med denna avhandling drar jag slutsatsen att Mg/Ca kan användas för att rekonstruera variationer i Arktiska Oceanens bottenvattentemperaturer givet att två kriterier uppfylls: hög sedimentationshastighet samt specifika arter.

## List of papers

This thesis overviews two years of Natalia Barrientos' PhD work where has been the main contributor in the laboratory analyses, figures and manuscript writing. The authors have contributed ideas, commentaries and revisions.

Manuscript I

**Barrientos, N.**, Lear, C.H., Jakobsson, M., Stranne, C., O'Regan, M., Cronin, T.M., Gukov, A.Y., Coxall, H.K. Benthic foraminiferal Mg/Ca paleothermometry in the Arctic Ocean.

Manuscript II

Barrientos, N., Coxall, H.K., Lear, C.H., Pearce, C., Muschitiello, F., O'Regan, M., Stranne, C., Koshurnikov, A., Jakobsson, M. Pacific-Arctic halocline variability through the late Holocene in the Herald Canyon, Chukchi Shelf.

---

The following paper is not included as part of this thesis:

Pearce, C., Varheyli, A., Wastegård, S., Jakobsson, M., Muschitiello, F., **Barrientos, N.**, O'Regan, M. and Cronin, T. M.: The 3.6 ka Aniakchak tephra in the Arctic Ocean: implications for the radiocarbon reservoir age of the Chukchi Sea in the late Holocene, Clim. Past, In prep.

**Licentiate Kappa**

Table of Contents



Appendix

# 1 Introduction

The Arctic region is experiencing faster warming compared to other regions of the planet, a phenomenon termed Arctic amplification [Serreze and Barry, 2011; Pithan and Mauritsen, 2014], which might be tied to the dynamic features of this region primordially consisting of a vast ocean with perennially sea ice covered parts. Satellite imaging operating since 1979 has revealed decreases in the summer mean sea-ice extent [Stroeve et al., 2012] (Figure 1) partly due to oceanographic feedbacks need to be further explored. Sea ice reduction will increasingly allow trans-arctic navigation and access to natural resources that if exploited may affect Arctic climate and ecosystems [ACIA, 2004], and most importantly influence vigorously global climate.

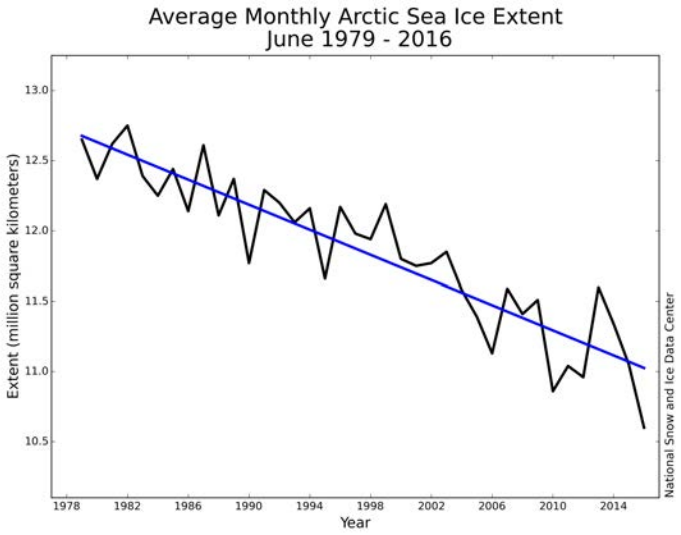


**Figure 1.** Illustration of the shrinking Arctic sea ice extent over the past four decades. Data are from the National Snow and Ice Data Center (NSIDC).

Another change observed in the Arctic Ocean is changing water mass temperatures altering the present Arctic water mass stratification (Figure 2). Temperature increases in Arctic intermediate depths have been reported as a consequence of stronger and/or warmer Atlantic water (200-800 mwd) inflow through the Fram Strait [Quadfasel et al. 1991; Carmack et al. 1995; Morison et al. 1998; Rudels et al. 2012]. Atlantic layer temperature increases, have been observed in the Nansen Basin continental slope [Quadfasel et al., 1991], the Laptev Sea [Schauer et al., 1997], the Arliss Plateau [Carmack et al., 1995], the Makarov Basin and Lomonosov Ridge [Aagaard et al., 1996; Swift et al., 1997 and Morison et al., 1998] and eastern Amundsen Basin [Rudels et al., 2000a and Schauer et al. 2002a]. As a response to this process, halocline thickness is reduced bringing warmer Atlantic waters closer to the sea surface and ice [Morison et al. 1998].

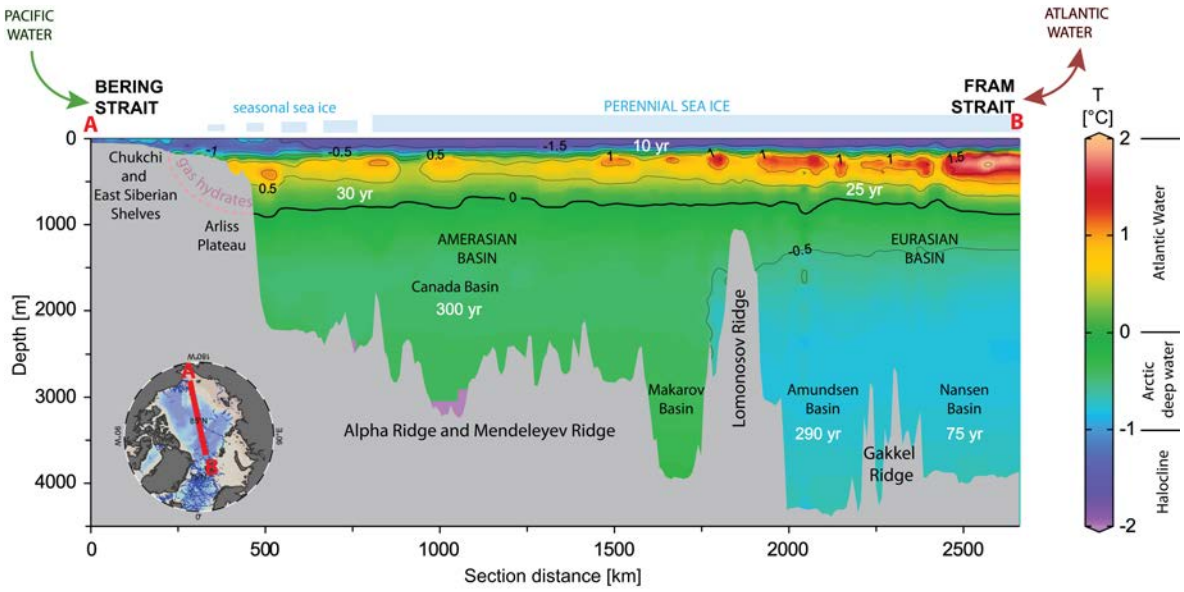


**Figure 2.** Arctic Ocean section from the Bering Strait (A) to the Fram Strait (B) showing modern temperatures. The profile illustrates the current water mass distribution in the Arctic Ocean with three main vertically stratified water masses (from surface to bottom water: Halocline, Atlantic water and Arctic deep water). Potential areas of subsea gas hydrate storage are drawn on the Chukchi and East Siberian Shelves. The section shows a simplified depiction of the main bathymetric features of the Arctic. Ages shown represent the approximate residence time of the Arctic water masses [e.g. Schlosser et al. 1994; Jones et al. 1995].

In addition, in the recent years there has been a substantial amount of research dedicated to comprehend and predict the stability fields of Arctic offshore permafrost and methane ($CH_4$) hydrates stable under optimal bottom water temperatures (BWT) and pressure conditions since their release could potentially lead to emission of $CH_4/CO_2$ to the atmosphere [Westbrook et al., 2009; Taylor et al., 2013; Shakhova et al., 2010; 2014; 2015; Stranne et al., 2016]. In order to place this hypothesized scenario into the past, reconstructing paleo-BWT variations in the Arctic Ocean is a first step to asses if this parameter had potential to exert climate system feedbacks.

One approach for understanding these Arctic Ocean water mass variations is reconstruction of bottom water temperatures from the past. However, the paleotemperature record from the Arctic Ocean is sparse and a better constrain of its variability over the Late Quaternary is crucial in this sensitive region.

## 1.1 Thesis objectives

Expedition SWERUS-C3 (Swedish- Russian-US Arctic Ocean Investigation of Climate-Cryosphere-Carbon Interactions) was built on a 90-days long expedition to the East Siberian Arctic Ocean (ESAO) during 2014 with Swedish icebreaker *Oden*. The main research topics of this expedition were to collect data to help test hypotheses concerning

Arctic cryosphere-carbon-climate system feedbacks. My PhD, fits into this by seeking to reconstruct Arctic BWT applying Mg/Ca paleothermometry in fossil benthic foraminifera from the recent geological past.

BWT paleotemperature records in the Arctic Ocean are very sparse. Cronin et al. [2012] established a first record from the last glacial cycle using Mg/Ca ratios in the calcite shells of ostracodes. The use of benthic foraminifera instead of ostracodes is challenging due to the low concentration of Mg in benthic foraminiferal tests compared to ostracodes (approximately 10 x lower). However, ostracode fossils are rather rare in Arctic marine sediments, whereas benthic foraminifera, although typically lacking from glacial intervals, are ubiquitous and often relatively common in interglacial-glacial transition sequences. This provides strong incentive to extend the method to Arctic benthic foraminifera. Exploring the controls on Mg concentration in Arctic benthic foraminifera and trying to build benthic foraminifera field temperature calibrations has thus been a major part of this Licentiate Thesis. The main goals were to:

(i) develop six field–based Mg/Ca-BWT calibrations combining modern temperature data with monospecific Mg/Ca values (Manuscript-1),

(ii) combine downcore benthic foraminifera stable isotopes and Mg/Ca data from a new late Holocene sediment core from the Chukchi Shelf (Herald Canyon, 72 m water depth) to test the success of Mg/Ca paleothermometry in capturing bottom water temperature variability in the Arctic Ocean (Manuscript-2).

## 2 Modern Arctic oceanography

The Arctic Ocean ($9.5\times 10^{12}$ $m^2$) is the smallest, shallowest and least salty of the world's oceans. Fifty-three % of the ocean consists of shelves [Jakobsson, 2002] while the deepest point, the Molloy Hole, is only 5600 m deep [Thiede et al., 1990]. Under the perennial sea-ice cover is hidden dynamic seafloor topography, with extensive underwater mountain ridges, i.e. the Alpha-Mendeleev, Lomonosov and Gakkel Ridges. These bathymetric features divide the Arctic Ocean into at least four basins and it is along the slopes of these shelves and ridges that the Atlantic waters flow anticlockwise [Björk et al., 2007; Rudels et al., 2012] (Figure 3).

Arctic instrumental oceanographic records go back to 1900 since the early work of Helland-Hansen and Nansen [1909], who discovered Atlantic origin waters brought through the Fram Strait flowing underneath the sea ice. These observations paved the

way to the current understanding of Arctic Ocean water mass stratification and circulation (Figure 2 and 3). In the following subsections the Arctic Ocean strata and sea-ice systems are introduced in more detail.

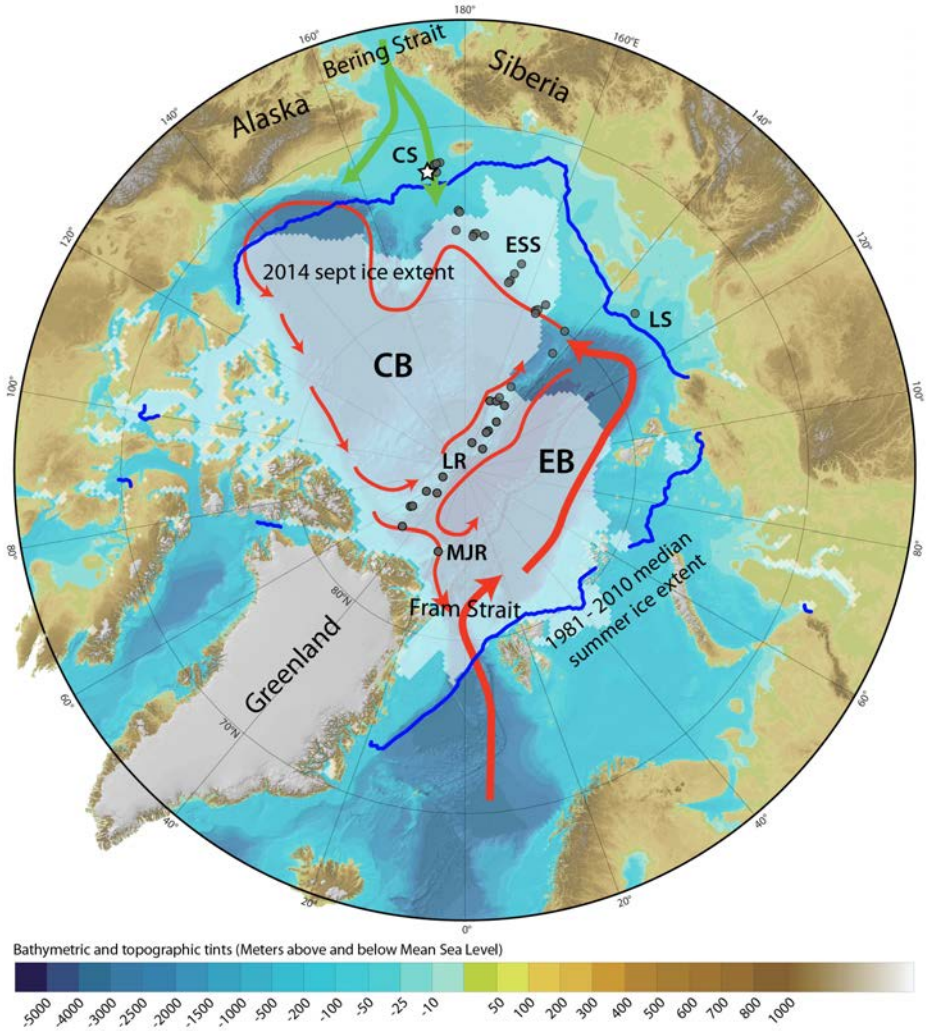


**Figure 3.** A simplified overview of the Arctic Ocean water sources are drawn with arrows (red: Atlantic water, green: Pacific Water). White shading shows the summer median sea ice extent in 2014 (NSIDC), the year of the SWERUS-C3 expedition, showing areal reduction as compared to the median 1981-2010 summer sea ice (blue contour line, NSIDC). Studied marine cores for Manuscript-1 are shown as grey circles and for Manuscript-2 as a white star. CB: Canadian Basin, LR: Lomonosov Ridge, EB: Eurasian Basin, CS: Chukchi Shelf, ESS: East Siberian Shelf, Laptev Shelf and MJR: Morris Jesup Rise. Basemap obtained from International Bathymetric Chart of the Arctic Ocean [Jakobsson et al., 2012].

## 2.1 Sea ice

Sea ice is considered part of the Arctic oceanography by acting as an atmospheric insulator of the water masses below. In the Arctic Ocean sea ice can be seasonal or perennial (surviving multiple years) and drifts with the transpolar surface current towards the Fram Strait. Its formation and melting, mainly along the shelves, produces brine enriched waters that sink to the bottom creating a dynamic physicochemical environment

that might remineralize organic material, leading to high nutrients and low oxygen [Rudels et al. 2004]. Wind modulated polynyas observed from sea ice charts (i.e. a stretches of open water surrounded by ice) have been found to play a role in modifying the salinity of the bottom waters by brine rejection in the vicinity of Wrangel Island on the Chukchi Shelf [Winsor and Björk, 2000].

### 2.2 Polar Mixed Layer (PML): 0–50 m water depth

This cold (0 to 2°C) and relatively fresh (~32 to 34 psu) surface water layer is primarily sourced from sea ice and Siberian shelf glacial melt and from the inflow of low salinity Pacific water through the Bering Strait [Anderson and Jones, 1992; Jones, 2001; Rudels et al., 2004; Woodgate et al., 2007; Rudels et al., 2012]. The PML is subjected to oceanographic variations depending on its geographical location. In the Eurasian Basin, the PML is more saline and Pacific water sources are practically absent [Rudels et al., 2004].

### 2.3 Pacific/Arctic Halocline: 50–200 m water depth

The transport budget of Pacific into the Arctic is 1.5 Sv (1 Sv = $1 \times 10^6$ $m^3/s$) at the Bering Strait [Rudels et al., 2012]. Seawater density depends on temperature and salinity, and at high latitudes the density is mainly determined by salinity rather than by temperature. Hence, in the Arctic, low salinity waters (cold, Pacific and polar mixed layer waters) overlay high salinity waters (warm, Atlantic waters) creating a ~150 m isothermal halocline that acts isolating the PML from the warmer Atlantic layer below [Coachman and Aagaard, 1974; Rudels et al., 1996].

### 2.4 Atlantic water (AW): 200–900 mwd

More than one century ago the presence of AW was already identified in the Arctic [Nansen, 1902]. The flow of North Atlantic waters through the Fram Strait into the Arctic is of 7.1 Sv [Rudels et al., 2012]. These Atlantic sourced waters are warmer by 1–2°C and saltier (~ 34.30–34.75) than the rest of Arctic water masses and they flow around the continental shelves and ocean ridges at depths between 150–900 mwd [Rudels et al., 2004; Björk et al., 2007; Rudels et al., 2012]. The warmest core of the AW is within 300–500 m sometimes reaching 2°C [Rudels et al., 2004]. The conduit for these waters is also the Fram Strait, through which they flow at a rate of 5–8 Sv [Worthington, 1970]. Once inside the Arctic, 1 Sv of AW enters the Central Arctic Ocean subducting counterclockwise (cyclonic) hugging the continental slope around the Arctic Ocean and making its heat unavailable to the atmosphere [Rudels, 1987; Bourke et al., 1988; Rudels et al 1994]. The first barrier that the AW flow encounters along its underwater flow is the Lomonosov Ridge. There AW splits into two branches, one diverting poleward along the ridge, and the other traversing the ridge and making its path along the continental slope of the Canadian Basin [Rudels et al., 2012]. This AW will split again at the opposite limb of

the Lomonosov Ridge, one part following the ridge slope poleward and another continuing along the Canadian Basin continental shelf and closing the loop.

### 2.5 Arctic deep water

Below the AW, sub-zero water temperatures reemerge as the Eurasian Basin Deep Water (EBDW) and Canadian Basin Deep Water (CBDW), the latter 0.5–0.3 °C warmer and saltier [Jones et al., 1995; Rudels et al., 2012]. This is because the AW has subducted to greater depths in the Canadian than in the Eurasian Basin since in the Canadian Basin it has mixed with shelf-sourced sinking brines that push the water deeper [Rudels et al., 2012]. CBDW and EBDW converge at the Lomonosov Ridge adjacent to the Greenland limb, then flow out of the Arctic through the Fram Strait into the Greenland Sea. This chilled, dense water mass contributes to the mixture that eventually becomes North Atlantic Deep Water (NADW). NADW enters the global thermohaline ocean circulation system and eventually returns the Arctic waters to the surface in the northeast Pacific Ocean 1200 years later [Rudels et al., 2012].

## 3 Methods

### 3.1 Studied material

Growing collections of sediment cores from the central Arctic from multiple polar expeditions, and new suites of multicores recovered from the Arctic margins and continental slopes during the SWERUS-C3 expedition in 2014 have been shown to contain diverse and at times abundant calcareous benthic foraminifera suitable for proxy analysis in the geological record and thus could potentially be useful for paleoreconstructions [e.g. Scott et al. 1989; Wollenburg et al., 2001; 2007; Hanslik et al., 2010; Farmer et al., 2011; Hanslik and Hermelin 2011].

In this thesis we present results from foraminifera found in 42 surface sediments from core tops and multicores (Manuscript-1) and one downcore record (Manuscript-2) distributed across different Arctic Ocean regions (Figure 3): Chukchi Shelf (6), East Siberian Slope (16), Laptev Shelf (1), Lomonosov Ridge (18) and Morris Jesup Rise (1). Altogether, the sites cover depths from 52–3814 m. The core tops belong to 16 trigger weight, piston and gravity cores from Arctic Ocean ’96, LOMROG I–III and SWERUS-C3 expeditions [Jakobsson et al., 2008; Marcussen et al., 2011; Marcussen et al. 2012]. The 25 multicores were obtained during the SWERUS-C3 expedition. The downcore study come from sediment samples retrieved from the Herald Canyon on the Chukchi Shelf at 72 m water depth. Below follows a description of the methods and considerations relevant this thesis.

### 3.2 Radiocarbon dating

Radiocarbon ($^{14}C$) dates obtained from planktic foraminifera *Neogloboquadrina pachyderma* (~700 specimens per date) and mollusk shell calcite have been the primary means of assessing the age of surface and downcore marine sediment sequences in this work. This radiogenic isotope of carbon forms in the upper atmosphere and gets incorporated into $CO_2$ molecules that ultimately dissolve in the upper ocean. There, the isotopic signature is captured in the shells of calcifying organisms such as foraminifera. Before interpreting marine $^{14}C$ dates, a correction is required to account for the time lag in gas exchange between the atmosphere and ocean $^{14}C$ reservoirs, a process known as the marine reservoir effect (R). This mechanism derives higher $^{14}C$ ages in the marine samples and therefore needs to be accounted for [Bard, 1988; Stuiver and Braziunas, 1993]. The modern global mean R value is 400 years [Bard, 1988; Hughen et al., 2004]. However, previous research shows that in reality the rate of air-sea $CO_2$ exchange varies considerably between regions due to the oceanography, thus $^{14}C$ dates need to be adjusted based on the location by adding an offset to R known as $\Delta R$ [Stuiver and Braziunas, 1993].

Generated $^{14}C$ dates have been used in my research to (i) determine the surface sediment age for the modern field Mg/Ca-temperature calibration presented in Manuscript-1, and (ii) work with co-authors in a separate study to produce a very detailed age model for the Herald Canyon [Pearce et al. in preparation] that was applied in Manuscript-2.

### 3.3 Arctic benthic foraminifera taxonomy and ecology

There are hundreds of different living benthic species identified in the central Arctic Ocean across the shelves and in deep water [Wollenburg and Kuhnt, 2000]. In order to use foraminifera as climatic proxies, one first needs to learn about their taxonomy, biology and ecology. This is because each species, even from the same genus, may be characterized by distinct biological effects related to their ecology that modifies sea water chemistry in the microenvironment around the organism, and thus in the test calcite. Known as 'vital effects', these effects are typically not climate related. Conveniently, many of these foraminiferal vital effects have been studied so that it is possible to predict which species will carry vital effects. The outcome is that careful attention to taxonomy is required to ensure that appropriate species of the same taxon are being analyzed together. The same problems do not exist for Arctic planktic foraminifera because there is only one true polar species, *Neogloboquadrina pachyderma* [Spindler and Dieckmann, 1986], the same that was used for $^{14}C$ dating the core top samples in Manuscript-1.

The Arctic Ocean taxonomy followed has been reviewed by several authors [e.g. Lagoe, 1979; Bilodeau et al., 1990; Scott and Vilks, 1991; Wollenburg and Kuhnt, 2000;

Wollenburg et al., 2001; Wollenburg et al., 2004]. Investigation of the benthic living species found in Arctic surface sediments in Manuscript-1, has shown depth preferences. Certain species had major occurrence in shelves (*E. clavatum* and *N. labradorica*) whereas others in the shelf break, shelf slope and ridges (*C. neoteretis*, *Q. arctica*, *C. wuellerstorfi*, *O. tener*). Initially, it was thought that the distribution of foraminiferal associations in the Arctic Ocean was guided by water masses [Vilks, 1989; Scott et al., 1989; Scott and Vilks, 1991; Bergsten, 1994]. However, it has also been proposed that biological factors controlling ecology are most important [Green, 1960; Lagoe, 1976; 1977; Wollenburg and Mackensen, 1998].

## 3.4 Geochemical proxies applied on Arctic benthic foraminifera

### 3.4.1 Stable isotopes

Stable isotopes ratios of oxygen ($\delta^{18}O$) and carbon ($\delta^{13}C$) measured in marine calcite are widely used in palaeoceanography for reconstructing ocean-climate parameters. For $\delta^{18}O$, the major controls on foraminiferal $\delta^{18}O$ are temperature and seawater $\delta^{18}O$, the latter changing as a function of global ice volume [e.g. Urey, 1947; Emiliani, 1955; Shackleton, 1974]. Foraminiferal $\delta^{13}C$ reflects seawater dissolved inorganic carbon $\delta^{13}C$, which varies as a consequence of bottom water circulation, productivity and vital effects [e.g. Broecker and Peng, 1982; Sayles and Curry, 1988; Mackensen and Bickert, 1999]. The isotopes measured ($^{18}O$, $^{16}O$ and $^{13}C$, $^{12}C$) occur in such small proportions that their absolute abundances are difficult to measure with sufficient accuracy. Thus, both oxygen and carbon isotopic ratios in a sample are compared with those in a standard. For foraminifer calcite the standard is calcite derived from the *Belemnitella americana* belemnite from the Late Cretaceous PeeDee Formation in South Carolina (PDB, now 'VPDB'), expressed in part per mille (‰). For water or ice sample the 'mean ocean water' standard (SMOW) is used.

### 3.4.2 Magnesium concentration in benthic foraminiferal tests and Mg/Ca palaeothermometry

Mg, like the other alkaline earth metals, is a highly reactive element and it occurs dissolved in seawater as $Mg^{2+}$ (aq). Foraminifers have the ability to control Mg uptake of seawater during calcification. They actively discriminate Mg during biomineralization processes since Mg inhibits calcification, as shown in culture and field measurements at known temperature [Chave, 1954; Izuka, 1988; Davis et al., 2000]. Modern seawater Mg/Ca content is 5.5 mol/mol and a foraminifera test ends up having approximately 1000-3000 times lower ratio of Mg over Ca than seawater [Lea et al., 1999].

Importantly, Mg/Ca has been shown to be an independent paleotemperature proxy that can also be measured on foraminifera shells. Used in combination with benthic foraminifera $\delta^{18}O$ it becomes possible to reconstruct $\delta^{18}O$-of sea water, and hence salinity variations, without the problems introduced by other temperature proxies like different seasonal signals or different habitat depths of the biotic carriers [Nürnberg, 2000]. Experimental works have shown that higher temperatures allow foraminifera to more easily incorporate $Mg^{2+}$ into their calcite tests. On time scales shorter than one million years, as is the focus in this thesis, where seawater Mg and Ca are thought to be constant, the control on higher Mg incorporation at warmer waters is based on inorganic thermodynamics [Lea et al., 1999], since molecules move and collide faster increasing bonds at higher temperatures.

Over long timescales changes in Mg concentration in the oceans must also be considered, e.g. more Mg is dissolved in the oceans during warmer climates [Broecker and Peng, 1982]. The Mg sources in seawater might originate from continental weathering from rivers, in the Arctic especially Arctic Canada. The major Mg sinks include formation of hydrothermal fluids, clays and dolomite [Holland, 2005]. While Mg is generally regarded as a conservative ion in the oceans it remains unclear if seawater Mg concentrations are in steady state [Holland, 2005; Tipper et al., 2006]; incoming studies suggest that seawater Mg concentrations actually evolve rapidly with time [Fantle and DePaolo, 2006; Coggon et al., 2010; Higgins and Schrag, 2012].

Nevertheless, biological processes also have an influence in the Mg fractionation to a lesser extent deriving from a distinct life habitat and calcification pathway [Bentov and Erez, 2006; de Nooijer et al., 2009] and therefore species-specific applications are required.

#### 3.4.2.1 Trace metal sample cleaning and inductively coupled plasma mass spectrometry (ICP-MS)

While $\delta^{18}O$ measurements in benthic foraminifera calcite is relatively straightforward, requiring little pre-sample preparation, a rigorous cleaning protocol is required prior to Mg/Ca analysis. This is necessary to remove products of diagenesis, organic matter and clay remains from the test surfaces that might interfere with the real biogenic ratios [Boyle, 1983; Boyle and Keigwin, 1985/1986; Boyle and Rosenthal, 1996; Barker et al., 2003]. The steps during cleaning consist of (i) a clay removal step, since remaining clays have the greatest effects on Mg/Ca ratios [Barker et al. 2003]; (ii) organic matter removal or oxidizing step, since adhering organic matter will influence Mg/Ca ratios [Rathburn and De Deckker, 1997]; (iii) Fe-Mn oxide coatings removal, a reductive step, which is necessary because sediments under redox conditions enhance the formation of diagenetic Mn-rich oxide coatings [Barker et al. 2003].

Once cleaned, the benthic foraminifera samples must be dissolved and the solutes diluted to appropriate concentrations for measuring both Ca concentration and then trace metals, which includes Mg. Analysis was carried out at the Cardiff University ICP-MS facility, in collaboration with Prof. Carrie Lear. During mass spectrometry, the sample liquids were carried through capillaries to the ICP-MS nebulizer where they were transformed into a spray that reaches the plasma torch (8000 K). Here the sample is ionized, i.e. separated into ions grouped by mass-to-charge ratios. The mass spectrometer out-puts raw data as intensity counts, i.e. counts per second (cps). This is then translated to molarity units by comparing the cps from the standards of known chemical composition. Long term precision and accuracy of the analysis is achieved by analyzing two in house standards, i.e. 'Cardiff consistency standards' (CS1 and CS2), which are run at the beginning and end of each batch of analysis. To maintain quality of the Arctic trace metal data calculated at Cardiff University ICP-MS facility we have followed these steps:

(i) Intensity signals less than 5 times the blank were excluded.

(ii) Individual standards with the same [Ca] are run after each sample or matrix matched to one standard of equal [Ca] composition and samples with more than 10% offsets were excluded. This process is required because increasing [Ca] reduces sensitivity to magnesium that in turn reduces the accuracy of each measurement [Lear et al., 2002].

(iii) All the Mg/Ca results were further screened to detect remaining clays, organic matter and Fe-Mn oxide coatings by observing the correlation between Mg/Ca against Fe/Ca, Al/Ca and Mn/Ca, a low correlation meaning that the samples were successfully cleaned [Barker et al., 2003].

## 4 Manuscript summaries

### 4.1 Manuscript-1

Mg/Ca-temperature calibrations in the Arctic Ocean need to be developed since only few published calibrations cover the coldest end of the temperature spectra. Thus, Mg/Ca readings by ICP-MS in living (i.e., Rose Bengal stained) benthic foraminifera from newly retrieved Arctic surface sediments were coupled to newly-acquired bottom water temperatures, salinity and carbonate ion (all environmental factors thought to interplay with Mg incorporation) to investigate if Mg/Ca paleothermometry can be applied in the Arctic Ocean. Six of the most commonly occurring foraminifera species found in Arctic surface sediments (*Elphidium clavatum, Nonionellina labradorica, Cassidulina*

*neoteretis*, *Quinqueloculina arctica*, *Oridorsalis tener* and *Cibicidoides wuellerstorfi*) were analyzed. Apart from Mg-rich test species *Q. arctica* implying strong biological controls on its calcification process, Arctic Mg/Ca showed coherent low ratios (0.5–1.8 mmol/mol) consistent with the cold Arctic bottom waters (-1.8–1 °C) measured at the coring sites. This low observed bottom water temperature range presents a challenge to optimizing the calibration. To overcome this, and to see if local or compiled temperature calibrations are preferable, our new Arctic Mg/Ca dataset was integrated with published species-specific Mg/Ca data from outside the Arctic. We conclude that our stained Mg/Ca data, alone or compiled, fall within the published linear/exponential Mg/Ca-temperature sensitivities but is far from reproducing realistic paleotemperatures. This finding is validated by a late Holocene temperature record from a pilot study in a marine sediment core (2-PC) retrieved on the Chukchi Shelf, which is the focus of Manuscript-2 in this thesis (see below).

Furthermore, investigation into the use of Mg/Ca palaeothermometry using core top foraminifera from the central Arctic Ocean produced different results. Firstly, radiocarbon dating of samples from the Lomonosov Ridge indicated that the core tops were rather 'old', possibly due to the very low sedimentation rates (~0.5 cm/kyr), giving Holocene dates averaging 5000 $^{14}$C yrs. Trace metal analysis of benthic foraminifera from these $^{14}$C-dated core tops show Mg/Ca values that double those of the stained foraminifera specimens measured at the shelf stations. Such high values are suggestive of seawater temperatures much higher than Holocene variability, suggesting some diagenetic Mg input to central Arctic core top foraminifera. Scanning electron microscopy (SEM) and elemental mapping using Energy Dispersive Spectroscopy (EDS) was used to provide further insight. The results reveal evidence for crystalline Mg-rich overgrowths and infillings on the tests of the Holocene $^{14}$C-dated core top foraminifera. This implies that Arctic shelf settings are better environments for Mg/Ca palaeothermometry, while post-depositional alteration effects appear to influence benthic fossil foraminifera from the central Arctic. Thus, these Mg/Ca results were excluded from the calibration set and are now subject to a new parallel line of study.

### 4.2 Manuscript-2

The Herald Canyon is located at modern average summer sea-ice edge close to the continental shelf break of the Chukchi Sea. This bathymetric feature allows the throughflow of Pacific origin waters into the Arctic making it a target area for paleoceanographic reconstructions. We benefited from a new SWERUS-C3 L2-2-PC1 sediment core retrieved at 72 m from the Herald Canyon, an area where sedimentary records are recovered for the first time. Moreover, a robust age model is built from this record [Pearce et al. *in preparation*] reaching back ~4300 cal. yr BP. The goal of this paper was to reconstruct the variability of bottom water temperature, salinity and DIC $\delta^{13}$C using benthic foraminifera Mg/Ca palaeothermometry and $\delta^{18}$O analysis. These

parameters were measured on paired samples of the benthic foraminifera species *E. clavatum*, which was shown to be most common in this setting. The new calibration from Manuscript-1 was applied and compared with an alternate method for constraining BWT using Mg/Ca-BWT sensitivities from Varekamp et al. [2010]. The absolute temperatures seemed somewhat unrealistic, or arbitrary. However, it was concluded that this relates to imperfections in the calibration data sets, while we can have confidence in the relative Mg/Ca changes with respect to bottom water temperature variability. Qualitative interpretation of the Mg/Ca record (i.e. relative increases or decreases of BWT) together with the stable isotopes records, provides important insights into the variability of seawater $\delta^{18}O$, and thus brine water production, as well as bottom water organic carbon content at the site. The results indicate millennial to centennial scale halocline variability with a shift to colder bottom waters at ~1200 cal. years BP coeval with higher sedimentation rates and a rapid lightning excursion in the stable isotopes supporting the presence of bottom brines. These change was attributed to two main factors: a reduction in Pacific Waters entering the Arctic Ocean through the Herald Canyon, and a change in the summer sea ice extent at the site. Lastly, comparison to Mount Logan (Yukon, Canada) $\delta^{18}O$ ice core record indicates a Pacific atmosphere-climate coupling in the geochemical signature captured by the Herald Canyon bottom waters.

## 5 Current work and future perspectives

The work conducted so far towards this PhD project has led to some interesting discoveries regarding the application of Mg/Ca palaeothermometry in the Arctic Ocean and the potential for identifying global signals that can influence Arctic Ocean climate variability. Our new data in Manuscript-1 provide important new constraints to the calibration data set at the cold end of the temperature spectrum and it identifies preferential areas for benthic Mg/Ca application based on test preservation. During the production of Manuscript 1, SEM imaging revealed post-depositional coatings and fillings in foraminiferal tests that were found in Central $^{14}C$-dated Arctic cores. These diagenetic precipitates were resistant and not removed by the sample cleaning treatment that was effectuated prior to ICP-MS analysis. Nevertheless, when the central Arctic specimens are crushed and the fragments inspected again under the SEM, they reveal intact smooth sections since no recrystallization occurred. A way forward would be to use Secondary ion mass spectrometry or Laser ablation spectroscopy techniques on selected targeted unaltered wall section spots instead of dissolving the whole test as done in the ICP-MS. This will allow reconstructing central Arctic paleotemperatures at cores extending back to Marine Isotope Stage 5. Another consideration and future line of research is to constrain seawater Mg in the Arctic, and possible fluxes/sources. Does for example rivers/glaciers eroding dolomite (limestone with high Mg content) on the Canadian continent influence Arctic bottom water chemistry? In addition, during the production of Manuscript-2, Pacific atmosphere-climate oscillations where found in the

bottom waters of the Herald Canyon (Chukchi Sea). This connection needs to be further explored by adding new insights into atmospheric-ocean dynamics.

Lastly, working with Arctic benthic foraminifera has shown that various post depositional effects are affecting their tests, namely diagenesis and dissolution (Figure 4), which are dependent on their geographic spatial and bathymetric locations (ridge, shelves and basins). Investigations of the processes altering foraminifera tests in the Arctic Ocean are underway since this knowledge is needed for general foraminifera geochemical proxy validation and application.

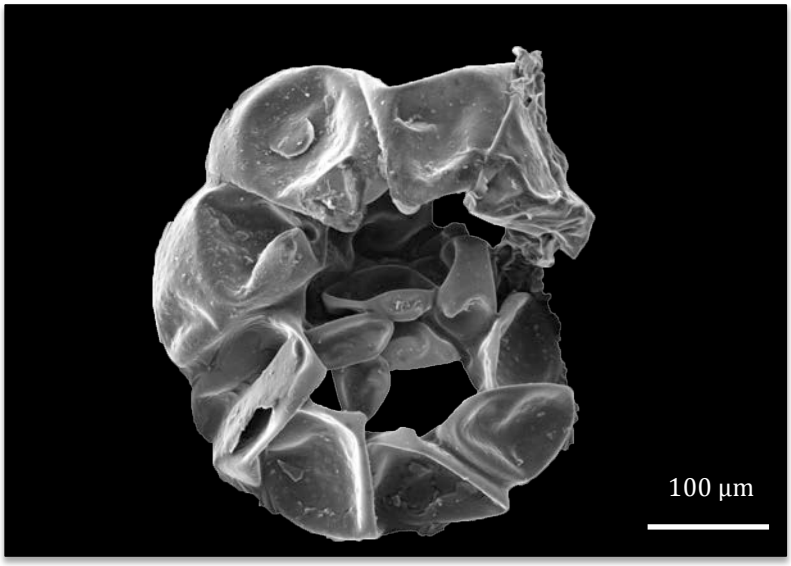


**Figure 4.** Fully dissolved calcite test of one *E. clavatum* specimen (‘ghost’ foraminifera). The image shows the organic lining preserved in the now acidic (~6 pH) marine sediment.

**Acknowledgments**

I deeply thank Helen Coxall and Martin Jakobsson who made this project possible giving me the opportunity to learn and grow at an academic and personal level. Thank you also for your respect and patience during the moments of slow progress. The bright discussions brought by Christof Pearce are also highly appreciated.

To the crew (scientific and nautical) onboard *Oden* summer 2014 during the SWERUS-C3 expedition for providing such a pleasant and familiar working environment. Especially, Carina, Pedrinho, Muschi, Sasha, Clint, Bull, Tom and Laura for creating such an enjoyable team environment. And thanks also to the cook who provided delicious Swedish food.

I also thank Carrie Lear, Elaine Mawbey and Anabel Morte Ródenas at Cardiff University for collaborating on this project and their guidance in measuring Mg/Ca in foraminifera.

Thanks to all amazing folk that I've come across during these two years along my PhD path, for bringing motivation and inspirational moments. The geo-badminton crew for all the fun games, get ready! A mis antípodas Albita y Tom, y 'Andigenous' Seb, gracias por llenar mi vida de magia.

A mi familia, y en especial a mi querida tía Gemma.

## References


ACIA (2004). Impacts of a warming Arctic: Arctic Climate Impact Assessment. Cambridge: Cambridge University Press, 139 pp.

Anderson,L.G., and Jones, E.P. (1992). Tracing upper waters of the Nansen Basin in the Arctic Ocean. Deep Sea Res., 39, Part A, S45-S433.

Bard, E. (1988). Correction of accelerator mass spectrometry $^{14}C$ ages measured in planktonic foraminifera: Paleoceanographic implications. Paleoceanography 3(6): 635-645.

Barker, S., M. and Greaves, E. H. (2003), A study of cleaning procedures used for foraminiferal Mg/Ca paleothermometry, Geochemistry Geophisics Geosystems, 4 (9), 1–20.

Bentov, S. and Erez, J. (2006), Impact of biomineralization processes on the Mg content of foraminiferal shells: A biological perspective. Geochemistry Geophisics Geosystems, 7 (1), 1–11.

Bergsten, H. (1994). Recent benthic foraminifera of a transect from the North Pole to the Yermak Plateau, eastern central Arctic Ocean. Marine Geology, 119, 251–267.

Bilodeau, G., de Vernal, A., Hillaire-Marcel, C., Josenhans, H.W., (1990). Postglacial paleoceanography of Hudson Bay: strati- graphic, microfaunal and palynological evidence. Canadian Journal of Earth Sciences 27, 946–963.

Björk, G., Jakobsson, M., Rudels, B., Swift, J.H., Anderson, L., Darby, D.A., Backman, J., Coakley, B., Winsor, P., Polyak, L., Edwards, M. (2007). Bathymetry and deep-water exchange across the central Lomonosov Ridge at 88–89oN. Deep Sea Research Part I: Oceanographic Research Papers 54 (8), 1197–1208.

Bourke, R. H., Weigel, A.M. and Paquette R. G. (1988) The westward-turning branch of the West Spitsbergen Current. J. Geophys. Res., 93, 14065–14077.

Boyle, E. (1983), Manganese carbonate overgrowths on foraminifera tests. Geochim. Cosmochim. Acta 47 (10), 1815–1819.

Boyle, E. A. and Keigwin, L. D. (1985/1986) Comparison of Atlantic and Pacific paleochemical records for the Last 215.000 years: Changes in deep ocean circulation and chemical inventories. Earth and Planetary Science Letters, 76, 135–150.

Boyle, E. A. and Rosenthal, Y. (1996). Chemical hydrography of the South Atlantic during the last glacial maximum: d13C vs. Cd, Berlin., Springer-Verlag, in: The South Atlantic: Present and Past Circulation, eds. G. Wefer, W. H. Berger, G. Siedler and D. Webb, Berlin., Springer-Verlag, 423-443.

Broecker, W., and Peng, T.-H. (1982), *Tracers in the sea*, Eldigo, Palisades, N.Y., 690 pp.

Chave, K.E., 1954, Aspects of the biochemistry of magnesium: 1. Calcareous marine organisms: Journal of Geology, v. 62, p. 266–283.

Coachman, L.K. and Aagaard, K. (1974). Physical Oceanography of Arctic and Subarctic Seas. 72 pp. Publisher: Springer Berlin Heidelberg.

Coggon, R. M., Teagle, D.A.H., Smith-Duque, C. E., Alt, J.C., and Cooper M.J. (2010). Reconstructing Past Seawater Mg/Ca and Sr/Ca from Mid-Ocean Ridge Flank Calcium Carbonate Veins. Science, 327, 1114-1117.

Davis, K. J., Dove, P. M. and De Yoreo, J. J. (2000). The role of $Mg^{2+}$ as an impurity in calcite growth, Science, 290, 1134–1137.

de Nooijer, L. J., Toyofuku, T. and Kitazato, H. (2009). Foraminifera promote calcification by elevating their intracellular ph, PNAS, 106 (36), 15374–15378.

Emiliani, C. (1955). Pleistocene temperatures. Journal of Geology (63), 538–578.

Fantle, M. S. and DePaolo, D. J. (2006). Sr isotopes and pore fluid chemistry in carbonate sediment of the Ontong Java Plateau: Calcite recrystallization rates and evidence for a rapid rise in seawater Mg over the last 10 million years. Geochim. Cosmochim. Acta, 70, 3883–3904.

Farmer, J. R., T. M. Cronin, A. de Vernal, G. S. Dwyer, L. D. Keigwin, and R. C. Thunell (2011). Western Arctic ocean temperature variability during the last 8000 years, *Geophysical Research Letters*, 38 (24), L24602.

Green, K.E. (1960). Ecology of Some Arctic Foraminifera. Micropaleontology, 6 (1), 57–78.

Hanslik, D., Jakobsson, M., Backman, J., Björck, S., Sellén, E., O'Regan, M., Fornaciari, E., Skog, G., 2010. Quaternary Arctic Ocean sea ice variations and radiocarbon reservoir age corrections. Quat. Sci. Rev. 29, 3430–3441.

Hanslik, D. (2011) Late Quaternary Biostratigraphy and Paleoceanography of the central Arctic Ocean. Doctoral thesis. Department of Geological Sciences, Stockholm University.

Helland-Hansen, B., and F. Nansen (1909), The Norwegian Sea. Report on Norwegian Fishery and Marine Investigation.

Higgins, J. A. and Schrag, D. P. (2012). Records of Neogene seawater chemistry and diagenesis in deep-sea carbonate sediments and pore fluids, Earth Planet. Sci. Lett., 357–358, 386–396.

Holland, H. D. (2005). Sea level, sediments and the composition of seawater, Am. J. Sci., 305, 220–239, 2005.

Hughen, K.A., Baillie, M.G.L, Bard, E., et al. (2004). MARINE04 marine radiocarbon age calibration, 0–26 cal kyr BP. Radiocarbon, 46 (3), 1059–1086.

Izuka, S. (1988). Relationship of magnesium and other minor elements in tests of *Cassidulina subglobosa* and *C. oriangulata* to physical oceanic properties, J. Foraminiferal Res., 18, 151–157.

Jakobsson, M., (2002). Hypsometry and volume of the Arctic Ocean and its constituent seas: Geochemistry, Geophysics, Geosystems, v. 3, no. 5, p. 1-18.

Jakobsson, M., Marcussen, C., and LOMROG Scientific Party (2008) Lomonosov Ridge off Greenland 2007 (LOMROG) – Cruise Report. Spetial publication Geological Survey of Denmark and Greenland, Copenhagen, Denmark, 122 pp.

Jakobsson, M., L. A. Mayer, B. Coakley, J. A. Dowdeswell, S. Forbes, B. Fridman, H. Hodnesdal, R. Noormets, R. Pedersen, M. Rebesco, H.-W. Schenke, Y. Zarayskaya A, D. Accettella, A. Armstrong, R. M.

Anderson, P. Bienhoff, A. Camerlenghi, I. Church, M. Edwards, J. V. Gardner, J. K. Hall, B. Hell, O. B. Hestvik, Y. Kristoffersen, C. Marcussen, R. Mohammad, D. Mosher, S. V. Nghiem, M. T. Pedrosa, P. G. Travaglini, and P. Weatherall, The International Bathymetric Chart of the Arctic Ocean (IBCAO) Version 3.0, Geophysical Research Letters, doi: 10.1029/2012GL052219. [Auxiliary Material]

Jones, E. P., Rudels, B. & Anderson, L. G. 1995: Deep waters of the Arctic Ocean: origins and circulation. *Deep-Sea Res. 42*, 737–760.

Jones, E. P. (2001). Circulation in the Arctic Ocean. Polar Research, 20: 139–146.

Lagoe, M.B. (1976). Species diversity of deep-sea benthic foraminifera from the central Arctic Ocean. Geol. Soc. Amer. Bull. 87, 1678.1683.

Lagoe, M.B. (1977). Recent benthic foraminifera from the Central Arctic Ocean. J. Foraminiferal Res. 7 (2), 106–129.

Lagoe, M.B. (1979). Recent benthonic foraminiferal biofacies in the Arctic Ocean. Micropaleontology 25, 214–224.

Lea, D.W. (1999). Trace elements in foraminiferal calcite. Modern foraminifera, 259–277.

Mackensen, A. and Bickert, T. (1999). Stable carbon isotopes in benthic foraminifera: proxies for deep and bottom water circulation and new production. In: Fischer, G & Wefer, G (eds.), Use of Proxies in Paleoceanography - Examples from the South Atlantic, Springer, Berlin, Heidelberg, 229–254.

Marcussen, C. and LOMROG II Scientific Party (2011). Lomonosov Ridge off Greenland 2011 (LOMROG II) – Cruise Report. Geological Survey of Denmark and Greenland, report 2011/106, 154 pp.

Marcussen, C. and LOMROG III Scientific Party (2012). Lomonosov Ridge off Greenland 2012 (LOMROG III) – Cruise Report. Geological Survey of Denmark and Greenland, report 2012/119, 220 pp.

Nansen, F. (1902). Oceanography of the North Polar Basin. The Norwegian North Polar Expedition, 1893-96. Scientific Results, 3(9), 427 pp.

National Snow and Ice Data Center, September 2016, www.nsidc.org

Nürnberg, D. (2000). Taking the temperature of past ocean surfaces. Science, 289, 1698-1699.

Pearce, C., Varheyli, A., Wastegård, S., Jakobsson, M., Muschitiello, F., Barrientos, N., O'Regan, M. and Cronin, T. M.: The 3.6 ka Aniakchak tephra in the Arctic Ocean: implications for the radiocarbon reservoir age of the Chukchi Sea in the late Holocene, Clim. Past, In prep.

Pithan, F., and Mauritsen, T., (2014). Arctic amplification dominated by temperature feedbacks in contemporary climate models: Nature Geosci, v. advance online publication.

Rathburn, A.E. and DeDeckker, P. (1997). Magnesium and strontium compositions of recent benthic foraminifera from the Coral Sea, Australia and Prydz Bay, Antarctica. Marine Micropaleontology 32, 231–248.

Rudels, B. (1987). On the mass balance of the Polar Ocean, with special emphasis on the Fram Strait. Norsk Polarinstitutt Skrifter 188.

Rudels, B., Jones, E.P., Anderson, L.G., and Kattner, G. (1994). On the intermediate depth waters of the Arctic Ocean, *in* The Polar Oceans and Their Role in Shaping the Global Environment (eds O. M.

Johannessen, R. D. Muench and J. E. Overland), American Geophysical Union, Washington, D. C. doi: 10.1029/GM085p0033.

Rudels, B., Anderson, L. G. & Jones, E. P. (1996). Formation and evolution of the surface mixed layer and halocline of the Arctic Ocean. Journal of Geophysical Research: Oceans, 101, 8807–8821.

Rudels, B., Jones, E.P., Schauer, U., Eriksson, P. (2004). Atlantic sources of the Arctic Ocean surface and halocline waters. Polar Res., 23, 181–208.

Rudels, B., Anderson, L., Eriksson, P. , Fahrbach, E., Jakobsson, M., Jones, E. P., Melling, H., Prinsenberg, S., Schauer, U. and Yao, T. (2012). Observations in the Ocean, *in* Lemke, P., ed., Arctic Climate Change: The ACSYS Decade and Beyond, Volume 43, Springer, 117–198.

Sayles, F.L. and Curry, W.B. (1988). $\delta^{13}C$, $TCO_2$, and the metabolism of organic carbon in deep sea sediments. Geochimica et Cosmochimica Acta, 52 (12), 2963–2978.

Schlosser, P., Kromer, B., Östlund, H.G., Ekwurzel, B., Bönisch, G., Loosli, H.H., and Purtschert, R. (1994). On the $^{14}C$ and $^{39}Ar$ distribution in the central Arctic Ocean: implications for deep water formation. Radiocarbon, 36, 327–343.

Scott, D.B., Mudie, P.J., Baki, V., MacKinnon, K.D., Cole, F.E. (1989) Biostratigraphy and Late Cenozoic paleoceanography of the Arctic Ocean: foraminiferal, lithostratigraphic, and isotopic evidence. Geological Society of America Bulletin 101, 260–277.

Scott, D.B., and Vilks, G. (1991). Benthonic foraminifera in the surface sediments of the deep-sea Arctic-Ocean. Journal of Foraminiferal Research 21 (1), 20–38.

Serreze, M. C. and Barry, R. G. (2011). Processes and impacts of Arctic amplification: A research synthesis. *Global and Planetary Change*, 77, 85–96.

Shackleton, N.J. (1974). Attainment of isotopic equilibrium between ocean water and the benthonic foraminifera genus *Uvigerina*, p. 203–209. In: Isotopic changes in the ocean during the last glacial. Cent. Nat. Rech. Sci. Colloq. Int., No. 219.

Shakhova, N., Semiletov, I., Salyuk, A., Yusupov, V., Kosmach, D., Gustafsson, Ö. (2010). Extensive methane venting to the atmosphere from sediments of the East Siberian Arctic Shelf. *Science* 327, 1246–1250.

Shakhova, N., Semiletov, I., Leifer, I., Sergienko, V., Salyuk, A., Kosmach, D., Chernykh, D., Stubbs, C., Nicolsky, D., Tumskoy, V., Gustafsson, Ö. (2014). Ebullition and storm-induced methane release from the East Siberian Arctic Shelf. *Nature Geoscience* 7, 64–70.

Shakhova, N., et al. (2015). The East Siberian Arctic Shelf: towards further assessment of permafrost-related methane fluxes and role of sea ice. Phil. Trans. R. Soc. A., 373 (2052), 20140451.

Spindler, M., Dieckmann, G.S., 1986. Distribution and abundance of the planktic foraminifer *Neogloboquadrina pachyderma* in sea ice of the Weddell Sea (Antarctica). Polar Biol. 5, 185–191.

Stranne, C., O'Regan, M., Dickens, G. R., Crill, P., Miller, C., Preto, P. and Jakobsson, M. (2016). Dynamic simulations of potential methane release from East Siberian continental slope sediments, Geochem. Geophys. Geosyst., 17.

Stroeve, J., Serreze, M., Holland, M., Kay, J., Malanik, J., and Barrett, A. (2012). The Arctic's rapidly shrinking sea ice cover: a research synthesis: Climatic Change, 110 (3-4), 1005–1027.

Stuiver, M., Braziunas, T.F. (1993). Modelling atmospheric C-14 influences and C-14 ages of marine samples to 10,000 BC. Radiocarbon 35, 137–189.

Taylor, A. E., Dallimore, S. R., Hill, P. R., Issler, D. R., Blasco, S., and Wright, F. (2013). Numerical model of the geothermal regime on the Beaufort Shelf, arctic Canada since the Last Interglacial. Journal of Geophysical Research: Earth Sruface. 118, 2365-2379.

Thiede, J., Pfirman, S., Schenke, H-W. and Reil, W. (1990). Batymetry of Molloy Deep: Fram Strait beteen Svalbard and Greenland. *Marine Geophysical Researches*, 12, 197–214.

Tipper, E. T., Galy, A., Gaillardet, J., Bickle, M. J., Elderfield, H., and Carder, E. A. (2006). The magnesium isotope budget of the modern ocean: Constraints from riverine magnesium isotope ratios, Earth Planet. Sci. Lett., 250, 241–253.

Urey, H. (1947). The thermodynamics of isotopic substances. J. Chem. Soc., 562–581.

Vilks, G. (1989). Ecology of recent foraminifera on the Canadian Continental shelf of the Arctic Ocean. In: Y. Herman (Ed.), The Arctic Seas, climatology, oceanography, geology and biology (pp. 497–569). New York: Van Nostrand Reinhold.

Westbrook, G.K. et al., (2009), Escape of methane gas from the seabed along the West Spitsbergen continental margin. Geophys. Res. Lett. 36, L15608.

Winsor, P. and Björk, G. (2000), Polynya activity in the Arctic Ocean from 1958 to 1997, J. Geophys. Res., 105(C4), 8789–8803.

Wollenburg, J. E. and Mackensen, A. (1998b). On the vertical distribution of living (Rose Bengal stained) benthic foraminifers in the Arctic Ocean, *Journal of foraminiferal research* 28 (4), 268–285.

Wollenburg, J.E. and Kuhnt, W. (2000). The response of benthicforaminifera to carbon flux and primary production in the Arctic Ocean. Mar. Micropaleontol. 40, 189–231.

Wollenburg, J.E., Kuhnt, W., Mackensen, A. (2001). Changes in Arctic Ocean paleoproductivity and hydrography during the last 145 kyrs: the benthic foraminiferal record. Paleoceanography 16, 65–77.

Wollenburg, J.E., Knies, J., Mackensen, A. (2004). High-resolution paleoproductivity fluctuations during the past 24 kyrs as indicated by benthic foraminifera in the marginal Arctic Ocean. Palaeogeogr. Palaeoclimatol. Palaeoecol. 204, 209–238.

Wollenburg, J.E., Mackensen, A., Kuhnt, W. (2007) Benthic foraminiferal biodiversity response to a changing Arctic palaeoclimate in the last 24.000 years. Palaeogeography, Palaeoclimatology, Palaeoecology 255, 195–222.

Woodgate, R. A., Weingartner, T. J. and Lindsay, R. W. (2007). The 2007 Bering Strait Oceanic Heat Flux and anomalous Arctic Sea-ice Retreat. Geophys. Res. Lett. 37, L01602.

Worthington, L.V. (1970). The Norwegian Sea as a Mediterranean basin. Deep Sea Research 17, 77–84.

Manuscript I

# Benthic foraminiferal Mg/Ca paleothermometry in the Arctic Ocean

**Benthic foraminiferal Mg/Ca paleothermometry in the Arctic Ocean**

Natalia Barrientos[1,2], Caroline H. Lear[3], Martin Jakobsson[1,2,4], Christian Stranne[1,2,5], Matt O'Regan[1,2], Thomas M. Cronin[6], Aleksander Y. Gukov[7], Helen K. Coxall[1,2]

[1] Department of Geological Sciences, Stockholm University, Stockholm 10691, Sweden. [2] Bolin Centre for Climate Research, Stockholm University, Stockholm 10691, Sweden. [3] School of Earth and Ocean Sciences, Cardiff University, Main Building, Park Place, Cardiff, CF10 3AT, UK. [4] UNIS - The University Centre in Svalbard, Longyearbyen N-9171, Svalbard. [5] Center for Coastal and Ocean Mapping, University of New Hampshire, 24 Colovos Road, Durham, New Hampshire 03824, USA. [6] U.S. Geological Survey, Reston, Virginia, USA. [7] Lena Delta Reserve, Akademika Fedorova Str. 28, 678400 Tiksi, Yakutia, Russia .

## Abstract

Reconstructions of Arctic bottom water temperatures (BWT) are needed to assess past millennial scale variability in ocean temperatures and future climate feedbacks linked to Arctic water warming. Foraminiferal Mg/Ca paleothermometry has proved useful for reconstructing BWT in other oceans on a variety of time scales. However, in the Arctic it has had limited application in part because existing calibrations lack data at the cold end of the BWT spectrum in the range of Arctic bottom waters (<3°C). In this study we explore the potential of foraminiferal Mg/Ca paleothermometry in the Arctic Ocean using six common species of benthic foraminifera (*Elphidium clavatum, Nonionellina labradorica, Cassidulina neoteretis, Oridorsalis tener, Cibicidoides wuellerstorfi* and *Quinqueloculina arctica*). The study set, which comprises 'live' Rose Bengal stained and Holocene 'fossil' radiocarbon ($^{14}$C) dated (3010–10800 $^{14}$C age years BP) specimens, were derived from 41 seafloor samples recovered from the Arctic shelves and central Arctic Ocean. Collectively the samples span depths of 52–3814 m and BWT ranges of -1.8–0.9 °C. Mg/Ca values of stained specimens show a weak linear correlation with BWT probably because Mg/Ca–BWT sensitivity is lower at low temperatures. When integrated with existing monospecific Mg/Ca datasets that span wider BWT (-1.8–25°C), the Arctic data, excluding data from *Q. arctica*, tend to fit in the Mg/Ca–BWT linear and/or exponential relationships. Application of the Mg/Ca method to a new down-core (late Holocene) *E. clavatum* record from the Chukchi Shelf produces 0.4 mmol/mol Mg/Ca variability. In contrast, benthic Mg/Ca from $^{14}$C-dated core tops from the Lomonosov Ridge have unexpectedly high Mg/Ca and variability (2 mmol/mol Mg/Ca), indicating controls additional to temperature on test Mg/Ca in the Central Arctic. Scanning electron microscopy combined with energy dispersive spectroscopy reveal evidence for inorganic calcite coatings on the benthic foraminifera from the central Arctic. We conclude that Arctic shelf areas are suitable for application of Arctic benthic foraminifera Mg/Ca palaeothermometry, especially for the genus *Elphidium*, whereas further work is required to understand controls on benthic foraminifer Mg/Ca in the Central Arctic. This study forms a part of the *SWERUS-C3* program (Swedish-Russian-US Arctic Ocean Investigation of Climate-Cryosphere-Carbon Interactions).

## 1. Introduction

The current rise in global temperature is affecting the Arctic more than twice the ratio of lower latitudes due to polar amplification processes and associated global positive feedbacks [Overland et al., 2015]. Key Arctic processes that are susceptible to change include shrinking sea ice cover, changes in the latitudinal heat flux, seasonal changes in cloud cover and carbon/greenhouse gas release from thawing permafrost and destabilized methane hydrates stored on Arctic continental shelves [ACIA, 2004; Serreze and Barry, 2011; Pithan and Mauritsen, 2014]. Temperature changes in the Artic Ocean will influence these processes where bottom waters intersect the extensive Arctic shelf areas. Predictions are that a 1°C warming outside the modeled stability zone could shift the upper limit of the methane hydrate stability zone [Westbrook et al., 2009], and likewise, rapidly degrade submarine permafrost with the potential for carbon venting from the sediments [Shakhova et al., 2010; 2014]. Moreover, warming of upper ocean waters could erode the cold Arctic halocline, exacerbating sea ice loss [Cronin et al., 2012].

Although recent observations and modeling suggest that carbon contributions from Arctic gas hydrates reaching the atmosphere may not be the threat initially thought [Thornton and Crill, 2015; Stranne et al., 2016], the vulnerability of stored permafrost carbon and associated potential for positive feedback processes remains poorly understood [Vonk and Gustafsson, 2013; Schuur et al., 2015]. It is clear from instrumental records that upper ocean temperatures in the Arctic have raised, for instance the Chukchi Sea has experienced a 0.8–2.4 °C increase over the past seven decades [Luchin and Panteleev, 2014]. However, the links between temperature changes in Arctic bottom waters and the proposed polar climate feedbacks on longer time scales are unknown. To address this, records of past millennial-scale variability in Arctic bottom water temperatures (BWT) and paleotemperature proxy exploration are needed.

Reconstructing Arctic BWT in the Quaternary using palaeoceanographic proxies has proved challenging due to the logistics of acquiring samples, the scarcity of microfossils in sediments and complex Arctic marine geochemistry that creates complications for interpreting paleoclimate signals. A growing micropalaeontological database [e.g. Scott et al., 1989; Osterman et al., 1999; Wollenburg et al., 2001; 2007; Hanslik, 2011] now provides a clearer picture of the spatial and temporal distribution of calcareous benthic foraminifera in the Arctic and highlighting potential for application of calcite based Mg/Ca palaeothermometry. The dominant environmental factor controlling benthic Mg/Ca values is assumed to be temperature [Chave, 1954; Izuka, 1988] with a 10±1% Mg/Ca increase per °C [e.g. Rosenthal et al., 1997; Martin et al., 2002; Lear et al., 2002]. This method for reconstructing past ocean temperatures is now widely used since the mid 1990s [Nürnberg et al., 1996; Rosenthal et al., 1997] and has the advantage over $\delta^{18}O$ paleothermometry of recording ambient sea water temperature at the time of calcification without

complications of changes in the chemical composition of seawater because of fluctuations in continental ice volume, sea ice or salinity [Billups and Schrag, 2002; Lear et al., 2000; 2004; Martin et al., 2002]. Importantly, Mg and Ca have long residence times in seawater (13 myr for Mg and 1myr for Ca [Broecker and Peng, 1982]), hence the method is suitable for reconstructing late Quaternary millennial scale temperature variability.

Some success in reconstructing Arctic BWT has come through using Mg/Ca paleothermometry in benthic ostracods, revealing 1–2 °C warmer intermediate (depth range) in bottom waters in the central Arctic region over the last 50 kyrs [Farmer et al., 2011; 2012; Cronin et al., 2012]. However, the ostracod data resolution is low due to a more sparse presence in the geological record, whereas benthic foraminifer fossils tend to be more common and stratigraphically continuous compared to ostracods. Thus, developing a method for utilizing benthic foraminifera Mg/Ca palaeothermometry is a primary goal.

In the northern high latitudes application of this proxy in benthic foraminifera has been limited to sites outside the Arctic basin proper as shown in the work of Kristjánsdóttir et al. [2007] using *Islandiella norcrossi, I. helenae, Melonis barleeanus* and *Cassidulina neoteretis* (*I. teretis, I. helenae* of some authors) from the North Iceland shelf. They found that Mg/Ca in these species living at cold temperatures could be used to discern BWT variability over the past 4000 years BP. Outside of the Arctic realm, benthic foraminifera Mg/Ca has been useful for reconstructing BWT in all ocean basins throughout the Cenozoic with Mg/Ca-BWT calibration data sets ranging across temperatures of -1 to 18°C [e.g. Rosenthal et al., 1997; Martin et al. 2002; Elderfield et al., 2006; Lear et al., 2010]. Other studies outside of the Arctic realm involve calibrations that range to temperatures < 1°C typical of the Arctic but from core tops retrieved from tropical and subtropical regions. While these studies include cold BWT, they do not factor in the unique salinity and chemical conditions of the Arctic Ocean proper. These factors may create their own influences on Mg/Ca partitioning into calcite; hence we explore not only the Arctic benthic Mg/Ca influence to temperature, but also to salinity and seawater carbonate chemistry.

Our primary goal here is to assess the benthic Arctic Mg/Ca relationship to temperature to develop new calibrations adapted to the Arctic environmental conditions. This data will then be combined into existing monospecific Mg/Ca datasets to refine calibrations and provide improved palaeothermometry tools suitable for reconstructing Arctic and global cold end bottom waters. Finally, we test the use of the Arctic vs. combined Mg/Ca–BWT relationship calibration in a low-resolution downcore Mg/Ca record from the Chukchi Shelf.

## 2. Materials and Methods

### 2.1 Marine sediment samples

The field calibration study is built on six species of benthic foraminifera found in surface sediments from 42 marine cores located across different regions of the Arctic Ocean (Figure 1): Chukchi Shelf (6), East Siberian Slope (16), Laptev Shelf (1), Lomonosov Ridge (18) and Morris Jesup Rise (1). All sites span water depths from 52–3814 m and temperatures of -1.8–0.9 °C, intersecting all three main Arctic water masses, halocline, Atlantic water and Arctic deep water [Rudels et al., 1994; 2012].

**Table 1.** Expedition and core label, location, age determination (note *Hanslik, 2011; and **Cronin and Gemery, 2016 unpublished) and chemical data (salinity, $\Delta[CO_3^{2-}]$ and oxygen) at all study sites part of this Mg/Ca field calibration. Temperature columns are in order of data preference. Last column depicts the number of RB stained calcareous benthic foraminifera (CBF). The geographic regions abbreviations are LR, Lomonosov Ridge; AB, Amundsen Basin; MB, Makarov Basin; MJR, Morris Jesup Rise; HC, Herald Canyon; AP, Arliss Plateau; ESS, Eastern Siberian Sea; LS, Laptev Shelf.

| Core top / Multicore ID | Lat (°N) | Lon (°E) | Water depth (m) | Arctic Ocean location | Age in *N. pachyderma* ($^{14}$C years BP) | BWT *SWERUS-C3* CTD (°C) | BWT *SWERUS-C3* CTD & WOD (°C) | BWT WOD (°C) | BWT WOA (°C) | Selected field BWT (°C) | Salinity | $\Delta[CO_3^{2-}]$ (µmol/kg) | Oxygen (µmol/kg) | Number of RB stained CBF at 0-6 cm |
|---|---|---|---|---|---|---|---|---|---|---|---|---|---|---|
| AO 96/09-1PC | 86.414 | 143.444 | 927 | LR crest | 4200 ± 90 | | | -0.17 | -0.21 | -0.17 | 34.89 | 50.69 | | |
| AO 96/12-TC | 87.098 | 144.773 | 1003 | LR crest | 4215 ± 70* | | | -0.18 | -0.21 | -0.18 | 34.88 | 47.35 | | |
| AO 96/13-TC | 87.153 | 145.169 | 978 | LR crest | 5180 ± 105 | | | -0.18 | -0.20 | -0.18 | 34.88 | 47.35 | | |
| AO 96/B1-1PC | 85.386 | 145.764 | 2525 | LR slope AB | 2010 ± 60 | | | | -0.59 | -0.59 | 34.92 | 23.25 | | |
| AO 96/B2-1PC | 85.406 | 152.279 | 611 | LR crest | 4900 ± 105 | | | 0.22 | 0.26 | 0.22 | 34.87 | 52.51 | | |
| AO 96/B7-TC | 85.553 | 156.599 | 2385 | LR slope MB | 5330 ± 105 | | | | -0.54 | -0.54 | 34.95 | 33.95 | | |
| LOMROG07-GC02 | 86.632 | -54.151 | 724 | LR crest | 8290 ± 180 | | | 0.11 | 0.13 | 0.11 | | | | |
| LOMROG07-PC04 | 86.701 | -53.767 | 810 | LR crest | 6625 ± 55* | | | 0.01 | 0.10 | 0.01 | | | | |
| LOMROG07-TC06 | 85.493 | -46.273 | 3007 | LR end slope AB | 4100 ± 120 | | | -0.73 | -0.80 | -0.73 | | | | |
| LOMROG07-PC08 | 85.295 | -14.892 | 1038 | MJR | 6720 ± 50* | | | -0.24 | -0.16 | -0.24 | 34.91 | 57.48 | | |
| LOMROG07-TC08 | 85.295 | -14.892 | 1038 | MJR | 8920 ± 55* | | | -0.24 | -0.16 | -0.24 | 34.91 | 57.48 | | |
| LOMROG09-GC03B | 88.164 | 156.362 | 3814 | LR slope MB | 5420 ± 105 | | | -0.29 | -0.46 | -0.29 | 34.96 | 2.19 | | |
| LOMROG12-TC05 | 87.821 | -59.632 | 1321 | LR crest | 10800 ± 275 | | | -0.37 | | -0.37 | | | | |
| LOMROG12-TC06 | 88.251 | -46.397 | 2923 | LR slope AB | 5120 ± 105 | | | | -0.59 | -0.59 | | | | |
| LOMROG12-TC09 | 89.027 | -73.734 | 1318 | LR crest | 10770 ± 786 | | | -0.39 | | -0.39 | | | | |
| LOMROG12-TC12 | 88.108 | 134.654 | 1366 | LR crest | 3010 ± 60 | | | -0.47 | -0.46 | -0.47 | 34.91 | 41.24 | | |
| SWERUS L2-1-KL | 72.337 | -176.439 | 73 | HC | RB stained | -1.66 | 0.73 | -0.03 | -1.27 | -1.66 | 32.89 | 0.67 | 239.08 | |
| SWERUS L2-2-KL | 72.567 | -175.265 | 71 | HC | RB stained | -0.72 | -1.03 | 0.45 | -1.19 | -0.72 | 32.88 | -4.27 | 240.77 | 133 |
| SWERUS L2-2-MC | 72.432 | -175.342 | 56 | HC | RB stained | -0.90 | -0.83 | 0.48 | -1.24 | -0.90 | 32.61 | 8.12 | 264.06 | 115 |
| SWERUS L2-2-PC | 72.517 | -175.320 | 72 | HC | RB stained | -0.72 | -1.06 | 0.74 | -1.18 | -0.72 | 32.71 | -4.31 | | |
| SWERUS L2-3-MC | 72.377 | -175.786 | 90 | HC | RB stained | -1.71 | -1.30 | -0.50 | -0.78 | -1.71 | 32.93 | -3.53 | 244.00 | 50 |
| SWERUS L2-4-MC | 72.861 | -175.711 | 124 | HC | RB stained | -0.26 | 0.22 | 0.38 | -0.87 | -0.26 | 34.36 | -10.35 | 110.92 | 195 |
| SWERUS L2-8-MC | 75.153 | 179.873 | 524 | AP | RB stained | 0.28 | 0.55 | 0.60 | 0.54 | 0.28 | 34.87 | 45.02 | 279.67 | 277 |
| SWERUS L2-9-MC | 75.057 | -179.820 | 446 | AP | RB stained | 0.45 | 0.68 | 0.71 | 0.58 | 0.45 | 34.86 | 47.37 | 276.99 | 116 |
| SWERUS L2-13-MC | 76.186 | -179.278 | 1118 | AP | RB stained | -0.22 | -0.22 | -0.22 | -0.24 | -0.22 | 34.89 | 37.55 | 286.04 | 78 |
| SWERUS L2-14-MC | 76.353 | 176.461 | 733 | ESS slope | RB stained | 0.25 | 0.27 | 0.34 | 0.10 | 0.25 | 34.89 | 42.50 | 285.00 | 72 |
| SWERUS L2-15-MC | 76.320 | 175.881 | 501 | ESS slope | RB stained | 0.52 | 0.62 | 0.74 | 0.56 | 0.52 | 34.86 | 46.65 | 282.02 | 187 |
| SWERUS L2-16-MC | 76.512 | 176.632 | 1023 | ESS slope | RB stained | -0.07 | -0.08 | -0.08 | -0.21 | -0.07 | 34.90 | 38.06 | 284.70 | 92 |
| SWERUS L2-18-MC | 76.409 | 173.879 | 349 | ESS slope | RB stained | 0.74 | 0.83 | 0.70 | 0.58 | 0.74 | 34.85 | 46.61 | 274.55 | 369 |
| SWERUS L2-21-MC | 77.579 | 163.308 | 153 | ESS slope | RB stained | -0.10 | -0.07 | | -1.16 | -0.10 | 34.50 | 25.42 | 232.93 | 153 |
| SWERUS L2-22-MC | 78.224 | 164.427 | 367 | ESS slope | RB stained | 0.91 | 0.94 | | 0.77 | 0.91 | 34.87 | 47.76 | 278.07 | 104 |
| SWERUS L2-23-MC | 78.664 | 165.033 | 522 | ESS slope | RB stained | 0.69 | 0.68 | | 0.60 | 0.69 | 34.90 | 49.99 | 288.46 | 78 |
| SWERUS L2-24-MC | 78.800 | 165.382 | 982 | ESS slope | RB stained | 0.02 | 0.12 | | -0.17 | 0.02 | 34.91 | 39.51 | 287.65 | 142 |
| SWERUS L2-25-MC | 79.226 | 152.676 | 101 | ESS slope | RB stained | -0.87 | -0.95 | | -1.33 | -0.87 | 34.24 | 28.80 | 263.22 | 102 |
| SWERUS L2-26-MC | 79.742 | 154.389 | 378 | ESS slope | RB stained | 0.53 | 0.69 | | 1.03 | 0.53 | 34.86 | 50.81 | 292.38 | 189 |
| SWERUS L2-27-MC | 79.665 | 154.126 | 276 | ESS slope | RB stained | 0.43 | 0.79 | | 0.82 | 0.43 | 34.82 | 49.99 | 290.05 | 125 |
| SWERUS L2-28-MC | 79.920 | 154.354 | 1145 | ESS slope | RB stained | -0.16 | -0.14 | | -0.20 | -0.16 | 34.91 | 36.98 | 290.85 | 112 |
| SWERUS L2-29-MC | 81.343 | 141.775 | 910 | LR crest | RB stained | 0.02 | -0.12 | -0.13 | -0.18 | 0.02 | 34.91 | 42.53 | 289.63 | 170 |
| SWERUS L2-29-MC, 0-1 cm | 81.343 | 141.775 | 910 | LR crest | 1080 ± 30 | | | | | | | | | |
| SWERUS L2-29-MC, 4-5 cm | 81.343 | 141.775 | 910 | LR crest | 2440 ± 30 | | | | | | | | | |
| SWERUS L2-29-MC, 6-7 cm | 81.343 | 141.775 | 910 | LR crest | 2700 ± 30 | | | | | | | | | |
| SWERUS L2-31-MC | 79.920 | 143.165 | 1157 | ESS slope-LR | RB stained | -0.21 | -0.18 | -0.20 | -0.30 | -0.21 | 34.91 | 37.70 | 291.44 | 8 |
| SWERUS L2-32-MC | 85.141 | 151.590 | 837 | LR crest | RB stained | -0.01 | -0.02 | -0.05 | -0.04 | -0.01 | 34.90 | 43.88 | 290.50 | 133 |
| SWERUS L2-32-MC, 2-3 cm | 85.141 | 151.590 | 837 | LR crest | 3410 ± 25** | | | | | | | | | |
| SWERUS L2-32-MC, 4-5 cm | 85.141 | 151.590 | 837 | LR crest | 6110 ± 20** | | | | | | | | | |
| SWERUS L2-32-MC, 5-6 cm | 85.141 | 151.590 | 837 | LR crest | 7920 ± 35** | | | | | | | | | |
| SWERUS L2-32-MC, 8-9 cm | 85.141 | 151.590 | 837 | LR crest | 8290 ± 30** | | | | | | | | | |
| SWERUS L2-32-MC, 11-12 cm | 85.141 | 151.590 | 837 | LR crest | 11000 ± 35** | | | | | | | | | |
| SWERUS L2-32-MC, 14-15 cm | 85.141 | 151.590 | 837 | LR crest | 11200 ± 40** | | | | | | | | | |
| SWERUS L2-32-MC, 19-20 cm | 85.141 | 151.590 | 837 | LR crest | 18650 ± 80** | | | | | | | | | |
| SWERUS L2-32-MC, 24-25 cm | 85.141 | 151.590 | 837 | LR crest | 29400 ± 280** | | | | | | | | | |
| SWERUS L2-32-MC, 31-32 cm | 85.141 | 151.590 | 838 | LR crest | 35400 ± 560** | | | | | | | | | |
| SWERUS L2-34-MC | 84.276 | 148.713 | 886 | LR crest | RB stained | -0.10 | 0.04 | -0.11 | -0.15 | -0.10 | 34.90 | 41.80 | 288.51 | 321 |
| SWERUS L1-26-MC/I | 76.473 | 132.044 | 52 | LS shelf | RB stained | -1.82 | -1.69 | -1.63 | -1.27 | -1.82 | 34.21 | 29.97 | 308.20 | 52 |

The foraminifera found in this surface sediments were retrieved from either core tops or multicores. The core tops belong to 16 trigger weight, piston and gravity cores from *Arctic Ocean '96, LOMROG I–III* and *SWERUS-C3* expeditions [Jakobsson et

al., 2008; Marcussen et al., 2011; 2012]. The 25 multicores were obtained during the *SWERUS-C3* expedition (Table 1). Down core sediment samples were also processed in core *SWERUS-C3* L2-2-PC1 (core 2-PC for abbreviation) retrieved from the Herald Canyon (Lat 72.517, Lon -175.320) on the Chukchi Shelf at 72 m water depth.

### 2.2 Field oceanographic data

For the *SWERUS-C3* multicores oceanographic data (temperature, salinity, alkalinity, $TCO_2$, pH and oxygen) were captured using conductivity temperature and depth (CTD) casts deployed while coring. For other cores, where no local CTD measurements were available, bottom water physical and chemical data from World Ocean Database (WOD) and CARINA database [Key et al., 2010] were used (Table 1). At each site, a thorough temperature study based on the arbitrary value of 50 km cell radius around each site was designed (Appendix, Table A) to compare inter- and intra-annual BWT variability. World Ocean Atlas (WOA) average ocean temperatures obtained by default gridded 3D dataset was used at locations lacking WOD or CTD information (Appendix, Table A and Figure A).

The degree of bottom water calcite saturation ($\Delta[CO_3^{2-}]$) is assumed to interfere with foraminiferal Mg/Ca inclusion at cold waters [Elderfield et al., 2006]. $\Delta[CO_3^{2-}]$ defined as $[CO_3^{2-}]_{measured}$ minus $[CO_3^{2-}]_{saturation}$ was calculated using $CO_2$ calc, Ver 1.3.0 [Robbins et al., 2010], where $[CO_3^{2-}]_{saturation}$ was obtained from $[CO_3^{2-}]_{sat}$ (µm/kg)= $[CO_3^{2-}]$ (µm/kg)/ $\Omega_{Calcite}$. Input parameters of the software were $CO_2$ dissociation constants K1 and K2 from Mehrbach et al. [1973] refit by Dickson and Millero [1987] (Appendix, Table B).

### 2.3 Sample preparation

All multicores (10 cm diameter) were vertically subsampled on average at 1 cm thick slices (Table D, Appendix). Each slice was sieved using deionized water over a 63 µm mesh sieve. The separated foraminifera-bearing sand-fractions were transferred to plastic containers and dosed immediately with laboratory Rose Bengal (RB) dye [Walton, 1952; Corliss and Emerson, 1990]. Previous studies have shown small offsets in foraminiferal trace metal values between living and dead (fossil) specimens from the same core top samples [Elderfield et al., 2006] that can be attributed to the up to thousands of years old core top particle ages differences. Living or recently dead specimens are, thus, best suited for building temperature calibrations since they directly experienced the measured BWT and no post depositional alteration. The RB solution was prepared according to the method described in Schönfeld et al. [2012] using 2 g of RB dissolved in 1L ethanol (99%) and each sample was kept inside the RB solution for a minimum of 14 days. Once staining was complete, the multicore samples were sieved again with deionized water using 125-250 µm, 250-355 µm and 355-500 µm mesh sieves. Each sample was inspected and wet-picked under the reflected light microscope using a Petri dish to better distinguish the pink-stained cytoplasm inside the tests. All stained (live) calcareous benthic foraminifera species were picked out, identified to species level and counted. Specimens qualified as

'stained foraminifera' only if all chambers except the ultimate chamber (youngest) were brightly rose-stained (Figure 2). Staining was difficult to assess in thick-shelled (porcelaneous) taxa (e.g. the miliolid *Quinqueloculina arctica*). Thus, for these species it was necessary to break the tests between glass plates to check if they contained stained cytoplasm and assess their age. For the trigger weight, piston and gravity 'unstained' core tops, the upper 1-cm (5 $cm^3$) was wet sieved over a 63 μm mesh sieve and oven dried at 50°C. The same procedure was applied to the downcore samples, although these were taken at 2-cm thick scoops (10 $cm^3$).

### 2.4 Core top age determination

The age of the benthic foraminifera found in multicore surface sediments was assessed by RB staining. Core top sediment age from the trigger weight, piston and gravity cores were $^{14}C$ dated on the planktic foraminifera *Neogloboquadrina pachyderma* (sinistral), a modern significant component of Arctic micro-zooplankton communities [Volkman, 2000; Bé, 1960; Steuerwald and Clark, 1972; Vilks, 1975]. This includes four published [Hanslik, 2011] and 12 new core top $^{14}C$ dates (Table 1). The material dated in both studies consisted on ~700 shells (5 to 6 mg of C) of the four-chambered morphotype *N. pachyderma* (125-250 μm) to avoid any bias from morphotypes [Healy-Williams, 1992]. Analyses were carried out at the Lund University (Sweden) and Beta Analytic (UK) Radiocarbon Dating Laboratories.

We will refer to these two distinct surface sediment sets as stained and unstained. Lastly, nine $^{14}C$-dates from planktic foraminifera *N. pachyderma* at multicores 29-MC (this study) and 32-MC (Cronin and Gemery, unpublished) were included in Table 1. This allowed testing the benthic-to-planktic age differences from the same depth interval since at these multicores the benthic foraminifera were RB stained.

### 2.5 Species selection and ecology

Six benthic foraminiferal species were found in sufficient quantities (3–40 specimens/sample) to build monospecific Mg/Ca-temperature field calibrations. The most common and abundant species across all locations from shallow to deep water habitats were *Elphidium clavatum* and *Nonionellina labradorica* in Halocline waters; *Cassidulina neoteretis* in Atlantic waters; and *Q. arctica, Cibicidoides wuellerstorfi* and *Oridorsalis tener* in Atlantic and Artic deep waters. Despite these observed distributions with depth/water masses it is believed that Arctic foraminiferal distribution is primarily controlled by productivity [Wollenburg, 1995].

These genera have been subject of previous Mg/Ca–temperature investigations [e.g. Izuka, 1988; Rosenthal et al., 1997; Toyofuku et al., 2000; Lear et al., 2002; Kristjánsdóttir et al., 2007]. All studied species build low Mg tests except *Q. arctica*, which has a high Mg-calcite test. Of these six, one species is epifaunal (*C. wuellerstorfi*), one is shallow infaunal (*Oridorsalis tener)* while the remaining four (*Q. arctica, C. neoteretis, N. labradorica, E. clavatum*) are deep infaunal [Wollenburg and Mackensen, 1998b; Murray, 2006]. Having this range of depth ecologies allows

us to explore the hypothesis that pore water buffers against carbonate corrosive bottom water, and hence infaunal habitat taxa make better Mg/Ca palaeothermometers [Lear et al., 2015].

Calcareous benthic foraminiferal counts were made within the upper 6 cm (125–500 μm size fraction) to constrain their living biomass distribution in the geographic range covered by the sites (Table 1 and Appendix Table D). Whole sample counts were standardized to a 471 $cm^3$ volume of sediment (6 cm subsurface sediment depth, 10 cm diameter multicore).

For the Chukchi Shelf, SWERUS L2-2-PC1 (2-PC) down core record analysis was carried out on *E. clavatum*. Foraminiferal extraction was carried out as for the other core top samples. The age model for this core is based on 17 mollusk shell $^{14}C$ dates at 14 distinct depths [Pearce et al., in preparation] and indicates that the sequence extends back to 4300 cal. yrs BP within 830 cm.

### 2.6 Trace metal analysis

Between 3-50 (depending on species) monospecific benthic foraminifera from the >125 μm size fraction (approx. 0.2-0.4 mg before cleaning) restricted to as narrow a size range as possible were picked out of each sample (Appendix, Table C). The shells were crushed between two glass plates and inspected under the microscope to remove impurities remaining in the inner chambers with a wet brush. The fragments were stored in polypropylene acid cleaned (10% HCl) Eppendorf safe lock tubes (0.5 ml) where the fragments were cleaned. Prior to trace metal analysis, benthic foraminiferal tests were rigorously cleaned at the Cardiff University Department of Ocean and Earth Sciences clean-lab facility to remove external metal sources derived from clays, organic matter and metal oxides, that might bias the intra-test elemental results [Boyle and Keigwin, 1985/1986; Barker et al., 2003].

Following Boyle and Keigwin [1985/1986] thorough cleaning protocol, the samples were first ultrasonically cleaned in a methanol/deionized-water solution to remove clays. Next, alkali-buffered hydrogen peroxide was used to remove organic matter. Samples were then treated with hydrazine hydrate, a strong reducing agent, to remove post depositional oxide metal coatings. Lastly, the samples were treated with 0.001M weak acid to leach any adsorbed contaminant. At this step the samples were free from impurities and they were finally dissolved with 120 μl of trace metal free 0.065N $HNO_3$, vortex stirred for a few seconds and centrifuged for three minutes. To promote dissolution, the tubes were stored cold in the fridge for at least 12 h. After dissolution, two aliquots were pipetted off from the tubes: a 10 μl aliquot for Ca analysis and a 100 μl aliquot for element/Ca. Each set was diluted using trace metal pure 0.5M Optima $HNO_3$ until a final volume of 350μl. The diluted samples with 350μl volume were analyzed at Cardiff University on a Thermo Element high-resolution inductively coupled plasma mass spectrometer (HR ICP-MS). At each run, Mg/Ca, B/Ca, Fe/Ca, Li/Ca, Mn/Ca, Al/Ca, U/Ca, Zn/Ca, Sr/Ca, Cd/Ca, Nd/Ca, Ba/Ca were simultaneously

measured (Appendix, Table E). Blanks composed of 0.5M Optima $HNO_3$ and in-house prepared independent consistency standards (CS1 4mM, MCS-A and CS2 4mM) were run in between every sample to determine analytical drift and long term precision, the latter determined to be with a precision of ~1% r.s.d. for Mg/Ca (Appendix, Table E). Mg/Ca ratios measured by the HR ICP-MS are dependent on the calcium concentration ([Ca]) of the same sample, with increasing [Ca] reducing sensitivity to Mg [Lear et al., 2002]. Therefore sets of individual standards with the same [Ca] as the diluted foraminiferal samples were run in sequence, i.e. matrix matched, to reduce compositional effect differences [Lear et al., 2002]. These matrix matched standards were prepared mixing blank 0.5M Optima $HNO_3$ and in-house MCS A 4mM standard. Samples with [Ca] smaller than 1mM were rejected since the sample values had a chemical composition close to the blank result of low sample content after cleaning. These were samples containing < 3 specimens. In addition, the thin hyaline tests from *Triloculina* genus found in Lomonosov Ridge core tops did not contain enough [Ca] to be analyzed for trace metal ratios meaning that their tests did not resist the trace metal cleaning method and could not be included in the study. Likewise, results from stations 25 and 31 were excluded in the results, due to the low concentrations of the analyte after cleaning.

The trace metal data were screened to determine their quality, precision (using the three in-house consistency standards) and accuracy (using the percentage of the matrix match effect). All data from samples with a blank intensity signal less than five and a matrix match difference of more than 15% were rejected. Results were screened for contamination of an unsuccessful cleaning and described in section 4.4.1; samples with anomalously high values of Fe/Ca, Al/Ca and Mn/Ca were excluded due to the risk of that the signals were coming from remaining clays, organic matter and/or metal coatings [Barker et al., 2003]. The thresholds of Al/Ca, Fe/Ca and Mn/Ca that a sample can present are site dependent and can be tested by exploring their relationship to Mg/Ca. Low correlation implies minimal contamination and thus reliable results derived from primary calcite Mg/Ca.

### 2.7 Scanning electron microscopy and energy dispersive spectrometry

To assess the quality of test preservation and explore evidence of post burial diagenesis we used Environmental Scanning Electron Microscopy (ESEM). This involved imaging and elemental analysis of internal and external test surfaces and broken wall sections in representative specimens of the 'live' (stained), and $^{14}C$-dated core top specimens. Analysis was carried out using a Philips XL-30- ESEM-FEG housed at Stockholm University, using first back-scattered electron detector mode (10 kv, working distance 10mm) to produce high-resolution SEM micrographs and second EDS (energy dispersive spectrometer) detector mode for elemental mapping. Specimens were mounted on steel SEM stubs and gold coated. Following imaging of whole specimens, individuals were crushed to break tests and remounted to reveal test wall cross sections. The EDS detector reports qualitative elemental chemistry by photon counting normalized to 100% with a ± 1% 2σ detection limit. Results were

rejected if they had < 10% dead time (X-Ray photon lag time). Average Mg content in foraminiferal calcite is 250 ppm [de Nooijer et al., 2014] (0.025 wt%). Biogenic Mg incorporation is usually outside EDS detection limits (1 wt%), thus allowing the detection of inorganic Mg if present in the shells.

Carbon was not included in the detection due to the carbon coated surfaces where foraminifera are mounted and that any gold present in the spectra may be related to the gold used to coat the samples to optimize conductivity of the electron beam across foraminiferal test surfaces in the SEM.

## 3. Results

### 3.1 Arctic field bottom water oceanography

Composite depth oceanographic profiles combining the captured CTD physical and chemical bottom water properties (temperature, salinity and $\Delta[CO_3^{2-}]$) at all *SWERUS-C3* sites are shown in Figure 3 (data source in Table 1). The bottom water composite covers water depths from 52 to 3814 m, thus spanning the full range of Arctic water masses (halocline, Atlantic water and Arctic deep water). The largest gradients in bottom temperature, salinity and $\Delta[CO_3^{2-}]$ are present at the upper 200 m water depth, which are bathed by polar mixed layer (<50 m) and halocline (50–200 m) waters that are unique of the Arctic Ocean. There we find progressive increases in temperature, salinity and $\Delta[CO_3^{2-}]$. Bottom temperatures rise 3°C (from -1.3 to 0.7°C), and salinity 2.2 psu (from 32.6 to 34.8). The $\Delta[CO_3^{2-}]$ profile shows undersaturation of $CO_3^{2-}$ (leading to negative $\Delta[CO_3^{2-}]$ on the Chukchi Shelf (sites 1-KL, 2-MC, 2-KL, 3-MC and 4-MC) and low values (25–30 µmol/kg) at the shallowest Eastern Siberian Sea slope sites (multicore sites 21-MC and 25-MC) and at the Laptev Shelf (site 26-MC/I).

A warmer and denser sub-halocline layer at 200–800 m presents positive BWT (from 0°C to 1°C) identified one century ago by Helland-Hansen and Nansen [1909] as Atlantic sourced water entering the Arctic through the Fram Strait. This deep-flowing Atlantic waters are saturated with respect to $\Delta[CO_3^{2-}]$, temperatures peak at 1°C within ~300-500 m while salinity shifts are steady at 34.8 psu values.

Below 800 m sits Arctic deep water (800–4000 m). There, BWT are nearly isothermal (less than 1°C decrease with depth) and salinity is homogeneous at 34.9 psu. The bottom $\Delta[CO_3^{2-}]$ content progressively decreases with depth reaching 2 µmol/kg in $\Delta[CO_3^{2-}]$ at the deepest water studied site (LOMROG09-GC03B, 3814 m). This value is consistent with Jutterström and Anderson [2005] estimations of Arctic calcite saturation horizons located at ~4000 m water depth.

These hydrographic data reveal that apart from BWT, strong variability ranges in salinity at halocline depths and $\Delta[CO_3^{2-}]$ at all depths might interfere with test Mg/Ca integration and thus need to be explored in conjunction to Mg/Ca values.

Bottom water oxygen levels (Figure 3e) are lower by ~30 μmol/kg in the upper continental shelf showing minimum values of 110.9 μmol/kg at the Herald Canyon (Chukchi Shelf) site 4-MC at 124 m water depth. An exception is found in the Laptev Shelf site, which has the most oxygenated bottom waters, with levels reaching 308.2 μmol/kg in multicore 26-MC/I that could be attributed to the proximity to Lena the Lena delta. This bimodal oxygen content on the Arctic shelf shows that although the sites are on the same stretch of shelf, they are influenced by two distinct surface water masses, 'old' oxygen depleted Pacific sourced waters on the Herald Canyon, and Eastern Siberian Shelf waters on the Laptev Shelf. Bottom water oxygen concentration is higher at intermediate water depths in the central Arctic consistent with a less organic carbon export to the seafloor.

Comparisons of the WOD and WOA temperature sets (Figure 4a) show the largest BWT temperature anomalies at the upper 500 m water depth. Expedition *SWERUS-C3* CTD temperatures were compared to WOD and WOA data sources (Figure 4b and 4c) showing that our measured temperatures compare well with each other over much of the upper 1200 m, except the uppermost 200 m, i.e. the polar mixed layer and halocline, where the differences are larger (up to 2.2 °C), while sub halocline conditions are more stable. The most consistent temperature comparison of all (i.e. the closest to 0°C BWT difference) is between WOD and *SWERUS-C3* CTD data, apart from a 2.4 °C offset value at site 1-KL on the Herald Canyon. From the temperature study we observe that these layers experience significant intra- and inter-annual temperature variability and thus the differences can likely be explained by a distinct sampling time of the year. For our Mg/Ca calibration experiments, we thus preferentially use field BWT sources from local *SWERUS-C3* CTD, followed by WOD and then WOA as last substitutes.

### 3.2 Spatial and depth distribution of Arctic stained benthic foraminifera

All *SWERUS-C3* sites are located at the edge of median summer sea ice limit and during winter are all fully ice covered and experience the polar night. The benthic foraminifera geographical distribution derived from all the 25 stained multicore surface sediments ranges from 52 to 1157 m water detph. In these sites, none of the six studied species inhabit the complete bathymetric range (Figures 5 and 6).

Assemblages from the shallowest sites on the Chukchi, East Siberian and Laptev shelves have high abundances of *E. clavatum* and *N. labradorica*. Chukchi shelf sites are bathed by cold nutrient-rich and oxygen depleted Pacific-Arctic halocline waters and there, presence of 63-125 μm diatoms (*Coscinodiscus* sp.) were diluting the foraminiferal samples. Interestingly, *E. clavatum* and *N. labradorica* can thrive in dysoxic pore waters since they have the ability to sequester chloroplasts that produce the necessary oxygen for cell functioning [Bernhard and Bowser, 1999]. These species can be also found in deeper sites in the Arctic [Polyak, 2016 *personal communication*], although not present at any of the deep sites in this study, likely due to the oligotrophic conditions at the Atlantic/Arctic deep water sampled locations.

Sites located on the Eastern Siberian slope and at shallow depths on the Lomonosov Ridge (~600–800 m), are bathed by warmer and saltier Atlantic waters and contain higher proportions of *C. neoteretis*. This species becomes dominant (>50 %) at sites 8-MC, 9-MC, 14-MC, 15-MC, 18-MC, 21-MC, 22-MC, 26-MC, 27-MC and 34-MC. *Quinqueloculina arctica*, *O. tener* and *C. wuellerstorfi* are the most abundant species below the Atlantic water layer, thriving in Arctic deep waters (>800 m). *Quinqueloculina arctica* is the most common species at sites 24-MC, 29-MC, 31-MC and 32-MC, at Arctic deep waters within 837 and 1157 m. *Cibicidoides wuellerstorfi* inhabits the ~1000 m on the Arliss Plateau (13-MC and 16-MC) that might relate to more eutrophic conditions brought by Pacific water inflow reaching the site. *Oridorsalis tener* starts appearing in small amounts at water depths around 500 m (15-MC and 23-MC) and becomes dominant at 1145 m (25-MC).

The total number of in-sediment living calcareous benthic foraminifera from the three studied locations at the Arliss Plateau and nine out of thirteen stations at the Eastern Siberian Sea slope shows that at 13 out of the 25 multicore stations (Stations 8-MC, 9-MC, 13-MC, 14-MC, 16-MC, 21-MC, 22-MC, 23-MC, 25-MC, 26-MC/I, 27-MC, 29-MC, 31-MC) >50 % stained specimens are concentrated in the first centimeter from the sampled multicore slices. Below 6 cm the number of stained individuals is almost zero (Table D Appendix). At stations 22-MC and 31-MC only the top two centimeters contained stained specimens, while stations 2-KL, 2-MC and 24-MC contained the highest percentages of stained benthic taxa at 2 cm subsurface (Table D Appendix). Living foraminifera occupied the deepest subsurface depths on the Laptev Shelf at 8 cm. The second deepest habitats occur on the Lomonosov Ridge where average living depths are 4 cm subsurface with extending to a maximum of 6 cm. The highest number of stained individuals within the topmost 6 cm subsurface depth was found at 18-MC with 369 counts followed by location SWERUS L2-34-MC1 with 321 counts and SWERUS L2-8-MC1 with 277 counts (Table D Appendix). Interestingly, all these three sites captured positive BWT characteristic of the Atlantic water layer. This observation highlights the significance of Atlantic water in supporting higher calcareous benthic foraminiferal biomass. In contrast, the lowest calcareous benthic foraminifera concentrations, 9 counts, were found at 31-MC (1157 m). Agglutinated benthic foraminifera dominate at this site, but the presence of three high-Mg calcite *Q. arctica*, the most soluble form of carbonate, suggests that corrosive waters at the site might not be the reason for abundant agglutinated.

### 3.3 Mg/Ca relationship to bottom water

#### 3.3.1 Temperature

Each monospecific Mg/Ca–BWT relationship covers a narrow temperature range. The ranges captured are of 1.56 °C in *E. clavatum*, 1.45 °C in *N. labradorica*, 1.45 °C in *Q. arctica*, 1.38 °C in *C. neoteretis*, 1.28 °C in *O. tener* and 0.74 °C in *C. wuellerstorfi*. Mg/Ca values from unstained *C. neoteretis*, *O. tener* and *C. wuellerstorfi* tend to be higher, doubled, and show more variability (Figure 7). Hence,

the stained data was plotted alone to remove any affecting environmental signal apart of temperature and/or post depositional Mg alteration (Figure 8). Exponential Mg/Ca–BWT fits were not calculated product of the small temperature gradients and linear fits were only applied to allow data description.

Mg/Ca ratios in stained *E. clavatum* from the seven multicores and ten measurements have average 0.66 mmol/mol and these vary between 0.521 and 0.795 mmol/mol. The analytical error based on two replicate analyses at three locations with the same field BWT is 0.2 mmol/mol, 0.194 mmol/mol, 0.036 mmol/mol (average 0.143 mmol/mol). Observed bottom temperatures at the sites range between -1.82 and -0.26 °C. The two variables present a low correlation of 0.05 mmol/mol change per °C (Figure 8a).

Mg/Ca values for *N. labradorica* obtained from six multicores are on average 1.25 mmol/mol. These are 0.6 mmol/mol higher than average *E. clavatum* Mg/Ca showing their monospecific Mg/Ca biological offset since they come from similar locations and thus similar field temperatures. The *N. labradorica* Mg/Ca range is 1.11–1.31 mmol/mol changing over a temperature gradient of -1.71 – -0.26 °C (Figure 8b). The Mg/Ca measurement error based on two replicate samples from the same location is 0.105 mmol/mol. There appears to be no positive correlation between *N. labradorica* Mg/Ca–BWT with a -0.017 mmol/mol per °C variability.

Mg/Ca values in stained *C. neoteretis* vary between 0.84–1.20 mmol/mol (average 1.05 mmol/mol) (Figure 8c) and corresponding field BWT range from -0.47 to 0.91 °C. The analytical error based on two samples having the same BWT is of 0.103 mmol/mol. The dataset captures a slight increase in stained Mg/Ca with increasing BWT giving a Mg/Ca change of 0.07 mmol/mol per °C. All unstained fossil Mg/Ca values are higher than modern stained individuals, and these are on the order of 1.29–3.33 mmol/mol (Figure 7c). One unstained Mg/Ca sample from LOMROG07/GC02 recorded exceptionally high values of 12.9 mmol/mol. This Mg/Ca outlier is excluded in this study although shown in the Appendix, Table F.

Porcelaneous tests as the ones secreted by *Q. arctica*, are known to incorporate more seawater Mg into their test than hyaline tests based on their distinct skeletal mineralogy, with values around 100–150 mmol/mol Mg/Ca at 10–25 °C [Toyofuku et al., 2000]. This is reflected in our measured *Q. arctica* Mg/Ca that are on average 40 times higher than the rest of the studied hyaline species (Figure 7). Stained Mg/Ca *Q. arctica* vary within 18.89–75.08 mmol/mol (average 49.58 mmol/mol) inside a -0.54–0.91 °C range and are positively correlated at a 35.2 mmol/mol per °C rate at the highest $R^2$ of the six studied species (0.37). Unstained *Q. arctica* samples tend to have higher and less scatter Mg/Ca values (50.47–73.53 mmol/mol) than stained results and these cover only the lowest field temperatures (from -0.5 to 0.3 °C) (Figure 7d). The lower Mg/Ca variability found within unstained samples could derive from the more homogeneous hydrographic setting, the central Arctic, from which they were obtained as compared to the stained data that mixes shelf, slope and central Arctic environments, while higher ratios could be attributed to central Arctic post

depositional effects.

Stained *O. tener* tests show Mg/Ca values of 1.43–1.78 mmol/mol (1.62 mmol/mol average) and these are higher in unstained $^{14}$C-dated fossil samples, 1.63–3.86 mmol/mol (Figure 7e). Their captured BWT vary between -0.59–0.69 °C and minor positive relationship to stained Mg/Ca at a 0.14 mmol/mol per °C. Based on this sensitivity, unstained Mg/Ca values present an unrealistically high relationship to BWT, although 3 out of 11 datapoints in *O. tener* align within the variation of the Mg/Ca from their stained specimens.

Three stained *C. wuellerstorfi* Mg/Ca measurements at two multicore sites have 1.15 and 1.32 mmol/mol at -0.22 °C and 1.48 mmol/mol at -0.07 °C (Figure 8f). The stained Mg/Ca error based on two replicates at the same site is of 0.17 mmol/mol. Unstained Mg/Ca values vary from 1.04–2.57 mmol/mol (average 1.52 mmol/mol) and only two out of the 8 unstained ratios are higher than the stained ones (Figure 7f).

### 3.3.2 Carbonate ion concentration ($\Delta[CO_3^{2-}]$)

Calcite solubility decreases with increasing depth (i.e. pressure) and decreasing temperature [Broecker and Peng, 1982]. In this study sites, the compilation of calculated bottom seawater $\Delta[CO_3^{2-}]$ with depth (Figure 3c) shows two saturation trends that do not linearly vary with depth. One presents undersaturated bottom waters at the shelf/slope *SWERUS-C3* sites. The other trend gradually decreases $\Delta[CO_3^{2-}]$ with depth from saturated to unsaturated bottom waters. These offsets derive from their wide Arctic geographical distribution covered by the sites where for instance Eastern Siberian Sea Shelf sites receive less riverine run off and are more influenced by Pacific waters [Chen et al., 2003].

We first construct Mg/Ca correlations with depth to observe if our Mg/Ca values are affected by bottom water $\Delta[CO_3^{2-}]$ (Figure 9). Halocline species (Figure 9a and b) and unstained Mg/Ca at all species (Figure 9c, d, e and f) show no particular Mg/Ca trend with depth. Stained *Cassidulina neoteretis* (Figure 9c) shows stable Mg/Ca values with depth. The strongest Mg/Ca-depth dependence of all species is depicted by stained specimens of *Q. arctica* (Figure 9d, $R^2 = 0.77$) implying that its Mg content is more controlled by $\Delta[CO_3^{2-}]$ than temperature (Figure 8d, $R^2 = 0.37$). Minor Mg/Ca decreases with depth are shown in stained *O. tener* (Figure 9e) and *C. wuellerstorfi* (Figure 9f), although it is difficult to asses their correlation due to the few number of data points.

Another reason for this undersaturated surface bottom waters could be related to the fact that in the Arctic, the coldest temperatures are present at the surface. The bottom water $\Delta[CO_3^{2-}]$–BWT relationship from different oceans displays a steep $\Delta[CO_3^{2-}]$ gradient below 3°C where $\Delta[CO_3^{2-}]$ varies considerably thus potentially having a major impact than temperature on Mg incorporation [Elderfield et al., 2006]. Arctic bottom waters are all < 3°C and therefore we need to explore first how bottom Arctic $\Delta[CO_3^{2-}]$ changes with BWT at the study sites. The Arctic $\Delta[CO_3^{2-}]$–BWT

relationship shows the clearest threshold gradient at 30 μmol/kg consistent with hydrographic data collected in the Nordic Sea [Elderfield et al., 2006]. At >30 μmol/kg bottom seawater $\Delta[CO_3^{2-}]$ values are more steady (~20 μmol/kg variability) and coincident to positive temperatures, while at <30 μmol/kg and negative bottom temperatures these are more scattered (~40 μmol/kg variability) (Figure 10, Table 1 for data sources).

Lastly, monospecific Mg/Ca–$\Delta[CO_3^{2-}]$ relationships (Figure 11) are not in agreement at *E. clavatum* or *N. labradorica* (Figure 11a and b) despite having wide $\Delta[CO_3^{2-}]$ ranges (-10 to 30 μmol/kg). We observe no covariance in the stained *C. neoteretis* Mg/Ca and a minor correlation in its unstained data (Figure 11c). Stained Mg/Ca *Q. arctica* (Figure 11d) shows a positive Mg/Ca–$\Delta[CO_3^{2-}]$ correlation over much of the data range apart from Pacific-Arctic halocline site 21-MC that is off trend (Figure 11d) presenting lowest $\Delta[CO_3^{2-}]$ (26 μmol/kg) but in trend with the rest of the Mg/Ca values at more saturated waters. Hence, this Mg/Ca data is not tracking this lowest 21-MC bottom water $\Delta[CO_3^{2-}]$. In contrast, unstained *Q. arctica* specimens show a more scattered Mg/Ca–$\Delta[CO_3^{2-}]$ pattern. For unstained and stained *O. tener* (Figure 11e) we find a slight Mg/Ca positive correlation to $\Delta[CO_3^{2-}]$. In *C. wuellerstorfi* (Figure 11f) unstained Mg/Ca values show a 1:1 relationship while stained data show a higher sensitivity, although their trend cannot be assessed since it is based in two data points. This species also shows a weaker sensitivity to BWT change (Figure 7f) compared to $\Delta[CO_3^{2-}]$ (Figure 9f).

### 3.3.3 Salinity

The Mg/Ca and salinity relationship found in halocline living species show no association in *E. clavatum* (Figure 12a) and a positive correlation ($R^2$= 0.52) between *N. labradorica* Mg/Ca and bottom water salinity (Figure 12b). Compilation with other data will benefit from these preliminary observations (Figure 18, section 4.2). Salinity Mg/Ca relationships are not shown for *C. neoteretis, Q. arctica, O. tener* and *C. wuellerstorfi* due to the constant values throughout the downwater where these species habit.

## 3.4 Radiocarbon dating

The new and published core top $^{14}C$ ages derived from unstained (dead/fossil) *N. pachyderma* range between 2010–10800 $^{14}C$ years (Table 1). This implies that *N. pachyderma* found in sediment core tops are not contemporaneous with the modern stained benthic fauna or hydrographic data. These core top age data however, are derived from planktic microfossils and the same age may not be obtained for benthic foraminifera from the same sample sediment. To explore this idea we obtained $^{14}C$ ages in 29-MC and 32-MC (Table 1) located on the Lomonosov Ridge side that is closer to the East Siberian Sea shelf. In both multicores 'living'/stained benthic foraminifera were found down to 3–4 cm sub-surface sediment depth, whereas planktic foraminifera picked over the same interval record dates of ~2100 $^{14}C$ years in 29-MC, and ~5000 $^{14}C$ years in 32-MC.

Four of the six studied species investigated in the Mg/Ca–BWT calibration study include both stained and unstained (dead) specimens (plots c, d, e and f in Figures 7 and 8). Therefore, it is worthwhile investigating any possible age effect on the Mg/Ca results (Figure 13). We observe positive linear trends between Mg/Ca and radiocarbon age at all species, more prominent in species *O. tener* and *C. wuellerstorfi*.

### 3.5 Down core Mg/Ca record on the Chukchi Shelf

Eleven selected samples of fossil *E. clavatum* spread throughout the ~800 cm of core SWERUS L2-2-PC1, 2-PC for simplification (Figure 1), retrieved at 72 m water depth. The core spans the entire late Holocene (age model in Pearce et al. in preparation). Fossil *E. clavatum* downcore Mg/Ca varies within 0.27 mmol/mol (Figure 14, Table 2) matching the little temperature variability assumed for the Late Holocene stable climate and suggesting non diagenetic results.

However, a wide range of paleotemperatures are obtained after application of distinct *E. clavatum* Mg/Ca-BWT fits (Table 2): (i) Arctic linear fit from section 3.4.1 (Figure 8a); (ii) fit obtained from compiling Mg/Ca from this study with Gabrielsson [2014, unpublished] and Varekamp et al. [2010]; (iii) Mg/Ca-BWT calibration from Varekamp et al. [2010]; (iv) Mg/Ca-BWT sensitivity from Varekamp et al. [2010] applied to average *SWERUS-C3* modern Mg/Ca results.

**Table 2.** Calculated downcore temperatures applying four different Mg/Ca-BWT sensitivities: Arctic, Arctic and compiled *E. clavatum* data, Varekamp et al. [2010] Mg/Ca calibration, Varekamp et al. [2010] sensitivity applied to average *SWERUS-C3* Mg/Ca values.

| | | Arctic (this study) | Arctic, Gabrielsson [2014] & Varekamp et al. [2010] | | Varekamp et al. [2010] | Varekamp et al. [2010] sensitivity applied to Arctic Mg/Ca data |
|---|---|---|---|---|---|---|
| Core 2-PC depth (cm) | Mg/Ca (mmol/mol) | BWT= (Mg/Ca - 0.711) / 0.048 (°C) | BWT= (Mg/Ca-0.743) / 0.07 (°C) | BWT= LN (Mg/Ca-0.719) / 0.062 (°C) | BWT= 4.42 LN (Mg/Ca) + 11.682 (°C) | using average 0.66 mmol/*mol SWERUS-C3* Mg/Ca BWT= LN (Mg/Ca / 0.812) / 0.1959 (°C) |
| 16 | 0.67 | -0.854 | -1.043 | -1.138 | 9.908 | -0.981 |
| 96 | 0.59 | -2.521 | -2.186 | -3.189 | 9.345 | -1.630 |
| 154 | 0.65 | -1.271 | -1.329 | -1.627 | 9.774 | -1.136 |
| 259 | 0.72 | 0.188 | -0.329 | 0.022 | 10.227 | -0.614 |
| 339 | 0.86 | 3.104 | 1.671 | 2.888 | 11.014 | 0.293 |
| 413 | 0.7 | -0.229 | -0.614 | -0.432 | 10.102 | -0.758 |
| 493 | 0.7 | -0.229 | -0.614 | -0.432 | 10.102 | -0.758 |
| 567 | 0.72 | 0.188 | -0.329 | 0.022 | 10.227 | -0.614 |
| 662 | 0.84 | 2.688 | 1.386 | 2.509 | 10.910 | 0.173 |
| 715 | 0.78 | 1.438 | 0.529 | 1.313 | 10.582 | -0.205 |
| 795 | 0.72 | 0.188 | -0.329 | 0.022 | 10.227 | -0.614 |
| | Minimum paleo-BWT (°C) | -2.521 | -2.186 | -3.189 | 9.345 | -1.630 |
| | Maximum paleo-BWT (°C) | 3.104 | 1.671 | 2.888 | 11.014 | 0.293 |
| | Paleo-BWT range (°C) | 5.625 | 3.857 | 6.078 | 1.669 | 1.923 |

The presented Arctic *E. clavatum* Mg/Ca-BWT calibration produces unlikely negative paleotemperatures (< -2°C) and the widest paleotemperature ranges (5.6 °C) of all the fits when substituting the Mg/Ca downcore values. The higher variability captured by the Arctic fit is a result from the lower gradient that Mg/Ca experiences at cold temperatures product of their exponential relationship. A different paleotemperature spread is obtained when Arctic Mg/Ca data is compiled to existing *E. clavatum* data, 3.9 °C if linear or 6.1 °C if exponential.

The application of Varekamp et al. [2010] calibration from the Long Island Sound gives very high temperatures and narrowest data spread due to their less scatter dataset at higher BWT. This suggests that other environmental factors between Arctic and Long Island Sound are affecting Mg/Ca in *E. clavatum*. Ultimately, the application of Varekamp et al. [2010] sensitivity using Arctic average stained Mg/Ca values gives the most accurate fit of all four explored with 2°C in paleo-BWT range and -1.6 °C as the minimum paleotemperature.

### 3.6 SEM and EDS analyses

SEM imaging provides insights into foraminiferal calcite preservation. Wall surfaces of the stained specimens, recently living at the time of collection and therefore thought to be unaffected by post-depositional effects, reveal smooth test surfaces and preservation of small details including apertural lips, pores, trans-wall pore canals and wall layering in *C. neoteretis*, *O. tener* and *C. wuellerstorfi* (Plate 1). In contrast, the unstained specimens, especially *C. neoteretis* and *O. tener* (Plate 2 Figs. 1, 2, 3 and 4), show high relieve test surfaces apparently due to presence of crystalline overgrowths. These large overgrowths mask the original wall porosity. Furthermore, images of crushed specimens reveal variable amounts of internal infilling (Plate 2 Figs. 1b, 2b, 3b, 4b). Of all species, *C. wuellerstorfi* calcite does not appear to be affected by overgrowths in the same way (Plate 2 Figs. 5 and 6).

EDS elemental mapping of a subset of the SEM imaged specimens untreated for trace metals provides further insight into shell chemistry, especially to examine the proportions and distribution of Mg. Carbon was not measured due to possible contaminations with the carbon tape where the specimens are mounted. The EDS spectra shown in Figure 15 reveals no Mg content at any of the three modern stained specimens from Plate 1 (*C. neoteretis* 2b, *O. tener* 4b and *C. wuellerstorfi* 6b). This is as expected since Mg is usually a trace element in foraminiferal calcite typically occurring at 250 ppm (0.025%) in low-Mg calcite species [de Nooijer et al., 2014], thus falling outside the EDS detection limits (1%).

In contrast, point spectra on the unsmooth surface for the three fossil unstained specimens from Plate 2 (*C. neoteretis* 1c, *O. tener* 4b and *C. wuellerstorfi* 5b) shown in Figure 16 have Mg content of 2.8 wt%, 2.7 wt%, and 2.3 wt% respectively, which is on the order of 100 times greater than in the stained examples.

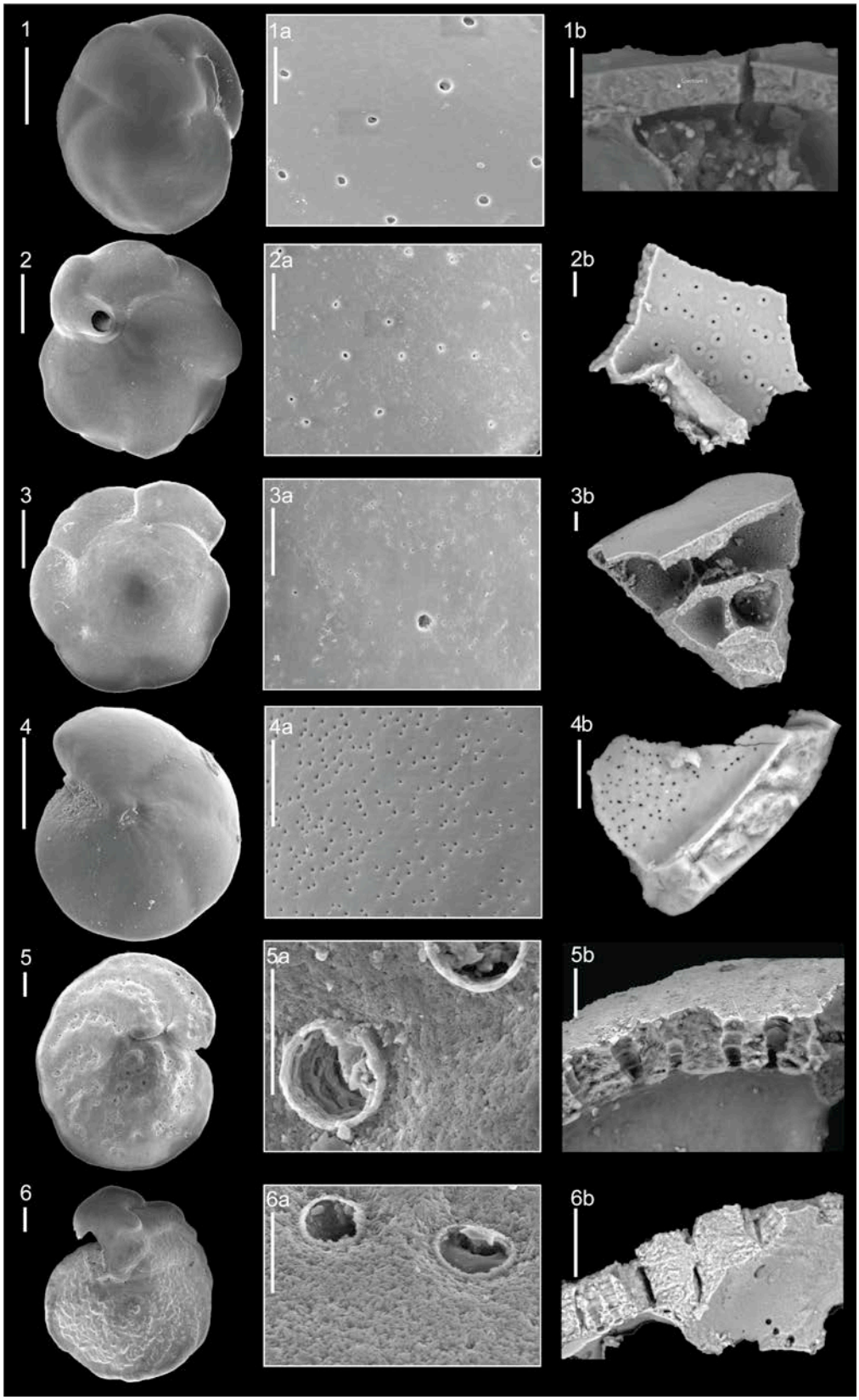


**Plate 1.** SEM images of modern (stained) benthic foraminifera from the multicore top samples showing whole specimens, close ups of wall textures and broken test sections for analysis of calcite preservation. Odd numbers = spiral side; even numbers = umbilical sides of *C. neoteretis* (1 and 2), *O. tener* (3 and 4) and *C. wuellerstorfi* (5 and 6) are shown. Scale bars: whole species = 100 μm, wall close ups = 40 μm and cross sections = 10 μm.

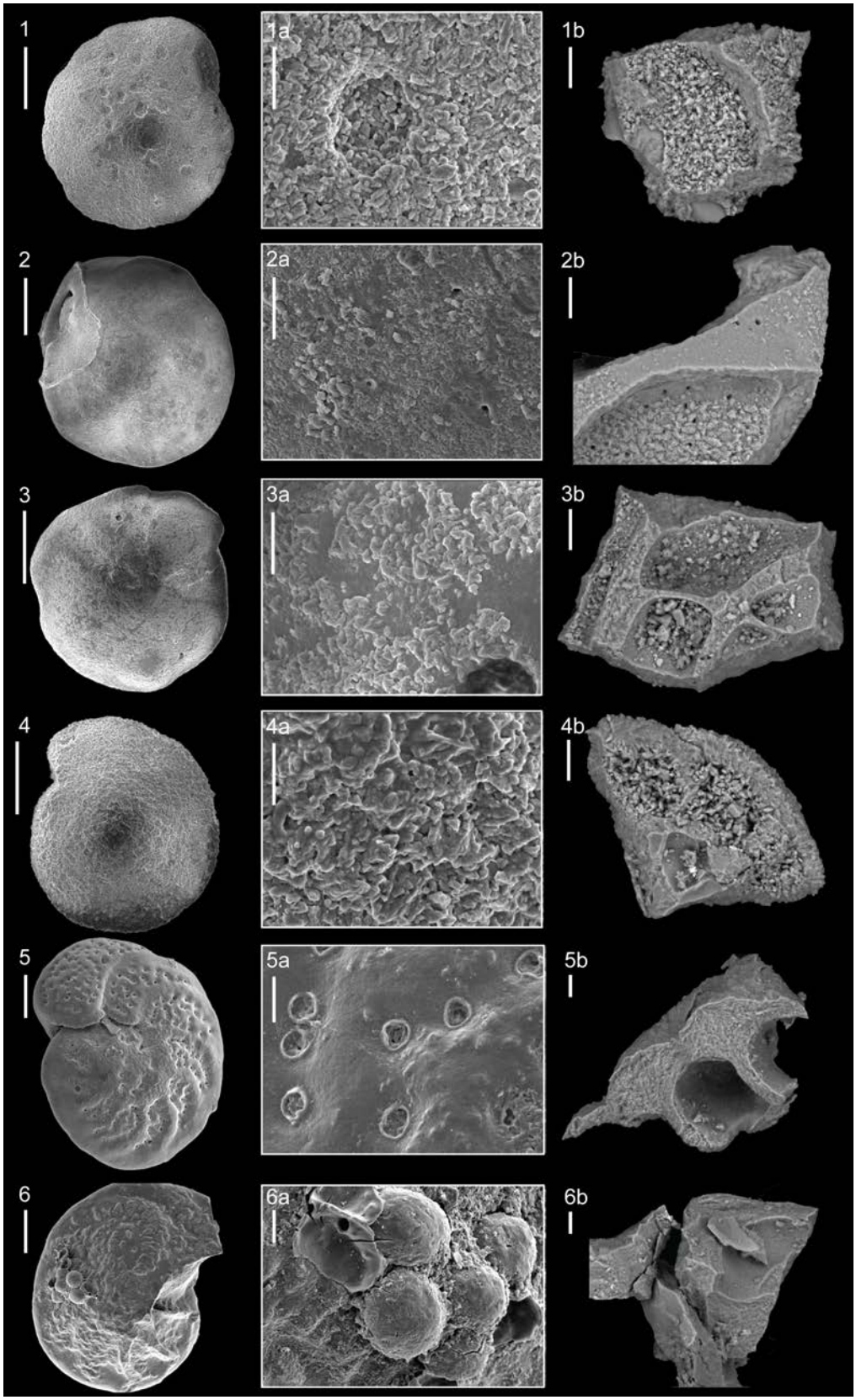


**Plate 2.** SEM images of benthic foraminifera specimens from $^{14}$C-dated core top samples showing whole specimens, close ups of wall textures and broken test sections for analysis of calcite preservation. Odd numbers = spiral side; even numbers = umbilical sides of *C. neoteretis* (1 and 2), *O. tener* (3 and 4) and *C. wuellerstorfi* (5 and 6) are shown. Scale bars: whole species = 100 μm, wall close ups = 40 μm and cross sections = 10 μm. Note in 6a the formation of framboidal pyrite.

## 4. Discussion

This study set out with the aim of exploring the application of Mg/Ca paleothermometry in the Arctic. The unique hydrological characteristics of the Arctic Ocean present challenges for understanding Mg concentration in benthic foraminiferal calcite and the potential for Mg/Ca palaeothermometry in this setting. Possible mechanisms that could interfere the Mg/Ca-BWT application are intrinsic to the Arctic hydrological characteristics, as the small and low field BWT ranges, seawater carbonate ion variations, strong salinity stratification and low sedimentation rates in the central Arctic allowing test alteration from old and poorly ventilated Arctic deep waters; all discussed below. Despite these difficulties, the captured oceanographic parameters at the studied sites present a good set of data to explore the controls on foraminiferal Mg/Ca paleothermometry at the coldest seawaters.

### 4.1 Building a Mg/Ca–temperature calibration at the cold end

In developing a Mg/Ca-T calibration at the coldest temperatures we lay at the end of the exponential sensitivity curve of the method thus giving highest variability of the temperature estimates. The choice of field temperatures at each site is a critical step, particularly where the ranges in temperature variability in the water column are so small (~3°C), and thus, a potential source of error. Seasonal changes in seawater temperature from the Japan Sea have shown fluctuations in foraminiferal calcite Mg/Ca, albeit dampened compared to full BWT seasonal swings [Toyofuku et al., 2000] and it is likely that a similar effect exists within the life span of Arctic benthic foraminifera. The significance of the annual BWT variability pattern is that CTD data collected and used in the calibration represent the temperature at one point in time when the cruise took place in August-September 2014, whereas benthic foraminifera live and calcify over months to 1–2 years [Myers, 1938; Boltovskoy and Wright, 1976] and therefore it is likely that the ambient temperature range captured in test Mg/Ca is integrating some degree of inter-annual temperature variability in the whole tests. However, it is believed that benthic foraminifera preferentially biomineralize during peak BWT of the year [Scourse et al., 2004] that for the Arctic would be September. Then, if our benthic foraminifera species are mainly calcifying in summer and the field temperatures were also taken in summer, the only temperature error will be dependent on how much temperature variability occurs over the summer season.

On the shallow Arctic shelves, wind mixing and intra-annual sea ice formation/melting processes especially interact in the upper 200 m. This is shown in the temperature study resulting in wide annual temperature ranges over the life span of foraminifera. In particular, the set of sites from the Chukchi Shelf, Herald Canyon area (50–100 m water depth), present the largest variations in BWT when compared to the rest of the Arctic as a result of Pacific origin waters entering the Arctic Ocean through the Bering Strait. In that region, annual temperature anomalies fluctuate between 1-4°C in the summer (summer Pacific water) and freezing point temperatures in winter (winter Pacific waters) [Steele et al., 2004; Woodgate et al., 2005]. Because

the annual temperature variability experienced (1-4°C) is bigger than the 1 to 2°C in the captured range in field Pacific origin halocline BWT we have to consider an increased noise in the calibration set in species *E. clavatum* and *N. labradorica*, species that inhabit this waters.

Previous empirical studies on the thermodynamic relationships of Mg concentration in benthic foraminiferal calcite have suggested the relationship to be either exponential [e.g. Rosenthal et al., 1997; Lear et al., 2002] or linear [e.g. Toyofuku et al., 2000; Marchitto et al., 2007]. In the Arctic, we have chosen linear fits only for simplification since we lay at lowest sensitivity part of the Mg/Ca-BWT exponential curve leading to horizontal line fits. The most striking observation is the anomalously high Mg/Ca values in our unstained samples discussed in sections 4.4 and 4.5. Scatter is observed in our stained dataset especially at the coldest halocline species, where similar BWT are related to different Mg/Ca values. However, studies outside the coldest end have also shown significant scatter among planktic Mg/Ca calibrations [Elderfield and Ganssen, 2000; Anand et al., 2003]. Leading mechanisms of the Mg/Ca scatter might be brought by field BWT error introduced at the shallow Arctic sites, species natural variation and/or other environmental factors.

From the coldest species studied *E. clavatum* and *N. labradorica*, this latest presents a negative Mg/Ca sensitivity, -0.017 mmol/mol per °C, and most scatter to BWT. This fact could be due to the wider variation in the physical and chemical properties on the Pacific origin waters bathing these sites. Pacific waters are also differentiated from the rest of Artic water masses by having lower salinity, $\Delta[CO_3^{2-}]$, oxygen and higher nutrients [e.g. Walsh et al., 1989; Chierici and Fransson, 2009], all parameters that could interfere with Mg/Ca incorporation. *Elphidium clavatum* presents a higher relationship to temperature of 0.05 mmol/mol per °C suggesting that its Mg incorporation is more related to temperature. The Atlantic water species *C. neoteretis* follows with a weak, positive linear correlation of 7% per °C. This sensitivity is nearly in line with the 8 or 9% per °C found in Kristjánsdóttir et al. [2007] over 6°C from the Iceland Shelf suggesting that local oceanographic parameters brought by different water masses are not affecting this species. The temperature sensitivity in *Q. arctica* Mg/Ca is scatter almost twenty times higher compared to species *Q. yabei* [Toyofuku et al. 2008] suggesting that these values cannot only be dependent on temperature. *Oridorsalis tener* was found at sites bathed by Atlantic and Arctic Deep Waters (Figures 5 and 6). Presumably *O. tener* is the polar variant of *O. umbonatus* [Wollenburg and Mackensen, 1998a] and has proved useful for Mg/Ca BWT reconstructions in a number of other calibration studies [Lear et al., 2002; Martin et al., 2002; Rathmann et al., 2004; Healey et al., 2008; Lear et al., 2010]. Stained specimens of *C. wuellerstorfi* were present at only two sites and their unstained values were not that elevated.

Based on this Arctic stained benthic foraminiferal data alone, any resulting calibration would not to be entirely reliable, but their mean values could allow inferring past

BWT variability. In the following sections we explore the various factors influencing the Mg/Ca sensitivity and move forward to developing calibrations that combine our new Arctic data with existing species-specific data sets.

### 4.2 Salinity effects on Mg/Ca

Culture [Lea et al., 1999; Dissard et al., 2010] and field studies [Ferguson et al., 2008] have shown that salinity can have more significant correlation to Mg/Ca than temperature having sensitivities from 2.8-60% per unit salinity. This process is hypothesized in Dissard et al. [2010] through showing that higher [$Mg^{2+}$] is incorporated into the foraminiferal calcification vacuoles at higher salinities.

Arctic Shelves lay under strong salinity stratified waters and therefore the Mg/Ca at the species present at these waters, *E. clavatum and N. labradorica* (Figures 5 and 6), were the ones inspected for possible salinity correlations. The Gabrielsson [2014, unpublished] salinity to Mg/Ca investigation in these same species from the Baltic and North Seas showed, despite the low number of datapoints, that *E. clavatum* Mg/Ca values were not affected by salinity whereas *N. labradorica* varied as Mg/Ca = $8*10^{-14}e^{0.8981*Sal}$, $R^2$=0.99 for n=3. We see a similar pattern in our Arctic specimens when compiled (Figure 18). For *E. clavatum*, the Mg/Ca–salinity compilation reveals no evidence for a systematic relationship (Figure 18a), whereas a significant correlation is strengthened in *N. labradorica* spanning a 2.5 psu field measured range and deriving the fit Mg/Ca = $9.32*10^{-6}*e^{(0.36**Sal)}$, $R^2$=0.87 for n=9 (Figure 18b) thus reducing Gabrielsson [2014, unpublished] Mg/Ca sensitivity to salinity.

Nevertheless, salinity covaries with temperature and $\Delta[CO_3^{2-}]$ [Zeebe and Wolf-Gladrow, 2001]. Thus, it is hard to differentiate the salinity signal unless having steady temperatures and seawater carbonate chemistry. However, in our field Arctic data set we only observe correlation with salinity, not temperature or $\Delta[CO_3^{2-}]$. This is an important finding and implying that *E. clavatum* is the best benthic tracer for reconstructing BWT on the shelf whilst *N. labradorica* for reconstructing salinities.

### 4.3 Saturation state effects on Mg/Ca

In other oceans, calcite saturation decreases with increasing water depths [e.g. Broecker and Peng, 1982]. However, in the Arctic the thick halocline layer, which extends to depths of ~200 m and therefore dominates shelves, is also undersaturated with respect to calcite at the Chukchi Shelf sites (Figure 3) as a consequence of old Pacific waters mixing in. Carbonate ion concentration of less than 30 μmol/kg has been shown to control benthic foraminiferal Mg/Ca more than temperature [Elderfield et al., 2006; Yu and Elderfield, 2008]. This threshold is found in the Arctic below 0°C, at which Mg/Ca incorporation shows higher variability to $\Delta[CO_3^{2-}]$ than it does to temperature. The low saturation found at the Pacific/Arctic halocline produces another source of uncertainty that might influence the Mg/Ca results. Therefore, the Mg/Ca scatter found in species living at the negative seawater Pacific-Arctic halocline temperatures, *E. clavatum* and *N. labradorica*, could be explained by $\Delta[CO_3^{2-}]$ bottom

water effects instead. However, Mg/Ca-$\Delta[CO_3^{2-}]$ relationships at these species (Figures 12a and 12b) show no significant relationship meaning that biological and/or other environmental factors (like salinity for *N. labradorica*, section 4.2) lead the Mg/Ca variations.

Previous studies have shown that Mg/Ca values of epifaunal species *C. wuellerstorfi*, are affected by temperature and $\Delta[CO_3^{2-}]$, while infaunal species appear to be unaffected to seawater $\Delta[CO_3^{2-}]$ as a consequence of using buffered $\Delta[CO_3^{2-}]$ porewaters for test calcification [Elderfield et al., 2010; Lear et al., 2015]. This is in line with our only epifitic species *Q. arctica* that shows the strongest Mg/Ca-$\Delta[CO_3^{2-}]$ relationship with a Mg/Ca-depth relationship of $R^2$=0.77, n=13.

### 4.4 Sample screening

An important observation is that specimens from unstained $^{14}C$-dated core tops have at least double the Mg/Ca concentration of stained multicore samples (<2 mmol/mol to ~4 mmol/mol in stained and unstained samples respectively). Foraminifera tend to reject Mg when segregating their $CaCO_3$ tests since it inhibits calcification [Davis et al., 2000]. Even for species building high-Mg calcite tests, Toyofuku et al. [2000] showed that the predicted Mg fractionation in inorganic calcite [Katz, 1973] is higher than in biogenic calcite. Therefore, anomalously high values cannot be biologically explained and we have to consider contamination as potential Mg rising sources. The Al/Ca and Fe/Ca content of each sample against the Mg/Ca were examined to observe presence of any detrital clays raising our biological Mg concentration. On the bases of published upper limits of Fe/Ca (175 μmol/mol) and Al/Ca (40 μmol/mol) [Bice et al., 2005; Lea et al., 2005], three out of seven Al/Ca values in *E. clavatum* are slightly higher (~10 μmol/mol), however, these not covary with Mg/Ca. All its Fe/Ca values are lower than 50 μmol/mol. *N. labradorica* has low Al/Ca (~10 mmol/mol average) and very high Fe/Ca content (~3000 μmol/mol), however they do not correlate to Mg/Ca and cannot help assessing Mg/Ca contamination. For *C. neoteretis* Al/Ca in the unstained specimens are all > 40 μmol/mol and 8 out of 15 in the stained ones. Fe/Ca was lower than 175 μmol/mol at both sets of samples. No significant Mg/Ca relationships were found between the two. Species *Q. arctica* have low Al/Ca in stained specimens but higher in unstained ones (average 78 μmol/mol), although without relationship to Mg/Ca. Fe/Ca, is always lower than the threshold. In *O. tener* Fe/Ca is lower than the limit value at all samples. Instead, Al/Ca tends to be higher with average 105 μmol/mol in unstained specimens, but lower in the stained ones with 35 μmol/mol average values. None of the ratios show covariance to Mg/Ca. For *C. wuellerstorfi* Al/Ca and Fe/Ca is lower than the limit at all samples and off-trend the Mg/Ca.

To sum up, we only observe high Fe/Ca in the stained specimens of *N. labradorica* and the Al/Ca is high at all species but *N. labradorica* and *C. wuellerstorfi*. These ratios are higher in the unstained samples that we attribute to an increase in diagenesis with age. The stained Fe/Ca and Al/Ca inter-species differences observed could be

attributed to the complex biological mechanisms that might control trace-element concentrations [Erez, 2003; Bentov and Erez, 2005].

The occurrence of test surface framboidal pyrite on a set of uncleaned specimens as shown in *C. wuellerstorfi* plate 2 (6a) from LOMROG12-TC12 core top, and in some *N. pachyderma* in the upper 1cm of multicore 34-MC, both retrieved from the Lomonosov Ridge crest provide further evidence of redox reactions occurring close to the sediment-seafloor interface in at least some Central Arctic core tops as posited in Butler and Rickard [2000]. Whether the processes driving this reaction also have an effect on Mg mobilization is unclear. Inorganically precipitated coatings that are resistant to the cleaning method tend to increase original test Mg/Ca ratio such that any original BWT signal is obliterated. The applied reducing step in the cleaning method extracts test adhered Mn oxyhydroxides formed under sediment oxidizing conditions but not the Mn carbonates product of reducing conditions [Groeneveld and Filipsson 2013]. This idea is supported by the progressive increase in Mg over the past 12 kyrs (Figure 14). Mn/Ca data can help assessing the presence of post-depositional iron-manganese coatings that could have formed by porewater reaction in the sediment redoxcline. For reliable Mg/Ca values, Boyle [1983] established an upper limit of 100 μmol/mol Mn/Ca. Species *E. clavatum* have average Mn/Ca of 76 μmol/mol. Two out of seven are 238 and 175 μmol/mol, however no linear covariance with Mg/Ca is shown. In *N. labradorica* Mn/Ca values are very high, averaging 884 μmol/mol although without Mg/Ca correlation whereas in *C. neoteretis* these are very low (average ~11 μmol/mol Mn/Ca). Stained *Q. arctica* Mn/Ca average 158 μmol/mol while unstained 922 μmol/mol. In *O. tener* Mn/Ca values are with very low, 8 μmol/mol. Finally, *C. wuellerstorfi* presents average 44 μmol/mol Mn/Ca.

Apart from metal rich coatings, secondary calcite precipitation could modify the biogenic Mg content. The fact that our unstained Mg/Ca directly increases with $\Delta[CO_3^{2-}]$ in *C. neoteretis, O. tener* and *C. wuellerstorfi*; and age at all unstained species could indicate that old Arctic saturated waters promote inorganic calcite precipitation on foraminiferal tests thus increasing the initial biogenic Mg/Ca content and steepening the calibration curve as found in earlier studies [e.g. Marchitto et al., 2007; Curry and Marchitto, 2008].

### 4.5 SEM and EDS analyses

The texture of foraminiferal test surfaces and pattern of Mg concentration on the internal and external surfaces of several representative unstained Central Arctic tests from Plate 2 provide further support for the idea of encrusted diagenetic coatings. The EDS mineralogical mapping method is semiquantitative, but it allows detecting inorganic calcite since it contains 2-3 wt% of Mg that equates to 2-3 times the EDS detection limit, whereas in 'fresh' tests biogenic Mg is under the EDS detection limit (<1 wt%) (Figures 16 and 17). Visually, the SEM micrographs in the fossil examples (Plate 2 and Figure 17) show heavily recrystallized surfaces obscuring original wall details. Interestingly, internal parts of the wall targeted by the electron beam appear to

reveal slightly lower Mg/Ca concentrations suggesting the original calcite still remains in protected parts of the wall. Average unstained-stained Mg/Ca in *C. wuellerstorfi* differ by only ~0.1 mmol/mol while for *C. neoteretis* and *O. tener* the differences are ~1 mmol/mol. Thus, after the vigorous cleaning method prior to trace metal analysis, Mg coating contributions to total test Mg/Ca are volumetrically smaller in larger size and wall thickness taxa (355-250 µm-sized *C. wuellerstorfi*) whereas coatings swamp the Mg/Ca signature in small and thinner walled species (250-125 µm-sized *C. neoteretis* and *O. tener*) due to their considerably higher surface to volume ratio [van Raden et al., 2011].

A plausible reason explaining the precipitation of these aggregates comes from the fact that core top Mg/Ca-$\Delta[CO_3^{2-}]$ is more linear in *C. neoteretis*, *O. tener* and *C. wuellerstorfi* fossil unstained than stained data. This could suggest that coatings form with increasing time of exposure under highly saturated $[CO_3^{2-}]$ bottom waters. More insights on the origin of these precipitates could include riverine inflow variability of $Mg^{2+}$ (aq) to Central Arctic bottom water. Mg can occur in sediments as a porewater solute [Wedepohl, 1978] and could result in Mg-rich porewaters that support its inorganic precipitation. Secondary calcite on test surface, interior or between could be product from the dissolution of the shell itself that has dissolved and recrystallized, or exogenous precipitating material that based on the presence of saturated waters is more likely to occur. Ostracode tests of *Krithe* were also imaged and less rugous surfaces were observed. Moreover, ostracodes are thought to have their biogenic Mg/Ca signal unaffected attributed to the ten times more Mg content in ostracodes than in benthic foraminifera [Cronin and Dwyer, 2016 *personal communication*].

### 4.6 Age effect

The methods to demonstrate the core top benthic foraminifera age might include some caveats. On the one hand, the use of Rose Bengal to stain the protoplasm may overestimate the numbers of recently living foraminifera [Bernhard et al., 2006], especially at the low oxygen settings found at the Herald Canyon sites where organic matter is not fully respired. On the other hand, the top sediment radiocarbon ages from planktic foraminifera *N. pachyderma* are rather old (3000–11000 kyrs), spanning the entire Holocene (~12 kyrs). This implies that the Mg/Ca measurements are not contemporary with the field BWT. Furthermore, planktic foraminifera settle down through the water column once dead a process that might lead to mixing ages between older planktic and younger living benthic foraminifera.

The Mg/Ca concentrations generally increase with increasing $^{14}C$ age over the Holocene (Figure 13). The ratios equate to ~20 °C warmer BWT in *C. neoteretis*, 25°C in *O. tener* and 16 °C in *C. wuellerstorfi* for the Holocene for these core top samples with the hypothetical Mg/Ca-temperature sensitivity of 0.1 mmol/mol per °C [e.g. Marchitto et al. 2007]. The Holocene is widely thought to be a rather stable climate where Arctic BWT cannot be perturbed on such a scale both with respect to seawater Mg or BWT. Rather, colder temperatures and thus lower ratios from the

oldest dated sample at end of the Younger Dryas (11 kyr) should be expected. Based on the EDS evidences we suggest that these higher than biogenically induced Mg/Ca ratios result from post-mortem diagenetic inorganic calcite coatings on test surfaces, that are thickening over time with the exposure to corrosive bottom waters through the low central Arctic burial rates. The reason for Mg concentration in Holocene fossil core-top foraminifera from the Central Arctic is unclear and conversely is not occurring in fossil from the shelf under higher sedimentation regimes as evidenced by the down core 2-PC Mg/Ca record from the Chukchi Shelf. These regional differences in Mg/Ca preservation might be attributed to the distinct sedimentation rates. Arctic sedimentation rates vary hugely from 5 – >10 cm/kyr on the Eastern Siberian Sea shelf and slopes, to 0.5–2 cm/kyr in the central Arctic Ocean with the lowest recorded being < 0.5 cm/kyr in the Makarov Basin [Backman et al., 2004; Stein, 2008]. This means that central Arctic surface sediments are exposed at the sediment water interface for longer times without being buffered by the sediments as it occurs at the shelf.

Furthermore, the old ages could result from erosion brought by bottom current action exposing older sediments on the Lomonosov Ridge. If sedimentation rates were modest (0.5-2 cm/kyr) it might simply be that the uppermost unconsolidated Holocene layer has been lost during coring operations. Piston and trigger weight coring (the methods used to recover the Central Arctic cores) are known to disturb the sediment-water interface, while the multicore method is optimal for capturing undisturbed surface sediment. A final possibility might be presence of bioturbation found in Lomonosov Ridge cores [Löwemark et al. 2012] giving 2.5 cm mixing rates [Clough et al., 1997]. If these bioturbation operate over central Arctic 0.5–1 cm/kyr sedimentation rates [Backman et al., 2004; Löwemark et al. 2012], mean age brought by mixing will be around 2500 years, yet younger than the ~5000 average measured ages.

### 4.7 Arctic *vs.* compiled Mg/Ca-BWT calibrations

Field BWT at the study sites span a very limited temperature range, however these are at the coldest end of seawater, like most of the deep ocean, and at it is at this portion of the temperature calibration that the method needs to be further tested. To address this and better test the reliability of our results, Arctic data was integrated with existing published and unpublished Mg/Ca-temperature calibration datasets that span a wider range of BWT (Figure 17, Table 3, and Appendix Table F).

Linear and exponential regressions were applied and our new data fits well in the calibration sets from all the oceans, for most species, and provide important cold end constraints (Figure 17). The unstained core top data fall anomalous when placed in the compiled trend giving us further evidence that their signal is not biological, thus excluded from all the fits.

**Table 3.** Available Mg/Ca–BWT data at the six studied species obtained from published and unpublished calibrations (all data compiled and sample location is supplemented in the Appendix,

Table F).

| species | reference | n | A | B | $R^2$ | Mg/Ca range (mmol/mol) | BWT gradient (°C) |
|---|---|---|---|---|---|---|---|
| Linear fit, Mg/Ca = (A*BWT) + B | | | | | | | |
| *E. clavatum* | This study (stained samples) | 10 | 0.048 | 0.711 | 0.12 | 0.52 – 0.80 | -1.82 – -0.26 |
| *E. clavatum* | Gabrielsson [2014 unpublished] | 3 | – | – | – | 0.82 – 1.58 | 3.78 – 6.53 |
| *E. clavatum* | Compilation (see Fig. 17a) | 25 | 0.070 | 0.743 | 0.78 | 0.52 – 2.58 | -1.82 – 15.71 |
| *N. labradorica* | This study (stained samples) | 6 | -0.017 | 1.236 | 0.02 | 1.11 – 1.31 | -1.71 – -0.26 |
| *N. labradorica* | Compilation (see Fig. 17b) | 9 | 0.163 | 1.407 | 0.66 | 1.11 – 3.42 | -1.71 – 6.55 |
| *C. neoteretis* | This study (stained samples) | 15 | 0.071 | 1.023 | 0.07 | 0.84 – 1.20 | -0.47 – 0.91 |
| *C. neoteretis* | Kristjánsdóttir et al. [2007] | 10 | 0.093 | 0.840 | 0.90 | 0.93 – 1.38 | 0.22 – 6.25 |
| *C. neoteretis* | Compilation (see Fig. 17c) | 25 | 0.049 | 1.011 | 0.62 | 0.84 – 1.38 | 0.96 – 5.47 |
| *Q. arctica* | This study (stained samples) | 13 | 35.198 | 40.882 | 0.37 | 18.89 – 75.08 | -0.54 – 0.91 |
| *Q. yabei* | Toyofuku et al. [2000] | 11 | 1.730 | 77.640 | 0.83 | 95.20 – 126.10 | 11.70 – 25.70 |
| *O. tener* | This study (stained samples) | 5 | 0.139 | 1.609 | 0.09 | 1.43 – 1.78 | -0.59 – 0.69 |
| *O. umbonatus* | Healey et al. [2008] | 24 | 0.449 | 0.773 | 0.67 | 1.25 – 2.60 | 0.85 – 3.8 |
| *O. umbonatus* | Lear et al. [2010] | 21 | 0.12 | 1.200 | 0.9 | 1.11 – 1.88 | -0.6 – 3.7 |
| *O. tener/umbonatus* | Compilation (see Fig. 17e) | 83 | 0.191 | 1.360 | 0.62 | 1.09 – 3.96 | -0.6 – 10.4 |
| *C. wuellerstorfi* | This study (stained samples) | 3 | 0.535 | 1.349 | 0.72 | 1.32 – 1.48 | -0.22 – -0.77 |
| *C. wuellerstorfi* | Rathburn and deDeckker [1997] | 38 | 0.342 | 1.390 | 0.78 | 1.27 – 8.7 | 2 – 6 |
| *C. wuellerstorfi* | Healey et al. [2008] | 33 | 0.295 | 0.670 | 0.90 | 0.79 – 2.05 | 0.95 – 3.8 |
| *C. wuellerstorfi* | Compilation (see Fig. 15f) | 225 | 0.311 | 0.681 | 0.71 | 0.68 –3.91 | -1.10 – 6.06 |
| Exponential fit, Mg/Ca = B * e^ (A*BWT) | | | | | | | |
| *E. clavatum* | Varekamp et al. [2010] | 12 | 0.1959 | 0.109 | 0.85 | 1.1 – 2.58 | 12.10 – 15.71 |
| *E. clavatum* | Compilation (see Fig. 17a) | 22 | 0.062 | 0.719 | 0.79 | 0.551 – 2.58 | -1.82 – 15.71 |
| *N. labradorica* | Gabrielsson (2014) unpublished | 3 | 0.273 | 0.421 | 0.10 | 1.84 – 3.42 | 5.87 – 6.55 |
| *N. labradorica* | Compilation (see Fig. 15b) | 9 | 0.086 | 1.359 | 0.68 | 1.11 – 3.42 | -1.71 – 6.55 |
| *C. neoteretis* | Kristjánsdóttir et al. [2007] | 10 | 0.082 | 0.864 | 0.90 | 0.93 – 1.38 | 0.22 – 6.25 |
| *C. neoteretis* | Compilation (see Fig. 17c) | 25 | 0.042 | 1.009 | 0.62 | 0.84 – 1.38 | -0.47 – 5.47 |
| *O. umbonatus* | Lear et al. [2002] | 23 | 0.114 | 1.008 | 0.40 | 1.09 – 3.43 | 0.8 – 9.9 |
| *O. umbonatus* | Rathmann et al. [2004] | 6 | 0.09 | 1.528 | – | 1.91 – 3.96 | 2.9 – 10.4 |
| *O. umbonatus* | Healey et al. [2008] | 24 | 0.252 | 0.988 | 0.67 | 1.25 – 2.60 | 0.85 – 3.8 |
| *O. umbonatus* | Tisserand et al. [2013] (fit Healey et al., 2008 and Rathman et al., 2004) | 12 | 0.110 | 1.360 | 0.53 | 2.26 – 3.1 | 4.17 – 6.06 |
| *O. tener/umbonatus* | Compilation (see Fig. 17e) | 83 | 0.096 | 1.372 | 0.60 | 1.09 – 3.96 | -0.6 – 10.4 |
| *C. wuellerstorfi* | Russell et al. [1994] | 15 | 0.206 | 0.953 | – | 1.32 – 2.25 | 1.7 – 2.8 |
| *C. wuellerstorfi* | Rosenthal et al. [1997] & Rosenthal [MIT unpublished] | 15 | – | – | – | 1.10 – 1.66 | 0.4 –2.8 |
| *C. wuellerstorfi* | Lear et al. [2002] | 16 | 0.280 | 0.652 | 0.58 | 0.92 – 2.10 | 1.7 – 4.4 |
| *C. wuellerstorfi* | Martin et al. [2002] | 27 | 0.309 | 0.448 | 0.81 | 0.68 – 1.46 | 1.8 – 3 |
| *C. wuellerstorfi* | Healey et al. [2008] | 33 | 0.230 | 0.781 | 0.91 | 0.79 – 2.05 | 0.95 – 3.8 |
| *C. wuellerstorfi* | Raitzsch et al. [2008] | 44 | 0.145 | 0.830 | 0.89 | 0.84 – 2.02 | 0.39 – 3.88 |
| *C. wuellerstorfi* | Tisserand et al. [2013] | 34 | 0.19 | 0.820 | 0.73 | 1.8 – 3.91 | 4.17 – 6.06 |
| *C. wuellerstorfi* | Compilation (see Fig. 17f) | 225 | 0.110 | 0.850 | 0.75 | 0.68 – 3.91 | -1.10 – 6.06 |

Statistically significant $R^2$ values were obtained in the compilation ($R^2 > 0.6$) applying either linear or exponential fits both presenting similar $R^2$ values. The resulting regression correlations are more significant in 3 of the 6 species. These are *E. clavatum* (Figure 17a) that adds the Arctic cold end data and lowers the Varekamp et al. [2010] exponential sensitivity from 20% per °C to 6% per °C (exponential) or 7% per °C (linear); *N. labradorica* (Figure 17b), that adds Mg/Ca to the cold end and lowers the Gabrielsson [2014, unpublished] exponential sensitivity from 0.273 mmol/mol/°C to 0.086 mmol/mol/°C (exponential) or 0.163 mmol/mol/°C (linear); and *C. neoteretis* (Figure 18c), lowers the sensitivity when combined to our stained *C. neoteretis* data with published data of Kristjánsdóttir et al. [2007] from the Iceland and Greenland margins. The relationship between Mg/Ca and BWT in this species can be described by either exponential (temperature sensitivity of 0.05 mmol/°C; $R^2$=0.60) or linear fits (sensitivity of 0.06 mmol/°C , $R^2$=0.61). Both fits reduce the Kristjánsdóttir et al. [2007] published sensitivity by ~0.03 mmol/mol/°C, since the published relationship is 0.082 mmol/mol/°C.

*Quinqueloculina arctica* Mg/Ca-BWT compiled data (Figure 18d), show a significantly different and larger range of Mg/Ca variability, 60 mmol/mol, over a small Arctic field BWT range, 1 °C, compared to data for another species in the genus, *Q. yabei*, that was based on culture experiments and field data from the Japan

Sea [Toyofuku et al. 2000] (Figure 18d). Like other taxa in the family Miliolidae, these two *Quinqueloculina* species have a porcelaneous test that is formed from high Mg calcite and in a fundamentally different way than hyaline low Mg-calcite taxa. Specifically, calcite crystals have been shown to precipitate within intracellular water vesicles, whose chemical composition is more controlled by the organism (thus represent cell-derived fluids) than in hyaline (perforate) taxa, which calcify the test within extracellular space [Angell, 1979, 1980]. The *Q. yabei* dataset records a strong correlation between Mg/Ca and temperature over a BWT range of 10-28°C. While there appears to be some correlation between BWT and Mg/Ca in the *Q. arctica* dataset alone (Figure 8d), the Mg/Ca-BWT sensitivity is quite different over the temperature ranges (35.2 mmol/mol/°C compared to 1.7 mmol/mol/°C respectively). Toyofuku et al. [2000] do not show $\Delta[CO_3^{2-}]$ in their study, however, our new data show that *Q. arctica* Mg/Ca is strongly influenced by $\Delta[CO_3^{2-}]$ evidenced first by the observed high Mg/Ca–depth covariance in stained samples ($R^2$=0.77) and second through the Mg/Ca–$\Delta[CO_3^{2-}]$ relationship ($R^2$=81) rejecting the 21-MC1 offset value (Figure 9d and 11d). This will be consistent if species *Q. arctica* had an epiphytic or epifaunal mode of life that records bottom water $\Delta[CO_3^{2-}]$ that is not buffered by pore water chemistry.

*Oridorsalis tener* (Figure 18e) stained Mg/Ca data are plotted together with *O. umbonatus* from multiple locations across the world oceans showing an offset with the overall linear or exponential by mean higher 0.25 mmol/mol values, although two datapoints are in line with Lear et al. [2010] dataset. Moreover, both studies show similar sensitivities (Arctic 0.14 mmol/mol/°C and Lear et al. [2010] 0.12 mmol/mol/°C). The coldest end of BWT is covered by Lear et al. [2002] study from the Pacific. If Mg/Ca is mainly dependent on thermodynamic and biological processes, a distinct oceanic source of waters should not be an issue, although Pacific and Atlantic waters do have different saturation states. Integrating data to build single-species Mg/Ca-BWT relationships might lead to extra noise in the data since different studies are built on wide test size fraction and different oceanic locations. On the one hand, Tisserand et al. [2013] indicated that differing size fractions result in varying intra-test Mg partitioning. In their study, *O. umbonatus* showed a ~0.4 mmol/mol Mg/Ca decrease at the 250–400 μm size samples when compared to the 150–250 μm data. This remark is important since Arctic hyaline foraminifera are typically smaller, within the 125–250 μm. Therefore our integrated Arctic data might be biased towards higher values product of ontogenetic and not environmental effects. This could be a possible explanation of the higher values obtained in stained *O. tener* when compared to the implemented data. Furthermore, previous studies suggest that infaunal species like this should be less sensitive to $\Delta[CO_3^{2-}]$ [Lear et al. 2015]. However, our *O. tener* data correlates more to $\Delta[CO_3^{2-}]$ and lead us to conclude that *O. tener* habitat depth might be slightly shallower than *O. umbonatus* due to the lower productivity of the Arctic. This could be another mechanism increasing our *O. tener* Mg/Ca as compared to the Lear et al. [2010] data from the coldest end.

Our Mg/Ca values for *C. wuellerstorfi* fall higher than the composite linear and exponential values by 1 mmol/mol in the linear fit and by 0.5 mmol/mol in the exponential fit (Figure 17f). From all species compiled and shown in Figure 17, this species presents the highest sensitivities, possibly product of its epifaunal habitat where bottom water $\Delta[CO_3^{2-}]$ effects interplay with Mg/Ca. *Cibicidoides wuellerstorfi* has been used in many previous Mg/Ca reconstructions of palaeo BWT at bathyal and abyssal depths outside of the Arctic Ocean and has been the subject of various calibration studies [Rosenthal et al., 1997; Lear et al., 2002; Martin et al., 2002; Healey et al., 2008; Raitzsch et al., 2008; Lear et al., 2010; Tisserand et al., 2013]. It occurs at sites bathed by Atlantic or Arctic Deep Water (Figures 5 and 6). Our Artic benthic *C. wuellerstorfi* are consistent with the only other published subzero deep water calibration point of -1.1°C, Greenland Sea, 78°N [Martin et al., 2002] (Figure 18f), and whether this is the result of the influence of low carbonate saturation ($\Delta[CO_3^{2-}]$=35-40 µmol/kg for the two samples stations) is unclear. Nonetheless, the new data suggest that *C. wuellerstorfi* is unsuitable for Arctic bottom water reconstructions, first because there are insufficient data points to constrain a cold water calibration and second, because of the inferred slightly parabolic behavior of *C. wuellerstorfi* Mg/Ca at low temperatures.

In sum, the implementation of this new stained Arctic data lowers the Mg/Ca-BWT sensitivity of previous fits favoring the exponential over the linear fit relationship (Table 3). Despite the Mg content in seawater thought to be conservative, discrepancies among Varekamp et al. [2010] and my dataset can be explained by other local intertwined physical, chemical and biological processes interfering with the Mg test incorporation. This phenomenon was observed in Ferguson et al. [2008], where planktic Mg/Ca values were affected by local variations inherited from different oceans.

## 5. Conclusions

We have investigated the relationship between Mg/Ca with temperature, salinity and carbonate ion concentration, in a set of 6 Rose Bengal stained benthic foraminifera species (*E. clavatum*, *N. labradorica*, *C. neoteretis*, *Q. arctica*, *C. wuellerstorfi* and *O. tener*) from the Arctic Ocean that occur in sufficient numbers and living across a wide range of Arctic water mass zones. Large variations in Mg/Ca are observed ranging from 0.5 mmol/mol in *E. clavatum* to 75 mmol/mol in *Q. arctica*. Regression analysis (linear fits) revealed $R^2$ values for Mg/Ca-temperature ranging from 0.02 to 0.72. Our Mg/Ca-BWT data distribution alludes to a generally weak relationship between Mg/Ca and BWT and thus unreliable absolute temperature calibration equations. For species *N. labradorica*, salinity appears to play a role ($R^2$= 0.52), while carbonate ion concentration may be affecting epifaunal *Q. arctica*. Thus, other Arctic environmental parameters changing in higher magnitude than temperature might influence Mg/Ca incorporation and that the effect of these processes is species dependent.

The weak Mg/Ca-temperature relationship could be explained by a combination of factors such as; the challenges of creating the field calibration set, including the possibility of mismatches between the 'snapshot' BWT field constraint (from SWERUS-C3 CTD data) (which spans both very low temperatures and small temperature ranges) compared to the longer time averaged growing period for the benthic foraminifera; limited numbers of data points in the calibrations (n ranging from 3–15); foraminiferal vital effects and the generally low sensitivity of the Mg/Ca-BWT dependency at low temperatures. *Elphidium clavatum* shows the most promise as a signal carrier for the Mg/Ca palaeothermometry method because they are common on the shelf and show no Mg/Ca-salinity or carbonate ion dependency, however the temperature - $R^2$ value is still weak (Mg/Ca-BWT $R^2 = 0.12$, n=10).

Despite the lack of clear correlation in our new Arctic data set, the absolute Mg/Ca values in our Rose Bengal stained samples fit well with existing data arrays and agree with linear/exponential Mg/Ca-BWT relationships, thus adding important constraints at the coldest end (-2 to 1°C) of the ocean temperature spectrum. However, this cold end of the compiled Mg/Ca data remains flat due to the exponential relationship between Mg/Ca and temperature observed over the much larger temperature ranges (-2 to 25°C), giving a wide range of possible temperatures for similar Mg/Ca values; equating to a temperature error of ±2°C. These limitations are clear when we apply the integrated equation (Arctic plus global data), or a version of this equation that integrates the new Arctic regression with the compiled data-set sensitivity, to a late Holocene down-core record of fossil benthic foraminifera Mg/Ca from the Chukchi Sea. The result is largely unrealistic BWT with large temperature spread. Thus, at this stage we have low confidence in the ability of Mg/Ca palaeothermometry to reconstruct absolute BWT in the Arctic, however, it is likely that time-averaged downcore patterns of benthic Mg/Ca variability do capture relative paleotemperature signals.

Holocene core tops from the central Arctic showed anomalously high Mg/Ca, implying controls additional to temperature on core top foraminiferal calcite from this region, an idea supported by SEM and EDS analysis that reveals evidence for Mg-rich diagenetic coatings and fillings. We speculate this to be the result of slow sedimentation and carbonate saturated deep waters in this setting. Fossil 'Mg-coated' core top specimens thus have been exposed to poorly ventilated old Arctic bottom waters for a longer time than live forms, allowing time for both corrosion of the test and secondary precipitation. This may limit the application of Mg/Ca palaeothermometry in this setting, although further work is required to explore this fully. Arctic shelves, where sedimentation is higher, are regarded as better settings to apply the downcore Mg/Ca method in benthic foraminifera.

**Acknowledgements** We thank E. Mawbey and A. Morte-Ródenas for teaching and explaining sample cleaning and ICP-MS operation. This research was supported by the Knut and Alice Wallenberg Foundation, Swedish Polar Research Secretariat, Stockhom University (SWERUS-C3 program), and the Swedish Research Council (VR).

## References


ACIA (2004). Impacts of a warming Arctic: Arctic Climate Impact Assessment. Cambridge: Cambridge University Press, 139 pp.

Anand, P., Elderfield, H., and Conte, M. H. (2003). Calibration of Mg/Ca thermometry in planktonic foraminifera from a sediment trap time series, Paleoceanography, 18 (2), 1050.

Angell, W. (1979). Calcification during chamber development in *Rosalina Floridana*, *Journal of Foraminiferal Research*, 9, 341–353.

Angell, W. (1980). Test morphogenesis (chamber formation) in the foraminifer *Spiroloculia Hyalina* Schulze. *Journal of Foraminiferal Research*, 10, 89–101.

Backman, J., Jakobsson, M., Løvlie, R., Polyak, L., Febo, L. A. (2004). Is the central Arctic Ocean a sediment starved basin?, *Quaternary Science Reviews*, 23, 1435–1454.

Barker, S., M. and Greaves, E. H. (2003). A study of cleaning procedures used for foraminiferal Mg/Ca paleothermometry, *Geochemistry Geophisics Geosystems*, 4 (9), 1–20.

Bé, A.W.H. (1960). Ecology of recent planktonic foraminifera: part 2. Bathymetric and seasonal distributions in the Sargasso Sea off Bermuda, *Micropaleontology*, 6, 372–392.

Bentov, S., Erez, J., (2005), Novel observations on biomineralization processes in foraminifera and implications for Mg/Ca ratio in the shells. Geology 33 (11), 841–844.

Bernhard J.M. and Bowser, S.S. (1999) Benthic foraminifera of dysoxic sediments: chloroplast sequestration and functional morphology. *Earth-Science Reviews*, 46, 149–165.

Bernhard, J. M., Ostermann, D. R., Williams, D. S., and Blanks, J. K. (2006). Comparison of two methods to identify live benthic foraminifera: A test between Rose Bengal and CellTracker Green with implications for stable isotope paleoreconstructions, Paleoceanography, 21, PA4210.

Bice, K., Layne, G., Dahl, K. (2005). Application of secondary ion mass spectrometry to the determination of Mg/Ca in rare, delicate, or altered planktonic foraminifera: examples from the Holocene, Paleogene, and Cretaceous. Geochem. Geophys. Geosystem 6 (12), Q12PO7.

Billups, K., and Schrag, D.P. (2002). Paleotemperatures and ice volume of the past 27 Myr revisited with paired Mg/Ca and $^{18}O/^{16}O$ measurements on benthic foraminifera, Paleoceanography, 17, PA000567.

Boltovskoy, E. and Wright, R. (1976). Recent Foraminifera, Junk, W. Publishers.

Boyle, E. (1983). Manganese carbonate overgrowths on foraminifera tests. Geochim. Cosmochim. Acta 47 (10), 1815–1819.

Boyle, E. A., and Keigwin, L. D. (1985/1986) Comparison of Atlantic and Pacific paleochemical records for the Last 215.000 years: Changes in deep ocean circulation and chemical inventories. Earth and Planetary Science Letters, 76, 135–150.

Broecker, W. and Peng, T.-H. (1982). Tracers in the sea, Eldigo, Palisades, N.Y., 690 pp.

Butler, I.B. and Rickard, D. (2000), Framboidal pyrite formation via the oxidation of iron (II) monosulfide by hydrogen sulphide, *Geochim. Cosmochim. Acta*, 64 (15), 2665–2672.

Chave, K.E. (1954). Aspects of the biochemistry of magnesium: 1. Calcareous marine organisms: Journal of Geology, v. 62, p. 266–283.

Chen, C.-T.A., Liu, K.-K. and Macdonald, R. (2003). Chapter 3: Continental Margin Exchanges, *in Ocean Biogeochemistry: The Role of the Ocean Carbon Cycle in Global Change*, 53–97, Springer Berlin Heidelberg.

Chierici, M. and Fransson, A. (2009). Calcium carbonate saturation in the surface water of the Arctic Ocean: undersaturation in freshwater influenced shelves, Biogeosciences, 6 (11), 2421–2431.

Clough, L.M., Ambrose, J.W.G., Kirk Cochran, J., Barnes, C., Renaud, P.E., Aller, R.C. (1997). Infaunal density, biomass and bioturbation in the sediments of the Arctic Ocean. Deep Sea Research Part II: Topical Studies in Oceanography 44 (8), 1683–1704.

Cronin, T. M., G. S. Dwyer, J. Farmer, H. A. Bauch, R. F. Spielhagen, M. Jakobsson, J. Nilsson, W. M. Briggs, and Stepanova, A. (2012). Deep Arctic ocean warming during the last glacial cycle, Nature Geoscience, 5 (9), 631–634.

Corliss, B.H. and Emerson, S. (1990). Distribution of Rose Bengal stained deep-sea benthic foraminifera from the Nova Scotian continental margin and Gulf of Maine. *Deep-sea Research*, 37 (3), 381–400.

Curry, W. B. and Marchitto, T. M. (2008). A SIMS calibration of *Cibicidoides pachyderma* Mg/Ca with temperature. Geochemistry, Geophysics, Geosystems, Q04009.

Davis, K.J., Dove, P.M., and De Yoreo, J.J. (2000), The role of $Mg^{2+}$ as an impurity in calcite growth, Science, 290, 1134–1137.

de Nooijer, L. J., Spero, H. J., Erez, J., Bijma, J. and Reichart, G. J. (2014). Biomineralization in perforate foraminifera, *Earth-Science Reviews*, 135, 48–58.

Dickson, A., and Millero, F. (1987). A comparison of the equilibrium-constants for the dissociation of carbonic-acid in seawater media. Deep-Sea Research Part A–Oceanographic Research Papers.

Dissard, D., Nehrke, G., Reichart, G.J., Bijma, J. (2010). The impact of salinity on the Mg/Ca and Sr/Ca ratio in the benthic foraminifera *Ammonia tepida*: Results from culture experiments. Geochim. Cosmochim. Acta, 74 (3), 928–940.

Elderfield, H. and Ganssen, G. (2000). Reconstruction of temperature and $\delta^{18}O$ of surface ocean waters inferred from foraminiferal Mg/Ca ratios. Nature, 405, 442–445.

Elderfield, H., Yu, J., Anand, P., Kiefer, T. and Nyland, B. (2006). Calibrations for benthic foraminiferal Mg/Ca paleothermometry and the carbonate ion hypothesis. Earth Planet. Sci. Lett., 250, 633–649.

Elderfield, H., G. M., S. Barker, I. R. Hall, A. Tripati, P. Ferretti, S. Crowhurst, L. Booth, and C. Daunt (2010). A record of bottom water temperature and seawater $\delta^{18}O$ for the southern ocean over the past 440 kyr based on Mg/Ca of benthic foraminiferal *Uvigerina* spp. Quaternary Science Reviews, 29, 160–169.

Erez, J. (2003). The source of ions for biomineralization in foraminifera and their implications for paleoceanographic proxies. Rev. Mineral. Geochem. 54, 115–149.

Farmer, J. R., Cronin, T. M., de Vernal, A., Dwyer, G. S., Keigwin, L. D. and Thunell, R. C. (2011). Western Arctic ocean temperature variability during the last 8000 years, Geophysical Research Letters, 38 (24), L24602.

Farmer, J. R., Cronin, T. M. and Dwyer, G. S. (2012) Ostracode Mg/Ca paleothermometry in the north atlantic and Arctic oceans: Evaluation of a carbonate ion effect, Paleoceanography, 27, PA2212.

Ferguson, J.E., Henderson, G.M., Kucera, M., Rickaby R.E.M. (2008). Systematic change of foraminiferal Mg/Ca ratios across a strong salinity gradient, Earth and Planetary Science Letters, 265, 153–166.

Gabrielsson, J. (2014). A study of Mg/Ca in benthic foraminifera sampled across a large salinity gradient, Masters thesis, Lund University, https://lup.lub.lu.se/student-papers/search/publication/5031779.

Groeneveld, J. and Filipsson H.L. (2013). Mg/Ca and Mn/Ca ratios in benthic foraminifera: the potential to reconstruct past variations in temperature and hypoxia in shelf regions. Biogeosciences, 10, 5125–5138.

Hanslik, D. (2011). Late Quaternary Biostratigraphy and Paleoceanography of the central Arctic Ocean. Doctoral thesis. Department of Geological Sciences, Stockholm University.

Healey, S., Thunell, R. and Corliss, B. (2008). The Mg/Ca-temperature relationship of benthic foraminiferal calcite: New core top calibrations in the < 4°C temperature range. Earth and Planetary Science Letters, 272 (3–4), 523–530.

Healy-Williams, N. (1992), Stable isotope differences among morphotypes of *Neogloboquadrina pachyderma* (Ehrenberg): implications for high-latitude palaeoceanographic studies. Terra Nova, 4, 693–700.

Helland-Hansen, B., and Nansen, F. (1909). The Norwegian Sea. Report on Norwegian Fishery and Marine Investigation.

Izuka, S. (1988). Relationship of magnesium and other minor elements in tests of *Cassidulina subglobosa* and *C. oriangulata* to physical oceanic properties, *J. Foraminiferal Res*., 18, 151–157.

Jakobsson, M., Marcussen, C., and LOMROG Scientific Party (2008) Lomonosov Ridge off Greenland 2007 (LOMROG) – Cruise Report. Spetial publication Geological Survey of Denmark and Greenland, Copenhagen, Denmark, 122 pp.

Jutterström, S. and Anderson, L.G. (2005). The saturation of calcite and aragonite in the Arctic Ocean. *Mar. Chem.* 94, 101–110.

Katz, A. (1973). The interaction of magnesium with calcite during crystal growth at 25–90°C and one atmosphere. Geochimica et Cosmochimica Acta, 37 (6), 1563–1586.

Key, R. M., Tanhua, T., Olsen, A., Hoppema, M., Jutterström, S., Schirnick, C., van Heuven, S., Kozyr, A., Lin, X., Velo, A., Wallace, D. W. R., and Mintrop, L. (2010). The CARINA data synthesis project: introduction and overview, *Earth Syst. Sci. Data*, 2, 105–121.

Kristjánsdóttir, G. B., D. W. Lea, A. E. Jennings, D. K. Pak, and C. Belanger (2007), New spatial Mg/Ca-temperature calibrations for three Arctic, benthic foraminifera and reconstruction of north Iceland shelf temperature for the past 4000 years, *Geochemistry, Geophysics, Geosystems*, 8 (3), 1–27.

Lea, D. (1999). Trace elements in foraminiferal calcite. In Modern Foraminifera (ed. B. K. S. Gupta). Kluwer Academic Publishers.

Lea, D., Pak, D., Paradis, G. (2005). Influence of volcanic shards on foraminiferal Mg/Ca in a core from the Galapagos region. Geochem. Geophys. Geosystem 6 (11), Q11P04.

Lear, C. H., Elderfield, H. and Wilson P. A. (2000). Cenozoic deep-sea temperatures and global ice volumes from Mg/Ca in benthic foraminiferal calcite, *Science*, 287, 269–272.

Lear, C. H., Y. Rosenthal, and N. Slowey (2002). Benthic foraminiferal Mg/ca-paleothermometry: a revised core top calibration, Geochimica et Cosmochimica Acta.

Lear, C. H., Rosenthal, Y., Coxall, H. K. and Wilson, P. A. (2004). Late Eocene to early Miocene ice sheet dynamics and the global carbon cycle. Paleoceanography, 19, PA4015.

Lear, C. H., Mawbey, E. M., and Rosenthal, Y. (2010). Cenozoic benthic foraminiferal Mg/Ca and Li/Ca records: Toward unlocking temperatures and saturation states, Paleoceanography, 25, PA4215.

Lear, C. H., Coxall, H. K., Foster, G. L., Lunt, D. J., Mawbey, E. M., Rosenthal, Y., Sosdian, S.M., Thomas, E. and Wilson, P.A. (2015). Neogene ice volume and ocean temperatures: Insights from infaunal foraminiferal Mg/Ca paleothermometry. Paleoceanography, 30 (11), 1437–1454.

Löwemark, L., O'Regan, M., Hanebuth, T., Jakobsson, M. (2012). Late Quaternary spatial and temporal variability in Arctic deep-sea bioturbation and its relation to Mn-cycles. Paleogeogr. Paleoclimatol. Paleoecol. 365–366, 192–208.

Luchin, V. and Panteleev, G. (2014). Thermal regimes in the Chukchi Sea from 1941 to 2008, Deep-Sea Research II, 109, 14–26.

Marchitto, T. M., Bryan, S. W., Curry, W. B., and McCorckle, D. C. (2007). Linear Mg/Ca temperature calibration for the benthic foraminifer Cibicidoides pachyderma. Paleoceanography. 22, PA1203.

Marcussen, C. and LOMROG II Scientific Party (2011). Lomonosov Ridge off Greenland 2011 (LOMROG II) – Cruise Report. Geological Survey of Denmark and Greenland, report 2011/106, 154 pp.

Marcussen, C. and LOMROG III Scientific Party (2012). Lomonosov Ridge off Greenland 2012 (LOMROG III) – Cruise Report. Geological Survey of Denmark and Greenland, report 2012/119, 220 pp.

Martin, P., Lea, D., Rosenthal, Y., Shackleton, N., Sarnthein, M. and Papenfusse, T. (2002). Quaternary deep-sea temperature histories derived from benthic foraminiferal Mg/Ca, Earth and Planetary Science Letters, 117, 193–209.

Mehrbach, C., C. Culberso, J. Hawley, and R. Pytkowic (1973). Measurement of apparent dissociation-constants of carbonic-acid in seawater at atmospheric-pressure. Limnology and Oceanography.

Murray, J. W. (2006). Ecology and Applications of Benthic Foraminifera, Cambridge University Press, 426 pp.

Myers, E. (1938). The present state of our knowlegde concerning the life-cycle of the foraminifera. Proc. U.S. Nat. Acad. Sci. 24 (1), 10-17.

Nürnberg, D., Bijma, J., and Hemleben, C. (1996). Assessing the reliability of magnesium in foraminiferal calcite as a proxy for water mass temperature, *Geochim. Cosmochim. Acta*, 60, 803–814.

Osterman, L.E., Poore, R.Z., and Foley, K.M. (1999). Distribution of benthic foraminifers (>125 μm) in the surface sediments of the Arctic Ocean: United States Geological Survey Bulletin 2164, 28 p.

Overland, J., Hanna, E., Hanssen-Bauer, I., Kim, S.-J., Walsh, J. E., Wang, M., Bhatt, U. S., Thoman, R. L. (2015). Surface Air Temperature. In *Arctic Report Card: Update for 2015*, http://www.Arctic.noaa.gov/reportcard/air_temperature.html

Pearce, C., Varheyli, A., Wastegård, S., Jakobsson, M., Muschitiello, F., Barrientos, N., O'Regan, M. and Cronin, T. M.: The 3.6 ka Aniakchak tephra in the Arctic Ocean: implications for the radiocarbon reservoir age of the Chukchi Sea in the late Holocene, Clim. Past, In prep.

Pithan, F. and Mauritsen, T. (2014). Arctic amplification dominated by temperature feedbacks in contemporary climate models. *Nature Geoscience* 7, 181–184.

Raitzsch, M., Kuhnert, H., Groeneveld, J., Bickert, T. (2008), Benthic foraminifer Mg/Ca anomalies in South Atlantic core top sediments and their implications for paleothermometry. *Geochemistry, Geophysics, Geosystems*, 9 (5), Q05010, doi:10.1029/2007GC001788.

Rathmann, S., Hess, S., Kuhnert, H., and Mulitza, S. (2004). Mg/Ca ratios of the benthic foraminifera *Oridorsalis umbonatus* obtained by laser ablation from core top sediments: Relationship to bottom water temperature. Geochemistry, Geophysics, Geosystems, 5 (12), 1–10.

Robbins, L., Hansen, M., Kleypas, J. and Meylan, S. (2010). $CO_2$ calc: A user-friendly seawater carbon calculator for Windows, Max OS X, and iOS (iPhone): U.S. Geological Survey Open-File Report 2010–1280, 17 p.

Rosenthal, Y., Boyle, E. and Slowey, N. (1997). Environmental controls on the incorporation of magnesium, strontium, fluorine and cd into benthic foraminiferal shells from little bahama bank: Prospects for thermocline paleoceanography, Geochim. Cosmochim. Acta, 61, 3633–3643.

Rudels, B., Jones, E.P., Anderson, L.G., and Kattner, G. (1994). On the intermediate depth waters of the Arctic Ocean, *in* The Polar Oceans and Their Role in Shaping the Global Environment (eds O. M. Johannessen, R. D. Muench and J. E. Overland), American Geophysical Union, Washington, D. C. doi: 10.1029/GM085p0033.

Rudels, B., Anderson, L., Eriksson, P., Fahrbach, E., Jakobsson, M., Jones, E. P., Melling, H., Prinsenberg, S., Schauer, U. and Yao, T. (2012). Observations in the Ocean, *in* Lemke, P., ed., Arctic Climate Change: The ACSYS Decade and Beyond, Volume 43, Springer, 117–198.

Shakhova, N., Semiletov, I., Salyuk, A., Yusupov, V., Kosmach, D., Gustafsson, Ö. (2010), Extensive methane venting to the atmosphere from sediments of the East Siberian Arctic Shelf. Science, 327, 1246–1250.

Shakhova, N., Semiletov, I., Leifer, I., Sergienko, V., Salyuk, A., Kosmach, D., Chernykh, D., Stubbs, C., Nicolsky, D., Tumskoy, V., Gustafsson, Ö. (2014), Ebullition and storm-induced methane release from the East Siberian Arctic Shelf. Nature Geoscience 7, 64–70.

Schönfeld, J., Alve E., Geslin, E., Jorissen, F., Korsun, S. and Spezzaferri, S. (2012). The fobimo (foraminiferal bio-monitoring) initiative – towards a standardised protocol for soft-bottom benthic foraminiferal monitoring studies. Marine Micropaleontology, 94–95, 1–13.

Schuur, E. A. G., McGuire, A. D., Schadel, C., Grosse, G., Harden, J. W., Hayes, D. J., Hugelius, G., Koven, C. D., Kuhry, P., Lawrence, D. M., Natali, S. M., Olefeldt, D., Romanovsky, V. E., Schaefer, K., Turetsky, M. R., Treat, C. C., Vonk, J. E. (2015). Climate change and the permafrost carbon feedback. Nature, 520, 171–179.

Scott, D.B., Mudie, P.J., Baki, V., MacKinnon, K.D., Cole, F.E., (1989). Biostratigraphy and Late Cenozoic paleoceanography of the Arctic Ocean: foraminiferal, lithostratigraphic, and isotopic evidence. Geological Society of America Bulletin 101, 260–277.

Scourse, J., Kennedy, H., Scott, G. and Austin, W. (2004). Stable isotopic analyses of modern benthic foraminifera from seasonally stratified shelf seas: disequilibria and the 'seasonal effect', The Holocene, 14 (5), 747–758.

Serreze, M. C., and Barry. R. G. (2011). Processes and impacts of Arctic amplification: A research synthesis. *Global and Planetary Change*, 77 (1–2), 85–96.

Steele, M., Morison, J., Ermold, W., Rigor, I., and Ortmeyer, M. (2004). Circulation of summer Pacific halocline water in the Arctic Ocean, *J. Geophys. Res.*, 109, C02027.

Stein, R. (2008). Chapter six: Quaternary variability of palaeoenvironment and its sedimentary record, in Arctic Ocean Sediments: Processes, Proxies, and Paleoenvironment, Developments in Marine Geology, vol. 2, edited by R. Stein, pp. 287–437, Elsevier.

Steuerwald, B.A. and Clark, D.L. (1972). *Globigerina pachyderma* in Pleistocene and Recent Arctic Ocean sediments. J. Paleontol, 46, 573–580.

Stranne, C., O'Regan, M., Dickens, G. R., Crill, P., Miller, C. G., Preto, P. and Jakobsson, M. (2016).

Dynamic simulations of potential methane release from East Siberian continental slope sediments, Geochemistry, Geophysics, Geosystems, 17 (3), 872–886.

Tisserand, A. A., Dokken, T. M., Waelbroeck, C., Gherardi, J.-M., Scao, V., Fontanier, C. and Jorissen, F (2013). Refining benthic foraminiferal Mg/Ca-temperature calibrations using core-tops from the western tropical Atlantic: Implication for paleotemperature estimation. Geochemistry, Geophysics, Geosystems, 14 (4), 929–946.

Thornton, B.F. and Crill, P. (2015). Arctic permafrost: Microbial lid on subsea methane. Nature Climate Change 5, 723–724.

Toyofuku, T., Kitazato, H., Kawahata, H., Tsuchiya, M. and Nohara M. (2000). Evaluation of Mg/Ca thermometry in foraminifera: Comparison of experimental results and measurements in nature. Paleoceanography, 15, 456–464.

Toyofuku, T., De Nooijer, L.J., Yamamoto, H., Kitazato, H. (2008). Real-time visualization of calcium ion activity in shallow benthic foraminiferal cells using the fluorescent indicator Fluo-3AM. Geochem. Geophys. Geosyst. 9, Q05005.

van Raden, U., Groeneveld, J., Raitzsch, M. and Kucera M. (2011). Mg/Ca in the planktonic foraminifera *Globorotalia inflata* and *Globigerinoides bulloides* from western mediterranean plankton tow and core top samples, Marine Micropaleontology, 78, 101–112.

Varekamp, J. C., Thomas, E., Altabet, M., Cooper, S., Brinkhuis, H., Sangiorgi, F., Donders, T. and Buchholtz ten Brink, M. (2010). Environmental Change in Long Island Sound in the Recent Past: Eutrophication and climate change. Final Report LISRF Grant CWF 334-R (FRS 525156).

Vilks, G. (1975). Comparison of *Globorotalia pachyderma* (Ehrenberg) in the water column and sediments of the Canadian Arctic, J. Foraminiferal Res., 5 (4), 313–325.

Volkmann, R. (2000). Planktic foraminifers in the outer Laptev Sea and the Fram Strait – Modern distribution and ecology. J. Foraminiferal Res., 30 (3), 157–176.

Vonk, J. E. and Gustafsson, Ö. (2013). Permafrost-carbon complexities. Nature Geoscience, 6, 675–676.

Walsh, J. J., C. P. McRoy, L. K. Coachman, J. J. Georing, J. J. Nihoul, T. E. Whitledge, T. H. Blackburn, P. L. Parker, C. D. Wirick, P. G. Shuert, J. M. Grebmeier, A. M. Springer, R. D. Tripp, D. A. Hansell, S. Djenidi, E. Deleersnijder, K. Henriksen, B. A. Lund, P. Andersen, F. E. Muller-Karger, and K. Dean (1989), Carbon and nitrogen cycling within the Bering/Chukchi Seas: Source regions for organic matter effecting AOU demands of the Arctic Ocean. Prog. Oceanogr., 22, 277–259.

Walton, W. (1952). Techniques for recognition of living foraminifera., Contrib. Cushman Found. Foraminiferal Res., 3, 56–60.

Wedepohl, K.H. (1978). Handbook of Geochemistry, Vol. II/5. Berlin–Heidelberg–New York. Springer-Verlag.

Westbrook, G.K. et al., (2009). Escape of methane gas from the seabed along the West Spitsbergen continental margin. Geophys. Res. Lett. 36, L15608.

Wollenburg, J. (1995). Benthic foraminiferal assemblages in the Arctic Ocean: indicators for water mass distribution, productivity, and sea ice drift. Berichte zur Polarforschung, 179, 227 pp.

Wollenburg, J.E. and Mackensen, A. (1998a). Living benthic foraminifers from the central Arctic Ocean: faunal composition, standing stock and diversity. Marine Micropaleontology 34, 153–185.

Wollenburg, J. E. and Mackensen, A. (1998b). On the vertical distribution of living (Rose Bengal stained) benthic foraminifers in the Arctic Ocean, Journal of foraminiferal research 28 (4), 268–285.

Wollenburg, J.E., Kuhnt, W., Mackensen, A., (2001). Changes in Arctic Ocean paleoproductivity and hydrography during the last 145 kyrs: the benthic foraminiferal record. Paleoceanography 16, 65–77.

Wollenburg, J.E., Mackensen, A., Kuhnt, W. (2007). Benthic foraminiferal biodiversity response to a changing Arctic palaeoclimate in the last 24.000 years. Palaeogeography, Palaeoclimatology, Palaeoecology 255, 195–222

Woodgate, R. A., K. Aagaard, and Weingartner, T. J. (2005). A year in the physical oceanography of the Chukchi Sea: Moored measurements from autumn 1990–1991, Deep Sea Res., Part II, 52 (24–26), 3116–3149.

World Ocean Atlas (WOA), http://www.nodc.noaa.gov/OC5/woa13/

World Ocean Database (WOD), http://www.nodc.noaa.gov/OC5/WOD/pr_wod.html

Yu, J. and Elderfield, H. (2008). Mg/Ca in the benthic foraminifera *Cibicidoides wuellerstorfi* and *Cibicidoides mundulus*: Temperature versus carbonate ion saturation, *Earth and Planetary Science Letters*, 276, 129–139.

Zeebe, R.E. and Wolf-Gladrow, D.A. (2001). $CO_2$ in Seawater: Equilibrium, Kinetics, Isotopes, xiii. Elsevier, Amsterdam. 346 pp.

**Figure 1.** Location of the 42 Arctic Ocean study sites used to build the field Mg/Ca–temperature calibration. Pink circles; 25 Rose Bengal stained multicore (MC) and kastenlot (KL) sites retrieved during the *SWERUS-C3* expedition. Grey circles; 16 radiocarbon dated core top sites. Star; location of the Mg/Ca pilot study. Equidistance of the contour lines is 1000 m. Geographic regions relevant to this study are CS, Chukchi Shelf; HC, Herald Canyon; AP, Arliss Plateau; ESSs, Eastern Siberian Sea slope; LS, Laptev Shelf; MB, Makarov Basin; AB, Amundsen Basin; LR, Lomonosov Ridge; MJR, Morris Jesup Rise.

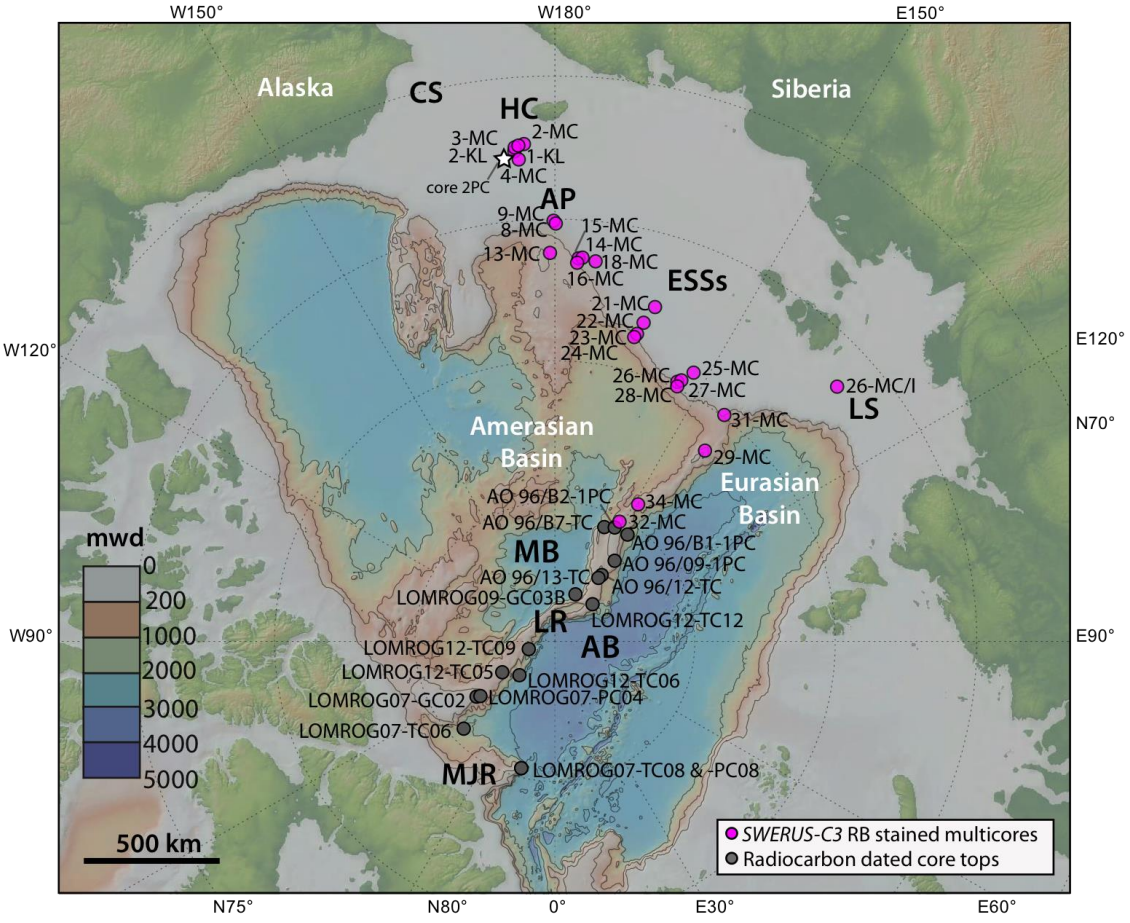

**Figure 2.** Representative light microscope views of foraminiferal samples from this study. Left, foraminifera in the sediment coarse fraction (SWERUS L2-16-MC1, 0-1 cm showing a Rose Bengal stained (live) specimen of *Cassidulina neoteretis* surrounded by unstained fossils. Right, close up view of the same stained specimen compared to a non-stained specimen of the same species (core top AO96/12-TC, 0-1 cm).

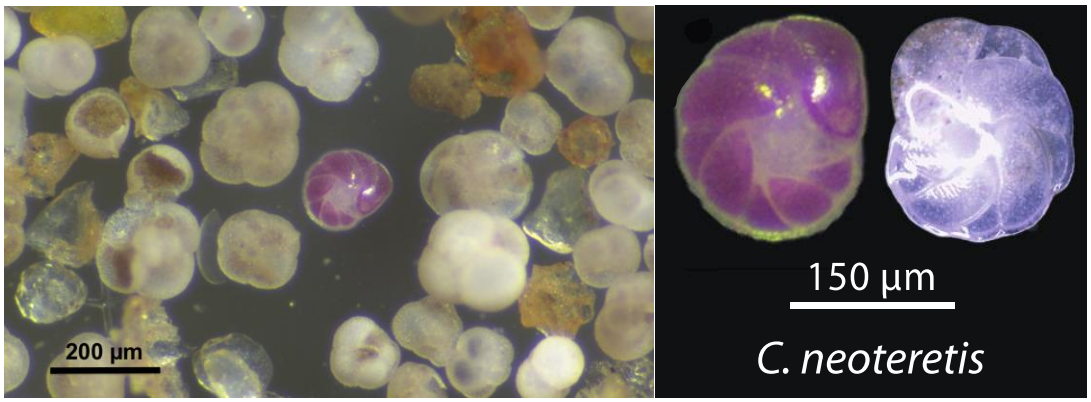

**Figure 3.** Composite bottom water hydrological data across all of the 41 study sites. (a) bottom water temperatures (BWT), (b) salinity, (c) calculated seawater $\Delta[CO_3^{2-}]$ and (d) SWERUS-C3 oxygen. For data source information see Table 1. Horizontal dashed lines identify the limits of the typical Arctic water masses named at the right side of the plot. Data points with bigger marker size correspond to data collected from the Chukchi Shelf (Herald Canyon) while the star depicts the Laptev Shelf site. The $\Delta[CO_3^{2-}]$ and oxygen values between these two regions differ the most as a result of old and nutrient rich Pacific waters bathing the Herald Canyon sites and thus creating more hydrological differences from this composite.

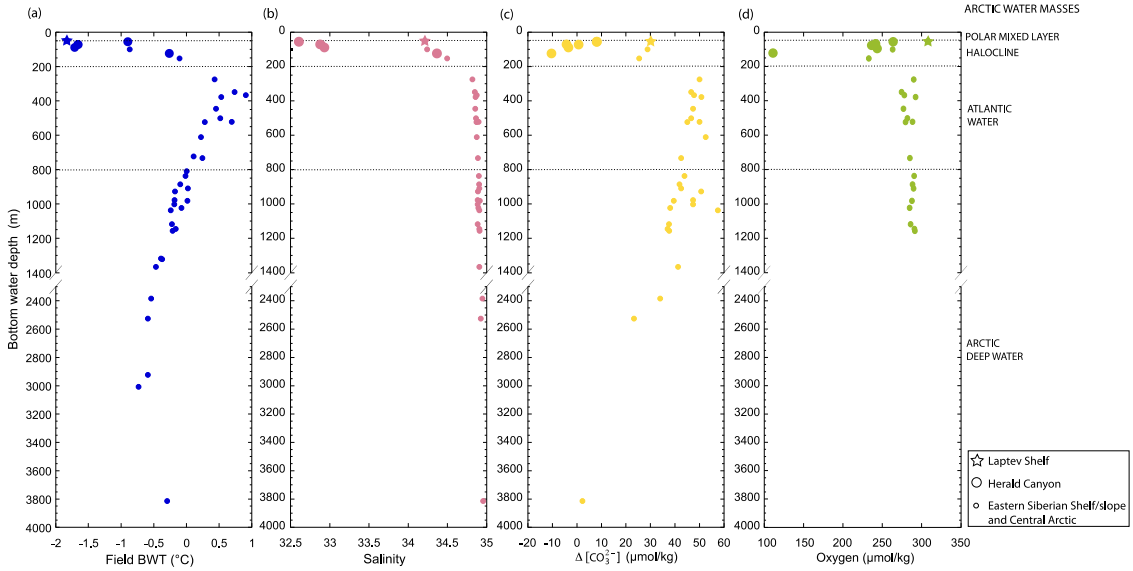

**Figure 4.** Bottom water temperature differences between observed (SWERUS CTD data covering the upper 1200 mwd) and nearest neighbor values derived from online ocean databases (World Ocean Database, WOD; and World Ocean Atlas, WOA): (a) WOD – WOA temperatures; (b) SWERUS-C3 CTD – WOD temperatures; (c) SWERUS-C3 CTD – WOA temperatures.

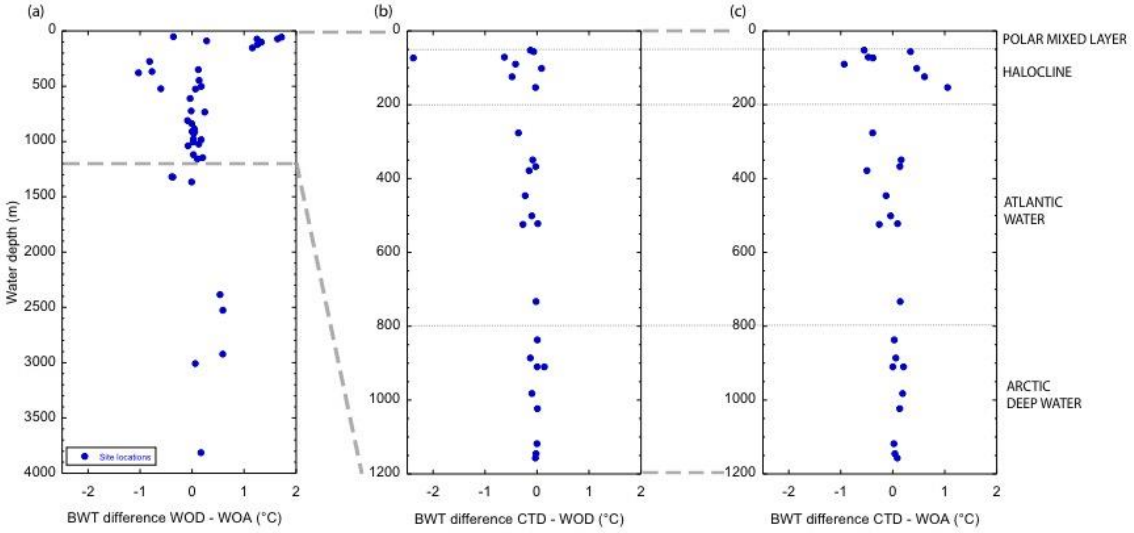

**Figure 5.** Spatial distribution and proportions of the 6 species of interest in this study as observed in 'live' benthic foraminiferal assemblages (Rose Bengal stained specimens) from the *SWERUS-C3* 25 multicore (MC) and kastenlot (KL) core top samples (pink circles). Counts were made on the >125 µm stained species found in the topmost 6 cm of each multicore. At these sites, the main control on assemblage composition is water depth, reflecting the different Arctic Ocean layers. *N. labradorica* and *E. clavatum* are restricted to the shelves; *C. neoteretis* and *Q. arctica* prefer continental slope and top ridge settings; *O. tener* and *C. wuellerstorfi* occur in the deepest cores. Geographic regions were the multicores were retrieved are are HC, Herald Canyon; AP, Arliss Plateau; ESSs, Eastern Siberian Sea slope; LS, Laptev Shelf; LR, Lomonosov Ridge. Equidistance of the contour lines is 500 m.

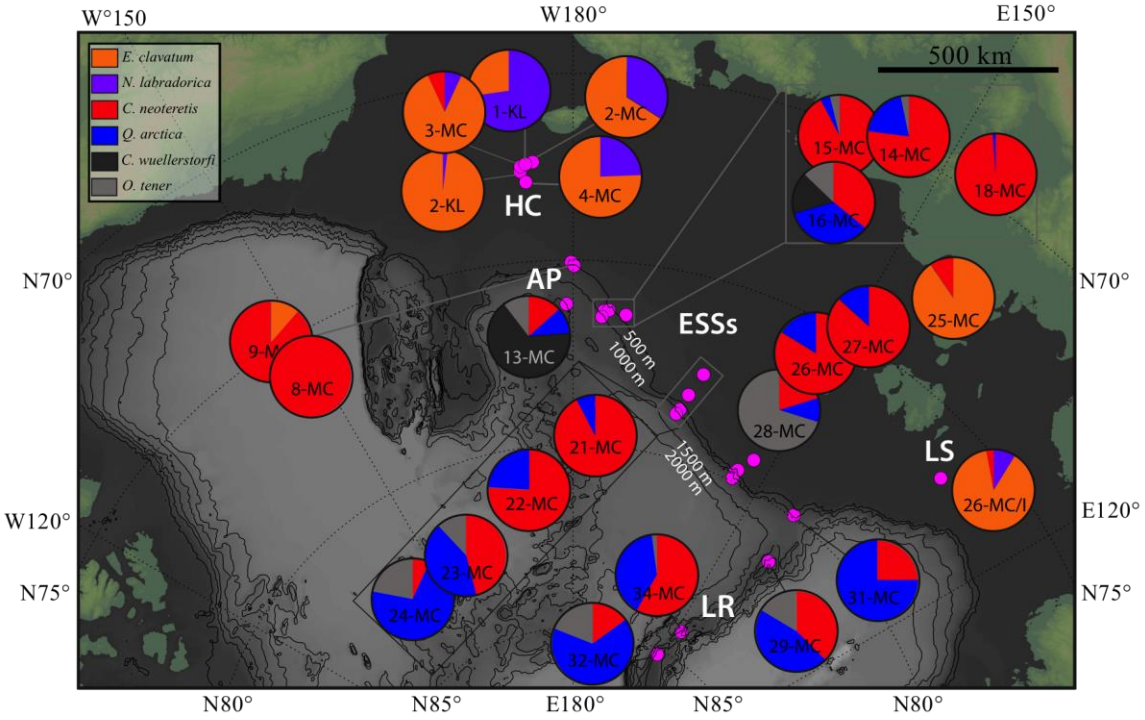

**Figure 6.** Water depth distribution of stained (living) individuals of the 6 species (sites and samples as in Figure 5). Temperature and salinity of the composite sites are depicted in blue and pink dots respectively. Arctic water masses linked to these depths are shown to the right. *Elphidium clavatum* and *N. labradorica* show preference for cold, fresh and nutrient rich halocline waters. *Cassidulina neoteretis* is the most abundant and cosmopolitan species. It shows a pronounced peak in abundance at 280-350 mwd coincident with the upper Atlantic water, which is the warmest Arctic Ocean layer. *Quinqueloculina arctica* and *Oridorsalis tener* show preference for deeper habitats bathed by the deepest Atlantic waters. *Cibicidoides wuellerstorfi*, occurs in only the deepest most core tops associated with Arctic deep water.

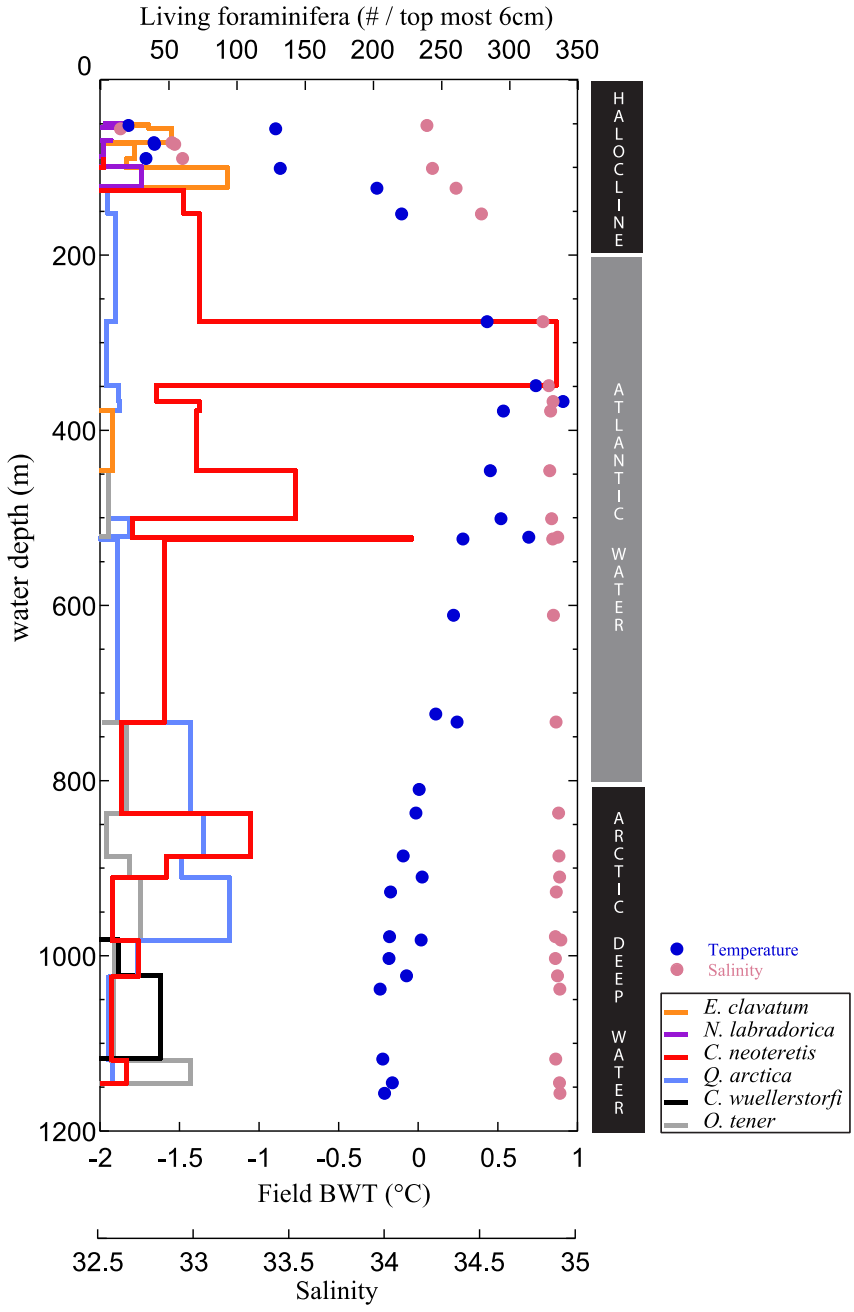

**Figure 7.** Benthic foraminifera Mg/Ca data for the 6 species investigated in this study plotted against field bottom water temperatures (BWT). Pink circles and black crosses distinguish stained and unstained samples respectively. Mg/Ca variability is highest in species inhabiting halocline waters, i.e. *E. clavatum* and *N. labradorica* (panels a and b) where BWT also shows a large gradient. Mg/Ca values of *Q. arctica* (d) are one order of magnitude higher than all other species because it builds its test using high-Mg calcite whereas the others produce low-Mg calcite.

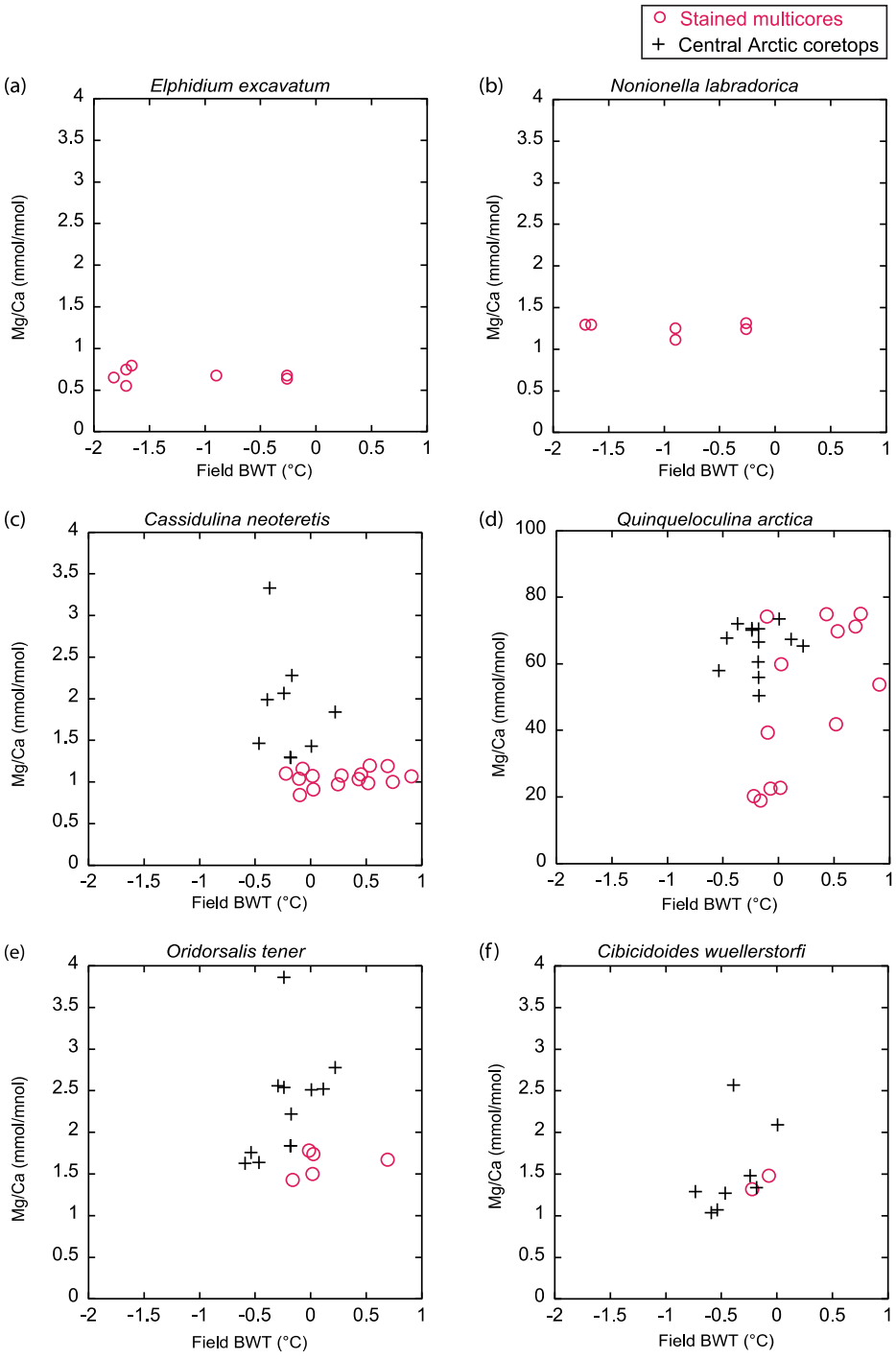

**Figure 8.** Mg/Ca data and field bottom water temperature (BWT) relationships based on stained foraminifera for the six studied species (from (a) to (f)) and linear regressions with associated equations. A suggested calibration based only on two *C. wuellerstorfi* samples is suggested as a dashed line.

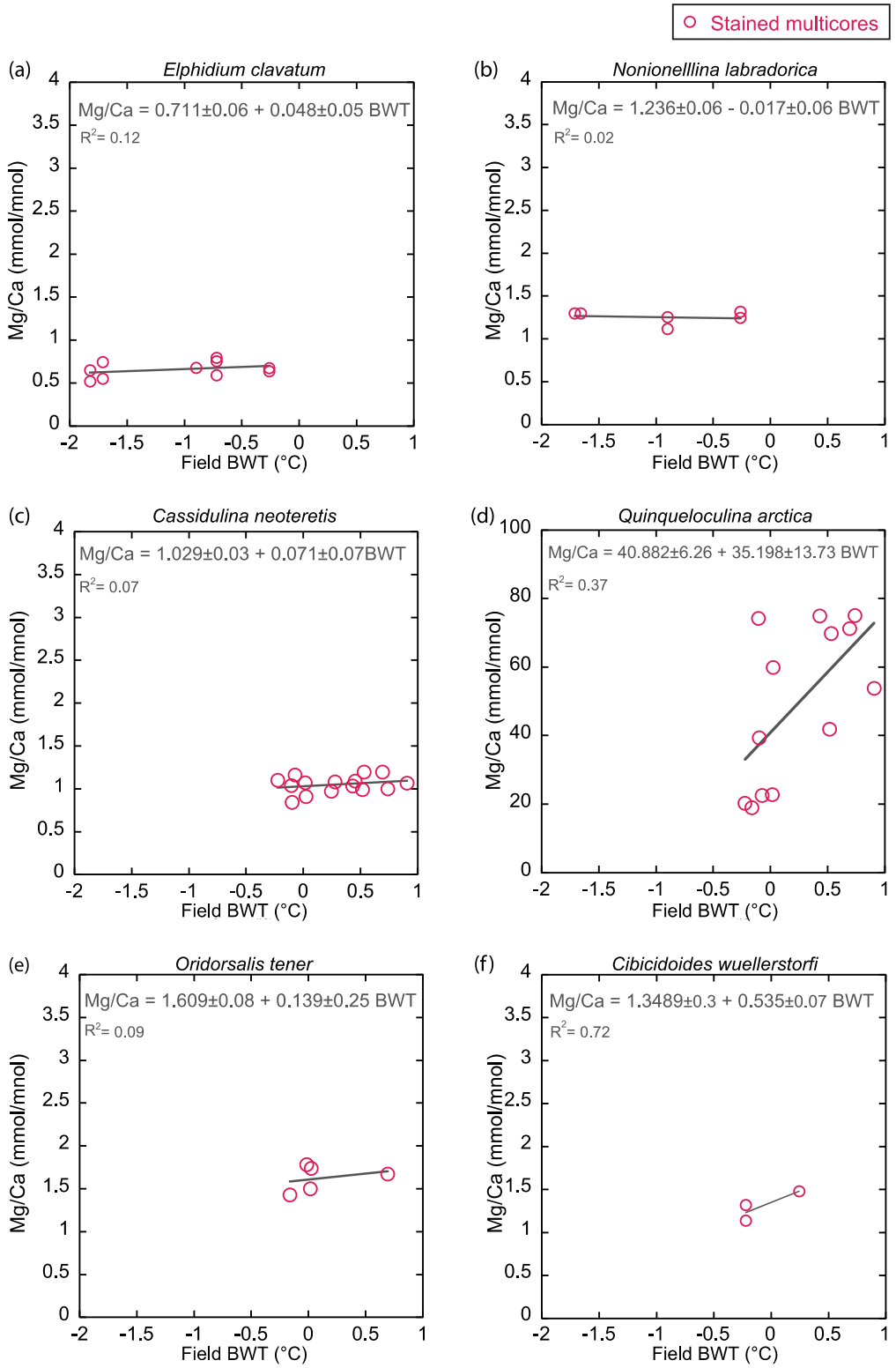

**Figure 9.** Depth-Mg/Ca plots of the six species showing that only stained *Q. arctica* has a strong gradient ($R^2$=0.77) and therefore might be affected by $\Delta[CO_3^{2-}]$ and or dissolution.

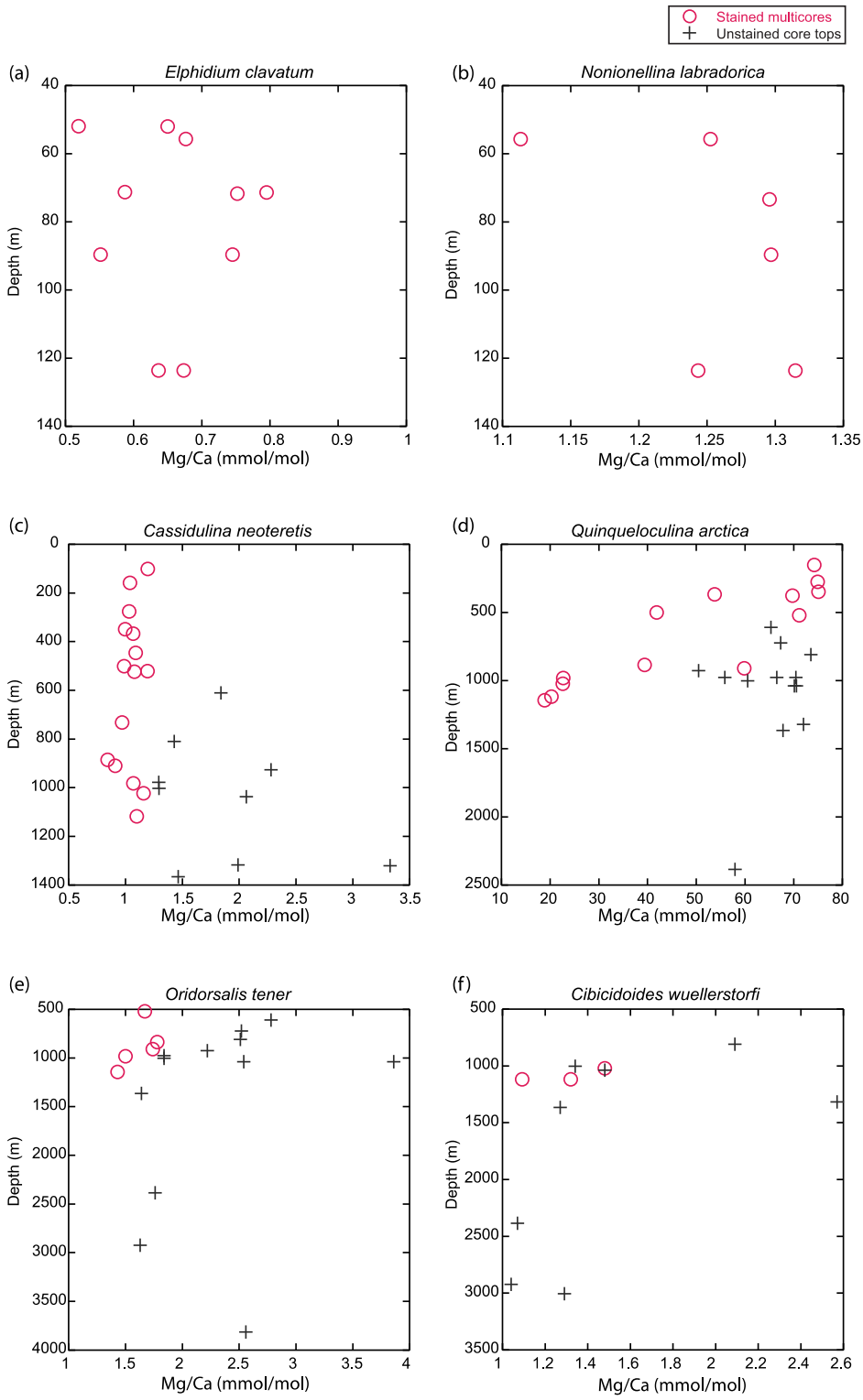

**Figure 10.** Bottom water carbonate ion effect and temperature relationship at all studied sites. The plot shows a change in gradient from steady $\Delta[CO_3^{2-}]$ values to more variable below -0.5 °C, with exception to 4-MC, 1-KL and 21-MC Pacific water sourced sites. This suggests that benthic foraminiferal Mg/Ca values with negative temperatures, i.e. shelf sites, could track $\Delta[CO_3^{2-}]$ changes rather than BWT.

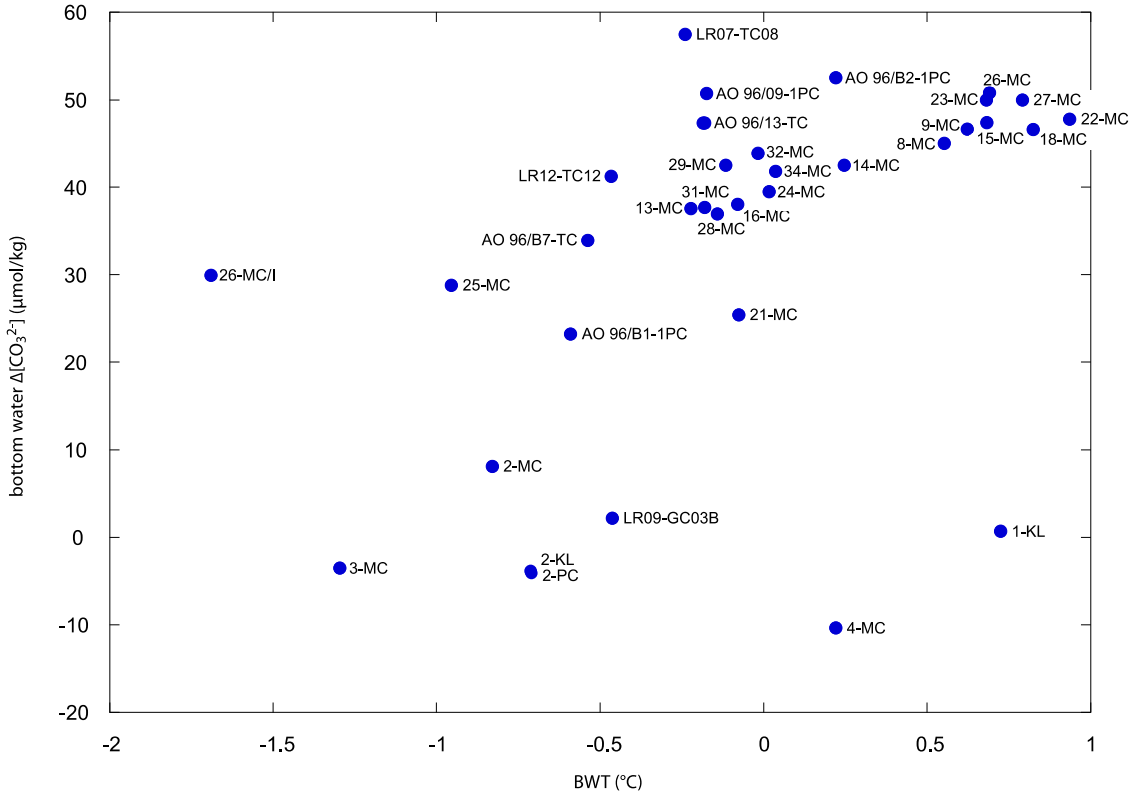

**Figure 11.** Benthic foraminifera Mg/Ca data and their effect to $\Delta[CO_3^{2-}]$. This correlation shows that unstained core tops in species (c), (e) and (f) bathed under more saturated waters present higher Mg/Ca ratios. Stained Q. arctica (d) show a positive relationship apart from Pacific-Arctic halocline water site 21-MC.

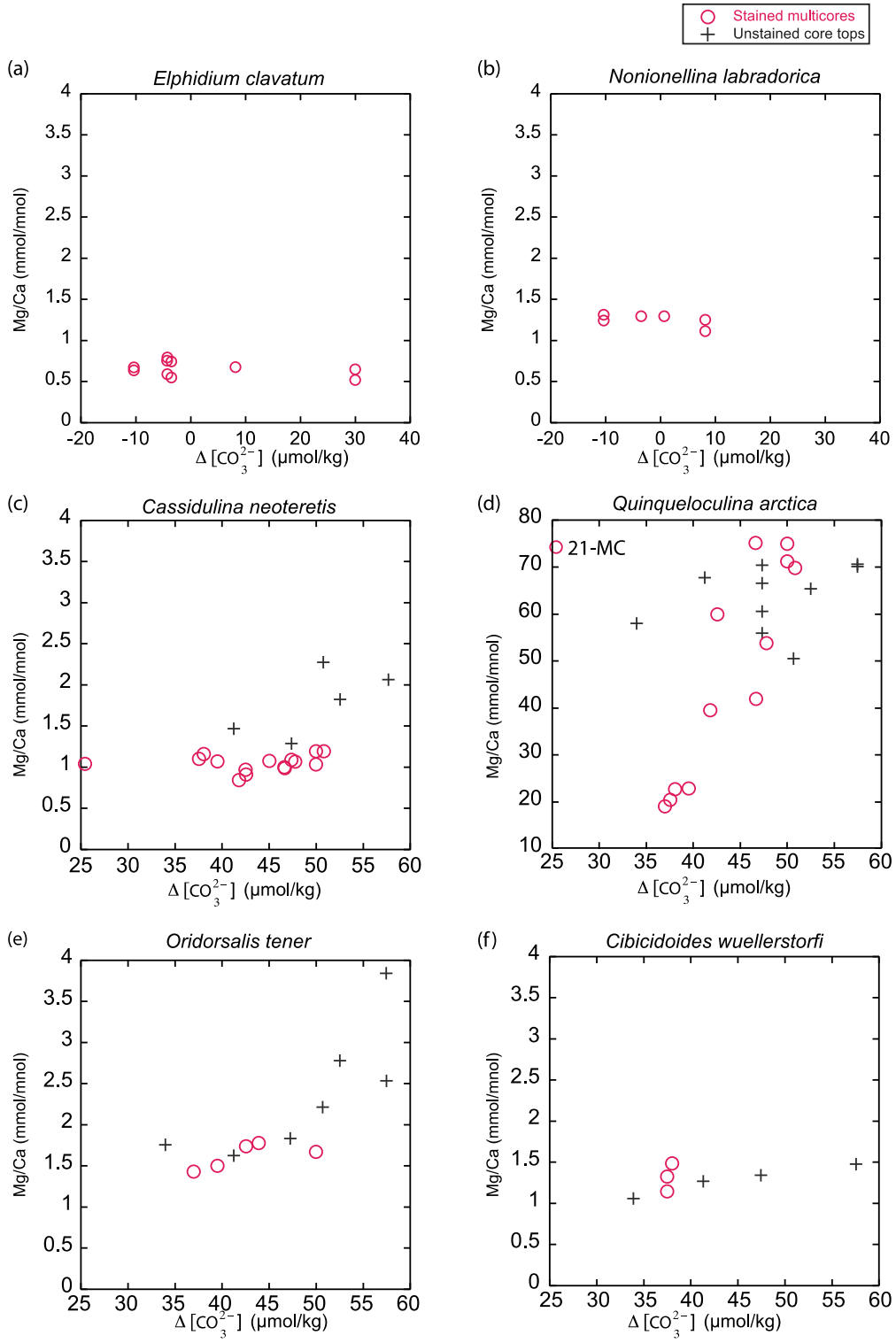

**Figure 12.** Salinity relationship to Mg/Ca in the halocline living Arctic species *E. clavatum* (a) and *N. labradorica* (b). Despite the low salinity ranges captured, species (b) show a positive correlation, bigger than the one obtained from Mg/Ca–BWT depicted in Figure 8b.

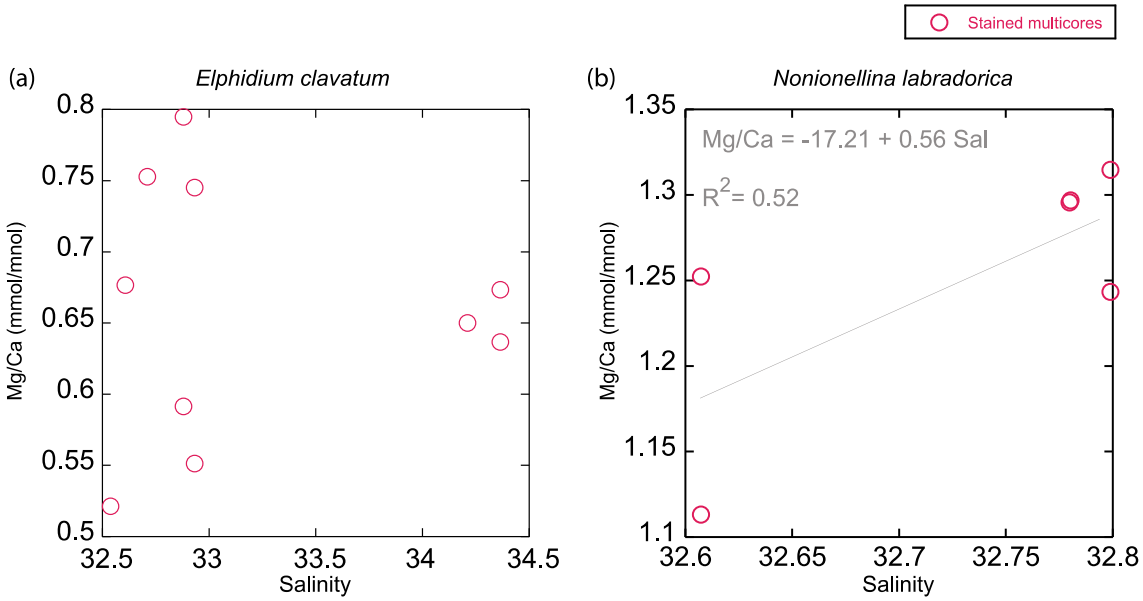

**Figure 13.** Core-top foraminiferal Mg/Ca data measured in four species compared to sample $^{14}C$ age showing a Mg/Ca–age effect. Red circles, modern stained specimens. Black crosses, radiocarbon dated core tops.

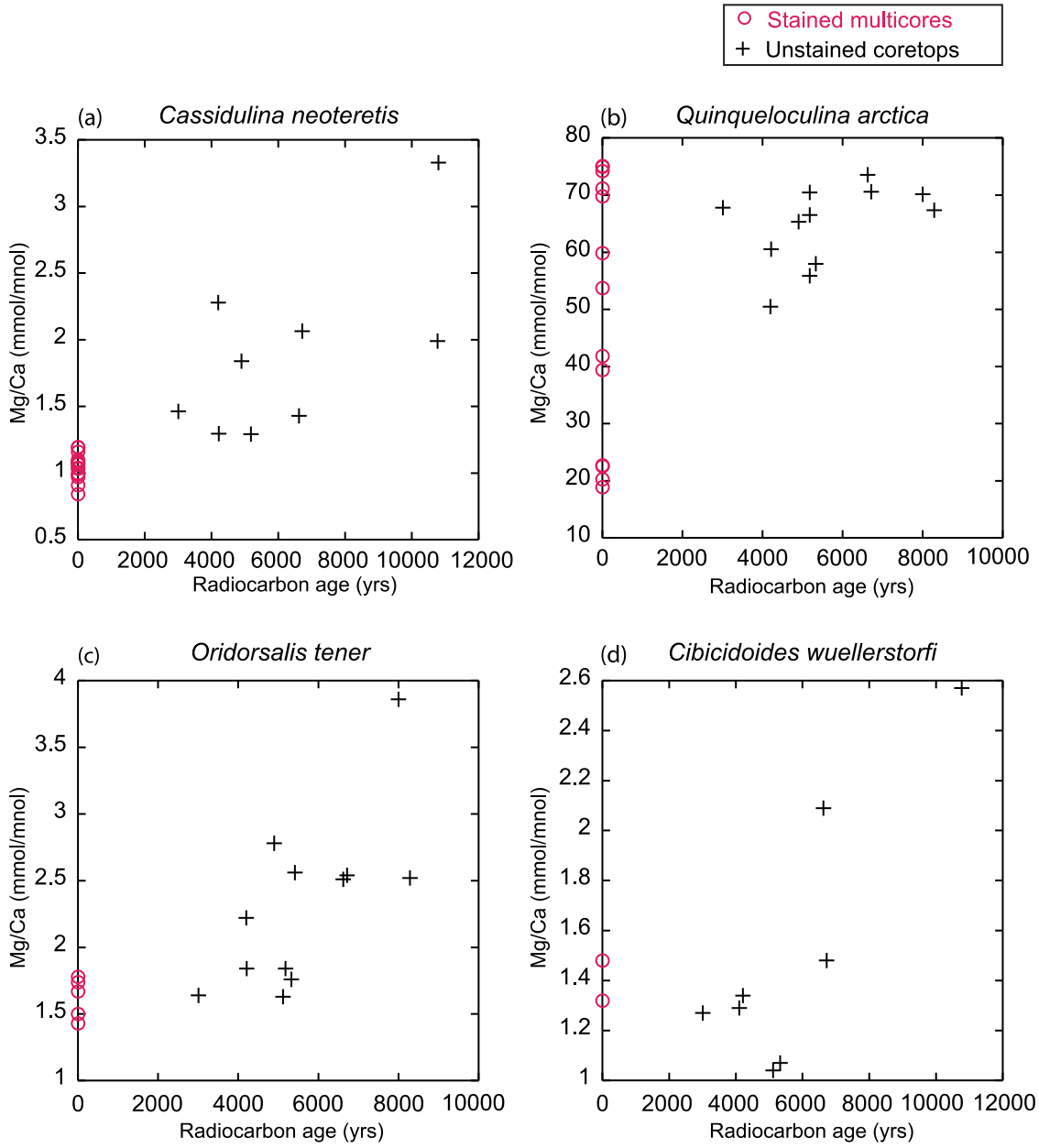

**Figure 14.** Down core Mg/Ca measured in fossil *E. clavatum* from *SWERUS* core L2-2-PC1 retrieved from the Chukchi Shelf (x-symbol). The temperature axis is based on several Mg/Ca–BWT calibration fits. The most reliable fit is given after applying the sensitivity of Varekamp et al. [2010] dataset in our mean *SWERUS-C3* core top data. The applied Varekamp et al. [2010] paleo-BWT results were not depicted since they fall around 10 °C paleo-BWT.

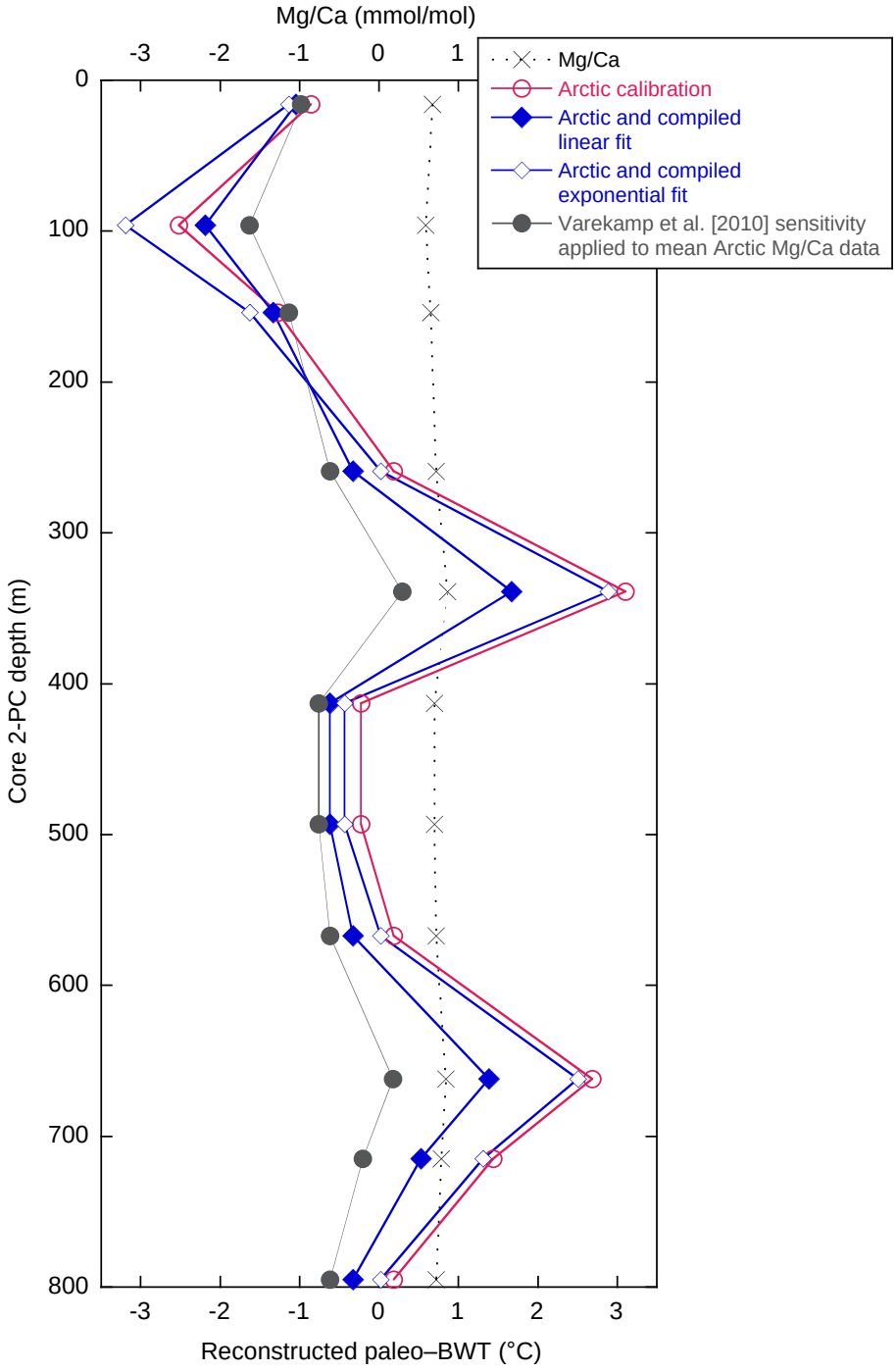

**Figure 15.** Stained foraminifera EDS elemental results (in weight %) from three specimens shown in Plate 1 (*C. neoteretis* 2b, *O. tener* 4b, *C. wuellerstorfi* 6b).

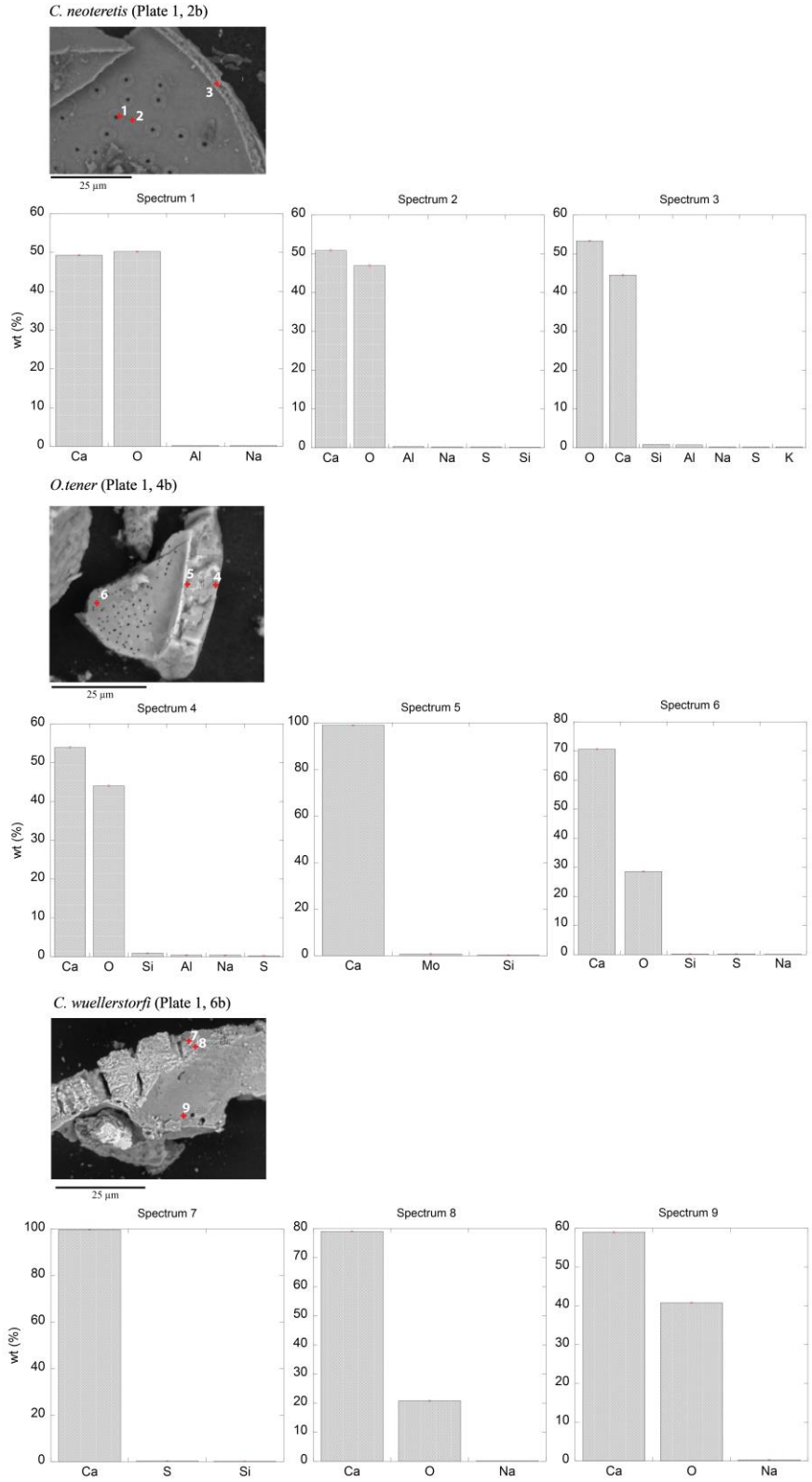

**Figure 16.** Unstained foraminifera EDS elemental results (in weight %) from specimens shown in Plate 2 (*C. neoteretis* 1c, *O. tener* 4b, *C. wuellerstorfi* 5b.

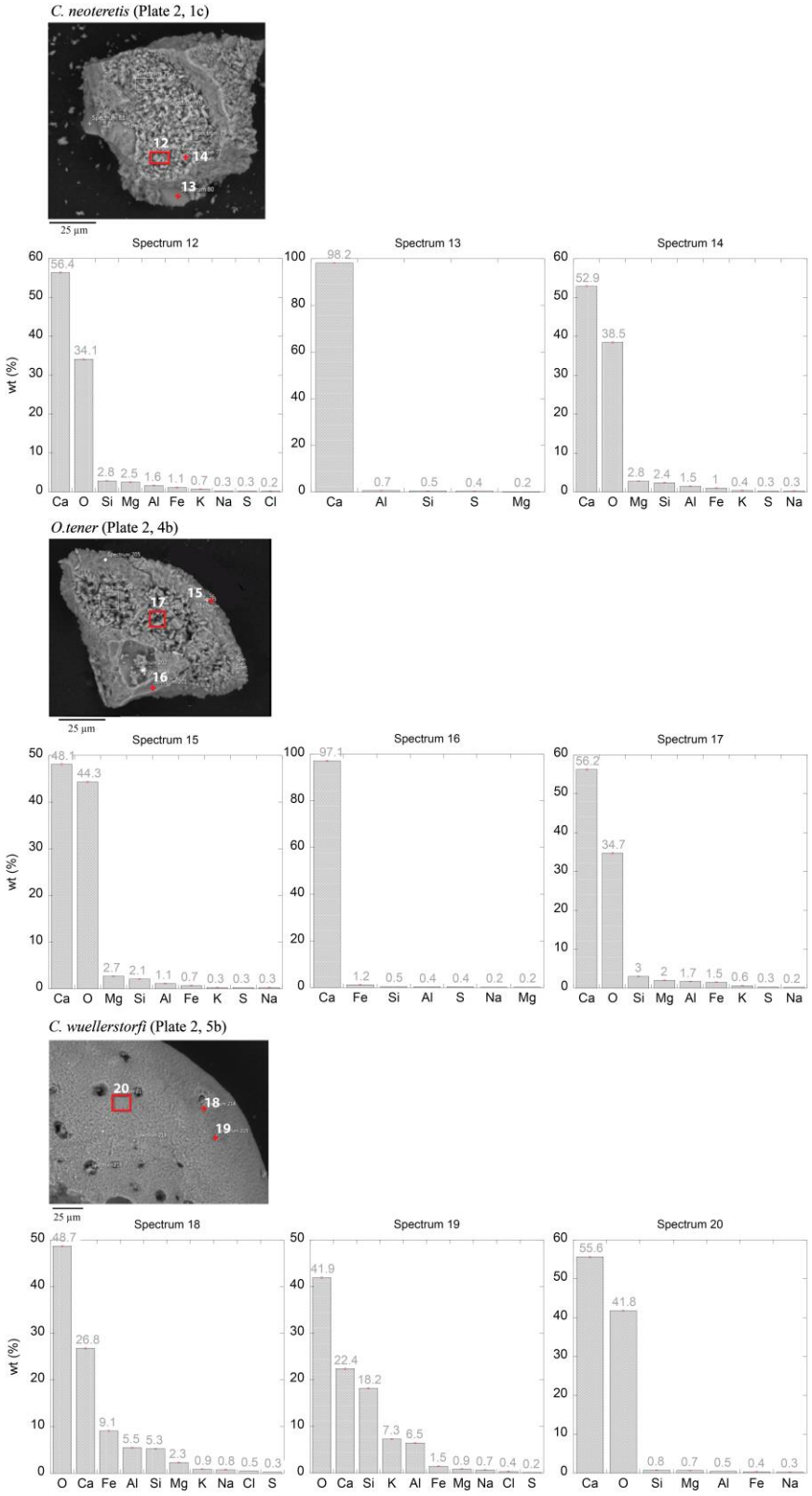

**Figure 17.** Arctic benthic foraminiferal trace metal data for the 6 species investigated in this study compared to published and unpublished data [Gabrielsson, Masters thesis, 2014; Rosenthal MIT/unpublished] from different oceans, excluding *Cassidulina neoteretis* data all compiled from Arctic samples. Zoom in of plot 15 (c) *C. neoteretis* Mg/Ca compilation after excluding unstained samples. The Mg/Ca and field BWT axes scales are customized per species reflecting the range of values typical for the taxon. Note that radiocarbon dated core top Mg/Ca values (crosses) are off-trend compared to the compilation and therefore were not included in the Mg/Ca-BWT regression calculations.

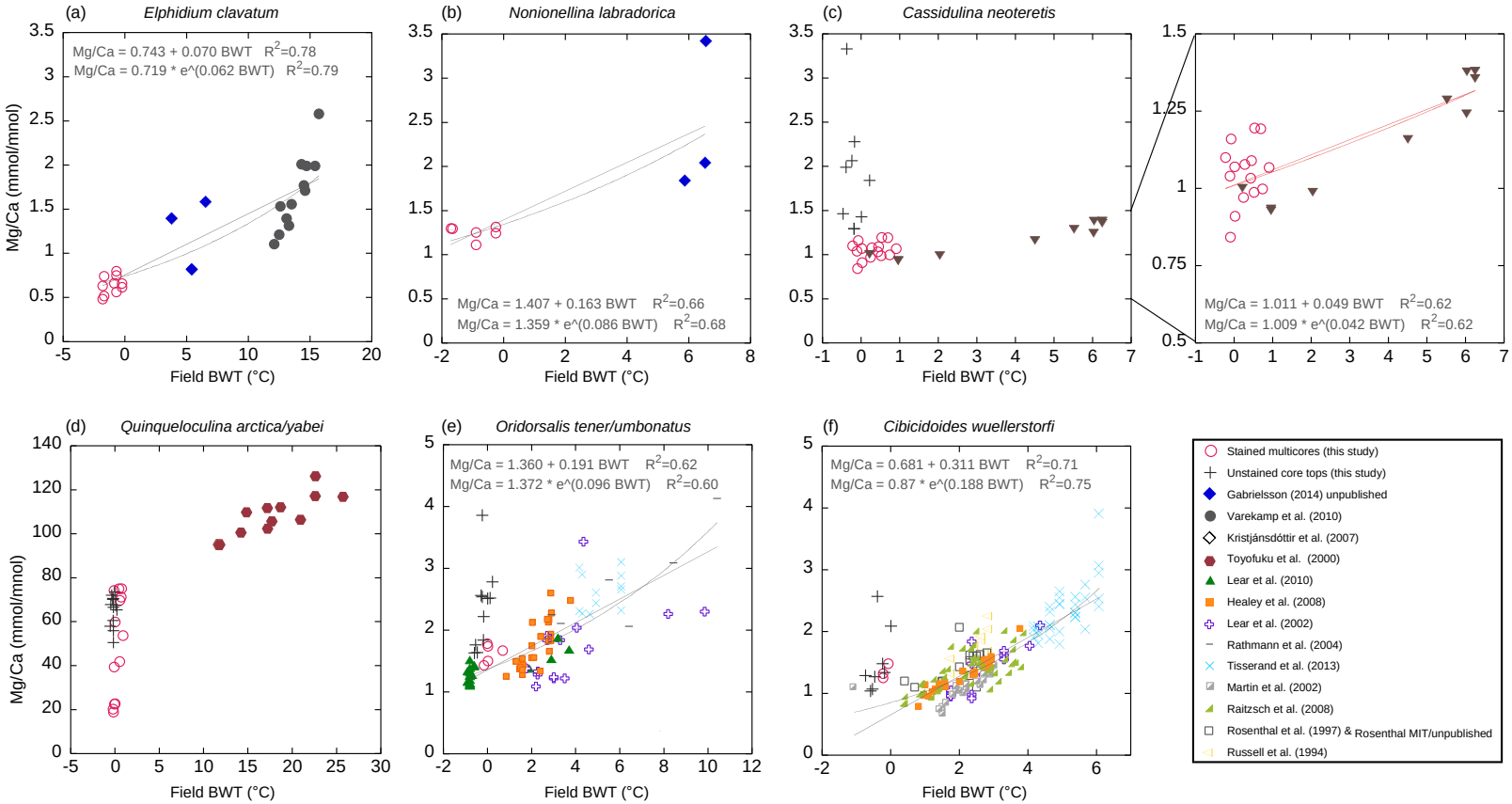

**Figure 18.** Core top foraminiferal Mg/Ca data vs. field salinity data in *E. clavatum* and *N. labradorica.* Red circles show data from this study (stained multicore samples from the Arctic halocline) together with existing unpublished data [Gabrielsson, Masters thesis, 2014] from the southern Baltic Sea and Skagerrak (North Sea).

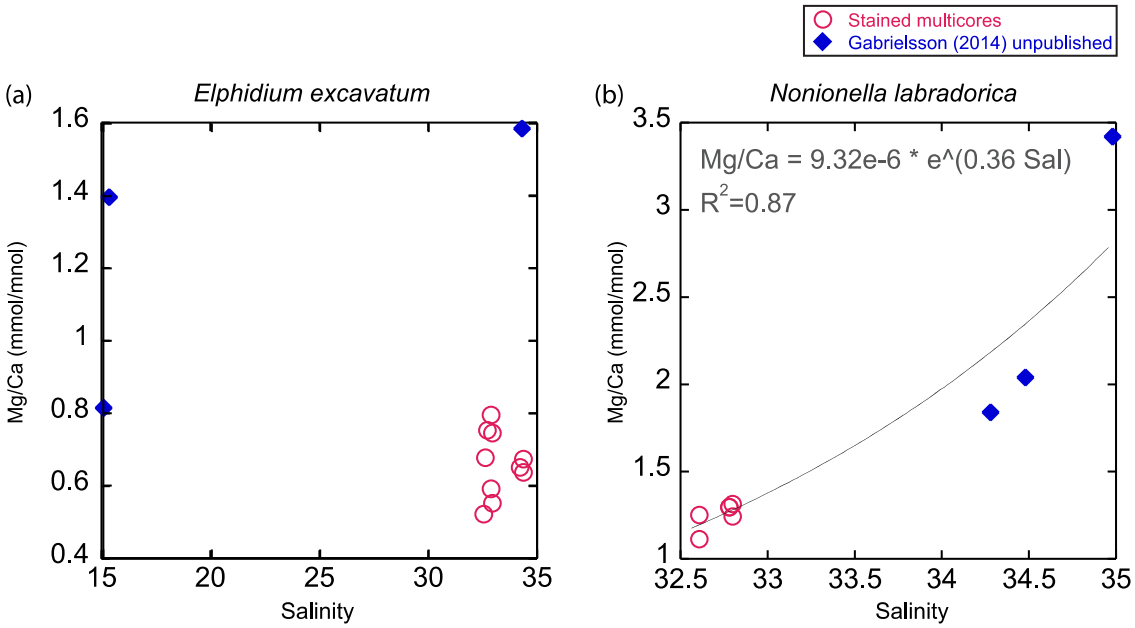

## Appendix

**Figures.** ODV plots constructed using the CARINA database.

**Figure A.** Chukchi to Atlantic water temperature depth profile section.

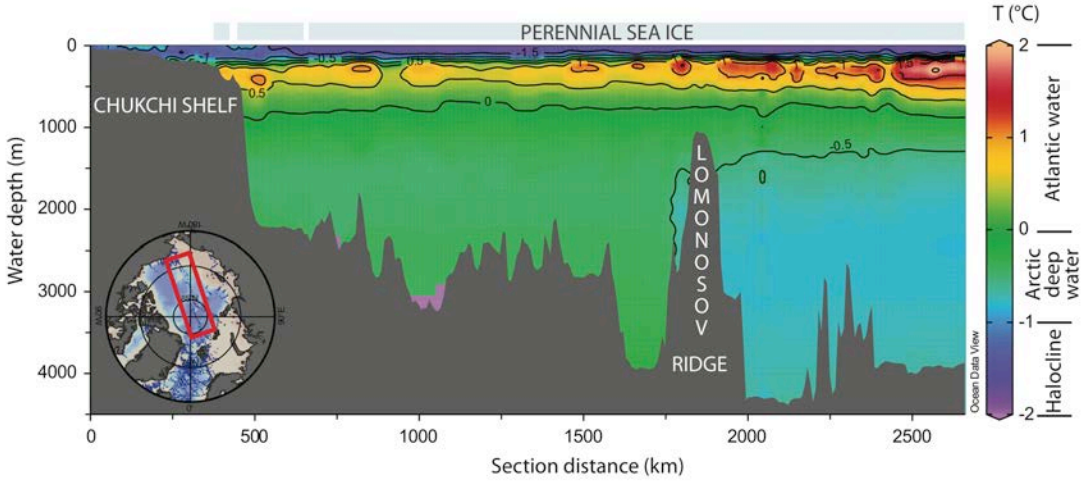


**Figure B.** Chukchi to Atlantic salinity profile of the water column.

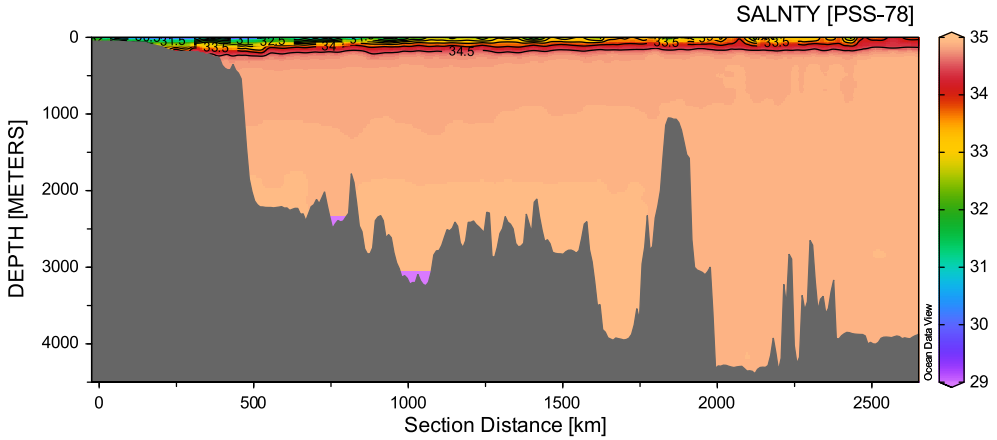


**Figure B1.** Chukchi to Atlantic salinity zoom in of the upper 1000 m of water depth. We can observe fresher water closer to the Bering Sea brought by Pacific water inflow to the Arctic.

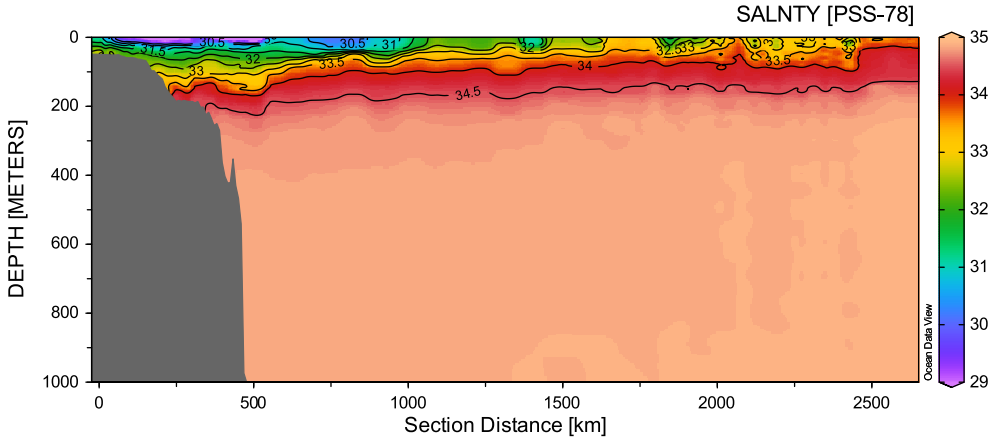

**Figure C.** Chukchi to Atlantic nutrient concentrations (phosphate and silicate). Observe the higher nutrient concentrations at the waters bathing the Chukchi Shelf, product of Pacific Water inflow through the Bering Strait.

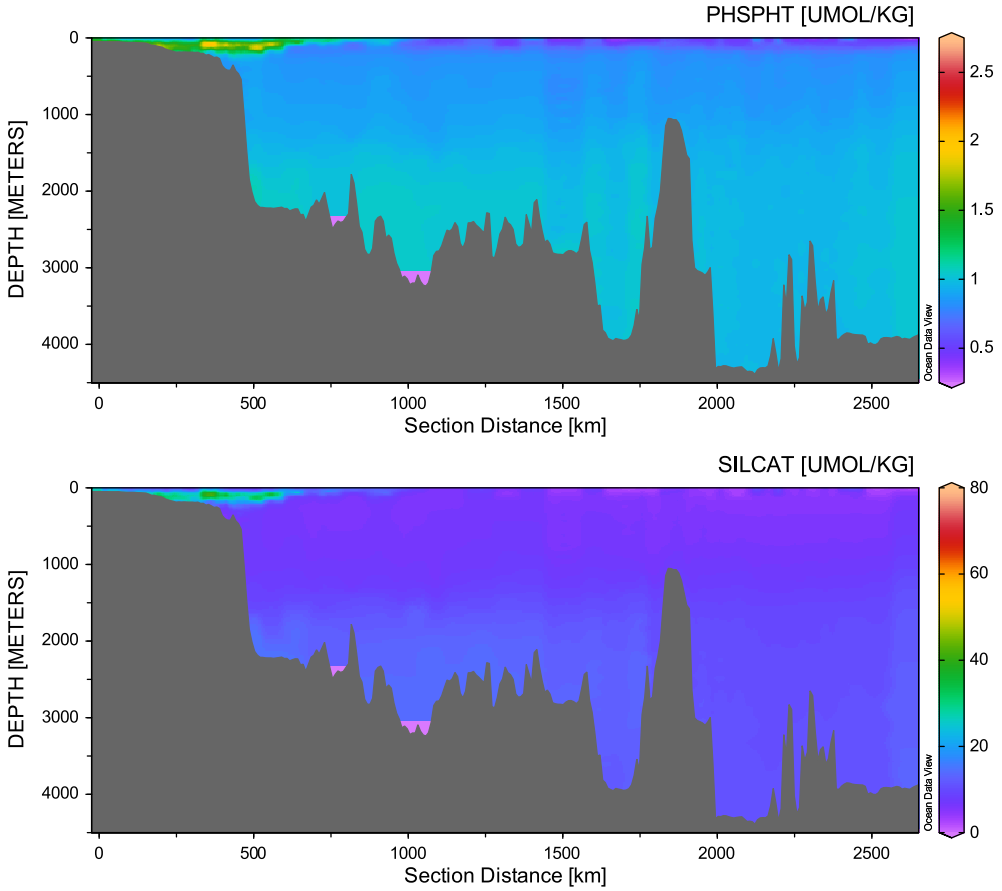

## Appendix

## Tables.

**Table A.** Field bottom water temperature comparison at each site using World Ocean database (wod, red columns), in situ CTD stations (ctd, green columns), wod and ctd combined together (orange columns) and World Ocean Atlas (woa, purple columns). The study is built on a 50 km cell grid around each site and depicts the minimum, maximum, average and distance to station for each temperature data source.

| Site | wod.Tmin | wod.Tmax | wod.Tavg | wod.Tstd | wod.numOK | ctd.Tmin | ctd.Tmax | ctd.Tavg | ctd.Tstd | ctd.numOK | ctd.Tnearest | ctd.minDist_km | ctd_wod.Tmin | ctd_wod.Tmax | ctd_wod.Tavg | ctd_wod.Tstd | ctd_wod.numOK | woa.Tmin | woa.Tmax | woa.Tam | woa.minDist_km |
|---|---|---|---|---|---|---|---|---|---|---|---|---|---|---|---|---|---|---|---|---|---|
| AO96/B2-1PC | 0.1710 | 0.2549 | 0.2213 | 0.0357 | 6 | 0.3053 | 0.3053 | 0.3053 | 0.0000 | 1 | 0.3053 | 43.0787 | 0.1710 | 0.3053 | 0.2333 | 0.0455 | 7 | 0.0849 | 0.3606 | 0.2619 | 3.5984 |
| AO96/B1-1PC | | | | | 0 | | | | | 0 | | | | | | | 0 | -0.8285 | -0.3522 | -0.8285 | 1.6108 |
| AO96/B7-TC | | | | | 0 | | | | | 0 | | | | | | | 0 | -0.7568 | -0.3340 | -0.5369 | 8.0428 |
| A096/09-1PC | -0.2282 | -0.1077 | -0.1739 | 0.0395 | 7 | | | | | 0 | | | -0.2282 | -0.1077 | -0.1739 | 0.0395 | 7 | -0.3424 | -0.1454 | -0.2056 | 4.4171 |
| A096/12-TC | -0.2300 | -0.1500 | -0.1843 | 0.0412 | 3 | | | | | 0 | | | -0.2300 | -0.1500 | -0.1843 | 0.0412 | 3 | -0.2835 | -0.1392 | -0.2058 | 3.0596 |
| AO96/13-TC | -0.2300 | -0.1403 | -0.1802 | 0.0409 | 5 | | | | | 0 | | | -0.2300 | -0.1403 | -0.1802 | 0.0409 | 5 | -0.2777 | -0.1400 | -0.2028 | 3.1635 |
| LOMROG09-GC03B | -0.2926 | -0.2926 | -0.2926 | 0.0000 | 2 | | | | | 0 | | | -0.2926 | -0.2926 | -0.2926 | 0.0000 | 2 | -0.6404 | -0.3352 | -0.4626 | 4.3788 |
| LOMROG12-TC12 | -0.5358 | -0.3464 | -0.4663 | 0.0852 | 4 | | | | | 0 | | | -0.5358 | -0.3464 | -0.4663 | 0.0852 | 4 | -0.8252 | -0.3519 | -0.4581 | 1.8454 |
| LOMROG12-PC11 | -0.6770 | -0.6532 | -0.6658 | 0.0107 | 4 | | | | | 0 | | | -0.6770 | -0.6532 | -0.6658 | 0.0107 | 4 | -0.7397 | -0.3464 | -0.6731 | 10.3917 |
| LOMROG12-TC06 | | | | | 0 | | | | | 0 | | | | | | | 0 | -0.8236 | -0.3549 | -0.7302 | 13.7916 |
| LOMROG07-PC04 | -0.0470 | 0.0584 | 0.0057 | 0.0745 | 2 | | | | | 0 | | | -0.0470 | 0.0584 | 0.0057 | 0.0745 | 2 | 0.0613 | 0.1695 | 0.0946 | 8.7905 |
| LOMROG07-GC02 | 0.0734 | 0.1538 | 0.1136 | 0.0569 | 2 | | | | | 0 | | | 0.0734 | 0.1538 | 0.1136 | 0.0569 | 2 | 0.1006 | 0.1946 | 0.1278 | 0.7797 |
| LOMROG07-TC06 | -0.7340 | -0.7340 | -0.7340 | 0.0000 | 1 | | | | | 0 | | | -0.7340 | -0.7340 | -0.7340 | 0.0000 | 1 | -0.7945 | -0.4113 | -0.7945 | 13.2036 |
| LOMROG07-PC08 | | | | | 0 | | | | | 0 | | | | | | | 0 | -0.2426 | 0.0704 | -0.1593 | 6.1445 |
| LOMROG07-TC08 | -0.3382 | -0.1770 | -0.2395 | 0.0495 | 14 | | | | | 0 | | | -0.3382 | -0.1770 | -0.2395 | 0.0495 | 14 | -0.2929 | 0.0032 | -0.2123 | 6.1435 |
| HLY0503-18TC | -0.6578 | -0.3870 | -0.5639 | 0.1533 | 3 | | | | | 0 | | | -0.6578 | -0.3870 | -0.5639 | 0.1533 | 3 | -0.5909 | -0.2590 | -0.5909 | 8.4051 |
| SWERUS L2-1-KL | -0.0990 | 0.0720 | -0.0271 | 0.0887 | 3 | -1.7143 | -0.7207 | -1.5682 | 0.3006 | 10 | -1.6610 | 0.3341 | -1.7143 | 0.0720 | -1.2126 | 0.7252 | 13 | -1.8449 | 0.0302 | -1.2747 | 4.7017 |
| SWERUS L2-2-MC | -1.8140 | 2.2813 | 0.4793 | 1.5066 | 8 | -1.7334 | -0.3250 | -1.5287 | 0.3407 | 15 | -0.3250 | 6.6881 | -1.8140 | 2.2813 | -0.8303 | 1.3238 | 23 | -1.8377 | -0.0452 | -1.2376 | 6.4117 |
| SWERUS L2 -2-PC | -0.0671 | 1.3000 | 0.7362 | 0.5903 | 5 | -1.7271 | -0.7204 | -1.5919 | 0.2289 | 17 | -0.7204 | 14.7782 | -1.7271 | 1.3000 | -1.0628 | 1.0505 | 22 | -1.8454 | 0.2739 | -1.1879 | 12.2098 |
| SWERUS L2-2-KL | -1.1300 | 1.3000 | 0.4508 | 0.9430 | 6 | -1.7291 | -0.7200 | -1.5880 | 0.2361 | 16 | -0.7200 | 20.6287 | -1.7291 | 1.3000 | -1.0320 | 1.0561 | 22 | -1.8451 | 0.2537 | -1.1902 | 7.4441 |
| SWERUS L2-3-MC | -0.7928 | -0.2000 | -0.4964 | 0.4192 | 2 | -1.7115 | -1.6815 | -1.6963 | 0.0141 | 4 | -1.7115 | 2.6046 | -1.7115 | -0.2000 | -1.2964 | 0.6475 | 6 | -1.8594 | 1.7952 | -0.7756 | 3.0088 |
| SWERUS L2-4-MC | 0.0616 | 0.6392 | 0.3819 | 0.2939 | 3 | -0.2602 | -0.2602 | -0.2602 | 0.0000 | 1 | -0.2602 | 8.6002 | -0.2602 | 0.6392 | 0.2214 | 0.4008 | 4 | -1.7000 | 0.4651 | -0.8714 | 31.3700 |
| SWERUS L2-8-MC | 0.4600 | 0.6999 | 0.6015 | 0.0958 | 9 | 0.3343 | 0.6021 | 0.4450 | 0.1155 | 4 | 0.3343 | 2.9149 | 0.3343 | 0.6999 | 0.5533 | 0.1229 | 13 | 0.3975 | 0.8644 | 0.5389 | 3.1397 |
| SWERUS L2-9-MC | 0.5368 | 0.8691 | 0.7144 | 0.1353 | 8 | 0.5372 | 0.8014 | 0.6216 | 0.1212 | 4 | 0.5705 | 6.4657 | 0.5368 | 0.8691 | 0.6835 | 0.1332 | 12 | 0.1934 | 1.1196 | 0.5828 | 7.7623 |
| SWERUS L2-13-MC | -0.3199 | -0.0300 | -0.2200 | 0.1309 | 4 | -0.2221 | -0.2221 | -0.2221 | 0.0000 | 1 | -0.2221 | 2.7686 | -0.3199 | -0.0300 | -0.2204 | 0.1133 | 5 | -0.3123 | -0.1464 | -0.2426 | 7.2961 |
| SWERUS L2-14-MC | 0.3450 | 0.3450 | 0.3450 | 0.0000 | 1 | 0.2123 | 0.2469 | 0.2296 | 0.0245 | 2 | 0.2469 | 1.4524 | 0.2123 | 0.3450 | 0.2681 | 0.0688 | 3 | -0.6726 | 0.4187 | 0.1024 | 3.3404 |
| SWERUS L2-15-MC | 0.6530 | 0.8236 | 0.7361 | 0.0854 | 3 | 0.5056 | 0.6574 | 0.5660 | 0.0601 | 6 | 0.5194 | 0.4165 | 0.5056 | 0.8236 | 0.6227 | 0.1063 | 9 | 0.2941 | 0.8429 | 0.5607 | 6.0910 |
| SWERUS L2-16-MC | -0.1000 | -0.0630 | -0.0815 | 0.0262 | 2 | -0.0737 | -0.0737 | -0.0737 | 0.0000 | 1 | -0.0737 | 6.1516 | -0.1000 | -0.0630 | -0.0789 | 0.0190 | 3 | -0.2778 | -0.1196 | -0.2073 | 12.5787 |
| SWERUS L2-18-MC | 0.6993 | 0.6993 | 0.6993 | 0.0000 | 1 | 0.7399 | 0.9217 | 0.8568 | 0.0803 | 4 | 0.7399 | 1.6746 | 0.6993 | 0.9217 | 0.8253 | 0.0990 | 5 | 0.0364 | 1.4614 | 0.5812 | 3.7975 |
| SWERUS L2-21-MC | | | | | 0 | -0.1129 | -0.0364 | -0.0746 | 0.0541 | 2 | -0.1129 | 0.7743 | -0.1129 | -0.0364 | -0.0746 | 0.0541 | 2 | -1.7890 | -0.4786 | -1.1592 | 5.3358 |
| SWERUS L2-22-MC | | | | | 0 | 0.9092 | 0.9767 | 0.9372 | 0.0352 | 3 | 0.9092 | 2.8318 | 0.9092 | 0.9767 | 0.9372 | 0.0352 | 3 | 0.2271 | 1.3533 | 0.7718 | 16.8635 |
| SWERUS L2-23-MC | | | | | 0 | 0.6148 | 0.7158 | 0.6819 | 0.0456 | 4 | 0.6943 | 1.0151 | 0.6148 | 0.7158 | 0.6819 | 0.0456 | 4 | 0.3943 | 1.0498 | 0.6016 | 4.8264 |
| SWERUS L2-24-MC | | | | | 0 | 0.0170 | 0.2154 | 0.1162 | 0.1403 | 2 | 0.0170 | 0.3698 | 0.0170 | 0.2154 | 0.1162 | 0.1403 | 2 | -0.3254 | -0.0554 | -0.1713 | 8.3471 |
| SWERUS L2-25-MC | | | | | 0 | -0.9981 | -0.8678 | -0.9548 | 0.0589 | 4 | -0.8678 | 0.2851 | -0.9981 | -0.8678 | -0.9548 | 0.0589 | 4 | -1.6985 | -0.6708 | -1.3281 | 11.3249 |
| SWERUS L2-26-MC | | | | | 0 | 0.4665 | 0.9956 | 0.6906 | 0.2749 | 5 | 0.5346 | 3.4769 | 0.4665 | 0.9956 | 0.6906 | 0.2749 | 5 | 0.5730 | 1.3185 | 1.0325 | 13.8621 |
| SWERUS L2-27-MC | | | | | 0 | 0.4323 | 1.1670 | 0.7919 | 0.2728 | 6 | 0.4323 | 4.4391 | 0.4323 | 1.1670 | 0.7919 | 0.2728 | 6 | -0.0307 | 1.4175 | 0.8205 | 4.4121 |
| SWERUS L2-28-MC | | | | | 0 | -0.1627 | -0.1184 | -0.1405 | 0.0313 | 2 | -0.1627 | 1.4585 | -0.1627 | -0.1184 | -0.1405 | 0.0313 | 2 | -0.3089 | -0.0939 | -0.2039 | 11.3256 |
| SWERUS L2-29-MC | -0.1980 | -0.0698 | -0.1347 | 0.0415 | 15 | -0.0485 | 0.0240 | -0.0224 | 0.0403 | 3 | 0.0240 | 4.2307 | -0.1980 | 0.0240 | -0.1160 | 0.0589 | 18 | -0.3866 | -0.0835 | -0.1808 | 3.9551 |
| SWERUS L2-31-MC | -0.4760 | 0.1020 | -0.1981 | 0.1453 | 18 | -0.2122 | -0.0670 | -0.1250 | 0.0481 | 6 | -0.2122 | 1.0625 | -0.4760 | 0.1020 | -0.1798 | 0.1310 | 24 | -0.3903 | -0.2443 | -0.2955 | 11.6879 |
| SWERUS L2-32-MC | -0.0761 | -0.0140 | -0.0500 | 0.0322 | 3 | -0.0083 | 0.0534 | 0.0161 | 0.0328 | 3 | -0.0083 | 19.4450 | -0.0761 | 0.0534 | -0.0170 | 0.0464 | 6 | -0.1490 | 0.0376 | -0.0412 | 1.8313 |
| SWERUS L2-34-MC | -0.1461 | -0.0391 | -0.1093 | 0.0310 | 15 | -0.0957 | -0.0240 | -0.0580 | 0.0360 | 3 | -0.0957 | 0.6644 | -0.1461 | -0.0240 | -0.1008 | 0.0365 | 18 | -0.2660 | -0.0704 | -0.1529 | 11.0580 |
| SWERUS L1-26-MC/I | -1.6400 | -1.6230 | -1.6315 | 0.0120 | 2 | -1.8068 | -1.8068 | -1.8068 | 0.0000 | 1 | -1.8068 | 0.1462 | -1.8068 | -1.6230 | -1.6899 | 0.1016 | 3 | -1.6967 | -0.8691 | -1.2705 | 11.1127 |

**Table B.** *SWERUS-C3* and CARINA chemical data at the sites. Carbonate ion parameters depicted in blue were calculated using the program $CO_2$ calc [Robbins et al., 2010].

| Site ID | Site depth (m) | Carbonate data source, Sta ID (sample) | P (db) | Temp (°C) | salinity (psu) | TA (µmol/kg) | $TCO_2$ (µm/kg) | pH | $CO_3^{=}$ measured (µmol/kgSW) | Ω Ca | $CO_3^{=}$ saturation (µmol/kgSW) | $\Delta[CO_3^{=}]$ (µmol/kg) |
|---|---|---|---|---|---|---|---|---|---|---|---|---|
| SWERUS L1-26-MC/I | 52 | SWERUS Leg 1, 15 (sam 1) | 48.00 | -1.81 | 34.21 | 2304.90 | 2224.40 | 7.96 | 71.88 | 1.72 | 41.91 | 29.97 |
| SWERUS L2-2-MC | 55.7 | SWERUS Leg 2, 54 (sam 1) | 50.00 | -0.89 | 32.60 | 2246.20 | 2214.00 | 7.80 | 49.77 | 1.20 | 41.65 | 8.12 |
| SWERUS L2-2-KL | 71.4 | SWERUS Leg 2, 53 (sam 1) | 70.00 | -1.55 | 32.70 | 2251.40 | 2254.40 | 7.68 | 37.56 | 0.90 | 41.83 | -4.27 |
| SWERUS L2-2-PC | 71.7 | SWERUS Leg 2, 53 (sam 1&2) | 71.65 | -1.55 | 32.71 | 2253.65 | 2256.80 | 7.68 | 37.56 | 0.90 | 41.87 | -4.31 |
| SWERUS L2-1-KL | 73.4 | SWERUS Leg 2, 50 (sam 1) | 70.30 | -1.66 | 32.80 | 2257.40 | 2245.10 | 7.73 | 42.53 | 1.02 | 41.86 | 0.67 |
| SWERUS L2-3-MC | 89.6 | SWERUS Leg 2, 52 (sam 1) | 89.10 | -1.71 | 32.93 | 2260.00 | 2260.30 | 7.68 | 38.51 | 0.92 | 42.04 | -3.53 |
| SWERUS L2-25-MC | 101 | SWERUS Leg 2, 87 (sam 1) | 99.60 | -0.87 | 34.24 | 2283.10 | 2203.40 | 7.94 | 71.23 | 1.68 | 42.42 | 28.80 |
| SWERUS L2-4-MC | 123.6 | SWERUS Leg 2, 59 (sam 1) | 114.70 | -0.26 | 34.37 | 2292.00 | 2320.00 | 7.56 | 32.26 | 0.76 | 42.61 | -10.35 |
| SWERUS L2-21-MC | 153 | SWERUS Leg 2, 79 (sam 1) | 154.90 | -0.11 | 34.50 | 2293.00 | 2220.00 | 7.90 | 68.43 | 1.59 | 43.01 | 25.42 |
| SWERUS L2-27-MC | 276 | SWERUS Leg 2, 91 (sam 2) | 270.40 | 0.39 | 34.81 | 2301.10 | 2177.40 | 8.03 | 94.14 | 2.13 | 44.16 | 49.99 |
| SWERUS L2-18-MC | 349 | SWERUS Leg 2, 74 (sam 1) | 342.42 | 0.73 | 34.85 | 2299.30 | 2180.50 | 8.01 | 91.46 | 2.04 | 44.86 | 46.61 |
| SWERUS L2-22-MC | 367 | SWERUS Leg 2, 81 (sam 1) | 363.40 | 0.89 | 34.87 | 2304.20 | 2183.10 | 8.01 | 92.82 | 2.06 | 45.06 | 47.76 |
| SWERUS L2-26-MC | 378 | SWERUS Leg 2, 92 (avg. sam 3 & 4) | 377.60 | 0.53 | 34.86 | 2297.95 | 2170.30 | 8.04 | 96.01 | 2.12 | 45.20 | 50.81 |
| SWERUS L2-9-MC | 446 | SWERUS Leg 2, 66 (avg. sam 1 & 2) | 437.75 | 0.56 | 34.86 | 2299.65 | 2174.40 | 8.03 | 91.73 | 2.07 | 44.36 | 47.37 |
| SWERUS L2-15-MC | 501 | SWERUS Leg 2, 70 (sam 1) | 504.60 | 0.50 | 34.86 | 2304.20 | 2181.80 | 8.02 | 93.07 | 2.01 | 46.42 | 46.65 |
| SWERUS L2-23-MC | 522 | SWERUS Leg 2, 82 (sam 1) | 495.70 | 0.67 | 34.90 | 2302.60 | 2174.20 | 8.03 | 96.33 | 2.08 | 46.33 | 49.99 |
| SWERUS L2-8-MC | 524 | SWERUS Leg 2, 63 (avg sam 1 & 2) | 522.80 | 0.34 | 34.87 | 2303.05 | 2183.10 | 8.05 | 91.63 | 1.97 | 46.61 | 45.02 |
| SWERUS L2-14-MC | 733 | SWERUS Leg 2, 69 (sam 1) | 734.50 | 0.21 | 34.89 | 2304.10 | 2184.00 | 8.01 | 91.25 | 1.87 | 48.74 | 42.50 |
| SWERUS L2-32-MC | 837 | SWERUS Leg 2, 109 (sam 6 & 7) | 799.40 | 0.05 | 34.90 | 2300.05 | 2175.50 | 8.02 | 93.30 | 1.89 | 49.42 | 43.88 |
| SWERUS L2-34-MC | 886 | SWERUS Leg 2, 103 (sam 2) | 888.20 | -0.13 | 34.90 | 2306.40 | 2183.80 | 8.01 | 92.17 | 1.83 | 50.36 | 41.80 |
| SWERUS L2-29-MC | 910 | SWERUS Leg 2, 97 (sam 1) | 851.60 | -0.01 | 34.91 | 2302.50 | 2179.30 | 8.01 | 92.51 | 1.85 | 49.98 | 42.53 |
| SWERUS L2-24-MC | 982 | SWERUS Leg 2, 84 (sam 1) | 971.80 | -0.03 | 34.91 | 2303.90 | 2183.60 | 8.00 | 90.76 | 1.77 | 51.25 | 39.51 |
| SWERUS L2-16-MC | 1023 | SWERUS Leg 2, 68 (sam 1) | 1001.20 | -0.12 | 34.90 | 2304.70 | 2186.40 | 8.00 | 89.63 | 1.74 | 51.57 | 38.06 |
| SWERUS L2-13-MC | 1118 | SWERUS Leg 2, 67 (sam 1) | 1112.30 | -0.27 | 34.89 | 2300.70 | 2180.30 | 8.00 | 90.35 | 1.71 | 52.81 | 37.55 |
| SWERUS L2-28-MC | 1145 | SWERUS Leg 2, 94 (sam 2) | 1147.50 | -0.24 | 34.91 | 2307.70 | 2187.80 | 8.00 | 90.20 | 1.70 | 53.21 | 36.98 |
| SWERUS L2-31-MC | 1157 | SWERUS Leg 2, 100 (avg. sam 2 & 3) | 1118.95 | -0.16 | 34.91 | 2301.80 | 2181.10 | 8.00 | 90.57 | 1.71 | 52.87 | 37.70 |
| AO96/B2-1PC, 0-1 cm | 611 | CARINA, 11561 (sam 16 & TA and TCO2 avg. sam 12- 21) | 593 | 0.24 | 34.87 | 2294.00 | 2157.00 | 7.70 | 99.81 | 2.11 | 47.30 | 52.51 |
| AO96/B1-1PC, 0-1 cm | 2525 | CARINA, 1154, (sam 25) | 2556 | -0.77 | 34.92 | 2295.00 | 2159.00 | 7.70 | 94.59 | 1.33 | 71.33 | 23.25 |
| AO96/B7-TC, 0-1 cm | 2385 | CARINA, 11564 (sam 24) | 2217 | -0.41 | 34.95 | 2300.00 | 2156.00 | 7.71 | 100.53 | 1.51 | 66.58 | 34.85 |
| A096/09-1PC, 0-1 cm | 927 | CARINA, 11557 (sam 20) | 944 | -0.19 | 34.89 | 2292.00 | 2152.00 | 7.69 | 101.23 | 2.00 | 50.54 | 50.69 |
| A096/12-ITWC, 1 cm | 1003 | CARINA, 11556 (sam 18) | 987 | -0.17 | 34.88 | 2293.00 | 2156.00 | 7.69 | 98.76 | 1.91 | 51.41 | 47.35 |
| AO96/13-TC, 0-1 cm | 978 | CARINA, 11556 (sam 18) | 987 | -0.17 | 34.88 | 2293.00 | 2156.00 | 7.69 | 98.76 | 1.91 | 51.41 | 47.35 |
| LOMROG09-GC03B, 0-1 cm | 3814 | CARINA, 15366 (sam 35) & TA 15365 (sam 24) | 3808 | -0.28 | 34.96 | 2297.00 | 2159.00 | 7.70 | 93.41 | 1.02 | 91.22 | 2.19 |
| LOMROG12-TC12, 0-1 cm | 1366 | CARINA, 15360 (sam 23) & pH 15361 (sam 24) | 1314 | -0.49 | 34.91 | 2298.00 | 2164.00 | 7.69 | 96.38 | 1.75 | 55.14 | 41.24 |
| LOMROG12-TC06, 0-2 cm | 2923 | – | | | | | | | | | | |
| LOMROG07-PC04, 0-1 cm | 810 | – | | | | | | | | | | |
| LOMROG07/GC02, 0-1 cm | 724 | – | | | | | | | | | | |
| LOMROG07-TC06, 0-2 cm | 3007 | – | | | | | | | | | | |
| LOMROG07-PC08, 0-0.5 cm | 1038 | CARINA, 15379 (sam 36) | 1023 | -0.22 | 34.91 | 2304.00 | 2148.00 | 7.75 | 109.32 | 2.11 | 51.83 | 57.48 |
| LOMROG07-TC08, 0-0.5 cm | 1038 | CARINA, 15379 (sam 36) | 1023 | -0.22 | 34.91 | 2304.00 | 2148.00 | 7.75 | 109.32 | 2.11 | 51.83 | 57.48 |

Color legend:

| | | |
|---|---|---|
| know 2 | Preferences: | |
| output results from CO2 calc program | KHSO4 | Dickson, 1990 |
| | pH scale | Seawater scale (mol/kg-SW) |
| know all | CO2 constants | K1, K2 from Mehrbach et al., 1973 refit by Dickson and Millero, 1987 |
| calculated | Total Boron | Lee et al., 2010 |
| | Air-sea Flux | Ho et al., 2006 |

**Table C.** Number of individuals picked for trace metal analysis per site and its size fraction.

| Trace metal sample ID | Multicore/Core top ID | Benthic foraminifera species | individuals run for trace metal | size fraction (µm) | Stained (S) Unstained (U) | comments |
|---|---|---|---|---|---|---|
| M1 | 26-MC/I | *E. excavatum* | 20 | 125-250 | S | |
| M2 | 26-MC/I | *N. labradorica* | 3 | 350-425 | S | |
| M3 | 1-KL1 | *N. labradorica* | 6 | 250-350 | S | |
| M4 | 2-KL1 | *E. excavatum* | 13 | 125-250 | S | |
| M5 | 2-KL1 | *N. labradorica* | 1 | 350-425 | S | |
| M6 | 2-MC1-4 | *E. excavatum* | 19 | 125-250 | S | |
| M7 | 2-MC1-4 | *N. labradorica* | 10 | 250-350 | S | |
| M8 | 3-MC1-4 | *E. excavatum* | 15 | 125-250 | S | |
| M9 | 3-MC1-4 | *N. labradorica* | 2 | 350-425 | S | |
| M10 | 4-MC1-4 | *E. excavatum* | 25 | 125-250 | S | |
| M11 | 4-MC1-4 | *N. labradorica* | 10 | 250-350 | S | |
| M12 | 8-MC1-4 | *C. neoteretis* | 21 | 125-250 | S | |
| M13 | 9-MC1-4 | *E. excavatum* | 8 | 125-250 | S | small sample |
| M14 | 9-MC1-4 | *C. neoteretis* | 20 | 125-250 | S | half stained |
| M15 | 13-MC1-4 | *C. neoteretis* | 8 | 125-250 | S | |
| M16 | 13-MC1-4 | *Q. arctica* | 4 | 250-425 | S | |
| M17 | 13-MC1-4 | *C. wuellerstorfi* | 7 | 350-425 | S | |
| M18 | 14-MC1-4 | *C. neoteretis* | 20 | 125-250 | S | |
| M19 | 14-MC1-4 | *Q. arctica* | 2 | 250-425 | S | |
| M20 | 15-MC1-4 | *C. neoteretis* | 20 | 125-250 | S | |
| M21 | 15-MC1-4 | *Q. arctica* | 3 | 250-425 | S | |
| M22 | 16-MC1-4 | *C. neoteretis* | 20 | 125-250 | S | |
| M23 | 16-MC1-4 | *Q. arctica* | 3 | 250-425 | S | |
| M24 | 16-MC1-4 | *C. wuellerstorfi* | 9 | 350-425 | S | |
| M25 | 18-MC1-4 | *C. neoteretis* | 28 | 125-250 | S | |
| M26 | 18-MC1-4 | *Q. arctica* | 2 | 250-425 | S | |
| M27 | 21-MC2-4 | *C. neoteretis* | 27 | 125-250 | S | |
| M28 | 21-MC2-4 | *Q. arctica* | 1 | 250-425 | S | |
| M29 | 22-MC1-4 | *Q. arctica* | 4 | 250-425 | S | |
| M30 | 22-MC1-4 | *C. neoteretis* | 28 | 125-250 | S | |
| M31 | 23-MC1-4 | *C. neoteretis* | 20 | 125-250 | S | |
| M32 | 23-MC1-4 | *Q. arctica* | 5 | 250-425 | S | |
| M33 | 23-MC1-4 | *O. tener* | 6 | 125-250 | S | |
| M34 | 24-MC1-4 | *C. neoteretis* | 8 | 125-250 | S | |
| M35 | 24-MC1-4 | *Q. arctica* | 5 | 250-425 | S | |
| M36 | 24-MC1-4 | *O. tener* | 16 | 125-250 | S | |
| M37 | 25-MC1-4 | *E. excavatum* | 18 | 125-250 | S | |
| M38 | 26-MC1-4 | *C. neoteretis* | 23 | 125-250 | S | |
| M39 | 26-MC1-4 | *Q. arctica* | 3 | 250-425 | S | |
| M40 | 27-MC1-4 | *C. neoteretis* | 22 | 125-250 | S | |
| M41 | 27-MC1-4 | *Q. arctica* | 3 | 250-425 | S | |
| M42 | 28-MC1-4 | *C. neoteretis* | 6 | 125-250 | S | half stained |
| M43 | 28-MC1-4 | *Q. arctica* | 3 | 250-425 | S | half stained |
| M44 | 28-MC1-4 | *O. tener* | 24 | 125-250 | S | half stained |
| M45 | 29-MC1-4 | *C. neoteretis* | 21 | 125-250 | S | |
| M46 | 29-MC1-4 | *Q. arctica* | 4 | 250-425 | S | |
| M47 | 29-MC1-4 | *O. tener* | 16 | 125-250 | S | |
| M48 | 32-MC1-4 | *C. neoteretis* | 14 | 125-250 | S | |
| M49 | 32-MC1-4 | *Q. arctica* | 5 | 250-425 | S | |
| M50 | 32-MC1-4 | *O. tener* | 15 | 125-250 | S | |
| M51 | 34-MC1-4 | *C. neoteretis* | 30 | 125-250 | S | |
| M52 | 34-MC1-4 | *Q. arctica* | 3 | 250-425 | S | |
| M53 | 2-MC1-5 | *E. excavatum* | 6 | 125-250 | S | |
| M54 | 2-MC1-5 | *N. labradorica* | 3 | 250-425 | S | |

| | | | | | | |
|---|---|---|---|---|---|---|
| M55 | 3-MC1-5 | *E. excavatum* | 13 | 125-250 | S | |
| M56 | 3-MC1-5 | *N. labradorica* | 4 | 250-425 | S | |
| M57 | 4-MC1-5 | *E. excavatum* | 6 | 125-250 | S | |
| M58 | 4-MC1-5 | *N. labradorica* | 7 | 250-425 | S | |
| LR9_1 | LOMROG12-TC09, 0-1 cm | *C. neoteretis* | 26 | 125-250 | U | |
| LR9_2 | LOMROG12-TC09, 0-1 cm | *Q. arctica* | 4 | 250-425 | U | |
| LR9_3 | LOMROG12-TC09, 0-1 cm | *O. tener* | 30 | 125-250 | U | |
| LR9_4 | LOMROG12-TC09, 0-1 cm | *C. wuellerstorfi* | 8 | 250-425 | U | |
| LR5_1 | LOMROG12-TC05, 0-1 cm | *Q. arctica* | 6 | 250-425 | U | |
| LR5_2 | LOMROG12-TC05, 0-1 cm | *O. tener* | 26 | 125-250 | U | |
| LR5_3 | LOMROG12-TC05, 0-1 cm | *C. wuellerstorfi* | 8 | 250-425 | U | |
| LR5_4 | LOMROG12-TC05, 0-1 cm | *C. neoteretis* | 4 | 125-250 | U | |
| 1.2 | AO96/B2-1PC, 0-1 cm | *Q. arctica* | 11 | 125-355 | U | |
| 1.3 | AO96/B2-1PC, 0-1 cm | *Triloculina* sp. | 3 | 125 | U | |
| 1.5 | AO96/B2-1PC, 0-1 cm | *C. neoteretis* | 10 | 125/250 | U | |
| 1.6 | AO96/B2-1PC, 0-1 cm | *O. tener* | 11 | 125 | U | |
| 2.1 | AO96/B1-1PC, 0-1 cm | *O. tener* | 13 | 125 | U | |
| 3.1 | AO96/B7-TC, 0-1 cm | *C. wuellerstorfi* | 18 | 125-355 | U | |
| 3.2 | AO96/B7-TC, 0-1 cm | *Q. arctica* | 11 | 125 | U | |
| 3.3 | AO96/B7-TC, 0-1 cm | *O. tener* | 15 | 125 | U | |
| 4.1 | A096/09-1PC, 0-1 cm | *C. neoteretis* | 12 | 125-250 | U | |
| 4.2 | A096/09-1PC, 0-1 cm | *O. tener* | 15 | 125-250 | U | |
| 4.3 | A096/09-1PC, 0-1 cm | *Q. arctica* | 14 | 125-355 | U | |
| 5.1 | A096/12-ITWC, 1 cm | *C. wuellerstorfi* | 6 | 250 | U | |
| 5.2 | A096/12-ITWC, 1 cm | *Q. arctica* | 9 | 300 | U | |
| 5.4 | A096/12-ITWC, 1 cm | *C. neoteretis* | 17 | 180 | U | |
| 5.5 | A096/12-ITWC, 1 cm | *O. tener* | 17 | 125 | U | |
| 6.1.1 | AO96/13-TC, 0-1 cm | *Q. arctica* | 4 | 500 | U | |
| 6.1.2 | AO96/13-TC, 0-1 cm | *Q. arctica* | 8 | 355 | U | |
| 6.1.3 | AO96/13-TC, 0-1 cm | *Q. arctica* | 12 | 125 | U | |
| 6.3 | AO96/13-TC, 0-1 cm | *C. neoteretis* | 13 | 125 | U | |
| 6.4 | AO96/13-TC, 0-1 cm | *O. tener* | 14 | 125 | U | |
| 7.1 | LOMROG09-GC03B, 0-1 cm | *Triloculina* sp. | 13 | 125 | U | |
| 7.2 | LOMROG09-GC03B, 0-1 cm | *O. tener* | 10 | 180 | U | No step VI |
| 8.1 | LOMROG12-TC12, 0-1 cm | *C. wuellerstorfi* | 7 | 250-425 | U | |
| 8.2 | LOMROG12-TC12, 0-1 cm | *Q. arctica* | 15 | 125-250 | U | |
| 8.4 | LOMROG12-TC12, 0-1 cm | *C. neoteretis* | 14 | 180 | U | |
| 8.5 | LOMROG12-TC12, 0-1 cm | *O. tener* | 16 | 125 | U | |
| 9.1 | LOMROG09-TC09, 0-2 cm | *O. tener* | 6 | 125 | U | |
| 11.1 | LOMROG12-TC06, 0-2 cm | *C. wuellerstorfi* | 5 | 250 | U | |
| 11.2 | LOMROG12-TC06, 0-2 cm | *O. tener* | 17 | 125 | U | |
| 12.1 | LOMROG07-PC04, 0-1 cm | *C. wuellerstorfi* | 3 | 125-355 | U | |
| 12.3 | LOMROG07-PC04, 0-1 cm | *Q. arctica* | 14 | 250 | U | |
| 12.5 | LOMROG07-PC04, 0-1 cm | *C. neoteretis* | 16 | 125 | U | |
| 12.6 | LOMROG07-PC04, 0-1 cm | *O. tener* | 16 | 125 | U | |
| 13.1 | LOMROG07/GC02, 0-1 cm | *Q. arctica* | 11 | 125-355 | U | |
| 13.2 | LOMROG07/GC02, 0-1 cm | *Triloculina* sp. | 5 | 125 | U | |
| 13.4 | LOMROG07/GC02, 0-1 cm | *C. neoteretis* | 20 | 125-250 | U | No step VI |
| 13.5 | LOMROG07/GC02, 0-1 cm | *O. tener* | 7 | 125 | U | No step VI |
| 14.1 | LOMROG07-TC06, 0-2 cm | *C. wuellerstorfi* | 10 | 125-355 | U | |
| 14.5 | LOMROG07-TC06, 0-2 cm | *O. tener* | 11 | 125 | U | No step VI |
| 15.1 | LOMROG07-PC08, 0-0.5 cm | *C. wuellerstorfi* | 15 | 250 | U | |
| 15.2 | LOMROG07-PC08, 0-0.5 cm | *Q. arctica* | 10 | 250 | U | |
| 15.3 | LOMROG07-PC08, 0-0.5 cm | *Triloculina* sp. | 17 | 355/125 | U | |
| 15.5 | LOMROG07-PC08, 0-0.5 cm | *C. neoteretis* | 17 | 125 | U | |
| 15.6 | LOMROG07-PC08, 0-0.5 cm | *O. tener* | 17 | 125 | U | |
| 15.7 | LOMROG07-TC08, 0-0.5 cm | *C. wuellerstorfi* | 13 | 250 | U | |
| 15.8 | LOMROG07-TC08, 0-0.5 cm | *Q. arctica* | 10 | 250 | U | |
| 15.9 | LOMROG07-TC08, 0-0.5 cm | *Triloculina* sp. | 5 | 180 | U | |
| 15.11 | LOMROG07-TC08, 0-0.5 cm | *C. neoteretis* | 20 | 180 | U | |
| 15.12 | LOMROG07-TC08, 0-0.5 cm | *O. tener* | 20 | 180 | U | |
| 16.1 | HLY0503-18TC, 3.3-6 cm | *C. wuellerstorfi* | 4 | 355 | U | |

**Table D.** Counts on Rose Bengal calcareous benthic foraminifera with depth at all the *SWERUS C3* multicores.

| Multicore sediment depth [cm] | # of RB stained calcareous benthic foraminifera |
|---|---|
| SWERUS L2-1 KL1, 0-2 | 17 |
| SWERUS L2-1 KL1, 2-4 | 2 |
| SWERUS L2-1 KL1, 4-6 | 4 |
| SWERUS L2-1 KL1, 6-8 | 2 |
| SWERUS L2-1 KL1, 8-10 | 0 |
| | |
| SWERUS L1-26-MC/I, 0-1 | 109 |
| SWERUS L1-26-MC/I, 1-2 | 35 |
| SWERUS L1-26-MC/I, 2-3 | 22 |
| SWERUS L1-26-MC/I, 3-4 | 19 |
| SWERUS L1-26-MC/I, 4-5 | 15 |
| SWERUS L1-26-MC/I, 5-6 | 21 |
| SWERUS L1-26-MC/I, 6-7 | 17 |
| SWERUS L1-26-MC/I, 7-8 | 16 |
| | |
| SWERUS L2-2-KL1, 0-2 | 50 |
| SWERUS L2-2-KL1, 2-4 | 16 |
| SWERUS L2-2-KL1, 4-6 | 67 |
| SWERUS L2-2-KL1, 6-8 | 13 |
| SWERUS L2-2-KL1, 8-10 | 0 |
| SWERUS L2-2-KL1, 10-12 | 0 |
| SWERUS L2-2-KL1, 12-14 | 0 |
| SWERUS L2-2-KL1, 14-16 | 0 |
| SWERUS L2-2-KL1, 16-18 | 0 |
| SWERUS L2-2-KL1, 18-20 | 0 |
| SWERUS L2-2-KL1, 20-22 | 0 |
| SWERUS L2-2-KL1, 22-24 | 0 |
| | |
| SWERUS L2-2-MC-4, 0-2 | 46 |
| SWERUS L2-2-MC-4, 2-3 | 53 |
| SWERUS L2-2-MC-4, 3-4 | 16 |
| SWERUS L2-2-MC-4, 4-5 | 1 |
| SWERUS L2-2-MC-4, 5-7 | 0 |
| SWERUS L2-2-MC-4, 7-9 | 0 |
| SWERUS L2-2-MC-4, 9-11 | 0 |
| SWERUS L2-2-MC-4,11-14 | 0 |
| SWERUS L2-2-MC-4, 14-17 | 0 |
| SWERUS L2-2-MC-4, 17-20 | 0 |
| SWERUS L2-2-MC-4, 20-24 | 0 |
| | |
| SWERUS L2-3-MC-4, 0-2 | 28 |
| SWERUS L2-3-MC-4, 2-4 | 16 |
| SWERUS L2-3-MC-4, 4-6 | 6 |
| | |
| SWERUS L2-3-MC-5, 0-2 | 0 |
| SWERUS L2-3-MC-5, 2-4 | 0 |
| SWERUS L2-3-MC-5, 4-6 | 0 |
| | |
| SWERUS L2-4-MC-4, 0-2 | 139 |
| SWERUS L2-4-MC-4, 2-4 | 45 |
| SWERUS L2-4-MC-4, 4-6 | 12 |
| SWERUS L2-4-MC-4, 6-8 | 1 |
| SWERUS L2-4-MC-4,8-10 | 0 |
| | |
| SWERUS L2-4-MC-5, 0-2 | 0 |
| SWERUS L2-4-MC-5, 2-4 | 0 |
| SWERUS L2-4-MC-5, 4-6 | 0 |
| | |
| SWERUS L2-8-MC-4, 0-1 | 202 |
| SWERUS L2-8-MC-4, 1-2 | 35 |

| Multicore sediment depth [cm] | # of RB stained calcareous benthic foraminifera |
|---|---|
| SWERUS L2-8-MC-4, 2-4 | 38 |
| SWERUS L2-8-MC-4, 4-6 | 2 |
| | |
| SWERUS L2-9-MC-4, 0-1 | 67 |
| SWERUS L2-9-MC-4, 1-2 | 9 |
| SWERUS L2-9-MC-4, 2-3 | 13 |
| SWERUS L2-9-MC-4, 3-4 | 24 |
| SWERUS L2-9-MC-4, 4-5 | 3 |
| SWERUS L2-9-MC-4, 5-6 | 1 |
| SWERUS L2-9-MC-4, 6-8 | 0 |
| SWERUS L2-9-MC-4, 8-10 | 0 |
| SWERUS L2-9-MC-4, 10-12 | 0 |
| SWERUS L2-9-MC-4, 12-14 | 0 |
| SWERUS L2-9-MC-4, 14-16 | 0 |
| SWERUS L2-9-MC-4, 16-18 | 0 |
| SWERUS L2-9-MC-4, 18-20 | 0 |
| SWERUS L2-9-MC-4, 20-24 | 0 |
| | |
| SWERUS L2-13-MC-4, 0-1 | 47 |
| SWERUS L2-13-MC-4, 1-2 | 18 |
| SWERUS L2-13-MC-4, 2-3 | 8 |
| SWERUS L2-13-MC-4, 3-4 | 6 |
| SWERUS L2-13-MC-4, 4-5 | 0 |
| SWERUS L2-13-MC-4, 5-6 | 0 |
| SWERUS L2-13-MC-4, 6-7 | 0 |
| SWERUS L2-13-MC-4, 7-8 | 0 |
| SWERUS L2-13-MC-4, 8-10 | 0 |
| SWERUS L2-13-MC-4, 10-12 | 0 |
| SWERUS L2-13-MC-4, 12-14 | 0 |
| SWERUS L2-13-MC-4, 14-16 | 0 |
| SWERUS L2-13-MC-4, 16-18 | 0 |
| | |
| SWERUS L2-14-MC-4, 0-1 | 58 |
| SWERUS L2-14-MC-4, 1-2 | 8 |
| SWERUS L2-14-MC-4, 2-3 | 5 |
| SWERUS L2-14-MC-4, 3-4 | 1 |
| SWERUS L2-14-MC-4, 4-5 | 0 |
| SWERUS L2-14-MC-4, 5-6 | 0 |
| SWERUS L2-14-MC-4, 6-7 | 0 |
| SWERUS L2-14-MC-4, 7-9 | 0 |
| SWERUS L2-14-MC-4, 9-11 | 0 |
| SWERUS L2-14-MC-4, 11-13 | 0 |
| SWERUS L2-14-MC-4, 13-15 | 0 |
| SWERUS L2-14-MC-4, 15-17 | 0 |
| SWERUS L2-14-MC-4, 17-19 | 0 |
| SWERUS L2-14-MC-4, 19-21 | 0 |
| SWERUS L2-14-MC-4, 21-22 | 0 |
| | |
| SWERUS L2-15-MC-4, 0-1 | 62 |
| SWERUS L2-15-MC-4, 1-2 | 51 |
| SWERUS L2-15-MC-4, 2-3 | 25 |
| SWERUS L2-15-MC-4, 3-4 | 21 |
| SWERUS L2-15-MC-4, 4-5 | 28 |
| SWERUS L2-15-MC-4, 5-6 | 0 |
| SWERUS L2-15-MC-4, 6-8 | 0 |
| SWERUS L2-15-MC-4, 8-10 | 0 |
| SWERUS L2-15-MC-4, 10-12 | 0 |
| SWERUS L2-15-MC-4, 12-14 | 0 |
| | |
| SWERUS L2-16-MC-4, 0-1 | 62 |

| | |
|---|---|
| SWERUS L2-16-MC-4, 1-2 | 19 |
| SWERUS L2-16-MC-4, 2-3 | 5 |
| SWERUS L2-16-MC-4, 3-4 | 3 |
| SWERUS L2-16-MC-4, 4-5 | 2 |
| SWERUS L2-16-MC-4, 5-6 | 1 |
| SWERUS L2-16-MC-4, 6-8 | 0 |
| SWERUS L2-16-MC-4, 8-10 | 0 |
| SWERUS L2-16-MC-4, 10-12 | 0 |
| SWERUS L2-16-MC-4, 12-14 | 0 |
| SWERUS L2-16-MC-4, 14-16 | 0 |
| SWERUS L2-16-MC-4, 16-18 | 0 |
| SWERUS L2-16-MC-4, 18-20 | 0 |
| SWERUS L2-16-MC-4, 20-24 | 0 |
| | |
| SWERUS L2-18-MC-4, 0-1 | 130 |
| SWERUS L2-18-MC-4, 1-2 | 67 |
| SWERUS L2-18-MC-4, 2-3 | 124 |
| SWERUS L2-18-MC-4, 3-4 | 40 |
| SWERUS L2-18-MC-4, 4-5 | 9 |
| SWERUS L2-18-MC-4, 5-6 | 0 |
| SWERUS L2-18-MC-4, 6-8 | 0 |
| SWERUS L2-18-MC-4, 8-10 | 0 |
| SWERUS L2-18-MC-4, 10-12 | 0 |
| SWERUS L2-18-MC-4, 12-14 | 0 |
| SWERUS L2-18-MC-4, 14-16 | 0 |
| SWERUS L2-18-MC-4, 16-18 | 0 |
| SWERUS L2-18-MC-4, 18-20 | 0 |
| | |
| SWERUS L2-21-MC-4, 0-1 | 100 |
| SWERUS L2-21-MC-4, 1-2 | 45 |
| SWERUS L2-21-MC-4, 2-4 | 8 |
| SWERUS L2-21-MC-4, 4-5 | 0 |
| SWERUS L2-21-MC-4, 5-6 | 0 |
| SWERUS L2-21-MC-4, 6-8 | 0 |
| SWERUS L2-21-MC-4, 8-10 | 0 |
| SWERUS L2-21-MC-4, 10-12 | 0 |
| SWERUS L2-21-MC-4, 12-14 | 0 |
| SWERUS L2-21-MC-4, 14-16 | 0 |
| SWERUS L2-21-MC-4, 16-18 | 0 |
| | |
| SWERUS L2-22-MC-4, 0-1 | 80 |
| SWERUS L2-22-MC-4, 1-2 | 24 |
| SWERUS L2-22-MC-4, 2-3 | 0 |
| SWERUS L2-22-MC-4, 3-4 | 0 |
| SWERUS L2-22-MC-4, 4-5 | 0 |
| SWERUS L2-22-MC-4, 5-6 | 0 |
| SWERUS L2-22-MC-4, 6-8 | 0 |
| SWERUS L2-22-MC-4, 8-10 | 0 |
| SWERUS L2-22-MC-4, 10-12 | 0 |
| SWERUS L2-22-MC-4, 12-14 | 0 |
| SWERUS L2-22-MC-4, 14-16 | 0 |
| SWERUS L2-22-MC-4, 16-18 | 0 |
| SWERUS L2-22-MC-4, 18-20 | 0 |
| SWERUS L2-22-MC-4, 20-22 | 0 |
| SWERUS L2-22-MC-4, 22-24 | 0 |
| SWERUS L2-22-MC-4, 24-26 | 0 |
| | |
| SWERUS L2-23-MC-4, 0-1 | 62 |
| SWERUS L2-23-MC-4, 1-2 | 10 |
| SWERUS L2-23-MC-4, 2-3 | 2 |
| SWERUS L2-23-MC-4, 3-4 | 4 |
| SWERUS L2-23-MC-4, 4-5 | 0 |
| SWERUS L2-23-MC-4, 5-6 | 0 |

| | |
|---|---|
| SWERUS L2-23-MC-4, 6-7 | 0 |
| SWERUS L2-23-MC-4, 7-8 | 0 |
| SWERUS L2-23-MC-4, 8-10 | 0 |
| SWERUS L2-23-MC-4, 10-12 | 0 |
| SWERUS L2-23-MC-4, 12-14 | 0 |
| SWERUS L2-23-MC-4, 14-16 | 0 |
| SWERUS L2-23-MC-4, 16-18 | 0 |
| SWERUS L2-23-MC-4, 18-20 | 0 |
| SWERUS L2-23-MC-4, 20-23 | 0 |
| SWERUS L2-23-MC-4, 23-24 | 0 |
| SWERUS L2-23-MC-4, 24-26 | 0 |
| | |
| SWERUS L2-24-MC-4, 0-1 | 22 |
| SWERUS L2-24-MC-4, 1-2 | 51 |
| SWERUS L2-24-MC-4, 2-3 | 44 |
| SWERUS L2-24-MC-4, 3-4 | 10 |
| SWERUS L2-24-MC-4, 4-5 | 12 |
| SWERUS L2-24-MC-4, 5-6 | 4 |
| SWERUS L2-24-MC-4, 6-7 | 4 |
| SWERUS L2-24-MC-4, 7-8 | 1 |
| SWERUS L2-24-MC-4, 8-9 | 0 |
| SWERUS L2-24-MC-4, 9-11 | 0 |
| SWERUS L2-24-MC-4, 11-13 | 0 |
| SWERUS L2-24-MC-4, 13-15 | 0 |
| SWERUS L2-24-MC-4, 15-17 | 0 |
| SWERUS L2-24-MC-4, 17-19 | 0 |
| SWERUS L2-24-MC-4, 19-21 | 0 |
| SWERUS L2-24-MC-4, 21-23 | 0 |
| | |
| SWERUS L2-25-MC-4, 0-1 | 58 |
| SWERUS L2-25-MC-4, 1-2 | 32 |
| SWERUS L2-25-MC-4, 2-4 | 10 |
| SWERUS L2-25-MC-4, 4-6 | 5 |
| SWERUS L2-25-MC-4, 6-8 | 0 |
| SWERUS L2-25-MC-4, 8-10 | 0 |
| SWERUS L2-25-MC-4, 10-12 | 0 |
| SWERUS L2-25-MC-4, 12-14 | 0 |
| SWERUS L2-25-MC-4, 14-16 | 0 |
| SWERUS L2-25-MC-4, 16-18 | 0 |
| SWERUS L2-25-MC-4, 18-21 | 0 |
| | |
| SWERUS L2-26-MC-4, 0-1 | 102 |
| SWERUS L2-26-MC-4, 1-2 | 57 |
| SWERUS L2-26-MC-4, 2-3 | 25 |
| SWERUS L2-26-MC-4, 3-4 | 4 |
| SWERUS L2-26-MC-4, 4-6 | 3 |
| SWERUS L2-26-MC-4, 6-8 | 0 |
| SWERUS L2-26-MC-4, 8-10 | 0 |
| SWERUS L2-26-MC-4, 10-12 | 0 |
| SWERUS L2-26-MC-4, 12-14 | 0 |
| SWERUS L2-26-MC-4, 14-16 | 0 |
| SWERUS L2-26-MC-4, 16-18 | 0 |
| SWERUS L2-26-MC-4, 18-20 | 0 |
| SWERUS L2-26-MC-4, 20-24 | 0 |
| SWERUS L2-26-MC-4, 24-28 | 0 |
| SWERUS L2-26-MC-4, 28-32 | 0 |
| SWERUS L2-26-MC-4, 32-36 | 0 |
| | |
| SWERUS L2-27-MC-5, 0-1 | 108 |
| SWERUS L2-27-MC-5, 1-2 | 12 |
| SWERUS L2-27-MC-5, 2-3 | 2 |
| SWERUS L2-27-MC-5, 3-4 | 1 |
| SWERUS L2-27-MC-5, 4-5 | 3 |

| | |
|---|---|
| SWERUS L2-27-MC-5, 5-6 | 0 |
| SWERUS L2-27-MC-5, 6-8 | 0 |
| SWERUS L2-27-MC-5, 8-10 | 0 |
| SWERUS L2-27-MC-5, 10-12 | 0 |
| SWERUS L2-27-MC-5, 12-15 | 0 |
| SWERUS L2-27-MC-5, 15-16 | 0 |
| SWERUS L2-27-MC-5, 16-18 | 0 |
| SWERUS L2-27-MC-5, 18-20 | 0 |
| SWERUS L2-27-MC-5, 20-22 | 0 |
| SWERUS L2-27-MC-5, 22-24 | 0 |
| | |
| SWERUS L2-28-MC-4, 0-1 | 48 |
| SWERUS L2-28-MC-4, 1-2 | 27 |
| SWERUS L2-28-MC-4, 2-3 | 26 |
| SWERUS L2-28-MC-4, 3-4 | 8 |
| SWERUS L2-28-MC-4, 4-5 | 5 |
| SWERUS L2-28-MC-4, 5-6 | 0 |
| SWERUS L2-28-MC-4, 6-7 | 0 |
| SWERUS L2-28-MC-4, 7-8 | 0 |
| SWERUS L2-28-MC-4, 8-10 | 0 |
| SWERUS L2-28-MC-4, 10-12 | 0 |
| SWERUS L2-28-MC-4, 12-14 | 0 |
| SWERUS L2-28-MC-4, 14-16 | 0 |
| SWERUS L2-28-MC-4, 16-18 | 0 |
| SWERUS L2-28-MC-4, 18-20 | 0 |
| SWERUS L2-28-MC-4, 20-22 | 0 |
| | |
| SWERUS L2-29-MC-4, 0-1 | 116 |
| SWERUS L2-29-MC-4, 1-2 | 27 |
| SWERUS L2-29-MC-4, 2-3 | 9 |
| SWERUS L2-29-MC-4, 3-4 | 15 |
| SWERUS L2-29-MC-4, 4-5 | 1 |
| SWERUS L2-29-MC-4, 5-6 | 2 |
| SWERUS L2-29-MC-4, 6-7 | 0 |
| SWERUS L2-29-MC-4, 7-8 | 0 |
| SWERUS L2-29-MC-4, 8-10 | 0 |
| SWERUS L2-29-MC-4, 10-12 | 0 |
| SWERUS L2-29-MC-4, 12-14 | 0 |
| SWERUS L2-29-MC-4, 14-16 | 0 |
| SWERUS L2-29-MC-4, 16-18 | 0 |
| SWERUS L2-29-MC-4, 18-20 | 0 |
| SWERUS L2-29-MC-4, 20-22 | 0 |
| SWERUS L2-29-MC-4, 22-23 | 0 |
| | |
| SWERUS L2-31-MC-4, 0-1 | 7 |
| SWERUS L2-31-MC-4, 1-2 | 2 |
| SWERUS L2-31-MC-4, 2-4 | 0 |
| SWERUS L2-31-MC-4, 4-6 | 0 |
| SWERUS L2-31-MC-4, 6-8 | 0 |
| SWERUS L2-31-MC-4, 8-10 | 0 |
| SWERUS L2-31-MC-4, 10-12 | 0 |
| SWERUS L2-31-MC-4, 12-15 | 0 |
| SWERUS L2-31-MC-4, 15-16 | 0 |
| SWERUS L2-31-MC-4, 16-18 | 0 |
| SWERUS L2-31-MC-4, 18-20 | 0 |
| SWERUS L2-31-MC-4, 20-22 | 0 |
| SWERUS L2-31-MC-4, 22-24 | 0 |
| SWERUS L2-31-MC-4, 24-26 | 0 |
| SWERUS L2-31-MC-4, 26-28 | 0 |
| SWERUS L2-31-MC-4, 28-30 | 0 |
| | |
| SWERUS L2-32-MC-4, 0-1 | 61 |
| SWERUS L2-32-MC-4, 1-2 | 35 |
| SWERUS L2-32-MC-4, 2-3 | 10 |
| SWERUS L2-32-MC-4, 3-4 | 12 |
| SWERUS L2-32-MC-4, 4-5 | 10 |
| SWERUS L2-32-MC-4, 5-6 | 6 |
| SWERUS L2-32-MC-4, 6-7 | 3 |
| SWERUS L2-32-MC-4, 7-8 | 0 |
| SWERUS L2-32-MC-4, 8-9 | 0 |
| SWERUS L2-32-MC-4, 9-10 | 0 |
| SWERUS L2-32-MC-4, 10-11 | 0 |
| SWERUS L2-32-MC-4, 11-12 | 0 |
| SWERUS L2-32-MC-4, 12-13 | 0 |
| SWERUS L2-32-MC-4, 13-14 | 0 |
| SWERUS L2-32-MC-4, 14-15 | 0 |
| SWERUS L2-32-MC-4, 15-16 | 0 |
| SWERUS L2-32-MC-4, 16-17 | 0 |
| SWERUS L2-32-MC-4, 17-18 | 0 |
| SWERUS L2-32-MC-4, 18-19 | 0 |
| SWERUS L2-32-MC-4, 19-20 | 0 |
| SWERUS L2-32-MC-4, 20-21 | 0 |
| SWERUS L2-32-MC-4, 21-22 | 0 |
| SWERUS L2-32-MC-4, 22-23 | 0 |
| SWERUS L2-32-MC-4, 23-24 | 0 |
| SWERUS L2-32-MC-4, 24-25 | 0 |
| SWERUS L2-32-MC-4, 25-26 | 0 |
| SWERUS L2-32-MC-4, 26-27 | 0 |
| SWERUS L2-32-MC-4, 27-28 | 0 |
| SWERUS L2-32-MC-4, 28-29 | 0 |
| SWERUS L2-32-MC-4, 29-30 | 0 |
| SWERUS L2-32-MC-4, 30-31 | 0 |
| SWERUS L2-32-MC-4, 31-32 | 0 |
| | |
| SWERUS L2-34-MC-4, 0-1 | 130 |
| SWERUS L2-34-MC-4, 1-2 | 64 |
| SWERUS L2-34-MC-4, 2-3 | 38 |
| SWERUS L2-34-MC-4, 3-4 | 32 |
| SWERUS L2-34-MC-4, 4-5 | 42 |
| SWERUS L2-34-MC-4, 5-6 | 15 |
| SWERUS L2-34-MC-4, 6-7 | 0 |
| SWERUS L2-34-MC-4, 7-8 | 0 |
| SWERUS L2-34-MC-4, 8-9 | 0 |
| SWERUS L2-34-MC-4, 9-10 | 0 |
| SWERUS L2-34-MC-4, 10-11 | 0 |
| SWERUS L2-34-MC-4, 11-12 | 0 |
| SWERUS L2-34-MC-4, 12-13 | 0 |

**Table E.** Trace metal data obtained by ICP-MS at all studied core top sites.

| Sample ID | Core top/multicore | BF species | Mg25/Ca43 | RSD |
|---|---|---|---|---|
| NBM_M01 | 26-MC/I | *Elphidium clavatum* | 0.65 | 1.69 |
| NBM_M04 | 2-KL1 | *Elphidium clavatum* | 0.79 | 2.28 |
| NBM_M06 | 2-MC1-4 | *Elphidium clavatum* | 0.68 | 1.48 |
| NBM_M08 | 3-MC1-4 | *Elphidium clavatum* | 0.55 | 1.26 |
| NBM_M10 | 4-MC1-4 | *Elphidium clavatum* | 0.64 | 1.89 |
| NBM_M55 | 3-MC1-5 | *Elphidium clavatum* | 0.75 | 1.53 |
| NBM_M57 | 4-MC1-5 | *Elphidium clavatum* | 0.67 | 0.71 |
| NBM_R3 | 2-PC1 | *Elphidium clavatum* | 0.75 | 1.00 |
| NBM_R1 | 26-MC/I | *Elphidium clavatum* | 0.52 | 3.95 |
| NBM_R2 | 2-KL1 | *Elphidium clavatum* | 0.59 | 1.85 |
| NBM_M03 | 1-KL1 | *Nonionellina labradorica* | 1.30 | 2.21 |
| NBM_M07 | 2-MC1-4 | *Nonionellina labradorica* | 1.25 | 2.02 |
| NBM_M11 | 4-MC1-4 | *Nonionellina labradorica* | 1.24 | 0.99 |
| NBM_M54 | 2-MC1-5 | *Nonionellina labradorica* | 1.11 | 1.78 |
| NBM_M56 | 3-MC1-5 | *Nonionellina labradorica* | 1.30 | 3.55 |
| NBM_M58 | 4-MC1-5 | *Nonionellina labradorica* | 1.31 | 0.20 |
| NBM_5_4 | A096/12-ITWC, 1 cm | *Cassidulina neoteretis* | 1.30 | 0.46 |
| NBM_6_3 | AO96/13-TC, 0-1 cm | *Cassidulina neoteretis* | 1.29 | 0.29 |
| NBM_8_4 | LOMROG12-TC12, 0-1 cm | *Cassidulina neoteretis* | 1.46 | 0.36 |
| NBM_12_5 | LOMROG07-PC04, 0-1 cm | *Cassidulina neoteretis* | 1.43 | 0.33 |
| NBM_15_5 | LOMROG07-PC08, 0-0.5 cm | *Cassidulina neoteretis* | 2.06 | 0.52 |
| NBM_13_4 | LOMROG07/GC02, 0-1 cm | *Cassidulina neoteretis* | 12.90 | 0.30 |
| NBM_LR9_1 | LOMROG12-TC09 | *Cassidulina neoteretis* | 1.99 | 1.45 |
| NBM_LR5_4 | LOMROG12-TC05 | *Cassidulina neoteretis* | 3.33 | 1.08 |
| NBM_1_5 | AO96/B2-1PC, 0-1 cm | *Cassidulina neoteretis* | 1.84 | 0.59 |
| NBM_4_1 | A096/09-1PC, 0-1 cm | *Cassidulina neoteretis* | 2.28 | 0.47 |
| NBM_M12 | 8-MC1-4 | *Cassidulina neoteretis* | 1.08 | 1.80 |
| NBM_M14 | 9-MC1-4 | *Cassidulina neoteretis* | 1.09 | 2.23 |
| NBM_M15 | 13-MC1-4 | *Cassidulina neoteretis* | 1.10 | 2.65 |
| NBM_M18 | 14-MC1-4 | *Cassidulina neoteretis* | 0.97 | 0.97 |
| NBM_M20 | 15-MC1-4 | *Cassidulina neoteretis* | 0.99 | 0.19 |
| NBM_M22 | 16-MC1-4 | *Cassidulina neoteretis* | 1.16 | 1.33 |
| NBM_M25 | 18-MC1-4 | *Cassidulina neoteretis* | 1.00 | 2.26 |
| NBM_M27 | 21-MC2-4 | *Cassidulina neoteretis* | 1.04 | 0.63 |
| NBM_M30 | 22-MC1-4 | *Cassidulina neoteretis* | 1.07 | 3.79 |
| NBM_M31 | 23-MC1-4 | *Cassidulina neoteretis* | 1.19 | 0.96 |
| NBM_M34 | 24-MC1-4 | *Cassidulina neoteretis* | 1.07 | 1.86 |
| NBM_M38 | 26-MC1-4 | *Cassidulina neoteretis* | 1.20 | 2.47 |
| NBM_M40 | 27-MC1-4 | *Cassidulina neoteretis* | 1.03 | 1.77 |
| NBM_M45 | 29-MC1-4 | *Cassidulina neoteretis* | 0.91 | 0.98 |
| NBM_M51 | 34-MC1-4 | *Cassidulina neoteretis* | 0.84 | 0.95 |
| NBM_1_2 | AO96/B2-1PC, 0-1 cm | *Quinqueloculina arctica* | 65.35 | 0.58 |
| NBM_3_2 | AO96/B7-TC, 0-1 cm | *Quinqueloculina arctica* | 57.96 | 0.36 |
| NBM_5_2 | A096/12-ITWC, 1 cm | *Quinqueloculina arctica* | 60.54 | 0.28 |
| NBM_6_1_1 | AO96/13-TC, 0-1 cm | *Quinqueloculina arctica* | 55.88 | 0.45 |
| NBM_6_1_2 | AO96/13-TC, 0-1 cm | *Quinqueloculina arctica* | 70.45 | 0.60 |
| NBM_6_1_3 | AO96/13-TC, 0-1 cm | *Quinqueloculina arctica* | 66.52 | 0.24 |
| NBM_8_2 | LOMROG12-TC12, 0-1 cm | *Quinqueloculina arctica* | 67.80 | 0.40 |
| NBM_12_3 | LOMROG07-PC04, 0-1 cm | *Quinqueloculina arctica* | 73.53 | 0.30 |
| NBM_13_1 | LOMROG07/GC02, 0-1 cm | *Quinqueloculina arctica* | 67.35 | 0.31 |
| NBM_15_2 | LOMROG07-PC08, 0-0.5 cm | *Quinqueloculina arctica* | 70.56 | 0.09 |

| Sample ID | Core top/multicore | BF species | Mg25/Ca43 | RSD |
|---|---|---|---|---|
| NBM_15_8 | LOMROG07-TC08, 0-0.5 cm | *Quinqueloculina arctica* | 70.15 | 0.50 |
| NBM_4_3 | A096/09-1PC, 0-1 cm | *Quinqueloculina arctica* | 50.47 | 0.29 |
| NBM_LR5_1 (M43_b) | LOMROG12-TC05, 0-1 cm | *Quinqueloculina arctica* | 72.04 | 2.23 |
| NBM_M43a | 28-MC1-4 | *Quinqueloculina arctica* | 18.89 | 0.97 |
| NBM_M16 | 13-MC1-4 | *Quinqueloculina arctica* | 20.26 | 0.89 |
| NBM_M21 | 15-MC1-4 | *Quinqueloculina arctica* | 41.85 | 1.06 |
| NBM_M23 | 16-MC1-4 | *Quinqueloculina arctica* | 22.55 | 0.64 |
| NBM_M26 | 18-MC1-4 | *Quinqueloculina arctica* | 75.08 | 1.87 |
| NBM_M28 | 21-MC2-4 | *Quinqueloculina arctica* | 74.22 | 1.37 |
| NBM_M29 | 22-MC1-4 | *Quinqueloculina arctica* | 53.74 | 0.90 |
| NBM_M32 | 23-MC1-4 | *Quinqueloculina arctica* | 71.18 | 0.99 |
| NBM_M35 | 24-MC1-4 | *Quinqueloculina arctica* | 22.71 | 1.85 |
| NBM_M39 | 26-MC1-4 | *Quinqueloculina arctica* | 69.78 | 0.97 |
| NBM_M41 | 27-MC1-4 | *Quinqueloculina arctica* | 74.95 | 0.48 |
| NBM_M46 | 29-MC1-4 | *Quinqueloculina arctica* | 59.88 | 0.69 |
| NBM_M52 | 34-MC1-4 | *Quinqueloculina arctica* | 39.40 | 1.29 |
| NBM_1_6 | AO96/B2-1PC, 0-1 cm | *Oridorsalis tener* | 2.78 | 0.67 |
| NBM_3_3 | AO96/B7-TC, 0-1 cm | *Oridorsalis tener* | 1.76 | 0.54 |
| NBM_4_2 | A096/09-1PC, 0-1 cm | *Oridorsalis tener* | 2.22 | 0.21 |
| NBM_5_5 | A096/12-ITWC, 1 cm | *Oridorsalis tener* | 1.84 | 0.29 |
| NBM_6_4 | AO96/13-TC, 0-1 cm | *Oridorsalis tener* | 1.84 | 0.69 |
| NBM_7_2 | LOMROG09-GC03B, 0-1 cm | *Oridorsalis tener* | 2.56 | 0.87 |
| NBM_8_5 | LOMROG12-TC12, 0-1 cm | *Oridorsalis tener* | 1.64 | 0.67 |
| NBM_11_2 | LOMROG12-TC06, 0-2 cm | *Oridorsalis tener* | 1.63 | 0.53 |
| NBM_12_6 | LOMROG07-PC04, 0-1 cm | *Oridorsalis tener* | 2.51 | 0.23 |
| NBM_13_5 | LOMROG07/GC02, 0-1 cm | *Oridorsalis tener* | 2.52 | 0.24 |
| NBM_15_6 | LOMROG07-PC08, 0-0.5 cm | *Oridorsalis tener* | 2.54 | 0.33 |
| NBM_15_12 | LOMROG07-TC08, 0-0.5 cm | *Oridorsalis tener* | 3.86 | 0.29 |
| NBM_M33 | 23-MC1-4 | *Oridorsalis tener* | 1.67 | 0.97 |
| NBM_M36 | 24-MC1-4 | *Oridorsalis tener* | 1.50 | 0.71 |
| NBM_M44 | 28-MC1-4 | *Oridorsalis tener* | 1.43 | 0.57 |
| NBM_M47 | 29-MC1-4 | *Oridorsalis tener* | 1.74 | 0.25 |
| NBM_M50 | 32-MC1-4 | *Oridorsalis tener* | 1.78 | 0.27 |
| NBM_15_1 | LOMROG07-PC08, 0-0.5 cm | *Cibicidoides wuellerstorfi* | 1.48 | 0.24 |
| NBM_3_1 | AO96/B7-TC, 0-1 cm | *Cibicidoides wuellerstorfi* | 1.07 | 0.25 |
| NBM_5_1 | A096/12-ITWC, 1 cm | *Cibicidoides wuellerstorfi* | 1.34 | 0.26 |
| NBM_8_1 | LOMROG12-TC12, 0-1 cm | *Cibicidoides wuellerstorfi* | 1.27 | 0.57 |
| NBM_11_1 | LOMROG12-TC06, 0-2 cm | *Cibicidoides wuellerstorfi* | 1.04 | 0.57 |
| NBM_12_1 | LOMROG07-PC04, 0-1 cm | *Cibicidoides wuellerstorfi* | 2.09 | 0.40 |
| NBM_14_1 | LOMROG07-TC06, 0-2 cm | *Cibicidoides wuellerstorfi* | 1.29 | 0.31 |
| NBM_LR9_4 | LOMROG12-TC05 | *Cibicidoides wuellerstorfi* | 2.57 | 0.82 |
| NBM_M17 | 13-MC1-4 | *Cibicidoides wuellerstorfi* | 1.32 | 1.26 |
| NBM_R4 | 13-MC1-4 | *Cibicidoides wuellerstorfi* | 1.15 | 1.34 |
| NBM_M24 | 16-MC1-4 | *Cibicidoides wuellerstorfi* | 1.48 | 1.21 |

**Table F.** Compiled Mg/Ca data and hydrological parameters (temperature and salinity) at the six studied species. Also shown are their core top locations.

| BF species | Data source | Location | Field BWT (°C) | Mg/Ca (mmol/mol) | Salinity |
|---|---|---|---|---|---|
| *E. excavatum* | Varekamp et al. [2010] | Long Island Sound | 12.10 | 1.10 | |
| *E. excavatum* | Varekamp et al. [2010] | Long Island Sound | 12.50 | 1.21 | |
| *E. excavatum* | Varekamp et al. [2010] | Long Island Sound | 13.28 | 1.32 | |
| *E. excavatum* | Varekamp et al. [2010] | Long Island Sound | 13.09 | 1.40 | |
| *E. excavatum* | Varekamp et al. [2010] | Long Island Sound | 12.59 | 1.53 | |
| *E. excavatum* | Varekamp et al. [2010] | Long Island Sound | 13.50 | 1.56 | |
| *E. excavatum* | Varekamp et al. [2010] | Long Island Sound | 14.59 | 1.71 | |
| *E. excavatum* | Varekamp et al. [2010] | Long Island Sound | 14.50 | 1.77 | |
| *E. excavatum* | Varekamp et al. [2010] | Long Island Sound | 14.30 | 2.01 | |
| *E. excavatum* | Varekamp et al. [2010] | Long Island Sound | 14.70 | 1.99 | |
| *E. excavatum* | Varekamp et al. [2010] | Long Island Sound | 15.40 | 1.99 | |
| *E. excavatum* | Varekamp et al. [2010] | Long Island Sound | 15.71 | 2.58 | |
| *E. excavatum* | Gabrielsson [2004] | Baltic and North Seas | 5.42 | 0.82 | 15.10 |
| *E. excavatum* | Gabrielsson [2004] | Baltic and North Seas | 3.78 | 1.39 | 15.36 |
| *E. excavatum* | Gabrielsson [2004] | Baltic and North Seas | 6.53 | 1.58 | 34.32 |
| *N. labradorica* | Gabrielsson [2004] | Baltic and North Seas | 5.87 | 1.84 | 34.28 |
| *N. labradorica* | Gabrielsson [2004] | Baltic and North Seas | 6.53 | 2.04 | 34.48 |
| *N. labradorica* | Gabrielsson [2004] | Baltic and North Seas | 6.55 | 3.42 | 34.98 |
| *C. neoteretis* | Kristjánsdóttir et al. [2007] | North Iceland Shelf | 6.03 | 1.24 | |
| *C. neoteretis* | Kristjánsdóttir et al. [2007] | North Iceland Shelf | 6.04 | 1.38 | |
| *C. neoteretis* | Kristjánsdóttir et al. [2007] | North Iceland Shelf | 0.22 | 1.00 | |
| *C. neoteretis* | Kristjánsdóttir et al. [2007] | North Iceland Shelf | 5.52 | 1.29 | |
| *C. neoteretis* | Kristjánsdóttir et al. [2007] | North Iceland Shelf | 2.04 | 0.99 | |
| *C. neoteretis* | Kristjánsdóttir et al. [2007] | North Iceland Shelf | 4.51 | 1.16 | |
| *C. neoteretis* | Kristjánsdóttir et al. [2007] | North Iceland Shelf | 6.25 | 1.35 | |
| *C. neoteretis* | Kristjánsdóttir et al. [2007] | North Iceland Shelf | 6.25 | 1.38 | |
| *C. neoteretis* | Kristjánsdóttir et al. [2007] | North Iceland Shelf | 0.96 | 0.93 | |
| *C. neoteretis* | Kristjánsdóttir et al. [2007] | North Iceland Shelf | 0.96 | 0.93 | |
| *Q. yabei* | Toyofuku et al. [2000] | Japan Sea | 17.20 | 111.70 | |
| *Q. yabei* | Toyofuku et al. [2000] | Japan Sea | 22.60 | 126.10 | |
| *Q. yabei* | Toyofuku et al. [2000] | Japan Sea | 25.70 | 116.90 | |
| *Q. yabei* | Toyofuku et al. [2000] | Japan Sea | 18.70 | 112.00 | |
| *Q. yabei* | Toyofuku et al. [2000] | Japan Sea | 14.80 | 109.80 | |
| *Q. yabei* | Toyofuku et al. [2000] | Japan Sea | 11.70 | 95.20 | |
| *Q. yabei* | Toyofuku et al. [2000] | Japan Sea | 17.20 | 102.30 | |
| *Q. yabei* | Toyofuku et al. [2000] | Japan Sea | 14.20 | 100.68 | |
| *Q. yabei* | Toyofuku et al. [2000] | Japan Sea | 17.70 | 105.61 | |
| *Q. yabei* | Toyofuku et al. [2000] | Japan Sea | 20.90 | 106.35 | |
| *Q. yabei* | Toyofuku et al. [2000] | Japan Sea | 22.60 | 117.11 | |
| *O. umbonatus* | Lear et al. [2002] | Little Bahama Bank | 9.86 | 2.30 | |
| *O. umbonatus* | Lear et al. [2002] | Little Bahama Bank | 8.20 | 2.26 | |
| *O. umbonatus* | Lear et al. [2002] | Little Bahama Bank | 4.35 | 3.43 | |
| *O. umbonatus* | Lear et al. [2002] | Little Bahama Bank | 4.05 | 2.04 | |
| *O. umbonatus* | Lear et al. [2002] | Hawaii Islands | 1.76 | 1.38 | |
| *O. umbonatus* | Lear et al. [2002] | Gulf of California | 3.50 | 1.22 | |
| *O. umbonatus* | Lear et al. [2002] | Gulf of California | 3.00 | 1.22 | |
| *O. umbonatus* | Lear et al. [2002] | Gulf of California | 3.00 | 1.24 | |
| *O. umbonatus* | Lear et al. [2002] | Okhotsk Sea | 2.20 | 1.09 | |
| *O. umbonatus* | Lear et al. [2002] | Okhotsk Sea | 2.27 | 1.28 | |
| *O. umbonatus* | Lear et al. [2002] | Okhotsk Sea | 2.28 | 1.33 | |
| *O. umbonatus* | Lear et al. [2002] | NE Atlantic | 3.30 | 1.84 | |
| *O. umbonatus* | Lear et al. [2002] | NE Atlantic | 2.70 | 1.91 | |
| *O. umbonatus* | Lear et al. [2002] | NE Atlantic | 2.70 | 1.84 | |
| *O. umbonatus* | Lear et al. [2002] | Timor Sea | 4.60 | 1.69 | |
| *O. umbonatus* | Rathmann et al. [2004] | continental slope off Namibia | 10.41 | 4.13 | |
| *O. umbonatus* | Rathmann et al. [2004] | continental slope off Namibia | 8.43 | 3.09 | |
| *O. umbonatus* | Rathmann et al. [2004] | continental slope off Namibia | 6.42 | 2.06 | |
| *O. umbonatus* | Rathmann et al. [2004] | continental slope off Namibia | 5.52 | 2.81 | |
| *O. umbonatus* | Rathmann et al. [2004] | continental slope off Namibia | 3.33 | 2.11 | |
| *O. umbonatus* | Rathmann et al. [2004] | continental slope off Namibia | 2.91 | 2.25 | |
| *O. umbonatus* | Healey et al. [2008] | Vema Channel | 1.45 | 1.38 | |
| *O. umbonatus* | Healey et al. [2008] | Vema Channel | 1.60 | 1.43 | |
| *O. umbonatus* | Healey et al. [2008] | Vema Channel | 2.00 | 1.55 | |
| *O. umbonatus* | Healey et al. [2008] | Vema Channel | 2.10 | 1.56 | |
| *O. umbonatus* | Healey et al. [2008] | Vema Channel | 2.41 | 1.90 | |
| *O. umbonatus* | Healey et al. [2008] | Vema Channel | 2.76 | 1.82 | |
| *O. umbonatus* | Healey et al. [2008] | Vema Channel | 2.88 | 2.60 | |
| *O. umbonatus* | Healey et al. [2008] | Vema Channel | 2.88 | 1.94 | |
| *O. umbonatus* | Healey et al. [2008] | Vema Channel | 2.76 | 2.13 | |

| | | | | | |
|---|---|---|---|---|---|
| *O. umbonatus* | Healey et al. [2008] | Vema Channel | 2.80 | 1.66 | |
| *O. umbonatus* | Healey et al. [2008] | Vema Channel | 0.85 | 1.25 | |
| *O. umbonatus* | Healey et al. [2008] | Vema Channel | 1.50 | 1.40 | |
| *O. umbonatus* | Healey et al. [2008] | Vema Channel | 2.39 | 1.34 | |
| *O. umbonatus* | Healey et al. [2008] | Vema Channel | 2.79 | 2.17 | |
| *O. umbonatus* | Healey et al. [2008] | Vema Channel | 2.90 | 2.28 | |
| *O. umbonatus* | Healey et al. [2008] | Vema Channel | 2.88 | 1.83 | |
| *O. umbonatus* | Healey et al. [2008] | Vema Channel | 2.71 | 2.18 | |
| *O. umbonatus* | Healey et al. [2008] | Indian Ocean | 1.58 | 1.28 | |
| *O. umbonatus* | Healey et al. [2008] | Indian Ocean | 1.58 | 1.54 | |
| *O. umbonatus* | Healey et al. [2008] | Indian Ocean | 1.58 | 1.36 | |
| *O. umbonatus* | Healey et al. [2008] | Indian Ocean | 1.30 | 1.50 | |
| *O. umbonatus* | Healey et al. [2008] | South China Sea | 3.77 | 2.48 | |
| *O. umbonatus* | Healey et al. [2008] | Other Atlantic | 2.02 | 1.75 | |
| *O. umbonatus* | Healey et al. [2008] | Other Atlantic | 2.04 | 2.12 | |
| *O. umbonatus* | Lear et al. [2010] | Norwegian Sea | -0.80 | 1.52 | |
| *O. umbonatus* | Lear et al. [2010] | Norwegian Sea | -0.90 | 1.17 | |
| *O. umbonatus* | Lear et al. [2010] | Norwegian Sea | -0.90 | 1.17 | |
| *O. umbonatus* | Lear et al. [2010] | Norwegian Sea | -0.80 | 1.34 | |
| *O. umbonatus* | Lear et al. [2010] | Norwegian Sea | -0.80 | 1.26 | |
| *O. umbonatus* | Lear et al. [2010] | Norwegian Sea | -0.80 | 1.32 | |
| *O. umbonatus* | Lear et al. [2010] | Norwegian Sea | -0.80 | 1.12 | |
| *O. umbonatus* | Lear et al. [2010] | Norwegian Sea | -0.80 | 1.11 | |
| *O. umbonatus* | Lear et al. [2010] | Norwegian Sea | -0.60 | 1.42 | |
| *O. umbonatus* | Lear et al. [2010] | Norwegian Sea | -0.60 | 1.44 | |
| *O. umbonatus* | Lear et al. [2010] | Norwegian Sea | -0.70 | 1.28 | |
| *O. umbonatus* | Lear et al. [2010] | Norwegian Sea | -0.80 | 1.39 | |
| *O. umbonatus* | Lear et al. [2010] | Norwegian Sea | -0.90 | 1.34 | |
| *O. umbonatus* | Lear et al. [2010] | Norwegian Sea | -0.80 | 1.20 | |
| *O. umbonatus* | Lear et al. [2010] | Norwegian Sea | -0.80 | 1.27 | |
| *O. umbonatus* | Lear et al. [2010] | Norwegian Sea | -0.80 | 1.15 | |
| *O. umbonatus* | Lear et al. [2010] | Norwegian Sea | -0.80 | 1.13 | |
| *O. umbonatus* | Lear et al. [2010] | Indo-Pacific | 3.70 | 1.69 | |
| *O. umbonatus* | Lear et al. [2010] | Indo-Pacific | 2.90 | 1.54 | |
| *O. umbonatus* | Lear et al. [2010] | Indo-Pacific | 1.90 | 1.38 | |
| *O. umbonatus* | Lear et al. [2010] | Southern Ocean | 3.20 | 1.88 | |
| *O. umbonatus* | Tisserand et al. [2013] | western tropical Atlantic | 6.06 | 3.10 | |
| *O. umbonatus* | Tisserand et al. [2013] | western tropical Atlantic | 6.06 | 2.88 | |
| *O. umbonatus* | Tisserand et al. [2013] | western tropical Atlantic | 6.06 | 2.66 | |
| *O. umbonatus* | Tisserand et al. [2013] | western tropical Atlantic | 6.06 | 2.32 | |
| *O. umbonatus* | Tisserand et al. [2013] | western tropical Atlantic | 6.06 | 2.71 | |
| *O. umbonatus* | Tisserand et al. [2013] | western tropical Atlantic | 4.92 | 2.44 | |
| *O. umbonatus* | Tisserand et al. [2013] | western tropical Atlantic | 4.92 | 2.61 | |
| *O. umbonatus* | Tisserand et al. [2013] | western tropical Atlantic | 4.64 | 2.26 | |
| *O. umbonatus* | Tisserand et al. [2013] | western tropical Atlantic | 4.30 | 2.90 | |
| *O. umbonatus* | Tisserand et al. [2013] | western tropical Atlantic | 4.30 | 2.27 | |
| *O. umbonatus* | Tisserand et al. [2013] | western tropical Atlantic | 4.17 | 3.01 | |
| *O. umbonatus* | Tisserand et al. [2013] | western tropical Atlantic | 4.17 | 2.31 | |
| *Cibicidoides wuellerstorfi* | Russell et al. [1994] | Atlantic | 2.80 | 2.25 | |
| *Cibicidoides wuellerstorfi* | Russell et al. [1994] | Atlantic | 2.80 | 2.04 | |
| *Cibicidoides wuellerstorfi* | Russell et al. [1994] | Atlantic | 2.60 | 1.86 | |
| *Cibicidoides wuellerstorfi* | Russell et al. [1994] | Atlantic | 2.60 | 1.92 | |
| *Cibicidoides wuellerstorfi* | Russell et al. [1994] | Atlantic | 2.40 | 1.77 | |
| *Cibicidoides wuellerstorfi* | Russell et al. [1994] | Atlantic | 2.30 | 1.46 | |
| *Cibicidoides wuellerstorfi* | Russell et al. [1994] | Atlantic | 2.30 | 1.54 | |
| *Cibicidoides wuellerstorfi* | Russell et al. [1994] | Atlantic | 2.10 | 1.32 | |
| *Cibicidoides wuellerstorfi* | Russell et al. [1994] | Atlantic | 2.10 | 1.32 | |
| *Cibicidoides wuellerstorfi* | Russell et al. [1994] | Atlantic | 1.70 | 1.32 | |
| *Cibicidoides wuellerstorfi* | Russell et al. [1994] | Atlantic | 1.70 | 1.56 | |
| *Cibicidoides wuellerstorfi* | Russell et al. [1994] | Pacific | 2.80 | 1.69 | |
| *Cibicidoides wuellerstorfi* | Russell et al. [1994] | Pacific | 2.80 | 1.69 | |
| *Cibicidoides wuellerstorfi* | Russell et al. [1994] | Pacific | 2.70 | 1.58 | |
| *Cibicidoides wuellerstorfi* | Russell et al. [1994] | Pacific | 2.70 | 1.65 | |
| *Cibicidoides wuellerstorfi* | Rathburn and de Decker [1997] | Coral Sea | 2.25 | 1.54 | |
| *Cibicidoides wuellerstorfi* | Rathburn and de Decker [1997] | Coral Sea | 2.25 | 1.86 | |
| *Cibicidoides wuellerstorfi* | Rathburn and de Decker [1997] | Coral Sea | 2.25 | 1.88 | |
| *Cibicidoides wuellerstorfi* | Rathburn and de Decker [1997] | Coral Sea | 2.25 | 1.27 | |
| *Cibicidoides wuellerstorfi* | Rathburn and de Decker [1997] | Coral Sea | 2.25 | 3.19 | |
| *Cibicidoides wuellerstorfi* | Rathburn and de Decker [1997] | Coral Sea | 2.25 | 2.80 | |
| *Cibicidoides wuellerstorfi* | Rathburn and de Decker [1997] | Coral Sea | 1.77 | 2.64 | |
| *Cibicidoides wuellerstorfi* | Rathburn and de Decker [1997] | Coral Sea | 1.72 | 2.64 | |
| *Cibicidoides wuellerstorfi* | Rathburn and de Decker [1997] | Coral Sea | 2.22 | 2.64 | |
| *Cibicidoides wuellerstorfi* | Rathburn and de Decker [1997] | Coral Sea | 3.82 | 2.64 | |
| *Cibicidoides wuellerstorfi* | Rathburn and de Decker [1997] | Coral Sea | 2.39 | 2.64 | |
| *Cibicidoides wuellerstorfi* | Rathburn and de Decker [1997] | Coral Sea | 2.87 | 2.64 | |
| *Cibicidoides wuellerstorfi* | Rathburn and de Decker [1997] | Coral Sea | 4.01 | 2.64 | |
| *Cibicidoides wuellerstorfi* | Rathburn and de Decker [1997] | Coral Sea | 2.05 | 2.64 | |
| *Cibicidoides wuellerstorfi* | Rathburn and de Decker [1997] | Coral Sea | 1.68 | 2.64 | |
| *Cibicidoides wuellerstorfi* | Rathburn and de Decker [1997] | Coral Sea | 1.43 | 2.95 | |
| *Cibicidoides wuellerstorfi* | Rathburn and de Decker [1997] | Coral Sea | 4.37 | 3.57 | |

| | | | | | |
|---|---|---|---|---|---|
| *Cibicidoides wuellerstorfi* | Rathburn and de Decker [1997] | Coral Sea | 2.47 | 3.57 | |
| *Cibicidoides wuellerstorfi* | Rathburn and de Decker [1997] | Coral Sea | 1.97 | 3.57 | |
| *Cibicidoides wuellerstorfi* | Rathburn and de Decker [1997] | Coral Sea | 2.67 | 3.57 | |
| *Cibicidoides wuellerstorfi* | Rathburn and de Decker [1997] | Coral Sea | 2.43 | 4.33 | |
| *Cibicidoides wuellerstorfi* | Rathburn and de Decker [1997] | Coral Sea | 2.22 | 4.33 | |
| *Cibicidoides wuellerstorfi* | Rathburn and de Decker [1997] | Coral Sea | 2.96 | 4.33 | |
| *Cibicidoides wuellerstorfi* | Rathburn and de Decker [1997] | Coral Sea | 2.61 | 4.33 | |
| *Cibicidoides wuellerstorfi* | Rathburn and de Decker [1997] | Coral Sea | 2.66 | 4.33 | |
| *Cibicidoides wuellerstorfi* | Rathburn and de Decker [1997] | Coral Sea | 2.08 | 4.33 | |
| *Cibicidoides wuellerstorfi* | Rathburn and de Decker [1997] | Coral Sea | 4.68 | 4.33 | |
| *Cibicidoides wuellerstorfi* | Rathburn and de Decker [1997] | Coral Sea | 2.54 | 4.33 | |
| *Cibicidoides wuellerstorfi* | Rathburn and de Decker [1997] | Coral Sea | 2.18 | 4.33 | |
| *Cibicidoides wuellerstorfi* | Rathburn and de Decker [1997] | Coral Sea | 2.80 | 4.33 | |
| *Cibicidoides wuellerstorfi* | Rathburn and de Decker [1997] | Coral Sea | 1.83 | 4.33 | |
| *Cibicidoides wuellerstorfi* | Rathburn and de Decker [1997] | Coral Sea | 2.08 | 4.33 | |
| *Cibicidoides wuellerstorfi* | Rathburn and de Decker [1997] | Coral Sea | 2.61 | 5.87 | |
| *Cibicidoides wuellerstorfi* | Rathburn and de Decker [1997] | Coral Sea | 2.50 | 5.87 | |
| *Cibicidoides wuellerstorfi* | Rathburn and de Decker [1997] | Coral Sea | 3.57 | 5.87 | |
| *Cibicidoides wuellerstorfi* | Rathburn and de Decker [1997] | Coral Sea | 2.75 | 8.70 | |
| *Cibicidoides wuellerstorfi* | Rathburn and de Decker [1997] | Coral Sea | 2.74 | 8.70 | |
| *Cibicidoides wuellerstorfi* | Rathburn and de Decker [1997] | Coral Sea | 3.29 | 8.70 | |
| *Cibicidoides wuellerstorfi* | Rosenthal et al. [1997] | Little Bahama Bank | 2.50 | 1.61 | |
| *Cibicidoides wuellerstorfi* | Rosenthal et al. [1997] | Little Bahama Bank | 2.30 | 1.29 | |
| *Cibicidoides wuellerstorfi* | Rosenthal et al. [1997] | Little Bahama Bank | 2.30 | 1.53 | |
| *Cibicidoides wuellerstorfi* | Rosenthal, MIT/unpub | Ceara Rise | 2.60 | 1.37 | |
| *Cibicidoides wuellerstorfi* | Rosenthal, MIT/unpub | Ceara Rise | 2.60 | 1.63 | |
| *Cibicidoides wuellerstorfi* | Rosenthal, MIT/unpub | Ceara Rise | 2.40 | 1.61 | |
| *Cibicidoides wuellerstorfi* | Rosenthal, MIT/unpub | Ceara Rise | 2.30 | 1.62 | |
| *Cibicidoides wuellerstorfi* | Rosenthal, MIT/unpub | Ceara Rise | 1.50 | 1.19 | |
| *Cibicidoides wuellerstorfi* | Rosenthal, MIT/unpub | Ceara Rise | 1.50 | 1.20 | |
| *Cibicidoides wuellerstorfi* | Rosenthal, MIT/unpub | Ontong Java Plateau | 2.80 | 1.66 | |
| *Cibicidoides wuellerstorfi* | Rosenthal, MIT/unpub | Ontong Java Plateau | 2.50 | 1.10 | |
| *Cibicidoides wuellerstorfi* | Rosenthal, MIT/unpub | Ontong Java Plateau | 2.00 | 2.07r | |
| *Cibicidoides wuellerstorfi* | Rosenthal, MIT/unpub | Ontong Java Plateau | 2.00 | 1.43 | |
| *Cibicidoides wuellerstorfi* | Rosenthal, MIT/unpub | South Atlantic | 0.70 | 1.10 | |
| *Cibicidoides wuellerstorfi* | Rosenthal, MIT/unpub | South Atlantic | 0.40 | 1.20 | |
| *Cibicidoides wuellerstorfi* | Lear et al. [2002] | Hawaii | 2.36 | 1.48 | |
| *Cibicidoides wuellerstorfi* | Lear et al. [2002] | Hawaii | 2.36 | 0.98 | |
| *Cibicidoides wuellerstorfi* | Lear et al. [2002] | Hawaii | 2.36 | 0.92 | |
| *Cibicidoides wuellerstorfi* | Lear et al. [2002] | Hawaii | 2.36 | 1.84 | |
| *Cibicidoides wuellerstorfi* | Lear et al. [2002] | Hawaii | 1.76 | 1.00 | |
| *Cibicidoides wuellerstorfi* | Lear et al. [2002] | Hawaii | 1.76 | 0.99 | |
| *Cibicidoides wuellerstorfi* | Lear et al. [2002] | Hawaii | 1.76 | 1.03 | |
| *Cibicidoides wuellerstorfi* | Lear et al. [2002] | Hawaii | 1.76 | 1.05 | |
| *Cibicidoides wuellerstorfi* | Lear et al. [2002] | Hawaii | 1.75 | 0.95 | |
| *Cibicidoides wuellerstorfi* | Lear et al. [2002] | Hawaii | 1.75 | 0.96 | |
| *Cibicidoides wuellerstorfi* | Lear et al. [2002] | NE Atlantic | 3.30 | 1.62 | |
| *Cibicidoides wuellerstorfi* | Lear et al. [2002] | NE Atlantic | 3.30 | 1.69 | |
| *Cibicidoides wuellerstorfi* | Lear et al. [2002] | NE Atlantic | 3.30 | 1.55 | |
| *Cibicidoides wuellerstorfi* | Lear et al. [2002] | NE Atlantic | 2.70 | 1.30 | |
| *Cibicidoides wuellerstorfi* | Lear et al. [2002] | Bahamas | 4.35 | 2.10 | |
| *Cibicidoides wuellerstorfi* | Lear et al. [2002] | Bahamas | 4.05 | 1.77 | |
| *Cibicidoides wuellerstorfi* | Martin et al. [2002] | Ceara Rise | 2.60 | 1.16 | |
| *Cibicidoides wuellerstorfi* | Martin et al. [2002] | Ceara Rise | 2.60 | 1.14 | |
| *Cibicidoides wuellerstorfi* | Martin et al. [2002] | Ceara Rise | 2.50 | 1.20 | |
| *Cibicidoides wuellerstorfi* | Martin et al. [2002] | Ceara Rise | 2.20 | 1.16 | |
| *Cibicidoides wuellerstorfi* | Martin et al. [2002] | Ceara Rise | 2.20 | 1.07 | |
| *Cibicidoides wuellerstorfi* | Martin et al. [2002] | Ceara Rise | 2.20 | 1.09 | |
| *Cibicidoides wuellerstorfi* | Martin et al. [2002] | Ceara Rise | 2.10 | 1.01 | |
| *Cibicidoides wuellerstorfi* | Martin et al. [2002] | Ceara Rise | 1.80 | 0.99 | |
| *Cibicidoides wuellerstorfi* | Martin et al. [2002] | Ceara Rise | 1.50 | 0.79 | |
| *Cibicidoides wuellerstorfi* | Martin et al. [2002] | Ceara Rise | 1.50 | 0.72 | |
| *Cibicidoides wuellerstorfi* | Martin et al. [2002] | Ceara Rise | 1.50 | 0.68 | |
| *Cibicidoides wuellerstorfi* | Martin et al. [2002] | Ontong Java Plateau | 2.80 | 1.37 | |
| *Cibicidoides wuellerstorfi* | Martin et al. [2002] | Ontong Java Plateau | 2.70 | 1.29 | |
| *Cibicidoides wuellerstorfi* | Martin et al. [2002] | Ontong Java Plateau | 2.70 | 1.32 | |
| *Cibicidoides wuellerstorfi* | Martin et al. [2002] | Ontong Java Plateau | 2.20 | 1.15 | |
| *Cibicidoides wuellerstorfi* | Martin et al. [2002] | Ontong Java Plateau | 2.00 | 1.05 | |
| *Cibicidoides wuellerstorfi* | Martin et al. [2002] | Ontong Java Plateau | 1.90 | 1.06 | |
| *Cibicidoides wuellerstorfi* | Martin et al. [2002] | Ontong Java Plateau | 1.90 | 1.12 | |
| *Cibicidoides wuellerstorfi* | Martin et al. [2002] | Ontong Java Plateau | 1.90 | 1.13 | |
| *Cibicidoides wuellerstorfi* | Martin et al. [2002] | Ontong Java Plateau | 1.60 | 0.86 | |
| *Cibicidoides wuellerstorfi* | Martin et al. [2002] | Other Atlantic sites | 3.00 | 1.45 | |
| *Cibicidoides wuellerstorfi* | Martin et al. [2002] | Other Atlantic sites | 3.00 | 1.46 | |
| *Cibicidoides wuellerstorfi* | Martin et al. [2002] | Other Atlantic sites | 2.90 | 1.31 | |
| *Cibicidoides wuellerstorfi* | Martin et al. [2002] | Other Atlantic sites | 2.90 | 1.34 | |
| *Cibicidoides wuellerstorfi* | Martin et al. [2002] | Other Atlantic sites | 2.70 | 1.22 | |
| *Cibicidoides wuellerstorfi* | Martin et al. [2002] | Other Atlantic sites | 1.40 | 0.75 | |
| *Cibicidoides wuellerstorfi* | Martin et al. [2002] | Other Atlantic sites | -1.10 | 1.11 | |
| *Cibicidoides wuellerstorfi* | Healey et al. [2008] | Vema Channel | 1.20 | 1.03 | |

| | | | | | |
|---|---|---|---|---|---|
| *Cibicidoides wuellerstorfi* | Healey et al. [2008] | Vema Channel | 1.30 | 1.07 | |
| *Cibicidoides wuellerstorfi* | Healey et al. [2008] | Vema Channel | 1.40 | 1.16 | |
| *Cibicidoides wuellerstorfi* | Healey et al. [2008] | Vema Channel | 1.40 | 1.08 | |
| *Cibicidoides wuellerstorfi* | Healey et al. [2008] | Vema Channel | 1.45 | 1.11 | |
| *Cibicidoides wuellerstorfi* | Healey et al. [2008] | Vema Channel | 1.60 | 1.11 | |
| *Cibicidoides wuellerstorfi* | Healey et al. [2008] | Vema Channel | 2.00 | 1.19 | |
| *Cibicidoides wuellerstorfi* | Healey et al. [2008] | Vema Channel | 2.10 | 1.36 | |
| *Cibicidoides wuellerstorfi* | Healey et al. [2008] | Vema Channel | 2.41 | 1.33 | |
| *Cibicidoides wuellerstorfi* | Healey et al. [2008] | Vema Channel | 2.45 | 1.35 | |
| *Cibicidoides wuellerstorfi* | Healey et al. [2008] | Vema Channel | 2.45 | 1.31 | |
| *Cibicidoides wuellerstorfi* | Healey et al. [2008] | Vema Channel | 2.76 | 1.48 | |
| *Cibicidoides wuellerstorfi* | Healey et al. [2008] | Vema Channel | 2.76 | 1.42 | |
| *Cibicidoides wuellerstorfi* | Healey et al. [2008] | Vema Channel | 2.88 | 1.44 | |
| *Cibicidoides wuellerstorfi* | Healey et al. [2008] | Vema Channel | 2.85 | 1.52 | |
| *Cibicidoides wuellerstorfi* | Healey et al. [2008] | Vema Channel | 2.93 | 1.60 | |
| *Cibicidoides wuellerstorfi* | Healey et al. [2008] | Vema Channel | 2.93 | 1.55 | |
| *Cibicidoides wuellerstorfi* | Healey et al. [2008] | Vema Channel | 2.88 | 1.48 | |
| *Cibicidoides wuellerstorfi* | Healey et al. [2008] | Vema Channel | 2.71 | 1.43 | |
| *Cibicidoides wuellerstorfi* | Healey et al. [2008] | Vema Channel | 2.88 | 1.44 | |
| *Cibicidoides wuellerstorfi* | Healey et al. [2008] | Vema Channel | 2.71 | 1.54 | |
| *Cibicidoides wuellerstorfi* | Healey et al. [2008] | Vema Channel | 2.76 | 1.50 | |
| *Cibicidoides wuellerstorfi* | Healey et al. [2008] | Indian Ocean | 1.00 | 1.14 | |
| *Cibicidoides wuellerstorfi* | Healey et al. [2008] | Indian Ocean | 1.50 | 1.12 | |
| *Cibicidoides wuellerstorfi* | Healey et al. [2008] | Indian Ocean | 1.58 | 1.18 | |
| *Cibicidoides wuellerstorfi* | Healey et al. [2008] | Indian Ocean | 0.95 | 0.98 | |
| *Cibicidoides wuellerstorfi* | Healey et al. [2008] | Indian Ocean | 0.96 | 0.97 | |
| *Cibicidoides wuellerstorfi* | Healey et al. [2008] | Indian Ocean | 1.10 | 0.96 | |
| *Cibicidoides wuellerstorfi* | Healey et al. [2008] | Indian Ocean | 0.81 | 0.79 | |
| *Cibicidoides wuellerstorfi* | Healey et al. [2008] | South China Sea | 3.77 | 2.05 | |
| *Cibicidoides wuellerstorfi* | Healey et al. [2008] | South China Sea | 2.40 | 1.30 | |
| *Cibicidoides wuellerstorfi* | Healey et al. [2008] | South China Sea | 2.71 | 1.44 | |
| *Cibicidoides wuellerstorfi* | Healey et al. [2008] | South China Sea | 2.89 | 1.42 | |
| *Cibicidoides wuellerstorfi* | Raitzsch et al. [2008] | South Atlantic | 2.51 | 1.57 | |
| *Cibicidoides wuellerstorfi* | Raitzsch et al. [2008] | South Atlantic | 2.36 | 1.73 | |
| *Cibicidoides wuellerstorfi* | Raitzsch et al. [2008] | South Atlantic | 0.86 | 0.99 | |
| *Cibicidoides wuellerstorfi* | Raitzsch et al. [2008] | South Atlantic | 2.67 | 1.44 | |
| *Cibicidoides wuellerstorfi* | Raitzsch et al. [2008] | South Atlantic | 2.85 | 1.38 | |
| *Cibicidoides wuellerstorfi* | Raitzsch et al. [2008] | South Atlantic | 3.05 | 1.33 | |
| *Cibicidoides wuellerstorfi* | Raitzsch et al. [2008] | South Atlantic | 3.58 | 1.72 | |
| *Cibicidoides wuellerstorfi* | Raitzsch et al. [2008] | South Atlantic | 3.59 | 1.51 | |
| *Cibicidoides wuellerstorfi* | Raitzsch et al. [2008] | South Atlantic | 2.57 | 1.50 | |
| *Cibicidoides wuellerstorfi* | Raitzsch et al. [2008] | South Atlantic | 3.16 | 1.20 | |
| *Cibicidoides wuellerstorfi* | Raitzsch et al. [2008] | South Atlantic | 3.66 | 1.50 | |
| *Cibicidoides wuellerstorfi* | Raitzsch et al. [2008] | South Atlantic | 1.43 | 1.08 | |
| *Cibicidoides wuellerstorfi* | Raitzsch et al. [2008] | South Atlantic | 3.46 | 1.34 | |
| *Cibicidoides wuellerstorfi* | Raitzsch et al. [2008] | South Atlantic | 2.95 | 1.42 | |
| *Cibicidoides wuellerstorfi* | Raitzsch et al. [2008] | South Atlantic | 2.43 | 1.79 | |
| *Cibicidoides wuellerstorfi* | Raitzsch et al. [2008] | South Atlantic | 3.59 | 1.87 | |
| *Cibicidoides wuellerstorfi* | Raitzsch et al. [2008] | South Atlantic | 2.35 | 1.74 | |
| *Cibicidoides wuellerstorfi* | Raitzsch et al. [2008] | South Atlantic | 2.36 | 1.49 | |
| *Cibicidoides wuellerstorfi* | Raitzsch et al. [2008] | South Atlantic | 3.88 | 1.98 | |
| *Cibicidoides wuellerstorfi* | Raitzsch et al. [2008] | South Atlantic | 3.55 | 1.48 | |
| *Cibicidoides wuellerstorfi* | Raitzsch et al. [2008] | South Atlantic | 0.94 | 1.02 | |
| *Cibicidoides wuellerstorfi* | Raitzsch et al. [2008] | South Atlantic | 1.20 | 0.94 | |
| *Cibicidoides wuellerstorfi* | Raitzsch et al. [2008] | South Atlantic | 1.39 | 1.04 | |
| *Cibicidoides wuellerstorfi* | Raitzsch et al. [2008] | South Atlantic | 2.36 | 1.16 | |
| *Cibicidoides wuellerstorfi* | Raitzsch et al. [2008] | South Atlantic | 2.18 | 1.28 | |
| *Cibicidoides wuellerstorfi* | Raitzsch et al. [2008] | South Atlantic | 2.18 | 1.30 | |
| *Cibicidoides wuellerstorfi* | Raitzsch et al. [2008] | South Atlantic | 2.43 | 1.54 | |
| *Cibicidoides wuellerstorfi* | Raitzsch et al. [2008] | South Atlantic | 2.51 | 2.01 | |
| *Cibicidoides wuellerstorfi* | Raitzsch et al. [2008] | South Atlantic | 2.41 | 1.58 | |
| *Cibicidoides wuellerstorfi* | Raitzsch et al. [2008] | South Atlantic | 2.11 | 1.73 | |
| *Cibicidoides wuellerstorfi* | Raitzsch et al. [2008] | South Atlantic | 1.77 | 1.76 | |
| *Cibicidoides wuellerstorfi* | Raitzsch et al. [2008] | South Atlantic | 1.68 | 1.40 | |
| *Cibicidoides wuellerstorfi* | Raitzsch et al. [2008] | South Atlantic | 0.43 | 0.84 | |
| *Cibicidoides wuellerstorfi* | Raitzsch et al. [2008] | South Atlantic | 1.53 | 1.37 | |
| *Cibicidoides wuellerstorfi* | Raitzsch et al. [2008] | South Atlantic | 3.35 | 1.55 | |
| *Cibicidoides wuellerstorfi* | Raitzsch et al. [2008] | South Atlantic | 3.81 | 1.43 | |
| *Cibicidoides wuellerstorfi* | Raitzsch et al. [2008] | South Atlantic | 0.39 | 0.84 | |
| *Cibicidoides wuellerstorfi* | Raitzsch et al. [2008] | South Atlantic | 1.27 | 1.23 | |
| *Cibicidoides wuellerstorfi* | Raitzsch et al. [2008] | South Atlantic | 0.93 | 1.15 | |
| *Cibicidoides wuellerstorfi* | Raitzsch et al. [2008] | South Atlantic | 0.43 | 0.95 | |
| *Cibicidoides wuellerstorfi* | Raitzsch et al. [2008] | South Atlantic | 1.57 | 1.27 | |
| *Cibicidoides wuellerstorfi* | Raitzsch et al. [2008] | South Atlantic | 0.92 | 1.17 | |
| *Cibicidoides wuellerstorfi* | Raitzsch et al. [2008] | South Atlantic | 3.33 | 2.02 | |
| *Cibicidoides wuellerstorfi* | Raitzsch et al. [2008] | South Atlantic | 2.91 | 1.07 | |
| *Cibicidoides wuellerstorfi* | Tisserand et al. [2013] | western tropical Atlantic | 6.06 | 2.95 | |
| *Cibicidoides wuellerstorfi* | Tisserand et al. [2013] | western tropical Atlantic | 6.06 | 2.95 | |
| *Cibicidoides wuellerstorfi* | Tisserand et al. [2013] | western tropical Atlantic | 6.06 | 2.41 | |
| *Cibicidoides wuellerstorfi* | Tisserand et al. [2013] | western tropical Atlantic | 6.06 | 2.53 | |

| | | | | | |
|---|---|---|---|---|---|
| *Cibicidoides wuellerstorfi* | Tisserand et al. [2013] | western tropical Atlantic | 6.06 | 3.07 | |
| *Cibicidoides wuellerstorfi* | Tisserand et al. [2013] | western tropical Atlantic | 6.06 | 3.91 | |
| *Cibicidoides wuellerstorfi* | Tisserand et al. [2013] | western tropical Atlantic | 5.67 | 2.55 | |
| *Cibicidoides wuellerstorfi* | Tisserand et al. [2013] | western tropical Atlantic | 5.67 | 2.76 | |
| *Cibicidoides wuellerstorfi* | Tisserand et al. [2013] | western tropical Atlantic | 5.67 | 2.04 | |
| *Cibicidoides wuellerstorfi* | Tisserand et al. [2013] | western tropical Atlantic | 5.38 | 2.56 | |
| *Cibicidoides wuellerstorfi* | Tisserand et al. [2013] | western tropical Atlantic | 5.38 | 2.23 | |
| *Cibicidoides wuellerstorfi* | Tisserand et al. [2013] | western tropical Atlantic | 5.38 | 2.24 | |
| *Cibicidoides wuellerstorfi* | Tisserand et al. [2013] | western tropical Atlantic | 5.38 | 2.31 | |
| *Cibicidoides wuellerstorfi* | Tisserand et al. [2013] | western tropical Atlantic | 5.38 | 2.44 | |
| *Cibicidoides wuellerstorfi* | Tisserand et al. [2013] | western tropical Atlantic | 5.38 | 2.30 | |
| *Cibicidoides wuellerstorfi* | Tisserand et al. [2013] | western tropical Atlantic | 4.92 | 2.44 | |
| *Cibicidoides wuellerstorfi* | Tisserand et al. [2013] | western tropical Atlantic | 4.92 | 2.65 | |
| *Cibicidoides wuellerstorfi* | Tisserand et al. [2013] | western tropical Atlantic | 4.92 | 2.55 | |
| *Cibicidoides wuellerstorfi* | Tisserand et al. [2013] | western tropical Atlantic | 4.92 | 1.80 | |
| *Cibicidoides wuellerstorfi* | Tisserand et al. [2013] | western tropical Atlantic | 4.92 | 2.45 | |
| *Cibicidoides wuellerstorfi* | Tisserand et al. [2013] | western tropical Atlantic | 4.92 | 2.00 | |
| *Cibicidoides wuellerstorfi* | Tisserand et al. [2013] | western tropical Atlantic | 4.64 | 2.40 | |
| *Cibicidoides wuellerstorfi* | Tisserand et al. [2013] | western tropical Atlantic | 4.64 | 2.11 | |
| *Cibicidoides wuellerstorfi* | Tisserand et al. [2013] | western tropical Atlantic | 4.64 | 2.32 | |
| *Cibicidoides wuellerstorfi* | Tisserand et al. [2013] | western tropical Atlantic | 4.64 | 1.88 | |
| *Cibicidoides wuellerstorfi* | Tisserand et al. [2013] | western tropical Atlantic | 4.64 | 2.05 | |
| *Cibicidoides wuellerstorfi* | Tisserand et al. [2013] | western tropical Atlantic | 4.64 | 2.10 | |
| *Cibicidoides wuellerstorfi* | Tisserand et al. [2013] | western tropical Atlantic | 4.30 | 2.08 | |
| *Cibicidoides wuellerstorfi* | Tisserand et al. [2013] | western tropical Atlantic | 4.30 | 2.02 | |
| *Cibicidoides wuellerstorfi* | Tisserand et al. [2013] | western tropical Atlantic | 4.30 | 1.95 | |
| *Cibicidoides wuellerstorfi* | Tisserand et al. [2013] | western tropical Atlantic | 4.30 | 1.81 | |
| *Cibicidoides wuellerstorfi* | Tisserand et al. [2013] | western tropical Atlantic | 4.17 | 1.91 | |
| *Cibicidoides wuellerstorfi* | Tisserand et al. [2013] | western tropical Atlantic | 4.17 | 2.09 | |
| *Cibicidoides wuellerstorfi* | Tisserand et al. [2013] | western tropical Atlantic | 4.17 | 2.03 | |

Manuscript II

# Pacific-Arctic halocline variability through the late Holocene in the Herald Canyon, Chukchi Shelf

Table of Contents

# Pacific-Arctic halocline variability through the late Holocene in the Herald Canyon, Chukchi Shelf

Natalia Barrientos[1], Helen Coxall[1], Caroline Lear[2], Christof Pearce[1,3], Francesco Muschitiello[1], Matt O'Regan[1], Christian Stranne[1.4], Andrey Koshurnikov[5,6], Martin Jakobsson[1].

[1]Department of Geological Sciences and Bolin Centre for Climate Research, Stockholm University, Stockholm, Sweden.
[2]School of Earth and Ocean Sciences, Cardiff University, Main Building, Park Place, Cardiff, CF10 3AT, UK.
[3]Department of Geoscience, Aarhus University, Aarhus, Denmark.
[5] Centre for Coastal and Ocean Mapping, University of New Hampshire, New Hampshire 03824, USA.
[5]Moscow State University, Geophysics, Russian Federation.
[6]National Research Tomsk Polytechnic University, Tomsk, 634050, Russia.

## Abstract

Marine sediment core SWERUS-L2-2-PC1 (830 cm) and a series of shorter (~30 cm) multicores accompanied by oceanographic data were collected at 6 stations in the Herald Canyon on the continental shelf of the Chukchi Sea. Sitting at 72 m water depth, seafloor at the 2-PC1 station is bathed by Pacific-Arctic halocline waters and thus is sensitively positioned to monitor variability in Pacific water inflow and halocline changes back in time. Down-core radiocarbon dating (Pearce et al., this volume) reveals exceptionally high late Holocene depositional rates at 2-PC1 (average 200 cm/kyr) allowing construction of detailed paleoceanographic histories in this region where few published measurements exist today. Here we present new high-resolution (~ 40 yrs sampling) records of benthic foraminifera carbon and oxygen stable isotopes and Mg/Ca from core 2-PC1 as proxies for changes in Arctic-Pacific bottom water temperature, upper ocean structure and water mass exchange during the past ~4000 kyrs. The data reveal switching between phases of warmer and cooler bottom water regimes during the Late Holocene. Between 4200 and 1200 cal. yr BP, Herald Canyon waters were warmer than today, suggesting greater influence of Pacific water and likely sea-ice free summers; while from 1200 cal. yr BP to 1950 AD the data suggest, cooler temperatures, more sea-ice formation and a more proximal summer sea-ice edge. The shallowest 2 cm of the core, representing modern times (i.e. post 1950 yrs BP), shows a pronounced excursion towards depleted benthic carbon isotope ratios (-0.8 ‰). This may be attributable to anthropogenic additions of $CO_2$ as a consequence of the combustion of fossil fuels (i.e. a 'Suess effect'), which has pervaded through the atmosphere into shallow Arctic Ocean subsurface layers and the dissolved inorganic carbon pool. The remarkable similarity between the timing of Mg/Ca BWT trends and millennial scale cycles captured in Canadian ice-core $\delta^{18}O$ record [Fischer et al., 2004; 2008] supports the idea that climatic/atmospheric processes affecting the North Pacific play an important role in setting Arctic-Pacific ocean thermo-halocline structure.

# 1 Introduction

Past decades of satellite imaging and ocean observation from drifting platforms and ship-based expeditions have revealed that the Pacific-Arctic region is subjected to ocean warming, receding summer sea-ice margins, ocean acidification and marine ecological changes [ACIA, 2004; Mathis et al., 2015; Wood et al., 2015]. The trigger mechanisms that drive the energy balance in the Arctic are paramount to understand why the rate of temperature increase is higher in the Arctic than the global mean and, more importantly, to understand the interplay between the atmosphere and ocean in response to a warming either by natural or anthropogenic contributions.

Observations of the patterns and variability of sea ice can provide important insights into this. About 40% of observed Arctic sea-ice retreat has been explained by atmospheric heat-flux factors [Francis et al., 2005] and linkages between sea-ice loss and atmospheric oscillation patterns have been found [Comiso, 2012; Dobricic et al., 2016]. Changes in atmospheric circulation patterns at quazi-decadal scale, such as the Arctic Oscillation [Thompson and Wallace, 1998], likely also play a role by steering Pacific water inflow directions. This is supported by observations showing that increases in the northward flux of Pacific waters entering the Arctic Ocean during 2007, as a response to stronger Pacific southerly winds, played a major role in driving the extreme retreat of the sea-ice margin that year [Zhang et al., 2008; Woodgate et al., 2010].

The other 60% contributing to sea-ice retreat must include forcing through oceanic advective/convective heat transport processes. However, in reality and over millennial time scales, the balance between atmospheric versus ocean mechanisms leading natural Arctic sea ice dynamics is uncertain [Comiso et al., 2008]. Over the past 3-4 decades, the most pronounced sea-ice retreat in the Arctic area occurs where Pacific waters, warmer than resident Arctic surface waters, enter the Arctic Ocean [Woodgate et al., 2006], despite that the heat flux is only 1/3rd of that arriving through the Fram Strait [Woodgate et al., 2010]. This can be explained by the higher buoyancy of Pacific waters compared to Atlantic waters; Pacific waters sit at shallower water depths and thus interact with and contribute more to the seasonal melt of sea ice [Woodgate et al., 2006].

The inflow of Pacific waters and reconfiguration of Arctic Ocean water masses have varied significantly over recent years. A few decades ago, hydrographic and chemical surveys identified traces of nutrient-rich Pacific waters reaching as far as the central Arctic Ocean [Kinney et al., 1970], although later, Pacific water was not even found in the Makarov Basin [McLaughlin et al., 1996], on the path towards the central Arctic Ocean. Also, a shallowing in the Pacific and Atlantic haloclines in western Canada Basin has been observed [McLaughlin et al., 2002]. Another example is that Atlantic water temperatures have increased [Quadfasel et al. 1991; Carmack et al., 1995] with a shoaling of the Atlantic layer manifested in the Amundsen and Makarov

Basins [Morison et al., 1998]. These particular changes are attributed to variations in the distribution of Pacific water in the Canadian Basin [Carmack et al., 1995; McLaughlin, et al., 1996] that might be connected to erosion of the uppermost polar mixed layer in these basins [Steele and Boyd 1998]. Therefore, we hypothesize that there might be a link between sea-ice decrease by atmospheric changes that is in turn linked to oceanographic variations at greater depths.

Here we analyse benthic foraminifera shell geochemistry from a piston core sequence retrieved in 2014 during the SWERUS-C3 expedition (Swedish-Russian-US Arctic Ocean investigation of Climate-Cryosphere-Carbon interactions) over an interesting time transition where both natural and anthropogenic processes are at play. Today at the study site in Herald Canyon (Chukchi Sea), warm, fresh and nutrient-rich 'Pacific Water' enters the Arctic Ocean from the Pacific Ocean via the Bering Strait, named as the 'Anadyr Current' (Fig. 1) [Coachman and Barnes, 1961]. Our study site lies under this incoming Pacific water mass and is thus sensitively positioned to capture variability in Pacific Water influx and sea-ice conditions over time. Importantly, the benthic foraminifera living at the seafloor in this setting inhabit and sample conditions of the Pacific-Arctic halocline. It should be possible, therefore, using sediment archives, to detect possible links between Pacific exchange, freshwater input and Arctic sea ice on the Chukchi Sea part of the Arctic Ocean, a region where very little other such data currently exit.

## 2 Herald Canyon Oceanography

The Chukchi Sea receives approximately 0.8 Sv Pacific water flow (1 Sv=$10^6$ $m^3/s$) [Ratmanov, 1937] through the shallow (~50 m deep) and narrow (~85 km wide) Bering Strait gateway. This transport of Pacific waters into the Arctic through the Bering Strait is caused by a 0.4–0.5 m higher water column on the Pacific compared to the Arctic side that counteracts the southward local wind velocity [Woodgate et al., 2010]. The pycnocline layer here, as elsewhere in the Arctic Ocean, is controlled by salinity rather than temperature differences, due to the extremely small spatial and vertical temperature gradients that exists in the Arctic (-2°C to 2°C) [Rudels et al., 2012]. The origin of the Arctic halocline water is still under investigation among oceanographers, some supporting mainly Atlantic sources [Steele and Boyd, 1998; Rudels et al., 2004], others suggesting Pacific and Atlantic admixtures [Woodgate et al., 2005], plus or minus significant local contributions from polynyas [Weingartner et al., 1998]. In the Chukchi Sea region, part of the halocline water is maintained from winter cold and fresh Pacific water entering through Bering Strait [Aagaard et al., 1981; Woodgate et al., 2012]. Once inside the Arctic Ocean, this layer is chilled to freezing point by the frigid Arctic air, causing sea ice to form over the shelves and in the process creating higher density brines (through the process of brine rejection). These brines sink below the polar mixed layer, thus delivering Pacific-derived waters to the halocline.

Spatially, Bering Strait waters flowing in from the Pacific split into three different shallow flowing water masses, from east to west; Alaskan Coastal waters, Bering Shelf waters (warm, low nutrient) and Anadyr waters (cold, high nutrient) [Coachman et al., 1975] (Figure 1). The Anadyr Current flows through the Herald Canyon and it can also reach the East Siberian Seas [Codispoti and Richards 1968]. It takes 10 years or less for Pacific waters to cross the Arctic [Danielson et al., 2014]. Barring additional sea ice changes, variation in the northward flow of these waters will interfere with the global hydrologic cycle [Aagaard and Carmack, 1989; Wijffels et al., 1992; Serreze et al., 2006] and the global thermohaline circulation [Shaffer and Bendtsen, 1994].

In the Herald Canyon two main water mass layers exist. A cold and fresh thin polar mixed layer of approximately 10 m (under zero wind action) followed by 50-100 meters of Pacific origin waters, representing the halocline. The Pacific waters are themselves, composed of slightly warm and saltier Pacific summer water (PSW) and cooler/fresher Pacific winter water (PWW) [Pickart et al., 2009]. These waters influence the Arctic Ocean in three major ways, (i) as a source of nutrient-rich waters [Walsh et al 1989] containing seven times more silica and twice as much nitrogen and phosphorus than typical Arctic waters [Heimdal, 1989]; (ii) as a source of heat; which is 1/3$^{rd}$ of that entering the Arctic through the Fram Strait heat [Woodgate et al, 2010] and (iii) as a source of fresh water inflow, 1/3$^{rd}$ of the total freshwater input to the Arctic [Aagaard and Carmack, 1989; Serreze et al., 2006]. The heat and fresh water aspects have important implications for surface freezing and thus Arctic sea ice extent [Aagaard et al., 1981].

With a mean depth of ~40 m, the Chukchi Sea encompasses the continental shelf from the Bering Strait to the shelf break towards the deep central Arctic Ocean basin [Jakobsson, 2002] (Figure 2). Herald Canyon is an important bathymetric feature since it cuts across shelf isobaths and steers water to flow northward from the Bering Strait even in the absence of wind [Woodgate et al., 2005b]. Oceanographic monitoring in the Herald Canyon over one year (1990–1991) [Woodgate et al., 2005b] has shown high seasonal temperature variability with a gradual cooling but little change in salinity (33.1 psu). The flanks of the Herald Canyon are dominated by two distinct water regimes. As seen from the Bering Strait side, our site lies on the eastern flank that is invaded by Pacific origin waters, while the western flank is bathed by Arctic origin waters. Interestingly, thermal regime surveys from 1941 to 2008 show that “warm” years have been characterized by a wider Pacific water distribution increasing the inflow through the Herald Canyon whereas in “cold” years Pacific waters follow the Alaskan coast [Luchin and Panteleev, 2014].

## 3 Materials and Methods

SWERUS-L2-2-PC1 piston core (hereafter 2-PC) was retrieved onboard the icebreaker R/V Oden at 72.516580 N, 175.319605 W (72 m water depth) in August 2014. The cored sediments comprise 8.3 m of homogeneous olive gray mud. The 6 x 1-1.5 m –long sections were sampled during the cruise (with 24h hours of core recovery) at 8 cm intervals. Where possible 2 cm wide scoops (10 $cm^3$) were taken.

### 3.1 Age model and reservoir correction

The chronology for 2-PC was developed in a parallel study by Pearce et al., (in preparation) (listed in this volume). The age model is based on 17 mollusk shell $^{14}C$ dates from 14 distinct depths in the core and calibrated using the Marine13 calibration curve [Reimer et al., 2013]. Correction of radiocarbon ages by subtraction of the local Arctic carbon reservoir effect ($\Delta R$) was possible based on the presence of the Aniakchak II tephra at ~700 cm depth with a value of 465 ± 60 years (details in Pearce et al. [in preparation]). The results revealed that the core extends from the present day back to approx. 4300 cal. yrs BP (BP= 1950 AD). The top most two mollusk dates (top 10 cm) gave "post-bomb" $^{14}C$ ages, implying that, despite the lack of a paired trigger weight core (known to minimize disturbance of the sediment ocean interface) at the 2-PC site, the youngest sediments are in place.

The age-depth curve reveals sedimentation rates that are exceptionally high, continuous and almost linear during the entire late Holocene (4300 years BP) allowing sampling at decadal-multidecadal resolution. However, three distinct depositional rates can be identified (Figure 5): (i) approx. 200 cm/kyr from 4300 to 2200 years BP followed by (ii) a 100 cm/kyr regime lasting until 1200 years BP that gradually increases to (iii) 300 cm/kyr at 700 years BP remaining stable until today (see Pearce et al., in preparation, this thesis).

### 3.2 Field oceanographic data

New oceanographic observations of the study area from SWERUS-C3 CTD casts (conductivity, temperature, depth measurements) deployed at the time of coring and the temperature, salinity and seawater $\delta^{18}O$ from previous RUSALCA 2004, 2009 and 2012 expeditions on the Chukchi Sea are used to provide a framework for interpretation of the paleo-reconstructed data. In Figure 4, we illustrate the regional relationship that Chukchi Sea oxygen isotopes have with temperature and salinity, showing a stronger correlation with salinity ($R^2$= 0.6) than with temperature ($R^2$=0.2).

The new Herald Canyon CTD casts capture local water column structure during the late summer of 2014 (Figure 3). The following water masses are recognized: a ~20 m of Polar Mixed Layer Waters and the Pacific-Arctic Halocline waters at ~50 to 100m. Pacific water is fresher than the mean salinity of the Arctic Ocean, thus its inputs provide net freshening [Chierci and Fransson, 2009]. However, locally in the Herald

Canyon, Pacific waters are saltier (32.5 psu at the Bering Strait and 32.8 psu at the Herald Valley) than the waters from the polar mixed layer (33.1 psu) [Aagaard and Carmack, 1989], a layer that includes inputs from seasonal melting.

### 3.3 Species selection

The availability and preservation of foraminifera in central Arctic Ocean sediment cores has typically been reported to be sporadic and patchy [Backman et al., 2004]. However, core 2-PC and adjacent multicores (Figure 1) from the Chukchi Shelf are rich in microfossils. These include benthic foraminifera (no miliolids), ostracods and diatoms (> 63μm diatoms of the *Coscinodiscus* genus indicative of high primary productivity at the surface waters). No planktonic foraminifera were present in the sediments. This might be due to either low salinity conditions that were unfavorable to the single Arctic species *Neogloboquadrina pachyderma* (typical *N. pachyderma* preference is 35 – 36 psu; Ravelo and Hillaire-Marcel [2007]), or the shallow water depths impeding the planktonic life cycle. The benthic foraminifera *Elphidium clavatum*, a diatom feeder [Varekamp et al., 2010] that lives partially buried in the sediment at approximately the first centimeter was the most common species and dominated assemblages in both 2-PC sediments and the multicore. Having, been shown previously to be suitable for geochemical analysis (Barrientos et al., Paper 1-, this thesis) this species was selected for use in this down-core study.

### 3.4 Geochemical paleoceanographic proxies measured in benthic foraminifera *Elphidium clavatum*

Mg/Ca and carbon and oxygen stable isotope analyses ($\delta^{13}C$ and $\delta^{18}O$) were used to infer late Holocene bottom water temperature, salinity and DIC $\delta^{13}C$ variability from sediments recovered in core 2-PC from Herald Canyon. Both types of analysis were carried out on the benthic foraminiferal species *E. clavatum*, (see Manuscript-1, this thesis). Use of a single species removes potential offsets introduced by vital effects such as different calcification depths or different growing seasons when trying to reconstruct salinity.

Mg/Ca ratios were analyzed at Cardiff University using a Thermo Element XR Inductively Coupled Plasma Mass Spectrometer (ICP-MS). Approximately 25 *E. excavatum* specimens (250–125 μm) per sample were crushed between two glass plates. These fragments were subjected to rigorous cleaning prior to Mg/Ca analysis to remove adhering contaminants. We followed a modified version of the cleaning protocol firstly described in Boyle and Keigwin (1985/1986). The cleaning method includes; (i) clay removal by ultrasonaticating the benthic test fragments in deionized water and methanol, (ii) a reductive step to remove metal oxides by introducing each sample in a hot bath after solution with hydrazine hydrate and citric acid in ammonia,

(iii) an oxidative step to remove organic matter by sonication of the sample with hydrogen peroxide in sodium hydroxide, and (iv) a weak acid leach step using Optima pure nitric acid to remove any adsorbed contaminant during the cleaning procedure. Based on three replicate analysis of benthic Mg/Ca from the same multicore site, Mg/Ca ratios in *E. excavatum* have an error of 0.115 mmol/mol. The resulting sampling resolution for Mg/Ca is at ~20 cm, equivalent to 100 yr.

$\delta^{13}C$ and $\delta^{18}O$ analyses were carried out at the Stockholm University Stable Isotope Lab using a Gasbench II coupled to a Thermo Scientific MAT 253 mass spectrometer. Based on these measurements the reproducibility was calculated to be better than 0.07‰ for $\delta^{13}C$ and 0.15‰ for $\delta^{18}O$. For stable isotope analysis each 0.2 mg of sample (approximately 40 specimens of *E. clavatum* from the 250–125 µm size fraction per sample) were flushed with helium gas in a septum-seal glass vial and a 100µl of 99% $H_3PO_4$ was added to each sample for reacting to carbon dioxide to finally detect the different mass-dependent fractionating ratios. The resulting stable isotopes record has a sampling interval of ~8cm (~40 years).

Foraminiferal based Mg/Ca paleothermometry has not being applied in this setting of the Arctic previously thus until recently (Barrientos et al., Manuscript-1, this thesis), no local calibrations existed. Here we experimented with reconstructing absolute bottom water temperatures (BWT) in the Herald Canyon using a new Arctic *E. clavatum* calibration as well as a modified version of this that incorporates Mg/Ca-temperature sensitivity constraints from another calibration based on other data sets [Varekamp et al., 2010].

## 4 Results

### 4.1 Stable isotopes in *E. clavatum*

The total isotopic variability throughout the 4300 cal. years BP is of 0.78 ‰ for $\delta^{18}O$ and 1.41 ‰ for $\delta^{13}C$ (Figure 6a and 6b). Overall, there is a very poor linear correlation between both stable isotopes ($R^2$= 0.09), however, a phase coupling between both signals is observed at certain intervals of time. From bottom to top, there is little systematic relationship between $\delta^{13}C$ and $\delta^{18}O$ values before ~2430 cal. yrs BP but thereafter the records covary apparently in phase until 1100 years BP. Sharp swings in $\delta^{13}C$ and $\delta^{18}O$ occur at ~1200 cal. years BP, with an excursion on the order of 1‰ in $\delta^{13}C$ (from -1.29 to -2.29 ‰) and 0.60 ‰ in $\delta^{18}O$ (from 2.81 to 2.21 ‰). Replicate analyses run for the samples registering the highest and lowest values produced very similar values and gave the same magnitude of isotopic shifts, implying that this was not an analytical issue.

Historical climate phases, i.e. the Roman Warm Period, Medieval Climate Anomaly, Little Ice Age and the Maunder Minimum are drawn on Figure 6 for reference, based

on their previous age calibrations. At the Medieval warm period (1000-700 cal. yrs BP) the signals become decoupled, with a decrease in $\delta^{18}O$ and an increase in $\delta^{13}C$, until 974 cal. years BP. Coincident with the onset of the Little Ice Age (500–300 cal. yrs BP) the $\delta^{18}O$ increases by a 0.3 ‰ and $\delta^{13}C$ lags this increase until 300 cal. yrs BP. Finally, after the start of the industrial revolution at 100 cal. yrs BP, both signals fall in phase again, showing abrupt decreases in both $\delta^{13}C$ and $\delta^{18}O$ extending to modern times (1.30 ‰ for $\delta^{13}C$ and 0.29 ‰ for $\delta^{18}O$), although the higher frequency variability in $\delta^{18}O$ partially masks this signal. A striking feature of the last 50 yrs (0 yr BP) is the further rapid decrease of benthic $\delta^{13}C$ and $\delta^{18}O$ on the order of 0.80 ‰ in $\delta^{13}C$ and 0.40 ‰ in $\delta^{18}O$. The uppermost (youngest) $\delta^{13}C$ sample (dated at ca. AD 1992 ± 15) records the lowest values for the entire record, and thus of the past 4200 cal. BP yrs.

### 4.2 Mg/Ca in *E. clavatum*

Down core *E. clavatum* Mg/Ca values vary between 0.51–0.93 mmol/mol (Figure 6c). The record shows a pattern of shifts between phases of higher and lower Mg/Ca on approximately 1000 yr cycles over the youngest 2000 cal. yr BP and 500 yr cycles during the oldest 2000 cal. yr BP. The topmost (youngest) core sample yields a Mg/Ca value of 0.79 mmol/mol. This is the highest value recorded in the past 1200 cal. yr BP. Peak values of 0.93 mmol/mol occur twice at 1586 ± 67 cal. yr BP and at 2196 ± 61 cal. yr BP (coincident with the start and end of the Roman Warm Period respectively). Higher than modern Mg/Ca values (> 0.79 mmol/mol) also occurred within 3077 ± 55 and 3526 ± 60 cal. yr BP. The minimum Mg/Ca (0.51 mmol/mol) occurs at 201 ± 34 cal. yr BP, within the Little Ice Age period, that is present in a 1200 cal. yr BP interval of lower than modern Mg/Ca values. Other phases of sustained low Mg/Ca (~0.65 mmol/mol) occur at 2404 ± 56 cal. yr BP and at 2787 ± 49 cal. yr BP. Within 4100–1200 cal. yr BP Mg/Ca ratios were on average higher (mean of 0.79 mmol/mol), than the following 1200 cal. yr BP-present (mean 0.66 mmol/mol).

## 5 Discussion

An important finding of the new Herald Canyon records is that benthic foraminifera Mg/Ca and $\delta^{13}C$ records show comparable systematic millennial to centennial scale variability over the past 4200 yrs (Figure 6b and 6c). Based on these we would predict that the Mg/Ca swings correspond to changes in BWT in the Herald Canyon and that this is imprinted in bottom water DIC $\delta^{13}C$, linked either to water mass mixing or local primary productivity. The lack of covariance between Mg/Ca and $\delta^{18}O$ trends suggests that our Herald Canyon benthic foraminifera $\delta^{18}O$ is largely recording seawater $\delta^{18}O$ fluctuations. To try and quantify BWT change we experimented with

applying Mg/Ca-temperature calibrations then compare the new Arctic record to a record of North Pacific climate change derived from a Canadian ice core.

### 5.1 Mg/Ca-temperature calibration and paleotemperature calculation

First we applied Mg/Ca-temperature constraints from a newly acquired Arctic Mg/Ca dataset based on modern (Rose Bengal stained) *E. excavatum* found in SWERUS-C3 multicore core tops (Figure 7, using the Barrientos et al. dataset from Manuscript-1). This provided important values at the coldest end of the bottom water temperature spectrum. Observed BWT at the multicore stations that were used in the calibration study range between -1.82 and -0.26 °C. The corresponding Mg/Ca ratios in stained *E. clavatum* average 0.66 mmol/mol between 0.521 and 0.795 mmol/mol. The resulting linear regression results in the following equation:

$$Mg/Ca = 0.711 \pm 0.06 + 0.048 \pm 0.05 \times BWT,\ R^2 = 0.12$$

This implies a Mg/Ca–BWT sensitivity of 0.048 mmol/mol change per °C that is half the average sensitivity of benthic foraminiferal Mg/Ca (0.1 mmol/mol per °C) [e.g. Marchitto et al. 2007; Lear et al. 2010]. With an $R^2$ value of only 0.12 this is a statistically weak relationship and suggests this would give unreliable absolute reconstructed BWT. When we apply this calibration to the downcore 2-PC Mg/Ca record the resulting BWT range (amplitude variability) is unreasonably large ~9 °C (Figure 8). We suggest that this poor correlation between Mg/Ca and temperature is due to a combination of factors, including; challenges of creating the field calibration set, with possibility of mismatches between the 'snapshot' BWT field constraint (from SWERUS-C3 CTD data) which spans both very low temperatures and small temperature ranges compared to the longer time averaged growing period for the benthic foraminifera; limited numbers of data points in the calibrations (n=10); and the generally low sensitivity of the Mg/Ca-temperature dependency at low temperatures (flat part of the exponential Mg/Ca-temperature relationship established with wider temperature spectra). Nevertheless, a better field calibration for the Arctic is hard to obtain and the low modern Mg/Ca values recorded are in-trend when compared published datasets.

We experimented with a second approach to reconstruct paleotemperatures, i.e. by applying the exponential relationship found in a previous *E. clavatum* calibration made in Long Island Sound (which covered a wider and warmer field bottom water temperature range [Varekamp et al., 2010]) to our Herald Canyon *E. clavatum* Mg/Ca values. This is the resulting calibration equation:

$$Mg/Ca = 0.1085\ (\pm 0.0412) \times e^{(0.1959(\pm 0.0264) \times BWT)},\ R^2 = 0.85$$

Here the Mg/Ca sensitivity is 0.1959 mmol/mol change per °C, implying a strong correlation between BWT and Mg/Ca ($R^2 = 0.85$). The reconstructed Mg/Ca-derived paleotemperatures in core 2-PC when substituting the Mg/Ca in the equation above have a much narrower spread but are unrealistically high (~10°C) for the Arctic setting.

Finally, we experimented with combining the Varekamp et al. [2010] Mg/Ca-T exponential sensitivity to our Arctic field data set. To do this, we shifted the y-intercept towards the mean core-top foraminiferal Mg/Ca value (0.66 mmol/mol) and mean field BWT from the SWERUS study. This results in a new equation:

$$Mg/Ca = 0.812 \times e^{(0.1959 \times BWT)}$$

This calibration has a 0.148 mmol/mol per °C higher sensitivity than the Arctic-only calibration. After applying this new equation to the down core Mg/Ca we obtained both a smaller temperature spread and more realistic BWTs (Figure 8); systematic increases and decreases in Mg/Ca correspond to BWT changes on the order of 3°C, varying between minima and maxima of -2°C to 1°C (Figure 8). These 3°C of total variability are consistent with modern end member observations of the temperature registered by the Herald Canyon water masses. These are Pacific waters flowing on the western flank of the Canyon (warmer) where core 2-PC is located vs. Arctic Shelf waters (colder) on the eastern flank of the Canyon (Figure 3a). Their temperatures differ by 3°C at the surface and by 1°C at depth. Thus, the reconstructed paleotemperature estimates could reflect the magnitude in temperature fluctuations derived from a shift between Pacific and Arctic shelf waters at the site.

We acknowledge that this approach is somewhat arbitrary, but the purpose was to produce some kind of realistic temperature target for discussion. As discussed by Barrientos et al. (Manuscript-1, this thesis), there are many challenges and limitations involved with building a field calibration due to the high degree of noise, low temperature range and low cold-end Mg/Ca-BWT sensitivity. Empirical experiments using *E. clavatum* could help improve our understanding of Mg incorporation at low temperatures, however the laboratory conditions bring additional biases because of the unnatural environment [Kontakiotis et al., 2016]. To summarize, we have confidence in Mg/Ca changes for recording relative increases and decreases in BWT but not the absolute temperature values. In the main palaeoceanographic interpretation figure (Figure 6), we use arrows to qualitatively indicate directional changes in BWT and water masses (Arctic Shelf vs. Pacific waters).

### 5.2 Chukchi Sea Mg/Ca variability and Pacific Ocean connections

To explore the possible cause of the millennial scale BWT temperature fluctuations in the Chukchi Sea record, and to test the hypothesis that the changes relate to variations

in Pacific water influence in the Arctic, we compared the new Mg/Ca data set to a high resolution 20000 year-long $\delta^{18}O$ ice core record retrieved from Prospector Russell Col (PRCol) on Mount Logan (Lat. 60.595, Long. 140.50 and 5.4 km a.s.l.) southwest Yukon (Canada) [Fischer et al., 2004; 2008]. The age model for this ice core is based on layer counting and dating of volcanic ash layers, and thus is entirely independent of our 2-PC Arctic chronology. The PRCol $\delta^{18}O$ record, shown as a smoothed curve (20 point moving average) (Figure 6f), shows a pattern of $\delta^{18}O$ variability that is remarkably similar to the 2-PC Mg/Ca BWT trend, revealing comparable millennial and centennial scale cycles that are largely in phase. From ~700 cal. yr BP the PRCol $\delta^{18}O$ and Mg/Ca records diverge, the ice core record showing a systematic shift to higher $\delta^{18}O$, peaking at 300 cal. yrs BP, during the Little Ice Age (LIA), while the 2-PC Mg/Ca shows sustained cold BWTs, including the coldest temperatures of the entire Late Holocene.

The climatic explanation for the Yukon record concludes that PRCol $\delta^{18}O$ is a moisture "source-meter" rather than a measure of past temperature [Fischer et al., 2004; 2008]. The phases of relatively high and low $\delta^{18}O$ are regarded as indicating the relative connectedness of the site to either tropical or North Pacific water sources, driven by millennial scale ENSO variability, causing changes in the balance between El Niño and La Niña modes; during periods of more frequent La Niña (stronger tropical easterlies) there is more zonal flow of water vapour transport to the Pacific Northwest and vice versa. The similarity between the Pacific and Chukchi Sea records suggests that the same climatic signals are communicated into the Arctic Ocean, thus providing evidence for a potential tropical Pacific-Arctic teleconnection. The precise ocean-climate mechanisms responsible for this are not fully understood, however, based on the Mg/Ca record we suggest that this involves changes in volume/rate or temperature of relatively warm Pacific waters, entering the Arctic through the Bering Strait. Using this hypothesis as a starting point we can proceed to interpret the 2-PC stable isotope records with respect to changes in Pacific water and the associated productivity, stratification and mixing processes related to interactions of Pacific waters on the Chukchi Shelf.

### 5.3 Herald Canyon stable isotopes: insights into BWT, sea-ice, brines, primary productivity and atmospheric $CO_2$

In terms of relating Herald Canyon $\delta^{18}O$ and $\delta^{13}C$ to the Chukchi oceanographic setting there are various complexities due to its current location at the Pacific gateway to the Arctic and close to the edge of mean summer sea ice extent. This environment hosts a wide variety of water masses and ocean systems that modify water chemistry (namely seasonal sea ice formation and melting, brine formation, as well as interactions between Pacific and Arctic shelf waters). Further details with respect to insights from $\delta^{18}O$ are discussed below.

It is well known that the process of sea ice formation alters seawater $\delta^{18}O$ due to the production of brines as salt is rejected during water freezing. Formation and sinking of these dense brines in the cold season and their subsequent dilution by summer melting effects $\delta^{18}O$ variability over the upper 100 m, the brines delivering $^{18}O$-depleted (low $\delta^{18}O$ values) to deeper levels [Hillaire-Marcel and de Vernal, 2008; Bauch et al., 2009; Xiao et al., 2014]. With respect to Arctic vs. Pacific surface $\delta^{18}O$ end-members, the $\delta^{18}O$ signature of the Arctic Ocean water masses is ~ -1‰ in Pacific sourced waters and ~0‰ in Atlantic origin waters, compared to -10 to -30 ‰ in water vapor and precipitation, ~ -20‰ in river runoff and ~ -2‰ in sea ice melt water [Östlund and Hut, 1984; Melling and Moore, 1995; Yamamoto-Kawai et al., 2008]. Modern seawater $\delta^{18}O$ observations from the area surrounding the study area, gathered by RUSALCA Expeditions (2004, 2009 and 2012), show a $\delta^{18}O$ average of -1‰, signaling typical Pacific water $\delta^{18}O$ signature, suggesting that 2-PC modern $\delta^{18}O$ signal is dominated by Pacific Waters.

Our 2-PC *E. clavatum* $\delta^{18}O$ record does not co-vary with the entire Mg/Ca record implying that the signal is related to both changes in salinity and temperature. We can observe from comparing $\delta^{18}O$ (Figure 6a) and Mg/Ca (Figure 6c) records that there is a decoupling in both signals when the waters are warmer (high Mg/Ca, low $\delta^{18}O$). In contrast, we observe a coupling at colder waters (low Mg/Ca, low $\delta^{18}O$). From this we infer that the $\delta^{18}O$ is a mixture of salinity and temperature parameters, suggesting that the $\delta^{18}O$ signal is dominated by salinity at colder waters and by temperature at warmer waters. This is consistent with the hypothesized scenario of more brines present at the site when the waters are colder with a concomitant reduced Pacific water inflow.

Dissolved inorganic carbon (DIC) in seawater is the primary source of carbonate for shell secretion. Infaunal species precipitate their tests with lower pore water $\delta^{13}C$ with respect to equilibrium seawater [Grossman 1984, 1987] consistent with the obtained negative $\delta^{13}C$ *E. clavatum* values (average -1.6 ‰). Moreover, brines are also depleted in $\delta^{13}C$ [Thornalley et al., 2010; Mackensen, 2013]. Therefore, our $\delta^{13}C$ is tracking local primary productivity at the site that in turn allows having insights into sea-ice upwelling. The proximity of the site to the summer sea ice edge will enhance primary productivity and sea-ice upwelling that acts lowering $\delta^{13}C$ due to higher organic matter decay. These factors together could explain the largest $\delta^{13}C$ shift of > 1‰ captured at ~1200 cal. yr BP. Based on microscopic evidence of >63 μm-sized diatoms and TOC measurements (1.8 % average) [Pearce, 2016 personal communication] modern Herald Canyon waters and sediments are highly organic-rich. The benthic $\delta^{13}C$ record suggests millennial scale variability comparable to the Mg/Ca time series (Figure 6b and 6c), with relatively high $\delta^{13}C$ corresponding to phases of low Mg/Ca and vice versa. This decoupled signal between Mg/Ca and $\delta^{13}C$ could be explained by higher BWT brought by nutrient rich Pacific waters promoting primary productivity (more Mg/Ca, less $\delta^{13}C$).

Furthermore, the abrupt and pronounced shift towards depleted $\delta^{13}C$ values reaching a minimum of ~ -2.6 ‰ in the past 50 years implies a change in DIC $\delta^{13}C$. One possibility is that this reflects a local increase in the flux of organic carbon matter to the seafloor due to higher primary productivity, i.e. the 'Mackensen Effect' [Mackensen et al., 1993, i.e , resulting in decreased $\delta^{13}C$ of benthic calcite, especially the quazi-infaunal species *E. excavatum*]. If a lowering of the $\delta^{13}C$ is due to more terrestrial input or enhanced primary productivity, we should most likely see a change in TOC. However, the TOC in topmost core 2-PC is more or less stable within the modern $\delta^{13}C$ decrease [Pearce, 2016 personal communication]. Another possibility is that this change reflects anthropogenic additions of isotopically light $CO_2$ to the system as a consequence of the combustion of fossil fuels (i.e. a 'Suess effect' [Quay et al., 1992]); we propose that the signal has pervaded through the atmosphere into shallow Arctic Ocean subsurface layers and thus dissolved inorganic carbon pool. Bauch et al. [2000] attributed a Suess effect in Arctic halocline waters of -0.9‰ ± 0.2, consistent with the observed 0.8‰ reduction in $\delta^{13}C$ since 1970.

Lastly, comparisons to the sedimentation rate changes at the site (Figure 6d) appear to mirror the Mg/Ca shift trends, with higher sedimentation rates matching colder bottom waters that also are in agreement with the interpretation of enhanced productivity at the site caused by the proximity of the summer sea ice edge at the surface.

## 6 Conclusions

A newly retrieved marine sediment core in the Herald Canyon (Chukchi Sea) an area where sparse sedimentological data exists, presented high Late Holocene sedimentation rates (~200 cm/kyr) exceptional for reconstructing the climate dynamics in terms of Pacific inflow water history. Despite the Late Holocene being regarded as having a relatively stable climate, our 4200 cal. yr BP geochemical records (Mg/Ca and stable isotopes in benthic foraminifera) capture climate related oscillations in the bottom waters of the Herald Canyon. This has been evidenced through benthic foraminifera *E. clavatum* Mg/Ca values that show millennial to centennial Mg/Ca variability trends. These fluctuations have been mainly interpreted as qualitative indicators of a change in halocline water sources.

Since Pacific waters are a source of heat to the Arctic, higher as modern Mg/Ca values have been associated with enhanced Pacific water inflow through the Herald Canyon that is in turn linked to summer sea ice free conditions. On the other hand, lower Mg/Ca trends indicate reduced Pacific water inflow and more Arctic shelf-derived halocline waters. Confidence that our new Arctic time series are capturing global climate signals comes from similarities of the pacing of change between the Herald Canyon Mg/Ca record and the Mount Logan (Yukon, Canada) $\delta^{18}O$ ice core record. This implies that Pacific Ocean-climate interactions influence Arctic thermal

and halocline structure on millennial and centennial times scales, with the potential to impact ice and carbon stocks on sensitive Arctic shelf regions. These interactions require further investigation.

The interpretation of the stable isotopes is more speculative since both seawater $\delta^{18}O$ composition and temperature signals are intimately mixed together in foraminiferal $\delta^{18}O$; whereas brines, primary productivity, ocean mixing and atmospheric $CO_2$ signals are intertwined in foraminiferal $\delta^{13}C$. However, by coupling Mg/Ca and stable isotopes in the same species we have found a way forward for interpretation where periods of warmer halocline are more sensitive to track temperature in the $\delta^{18}O$ signal and colder halocline waters suggests a more salinity dominating $\delta^{18}O$ signal. Independent quantifications on sea-ice extent from diatom and organic biomarker studies will provide additional constraints that will help disentangle these effects.

Altogether, the core shows two main regimes separated at 1200 cal. yr BP, time at where the major climate perturbation is captured by both stable isotopes and Mg/Ca ratios. This time boundary separates higher mean Mg/Ca values present at the bottom of the sequence (0.79 mmol/mol) from lower mean Mg/Ca values at the top (0.66 mmol/mol). Below 1200 cal. yr BP, three centennial-scale alternating pulses of enhanced Pacific inflow vs. Arctic shelf waters are recorded. From 1200 cal. yr BP to ~1950 AD, we find one millennial-scale cold phase attributed to a reduced Pacific inflow through the Herald Canyon. Inside this cold regime, the Little Ice Age interval registers the lowest Mg/Ca values of the Late Holocene. Lastly, the marine anthropogenic $CO_2$ imprint (Suess effect) is captured over the last 50 years of the core as a 0.8 ‰ benthic foraminiferal $\delta^{13}C$ reduction.

**Acknowledgements**

Lee W. Cooper (University of Maryland Center for Environmental Science) for kindly sharing RUSALCA 2004, 2009 and 2012 seawater oxygen isotope data. Heike Siegmund and Malin Söderman (Stable isotope Lab, Stockholm University) for running the stable isotopes. The SWERUS-C3 expedition was financed by grants from Knut and Alice Wallenberg Foundation (KAW), Swedish Polar Research Secretariat (SPRS), Swedish Research Council (VR) and Stockholm University.

## References


Aagaard, K., Coachman, L. K. and Carmack, E. (1981). On the halocline of the Arctic Ocean, Deep Sea Res., Part A, 28 (6), 529–545.

Aagaard, K., Carmack, E.C. (1989). The role of sea ice and other fresh water in the Arctic circulation. Journal of Geophysical Research 94 (C14), 14485–14498.

ACIA (2004). Impacts of a warming Arctic: Arctic Climate Impact Assessment. Cambridge: Cambridge University Press, 139 pp.

Backman, J., Jakobsson, M., Løvlie, R., Polyak, L., and Febo, L. A., 2004, Is the central Arctic Ocean a sediment starved basin? Quaternary Science Reviews, 23, 1435–1454.

Bauch, D., Carstens, J., Wefer, G. & Thiede, J. (2000): The imprint of anthro- pogenic CO2 in the Arctic Ocean: evidence from planktonic ∂13C data from water column and sediment surfaces. Deep-Sea Res. II, 47, 1791–1808.

Bauch, D., Dmitrenko, I.A., Wegner, C., Hölemann, J., Kirillov, S.A., Timokhov, L.A. & Kassens, H. (2009). Exchange of Laptev Sea and Arctic Ocean halocline waters in response to atmospheric forcing. J. Geophys. Res. 114, C05008.

Bemis, B.E., Spero, H. J., Bijma, J., and Lea, D.W. (1998). Reevaluation of the oxygen isotopic composition of planktonic foraminifera: Experi- mental results and revised palaeotemperature equations. Paleoceanography, 13, 150–160.

Berger, A.L., 1978. Long-term variations of daily insolation and Quaternary climatic changes. Journal of the Atmospheric Sciences, 35 (12), 2362–2367.

Boyle, E. A., and Keigwin, L. D. (1985/1986) Comparison of Atlantic and Pacific paleochemical records for the Last 215.000 years: Changes in deep ocean circulation and chemical inventories. Earth and Planetary Science Letters, 76, 135–150.

Carmack, E.C., Macdonald, R.W., Perkin, R.G., McLaughlin, F.A. (1995). Evidence for warming of Atlantic water in the southern Canadian Basin. Geophys. Res. Lett. (22), 1961–1964.

Chierici, M., Fransson, A. (2009). Calcium carbonate saturation in the surface water of the Arctic Ocean: undersaturation in freshwater influenced shelves. Biogeosciences 6 (11), 2421–2431.

Coachman, L. K., and Barnes, C. A. (1961), The contribution of Bering Sea Water to the Arctic Ocean, Arctic, 14 (3), 147–161.

Coachman, L. K., Aagaard, K., Tripp, R.B. (1975). Bering Strait: the regional physical oceanography. University of Washington Press, Seattle.

Codispoti, L.A. and Richards, F.A. (1968). Micronutrient distributions in the East Siberian and Laptcv Seas during summer, 1963. Arctic 21: 67-83.

Comiso, J.C., Parkinson, C.L., Gersten, R., Stock, L. (2008). Accelerated decline in the Arctic Sea ice cover. Geophys. Res. Lett., 35 (1), L01703.

Comiso JC. 2012. Large decadal decline of the Arctic multiyear ice cover. J. Clim. 25, 1176–1193.

Danielson S.L., Weingartner, T.J., Hedstrom, K.S. et al. (2014). Coupled wind-forced controls of the Bering-Chukchi shelf circulation and the Bering Strait throughflow: Ekman transport, continental shelf waves, and variations of the Pacific-Arctic sea surface height gradient. Progress in Oceanography, 125, 40–61.

Dobricic, S., Vignati, E. and Russo, S. (2016). Large-Scale atmospheric warming in winter and the Arctic sea ice retreat. Journal of Climate, 29 (8), 2869–2888.

Fisher, D.A., Wake, C., Kreutz, K., Yalcin, K., Steig, E., Mayewski, P., Anderson, L., Zheng, J., Rupper, S., Zdanowicz, C., Demuth, M., Waszkiewicz, M., Dahl-Jensen, D., Goto-Azuma, K., Bourgeois, J.B., Koerner, R.M., Sekerka, J., Osterberg, E., Abbott, M.B., Finney, B.P. and Burns, S.J. (2004). Stable isotope records from Mount Logan and Eclipse ice cores and nearby Jellybean Lake; water cycle of the North Pacific over 2 000 years and over 5 vertical kilometres; sud- den shifts and tropical connections. Géographie physique et Quaternaire, 58, 337–52.

Fisher, D.A., Osterberg, E., Dyke, A.S., et al. (2008). The Mt Logan Holocene–late Wisconsinan isotope record: Tropical Pacific– Yukon connections. The Holocene 18(5): 667–677.

Francis, J. A., E. Hunter, J. R. Key, and X. Wang (2005), Clues to variability in Arctic minimum sea ice extent, Geophys. Res. Lett., 32, L21501.

Grossman EL (1984) Carbon isotopic fractionation in live benthic foraminifera - comparison with inorganic pre- cipitate studies. Geochim Cosmochim Acta 48, 1505-1512.

Grossman, E.L. (1987). Stable isotopes in modern benthic foraminifera: a study of vital effect. Journal of Foraminiferal Research, 17, 48–61.

Heimdal, B.R. (1989). Arctic Ocean phytoplankton, in Herman, Yvonne, ed., The Arctic seas: New York, Van Nostrand Reinhold, p. 193–222.

Hillaire-Marcel, C. and de Vernal, A. (2008). Stable isotope clue to episodic sea ice formation in the glacial North Atlantic. Earth and Planetary Science Letters 268, 143–150.

Jakobsson, M., 2002, Hypsometry and volume of the Arctic Ocean and its constituent seas: Geochemistry, Geophysics, Geosystems, v. 3, no. 5, p. 1-18.

Kinney, P., Arhelger, M.E, and Burrell, D.C. (1970) Chemical characteristics of water masses in the Amerasian basin of the Arctic Ocean. J. Geophys. Res., 75, 4097–4104.

Kontakiotis, G., Mortyn, P.G., Antonarakou, A. and Drinia, H. (2016). Assessing the reliability of foraminiferal Mg/Ca thermometry by comparing field-samples and culture experiments: a review. Geological Quarterly, 2016, 60 (3): 547–560.

Lear, C. H., Mawbey, E. M., and Rosenthal, Y. (2010), Cenozoic benthic foraminiferal Mg/Ca and Li/Ca records: Toward unlocking temperatures and saturation states, *Paleoceanography*, 25, PA4215.

Luchin, V. and Panteleev, G. (2014), Thermal regimes in the Chukchi Sea from 1941 to 2008, Deep-Sea Research II, 109, 14–26.

Mackensen, A. (2001). Late Pleistocene deep-water circulation in the subantarctic eastern Atlantic. Global and Planetary Change, 30 (3-4), 197–229.

Mackensen, A. (2013). High epibenthic foraminiferal $\delta^{13}C$ in the recent deep Arctic Ocean: implications for ventilation and brine release during stadials. Paleoceanography, 28.

Marchitto, T. M., Bryan, S. W., Curry, W. B. and McCorckle, D. C. (2007). Linear Mg/Ca temperature calibration for the benthic foraminifer *Cibicidoides pachyderma*. Paleoceanography. 22, PA1203.

Mathis, J.T., Cross, J.N., Evans, W. and Doney, S.C. (2015). Ocean acidification in the surface waters of the Pacific-Arctic boundary regions. Oceanography 28 (2), 122–135.

McGann, M. (2008). High-resolution foraminiferal, isotopic, and trace element records from Holocene estuarine deposits of San Francisco Bay. California: Journal of Coastal Research 24 (5), 1092–1109.

McLaughlin FA, Carmack EC, Macdonald RW, Bishop JKB (1996) Physical and geochemical properties across the Atlantic/Pacific water mass boundary in the southern Canada Basin. J Geophys Res, 101, 1183–1197.

McLaughlin FA, Carmack EC, MacDonald RW, Weaver AJ, Smith J (2002) The Canada Basin 1989–1995: upstream events and far-field effects of the Barents Sea branch. J. Geophys. Res., 107. doi:1029/2001JC000904

Melling, H. and Moore, R. (1995). Modification of halocline source waters during freezing on the Beauford Sea shelf: Evidence from oxygen isotopes and dissolved nutrients. Cont. Shelf Res., 15, 89–113.

Morison JH, Steele M, Anderson R (1998) Hydrography of the upper Arctic Ocean measured form the nuclear submarine USS Pargo. Deep Sea Res I, 45: 15–38

Östlund, H. & Hut, G. (1984): Arctic Ocean water mass balance from isotope data. J. Geophys. Res., 89 (C4), 6373–6381.

Pearce, C., Varheyli, A., Wastegård, S., Jakobsson, M., Muschitiello, F., Barrientos, N., O'Regan, M. and Cronin, T. M.: The 3.6 ka Aniakchak tephra in the Arctic Ocean: implications for the radiocarbon reservoir age of the Chukchi Sea in the late Holocene, Clim. Past, In prep.

Pearson, P.N. (2012). Oxygen isotopes in foraminifera: overview and historical review. In Reconstructing Earth's Deep-Time Climate—The State of the Art in 2012, Paleontological Society Short Course, November 3, 2012. The Paleontological Society Papers, Volume 18, Linda C. Ivany and Brian T. Huber (eds.), pp. 1–38.

Pickart, R. S., G. W. K. Moore, A. M. Macdonald, I. A. Renfrew, J. E. Walsh, and W. S. Kessler, (2009). Seasonal evolution of Aleutian low-pressure systems: Implications for the North Pacific sub-polar circulation. Journal of Physical Oceanography, 39, 1316–1339.

Quadfasel, D., Sy, A., Wells, D., Tunik, A. (1991). Warming in the Arctic. Nature, 350, 385.

Quay, P. D., Tilbrook, B. and Wong, C. S. (1992). Oceanic uptake of fossil fuel $CO_2$: Carbon-13 evidence, Science, 256, 74–79.

Ratmanov, G.E. (1937). On the question of water exchange through Bering Strait. Issledovaniya Morei SSSR 25, 119–135.

Ravelo, A. C. and Hillaire-Marcel, C. (2007). Chapter Eighteen: The Use of Oxygen and Carbon Isotopes of Foraminifera in Paleoceanography, 1, 735–764.

Reimer, P.J., Bard, E., Bayliss, A., Beck, J.W., Blackwell, P.G., Ramsey, C.B., Buck, C.E., Cheng, H., Edwards, R.L., Friedrich, M., Grootes, P.M., Guilderson, T.P., Haflidason,H.,Hajdas,I.,Hatte ,C.,Heaton,T.J.,Hoffmann,D.L.,Hogg,A.G., Hughen, K.A., Kaiser, K.F., Kromer, B., Manning, S.W., Niu, M., Reimer, R.W., Richards, D.A., Scott, E.M., Southon, J.R., Staff, R.A., Turney, C.S.M., Plicht, J.v.d., (2013). IntCal13 and Marine13 radiocarbon age calibration curves 0-50,000 years cal BP. Radiocarbon 55, 1869–1887.

Rudels, B., Jones, E.P., Schauer, U., Eriksson, P. (2004). Atlantic sources of the Arctic Ocean surface and halocline waters. Polar Res., 23, 181–208.

Rudels, B., Anderson, L., Eriksson, P. , Fahrbach, E., Jakobsson, M., Jones, E. P., Melling, H., Prinsenberg, S., Schauer, U. and Yao, T. (2012), Observations in the Ocean, in Lemke, P., ed., Arctic Climate Change: The ACSYS Decade and Beyond, Volume 43, Springer, 117–198.

Sabine, C.L., et al., 2004. The oceanic sink for anthropogenic $CO_2$. Science 305 (5682), 367–371.

Serreze, M. C., A. P. Barrett, A. G. Slater, R. A. Woodgate, K. Aagaard, R. B. Lammers, M. Steele, R. Moritz, M. Meredith, and C. M. Lee (2006). The large-scale freshwater cycle of the Arctic, J. Geophys. Res., 111, C11010.

Shackleton, N. J. (1974). Attainment of isotopic equilibrium between ocean water and the benthonic foraminifera genus *Uvigerina*, p. 203–209. In Isotopic changes in the ocean during the last glacial. Cent. Nat. Rech. Sci. Colloq. Int., No. 219.

Shaffer, G., Bendtsen, J., 1994. Role of the Being Strait in controlling North Atlantic Ocean circulation and climate. Nature 367, 354–357. http://dx.doi.org/10.1038/ 367354a0.

Shimada, K., T. Kamoshida, M. Itoh, S. Nishino, E. Carmack, F. A. McLaughlin, S. Zimmermann, and A. Proshutinsky (2006). Pacific Ocean inflow: Influence on catastrophic reduction of sea ice cover in the Arctic Ocean, Geophys. Res. Lett., 33, L08605

Steele, M. and Boyd, T. (1998) Retreat of the cold halocline layer in the Arctic Ocean. J Geophys Res, 103: 10419–10435 .

Thompson, D. W. J. and Wallace, J. M. (1998), Arctic Oscillation signature in the wintertime geopotential height and temperature fields. Geophys. Res. Lett. 25, 1297-1300.

Thornalley, D. J. R., Elderfield, H. and McCave, I. N. (2010). Intermediate and deep water paleoceanography of the northern North Atlantic over the past 21,000 years. Paleoceanography, 25, PA1211,.

Urey, H. C. (1947), The thermodynamic properties of isotopic substances. Journal of the Chemical Society of London, 1947:562–581.

Varekamp, J. C., Thomas, E., Altabet, M., Cooper, S., Brinkhuis, H., Sangiorgi,F., Donders, T., and Buchholtz ten Brink, M. (2010). Environmental Change in Long Island Sound in the Recent Past: Eutrophication and climate change. Final Report LISRF Grant CWF 334-R (FRS 525156).

Walsh, J. J., C. P. McRoy, L. K. Coachman, J. J. Georing, J. J. Nihoul, T. E. Whitledge, T. H. Blackburn, P. L. Parker, C. D. Wirick, P. G. Shuert, J. M. Grebmeier, A. M. Springer, R. D. Tripp, D. A. Hansell, S. Djenidi, E. Deleersnijder, K. Henriksen, B. A. Lund, P. Andersen, F. E. Muller-Karger, and K. Dean (1989), Carbon and nitrogen cycling within the Bering/Chukchi Seas: Source regions for organic matter effecting AOU demands of the Arctic Ocean. Prog. Oceanogr. 22, 277-259.

Weingartner, T., Cavalieri, D., Aagaard, K. and Sasaki, Y. (1998). Circulation, dense water formation, and outflow on the northeast Chukchi Shelf. J. Geophys. Res., 103 (C4), 7647– 7661.

Wijffels, S.E., Schmitt, R.W., Bryden, H.L., Stigebrandt, A. (1992). Transport of freshwater by the oceans. Journal of Physical Oceanography 22, 155–162.

Wood, K.R., Bond, N.A., Danielson, S.L., Overland, J.E., Salo, S.A., Stabeno, P.J., Whitefield J., 2015. A decade of environmental change in the Pacific Arctic region. Progress in Oceanography 136, 12–31.

Woodgate, R. A., Aagaard, K. and Weingartner, T. J. (2005), A year in the physical oceanography of the Chukchi Sea: Moored measurements from autumn 1990–1991, Deep Sea Res., Part II, 52 (24–26), 3116–3149.

Woodgate, R. A., Aagaard, K. and Weingartner, T. J. (2006) Interannual Changes in the Bering Strait Fluxes of Volume, Heat and Freshwater between 1991 and 2004. Geophys. Res. Lett. 33, L15609.

Woodgate, R. A., Weingartner, T. J. & Lindsay, R. W., (2010) The 2007 Bering Strait Oceanic Heat Flux and anomalous Arctic Sea-ice Retreat. Geophys. Res. Lett., 37, L01602.

Xiao, W., Wang, R., Polyak, L., Astakhov, A., Cheng, X., (2014) Stable oxygen and carbon isotopes in planktonic foraminifera Neogloboquadrina pachyderma in the Arctic Ocean: An overview of published and new surface-sediment data. Marine Geology, 352, 397–408.

Yamamoto-Kawai, M., McLaughlin, F.A., Carmack, E.C., Nishino, S. and Shimada, K. (2008): Freshwater budget of the Canada Basin, Arctic Ocean, from salinity, $\delta^{18}O$, and nutrients. J. Geophys. Res., 113 (C01007), doi:10.1029/2006JC003858.

Zhang, J., M. Steele, and R. Woodgate (2008), The role of Pacific water in the dramatic retreat of arctic sea ice during summer 2007, J. Polar Science, 19(2), 93-107.

**Figure 1.** Bathymetric maps showing the present day geographic location of the Herald Canyon and spatial pattern of the Chukchi Shelf currents. The warm and fresh Alaskan Coastal Current (red) and nutrient rich Anadyr Water (green) enter the Arctic from the Pacific side across the Bering Strait. Arctic fresh shelf waters, termed Siberian Coastal Current (blue) flow in the opposite direction. The core sites are located in the path of Anadyr waters. These are the piston core 2-PC and shallow surface sediments used to build the Mg/Ca-BWT calibration (KL: kastenlott and MC: multicores). Basemap obtained from International Bathymetric Chart of the Arctic Ocean [Jakobsson et al., 2012].

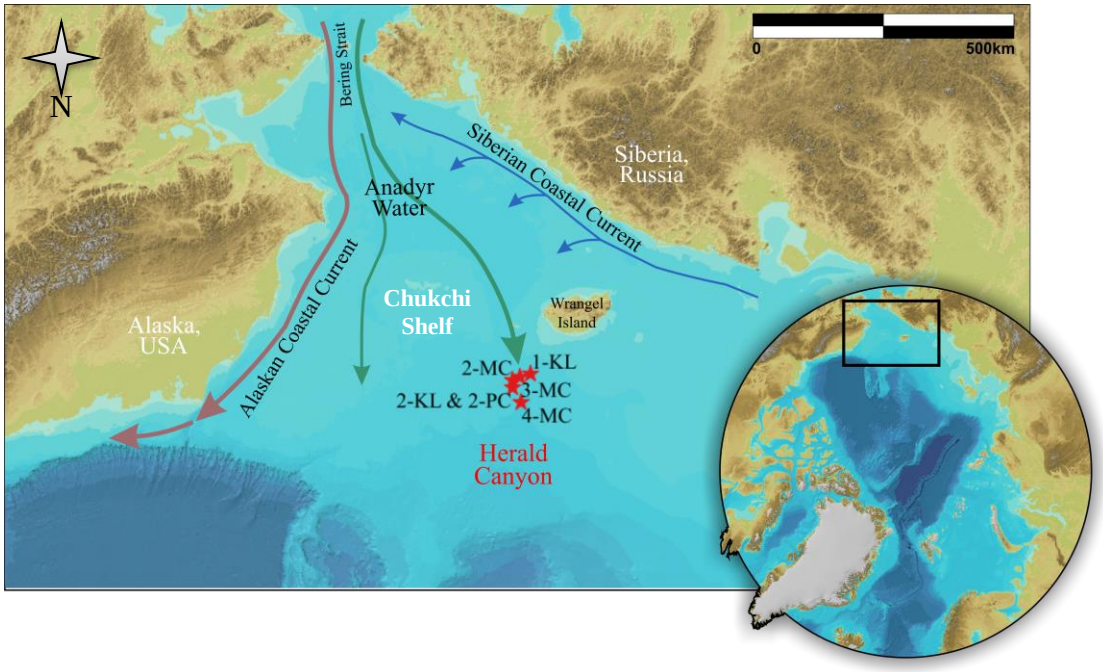

**Figure 2.** Transects showing North Pacific and Arctic Oceans separated by the Chukchi Shelf and their distinct hydrographic regimes (A. Temperature, B. Salinity). The large flat-topped region is the Chukchi Shelf. The red rectangular area on the map shows the transect depicted in the profiles and the star shows the location of site 2-PC.

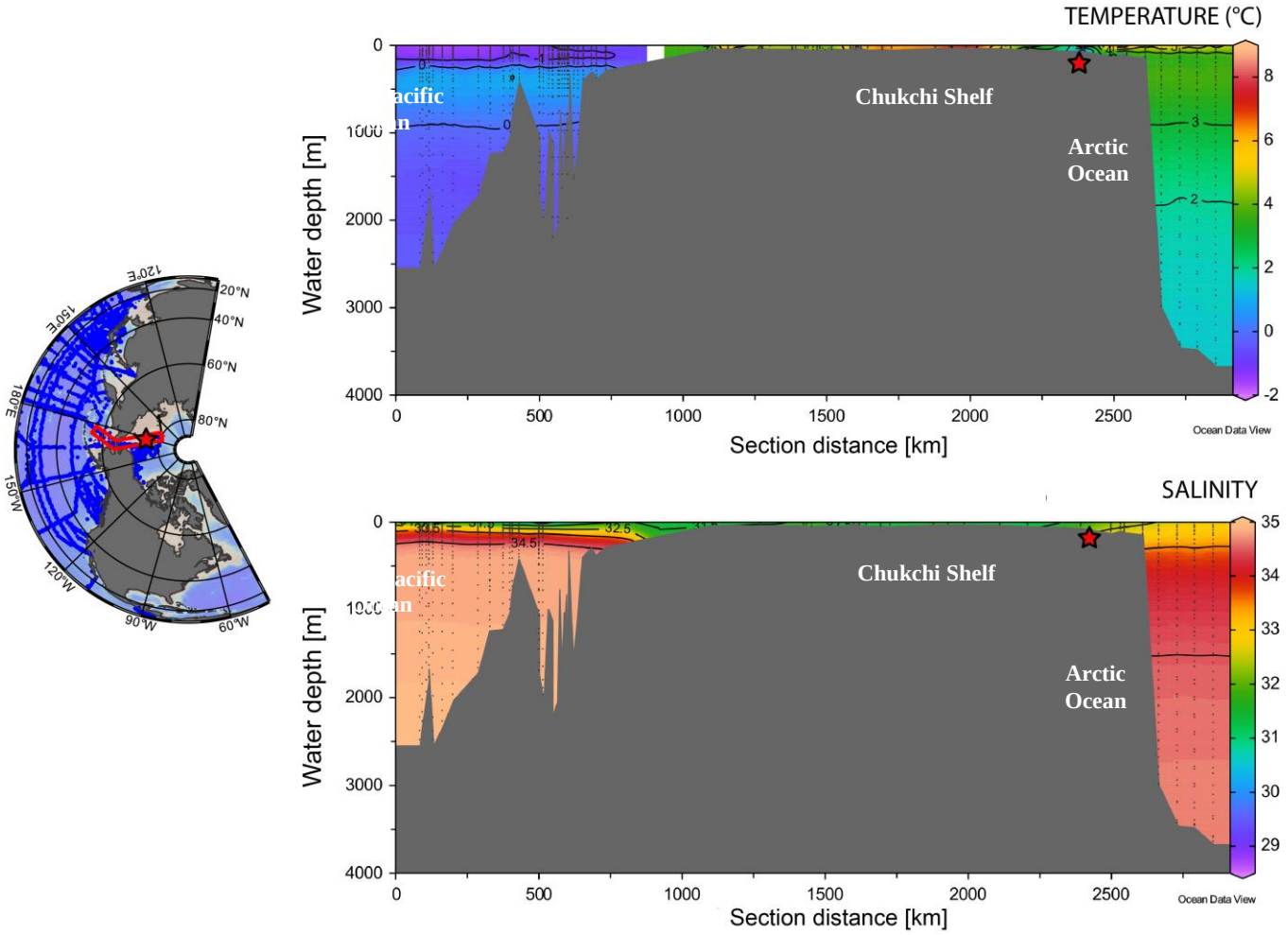

**Figure 3.** Observed water column oceanographic profiles from the study region. (a) Herald Canyon CTD temperature (SWERUS-C3 expedition in August 2014), (b) Herald Canyon salinity (SWERUS-C3 expedition in August 2014) and (c) a compilation of summer oxygen isotope seawater data (RUSALCA 2004, 2009 and 2012) from water samples taken in the Chukchi Sea. The thicker red line in plots (a) and (b) depicts the oceanographic data collected at the exact location of core 2-PC. The horizontal grey-shaded line depicts the water depth at the SWERUS-C3 2-PC coring station.

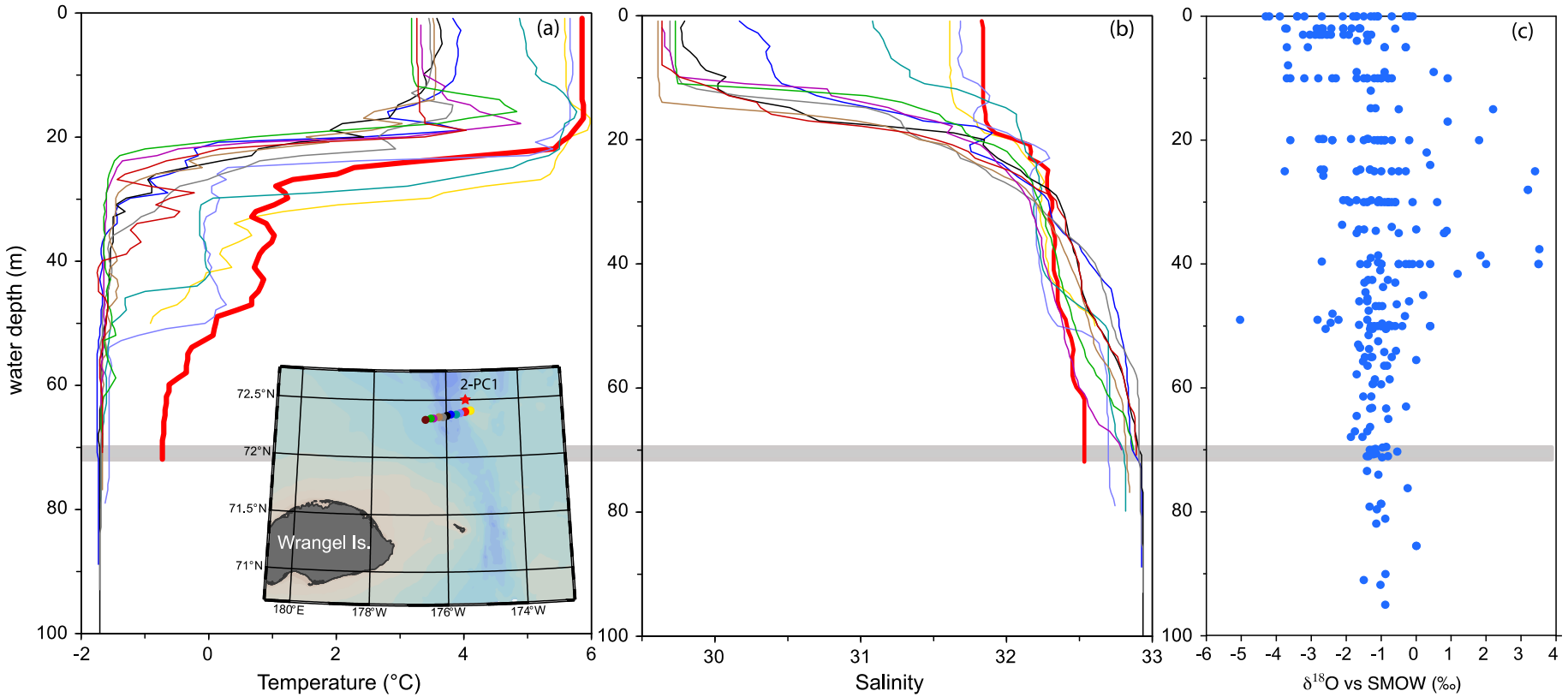

**Figure 4.** Relationship of modern Chukchi seawater $\delta^{18}O$ with ambient seawater temperature and salinity. The measurements are derived from the RUSALCA expeditions 2004, 2009 and 2012. Based on the high correlation coefficient, salinity covaries the most with seawater $\delta^{18}O$.

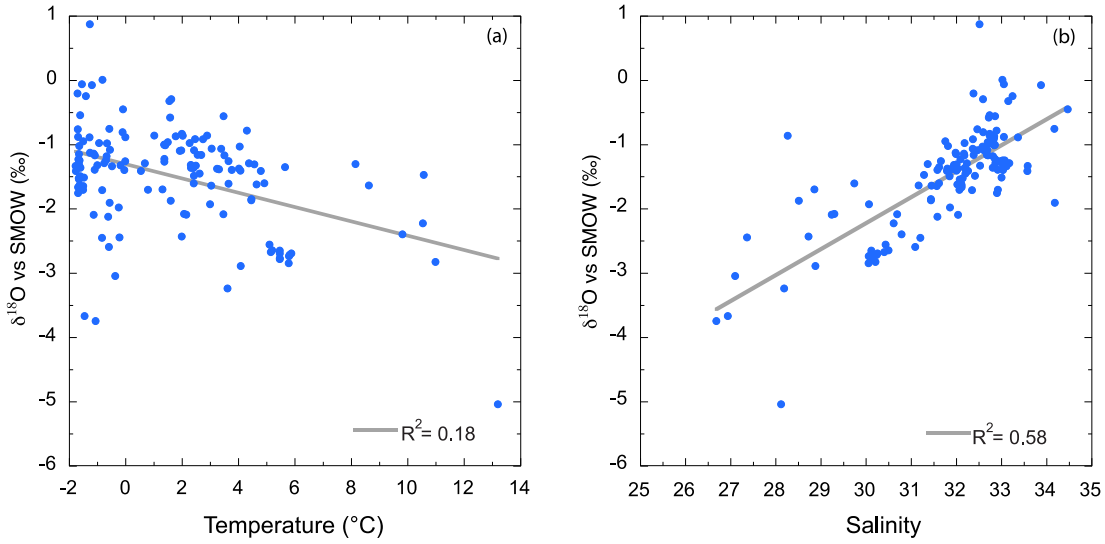

**Figure 5.** Age model for SWERUS-C3 core 2-PC based on 17 radiocarbon dates measured on mollusk shells [Pearce et al., *in preparation*]. The text labels for each $^{14}$C-date refer to the analyzing laboratory.

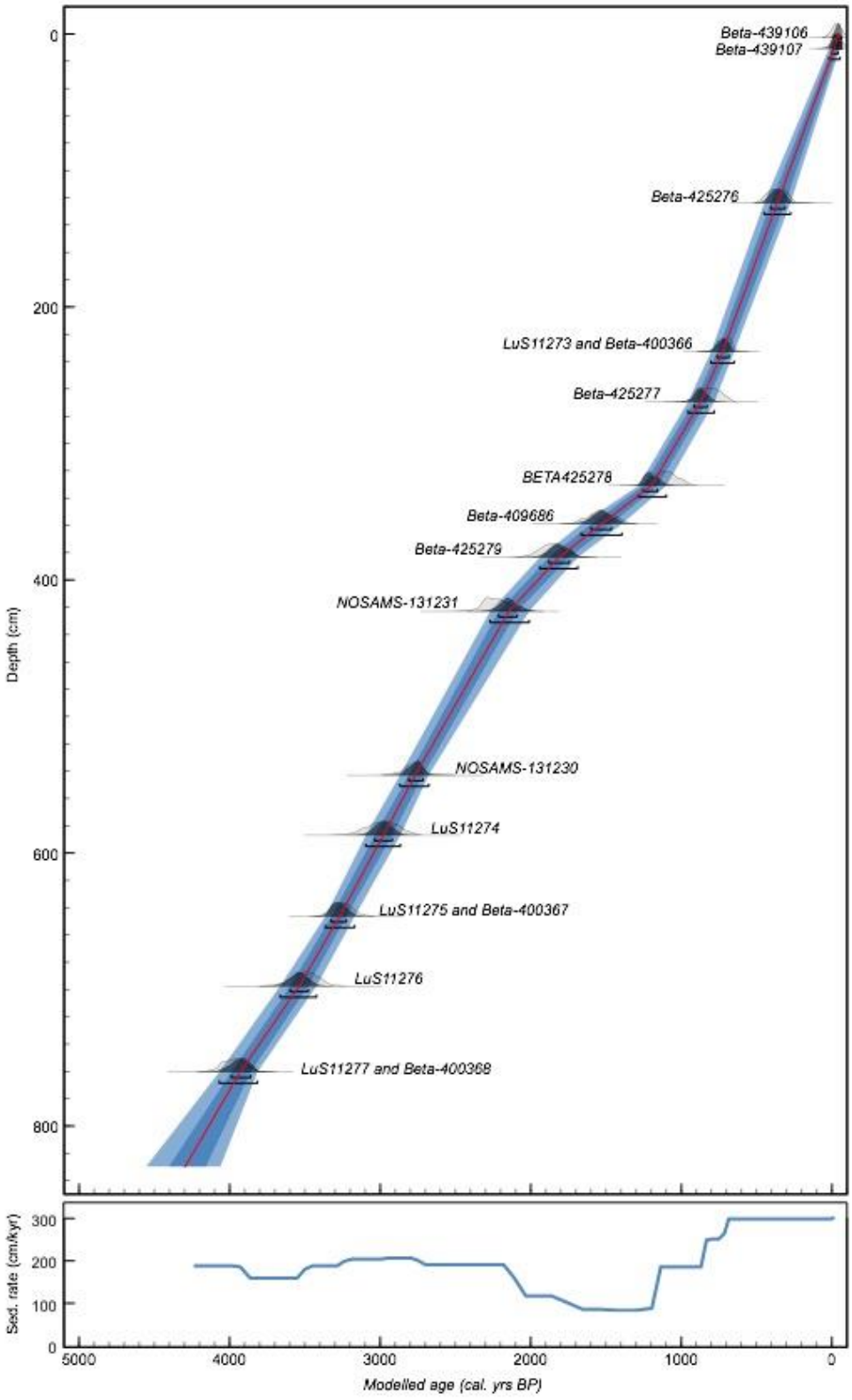

**Figure 6.** Herald Canyon palaeoceanographic proxies compared to $\delta^{18}O$ from the Yukon Mount Logan ice core. Stable isotopes of oxygen (a) and carbon (b), and Mg/Ca (c) measurements on benthic foraminifera *Elphidium clavatum* from core 2-PC. Dark and lighter color shading shows the 1sigma and 2sigma error of both the age model and the proxy data. The arrows show a schematic view of the interpreted oceanographic signals in terms of relative increases and decreases in bottom water temperature (linked to Pacific or Arctic Shelf waters respectively), brines and local primary productivity. Sedimentation rates (d) are derived from the radiocarbon age model. (e) Mg/Ca data repeated using the same presentation style as panel (c). (f) Smoothed (20 point moving average) $\delta^{18}O$ record from the Prospector Russell Col (PRcol) ice core recovered from Mt. Logan, Yukon. The highlighted red and blue shadings in (e) and (f) identify warm and cool phases as inferred independently from the respective records. Pink and grey rectangle shadings show distinct climatic events (as identified and calibrated preciously) for historical reference.

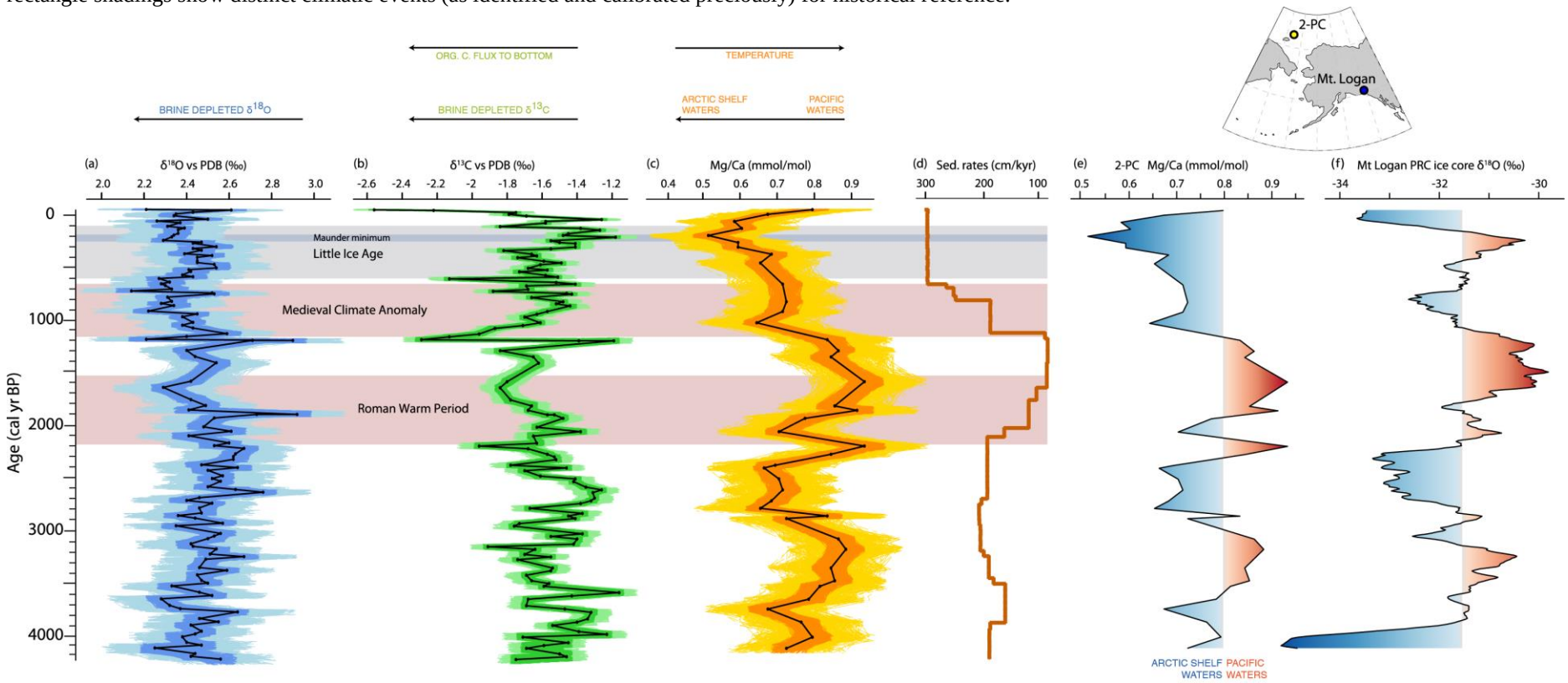

**Figure 7.** Modern Mg/Ca in Rose Bengal stained *Elphidium clavatum* showing its relationship to field SWERUS-C3 August 2014 bottom water temperatures (Barrientos et al., in preparation). The Mg/Ca values at this cold end of the temperature calibration are low deriving in weak/low sensitivity Mg/Ca-BWT fits.

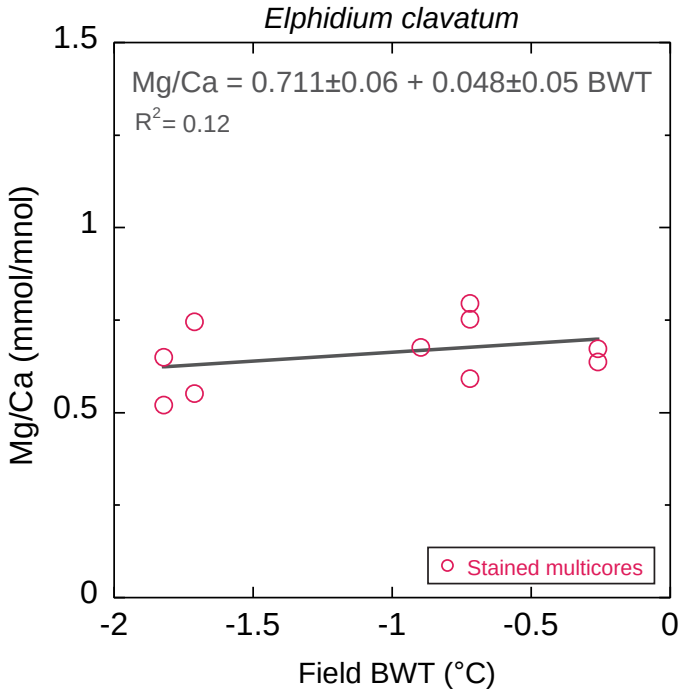

**Figure 8.** Mg/Ca-reconstructed Herald Canyon bottom water temperatures. Bottom water temperatures are based on two different Mg/C-temperature calibrations; (i) local SWERUS-C3 2-PC multicore calibration (dotted line) shown in Figure 7 and (ii) the sensitivity of Varekamp et al. [2010] calibration applied to average SWERUS-C3 Mg/Ca and field BWT core top values shown in Figure 7 (line). This second approach provides the most realistic Late Holocene magnitude of bottom water temperature variability.

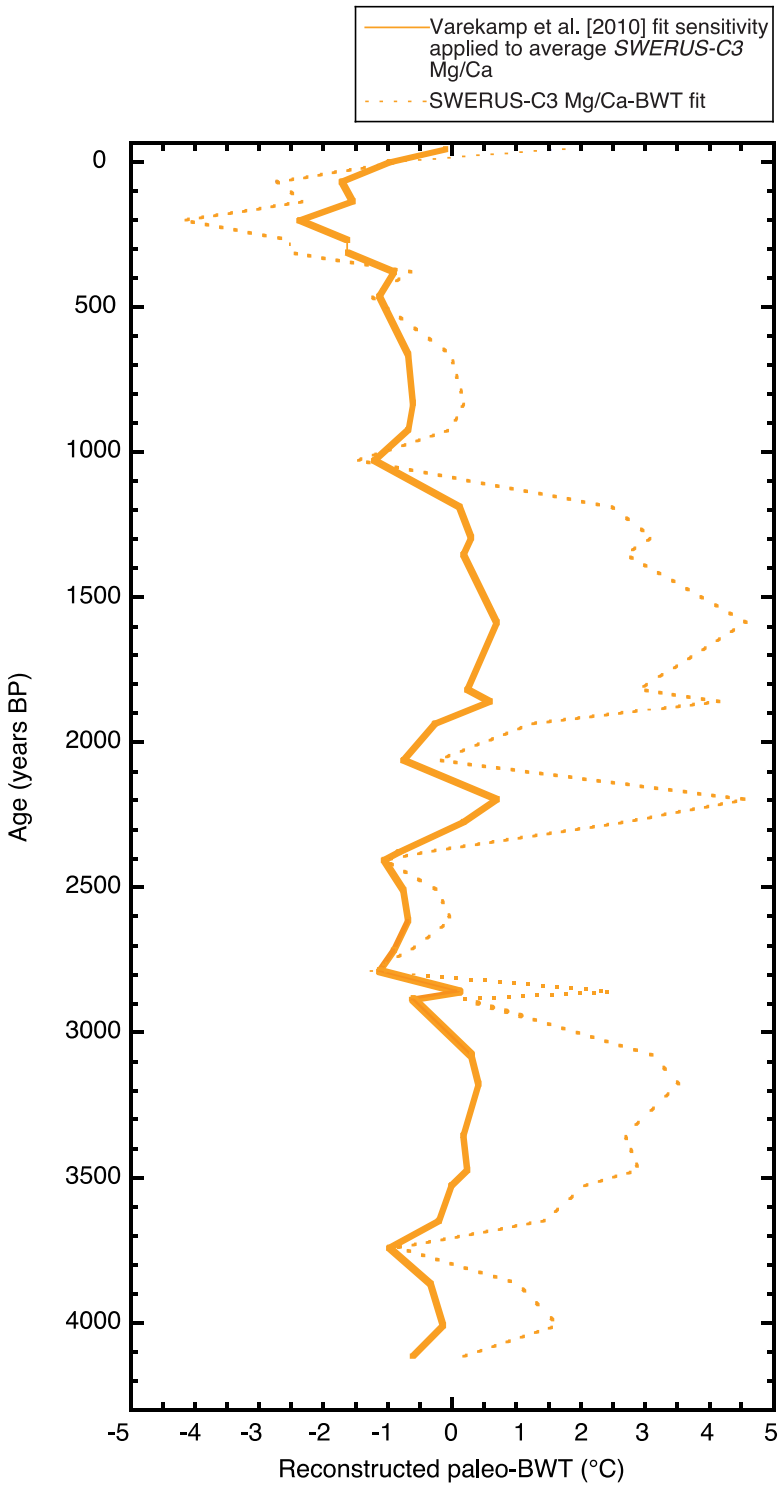

## Appendix

**Figures.**

**Figure A.** SWERUS-C3 core description of core 2-PC by Laura Gemery.

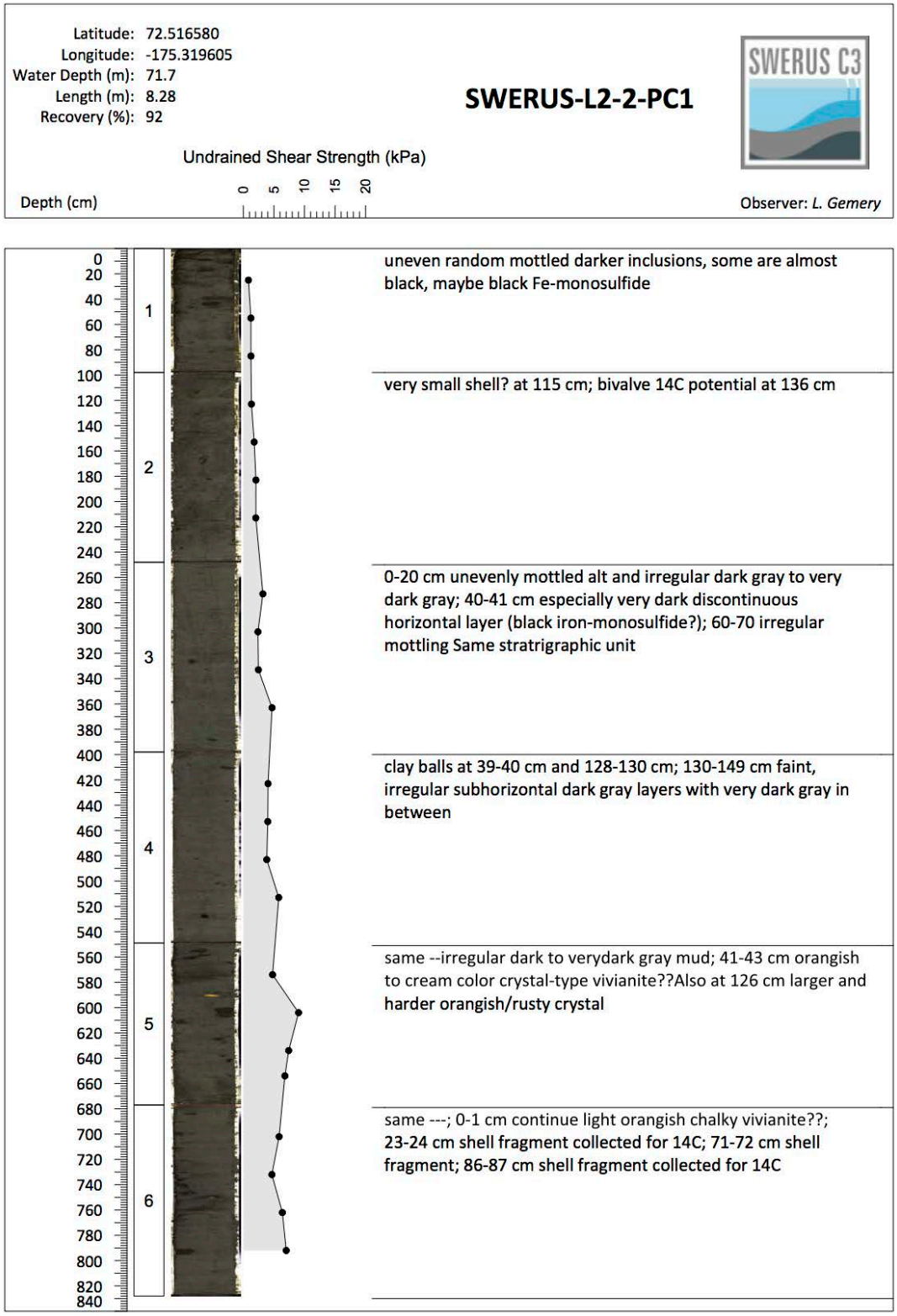

# Appendix

## Tables.

**Table A.** Stable isotope data from core 2-PC1 and their associated depth and age.

| Depth (cm) | Age (cal yrs BP) | 1σ error (yrs) | δ13C vs PDB (‰) | δ13C error (‰) | δ18O vs PDB (‰) | δ18O error (‰) |
|---|---|---|---|---|---|---|
| 1 | -41.8 | 14.6 | -2.56 | 0.07 | 2.21 | 0.15 |
| 3 | -36.8 | 15.3 | -2.22 | 0.07 | 2.61 | 0.15 |
| 11 | -16.4 | 18.5 | -1.75 | 0.07 | 2.43 | 0.15 |
| 16 | 0.3 | 19.6 | -1.79 | 0.07 | 2.35 | 0.15 |
| 21 | 17 | 20.8 | -1.69 | 0.07 | 2.34 | 0.15 |
| 31 | 50.4 | 23.2 | -1.26 | 0.07 | 2.50 | 0.15 |
| 36 | 67.1 | 24.4 | -1.58 | 0.07 | 2.26 | 0.15 |
| 41 | 83.8 | 25.5 | -1.58 | 0.07 | 2.37 | 0.15 |
| 51 | 117.2 | 27.9 | -1.84 | 0.07 | 2.31 | 0.15 |
| 56 | 133.9 | 29.1 | -1.38 | 0.07 | 2.39 | 0.15 |
| 61 | 150.6 | 30.2 | -1.27 | 0.07 | 2.36 | 0.15 |
| 71 | 184.1 | 32.6 | -1.45 | 0.07 | 2.36 | 0.15 |
| 76 | 200.8 | 33.8 | -1.48 | 0.07 | 2.34 | 0.15 |
| 81 | 217.5 | 35 | -1.18 | 0.07 | 2.33 | 0.15 |
| 91 | 250.9 | 37.3 | -1.55 | 0.07 | 2.29 | 0.15 |
| 96 | 267.6 | 38.5 | -1.50 | 0.07 | 2.47 | 0.15 |
| 99 | 277.6 | 39.2 | -1.41 | 0.07 | 2.43 | 0.15 |
| 109 | 311 | 41.6 | -1.41 | 0.07 | 2.54 | 0.15 |
| 114 | 327.7 | 42.7 | -1.55 | 0.07 | 2.43 | 0.15 |
| 119 | 344.5 | 43.9 | -1.82 | 0.07 | 2.47 | 0.15 |
| 129 | 377.9 | 44.8 | -1.66 | 0.07 | 2.39 | 0.15 |
| 134 | 394.6 | 44.5 | -1.63 | 0.07 | 2.52 | 0.15 |
| 139 | 411.4 | 44.2 | -1.74 | 0.07 | 2.45 | 0.15 |
| 149 | 444.8 | 43.6 | -1.59 | 0.07 | 2.45 | 0.15 |
| 154 | 461.6 | 43.3 | -1.49 | 0.07 | 2.45 | 0.15 |
| 159 | 478.3 | 43 | -1.61 | 0.07 | 2.53 | 0.15 |
| 169 | 511.8 | 42.4 | -1.68 | 0.07 | 2.54 | 0.15 |
| 174 | 528.5 | 42.1 | -1.57 | 0.07 | 2.41 | 0.15 |
| 179 | 545.2 | 41.8 | -1.73 | 0.07 | 2.42 | 0.15 |
| 189 | 578.7 | 41.2 | -1.58 | 0.07 | 2.38 | 0.15 |
| 194 | 595.4 | 40.9 | -1.51 | 0.07 | 2.43 | 0.15 |
| 199 | 612.1 | 40.6 | -2.13 | 0.07 | 2.27 | 0.15 |
| 209 | 645.6 | 40.1 | -1.52 | 0.07 | 2.32 | 0.15 |
| 214 | 662.3 | 39.8 | -1.41 | 0.07 | 2.28 | 0.15 |
| 219 | 679.1 | 39.5 | -1.69 | 0.07 | 2.30 | 0.15 |
| 229 | 712.5 | 38.9 | -1.68 | 0.07 | 2.33 | 0.15 |
| 234 | 729.9 | 38.7 | -1.88 | 0.07 | 2.14 | 0.15 |
| 239 | 749.7 | 39.3 | -1.46 | 0.07 | 2.52 | 0.15 |
| 241 | 757.6 | 39.5 | -1.43 | 0.07 | 2.53 | 0.15 |
| 249 | 789.2 | 40.3 | -1.66 | 0.07 | 2.31 | 0.15 |
| 259 | 828.8 | 41.4 | -1.48 | 0.07 | 2.33 | 0.15 |
| 264 | 848.6 | 41.9 | -1.52 | 0.07 | 2.28 | 0.15 |
| 269 | 868.4 | 42.4 | -1.44 | 0.07 | 2.34 | 0.15 |
| 279 | 921.1 | 43.2 | -1.57 | 0.07 | 2.22 | 0.15 |
| 284 | 947.8 | 43.6 | -1.63 | 0.07 | 2.45 | 0.15 |
| 289 | 974.6 | 44 | -1.70 | 0.07 | 2.38 | 0.15 |
| 299 | 1028 | 44.9 | -1.61 | 0.07 | 2.43 | 0.15 |
| 304 | 1054.7 | 45.3 | -1.71 | 0.07 | 2.38 | 0.15 |
| 309 | 1081.4 | 45.7 | -1.87 | 0.07 | 2.43 | 0.15 |
| 319 | 1134.9 | 46.5 | -1.96 | 0.07 | 2.59 | 0.15 |
| 324 | 1161.6 | 46.9 | -2.13 | 0.07 | 2.40 | 0.15 |
| 329 | 1188.3 | 47.3 | -2.29 | 0.07 | 2.21 | 0.15 |
| 331 | 1199 | 47.4 | -1.39 | 0.07 | 2.90 | 0.15 |
| 331 | 1199 | 47.4 | -1.19 | 0.07 | 2.71 | 0.15 |
| 339 | 1293.1 | 53.2 | -1.84 | 0.07 | 2.40 | 0.15 |
| 344 | 1351.9 | 56.8 | -1.65 | 0.07 | 2.44 | 0.15 |
| 349 | 1410.7 | 60.4 | -1.62 | 0.07 | 2.54 | 0.15 |
| 364 | 1586.2 | 67.1 | -1.80 | 0.07 | 2.42 | 0.15 |
| 369 | 1644.1 | 66.5 | -1.84 | 0.07 | 2.29 | 0.15 |
| 379 | 1759.9 | 65.5 | -1.78 | 0.07 | 2.42 | 0.15 |
| 384 | 1816.2 | 65 | -1.66 | 0.07 | 2.49 | 0.15 |
| 389 | 1858.3 | 64.6 | -1.68 | 0.07 | 2.41 | 0.15 |
| 394 | 1900.4 | 64.2 | -1.57 | 0.07 | 2.92 | 0.15 |

| Depth (cm) | Age (cal yrs BP) | 1σ error (yrs) | δ13C vs PDB (‰) | δ13C error (‰) | δ18O vs PDB (‰) | δ18O error (‰) |
|---|---|---|---|---|---|---|
| 394 | 1900.4 | 64.2 | -1.53 | 0.07 | 2.73 | 0.15 |
| 398 | 1934.1 | 63.9 | -1.48 | 0.07 | 2.53 | 0.15 |
| 408 | 2018.3 | 63.2 | -1.63 | 0.07 | 2.48 | 0.15 |
| 413 | 2060.4 | 62.9 | -1.38 | 0.07 | 2.61 | 0.15 |
| 418 | 2102.5 | 62.5 | -1.65 | 0.07 | 2.41 | 0.15 |
| 428 | 2170.5 | 61.5 | -1.63 | 0.07 | 2.60 | 0.15 |
| 433 | 2196.5 | 60.9 | -1.96 | 0.07 | 2.53 | 0.15 |
| 438 | 2222.4 | 60.3 | -1.68 | 0.07 | 2.67 | 0.15 |
| 448 | 2274.4 | 59.2 | -1.57 | 0.07 | 2.63 | 0.15 |
| 453 | 2300.3 | 58.6 | -1.53 | 0.07 | 2.62 | 0.15 |
| 458 | 2326.3 | 58 | -1.52 | 0.07 | 2.62 | 0.15 |
| 468 | 2378.2 | 56.8 | -1.78 | 0.07 | 2.47 | 0.15 |
| 473 | 2404.2 | 56.2 | -1.46 | 0.07 | 2.64 | 0.15 |
| 478 | 2430.1 | 55.6 | -1.70 | 0.07 | 2.50 | 0.15 |
| 488 | 2482 | 54.4 | -1.61 | 0.07 | 2.57 | 0.15 |
| 493 | 2508 | 53.8 | -1.41 | 0.07 | 2.52 | 0.15 |
| 498 | 2533.9 | 53.2 | -1.42 | 0.07 | 2.56 | 0.15 |
| 508 | 2585.9 | 52 | -1.35 | 0.07 | 2.50 | 0.15 |
| 513 | 2611.8 | 51.4 | -1.26 | 0.07 | 2.63 | 0.15 |
| 518 | 2637.8 | 50.8 | -1.31 | 0.07 | 2.76 | 0.15 |
| 528 | 2689.7 | 49.7 | -1.30 | 0.07 | 2.46 | 0.15 |
| 533 | 2715.6 | 49.1 | -1.32 | 0.07 | 2.40 | 0.15 |
| 538 | 2741.6 | 48.5 | -1.38 | 0.07 | 2.52 | 0.15 |
| 547 | 2786.8 | 48.7 | -1.67 | 0.07 | 2.46 | 0.15 |
| 557 | 2835.1 | 50.9 | -1.37 | 0.07 | 2.47 | 0.15 |
| 562 | 2859.2 | 52 | -1.45 | 0.07 | 2.36 | 0.15 |
| 567 | 2883.3 | 53.1 | -1.41 | 0.07 | 2.44 | 0.15 |
| 577 | 2931.5 | 55.3 | -1.73 | 0.07 | 2.57 | 0.15 |
| 582 | 2955.6 | 56.3 | -1.76 | 0.07 | 2.35 | 0.15 |
| 597 | 3028.6 | 56.2 | -1.37 | 0.07 | 2.56 | 0.15 |
| 602 | 3053 | 55.6 | -1.55 | 0.07 | 2.53 | 0.15 |
| 607 | 3077.4 | 55 | -1.40 | 0.07 | 2.50 | 0.15 |
| 617 | 3126.3 | 53.7 | -1.42 | 0.07 | 2.42 | 0.15 |
| 622 | 3150.7 | 53.1 | -1.91 | 0.07 | 2.43 | 0.15 |
| 627 | 3175.1 | 52.5 | -1.64 | 0.07 | 2.54 | 0.15 |
| 637 | 3224 | 51.3 | -1.70 | 0.07 | 2.51 | 0.15 |
| 642 | 3248.4 | 50.7 | -1.55 | 0.07 | 2.67 | 0.15 |
| 647 | 3273 | 50.2 | -1.74 | 0.07 | 2.49 | 0.15 |
| 662 | 3352.1 | 53.1 | -1.54 | 0.07 | 2.46 | 0.15 |
| 667 | 3378.5 | 54.1 | -1.55 | 0.07 | 2.59 | 0.15 |
| 675 | 3420.6 | 55.6 | -1.69 | 0.07 | 2.45 | 0.15 |
| 685 | 3473.4 | 57.6 | -1.66 | 0.07 | 2.47 | 0.15 |
| 690 | 3499.7 | 58.5 | -1.56 | 0.07 | 2.50 | 0.15 |
| 695 | 3526.1 | 59.5 | -1.59 | 0.07 | 2.33 | 0.15 |
| 705 | 3585.9 | 60.5 | -1.16 | 0.07 | 2.46 | 0.15 |
| 710 | 3617 | 60.9 | -1.43 | 0.07 | 2.52 | 0.15 |
| 715 | 3648.1 | 61.2 | -1.68 | 0.07 | 2.28 | 0.15 |
| 725 | 3710.3 | 62 | -1.69 | 0.07 | 2.32 | 0.15 |
| 730 | 3741.4 | 62.3 | -1.47 | 0.07 | 2.37 | 0.15 |
| 735 | 3772.5 | 62.7 | -1.32 | 0.07 | 2.64 | 0.15 |
| 745 | 3834.7 | 63.4 | -1.34 | 0.07 | 2.46 | 0.15 |
| 750 | 3865.8 | 63.8 | -1.40 | 0.07 | 2.55 | 0.15 |
| 755 | 3896.9 | 64.1 | -1.54 | 0.07 | 2.42 | 0.15 |
| 765 | 3955 | 68.4 | -1.39 | 0.07 | 2.47 | 0.15 |
| 770 | 3981.4 | 72.8 | -1.23 | 0.07 | 2.44 | 0.15 |
| 775 | 4007.9 | 77.1 | -1.71 | 0.07 | 2.38 | 0.15 |
| 785 | 4060.9 | 85.8 | -1.45 | 0.07 | 2.40 | 0.15 |
| 790 | 4087.3 | 90.2 | -1.59 | 0.07 | 2.47 | 0.15 |
| 795 | 4113.8 | 94.5 | -1.69 | 0.07 | 2.25 | 0.15 |
| 805 | 4166.8 | 103.2 | -1.50 | 0.07 | 2.44 | 0.15 |
| 810 | 4193.3 | 107.6 | -1.46 | 0.07 | 2.42 | 0.15 |
| 815 | 4219.7 | 112 | -1.75 | 0.07 | 2.56 | 0.15 |

**Table B.** Mg/Ca data from core 2-PC1 and their associated depth and age.

| Depth (m) | Age (cal yrs BP) | 1σ error (yrs) | Mg/Ca (mmol/mol) | Mg/Ca error (mmol/mol) |
|---|---|---|---|---|
| 0 | -44.4 | 14.3 | 0.79 | 0.1 |
| 16 | 0.3 | 19.6 | 0.67 | 0.1 |
| 36 | 67.1 | 24.4 | 0.58 | 0.1 |
| 56 | 133.9 | 29.1 | 0.60 | 0.1 |
| 76 | 200.8 | 33.8 | 0.51 | 0.1 |
| 96 | 267.6 | 38.5 | 0.59 | 0.1 |
| 109 | 311 | 41.6 | 0.59 | 0.1 |
| 129 | 377.9 | 44.8 | 0.68 | 0.1 |
| 154 | 461.6 | 43.3 | 0.65 | 0.1 |
| 214 | 662.3 | 39.8 | 0.71 | 0.1 |
| 259 | 828.8 | 41.4 | 0.72 | 0.1 |
| 279 | 921.1 | 43.2 | 0.71 | 0.1 |
| 299 | 1028 | 44.9 | 0.64 | 0.1 |
| 329 | 1188.3 | 47.3 | 0.83 | 0.1 |
| 339 | 1293.1 | 53.2 | 0.86 | 0.1 |
| 344 | 1351.9 | 56.8 | 0.84 | 0.1 |
| 364 | 1586.2 | 67.1 | 0.93 | 0.1 |
| 384 | 1816.2 | 65 | 0.85 | 0.1 |
| 389 | 1858.3 | 64.6 | 0.91 | 0.1 |
| 398 | 1934.1 | 63.9 | 0.77 | 0.1 |
| 413 | 2060.4 | 62.9 | 0.70 | 0.1 |
| 433 | 2196.5 | 60.9 | 0.93 | 0.1 |
| 448 | 2274.4 | 59.2 | 0.84 | 0.1 |
| 468 | 2378.2 | 56.8 | 0.69 | 0.1 |
| 473 | 2404.2 | 56.2 | 0.66 | 0.1 |
| 493 | 2508 | 53.8 | 0.70 | 0.1 |
| 513 | 2611.8 | 51.4 | 0.71 | 0.1 |
| 533 | 2715.6 | 49.1 | 0.68 | 0.1 |
| 547 | 2786.8 | 48.7 | 0.65 | 0.1 |
| 562 | 2859.2 | 52 | 0.83 | 0.1 |
| 567 | 2883.3 | 53.1 | 0.72 | 0.1 |
| 607 | 3077.4 | 55 | 0.86 | 0.1 |
| 627 | 3175.1 | 52.5 | 0.88 | 0.1 |
| 662 | 3352.1 | 53.1 | 0.84 | 0.1 |
| 685 | 3473.4 | 57.6 | 0.85 | 0.1 |
| 695 | 3526.1 | 59.5 | 0.81 | 0.1 |
| 715 | 3648.1 | 61.2 | 0.78 | 0.1 |
| 730 | 3741.4 | 62.3 | 0.67 | 0.1 |
| 750 | 3865.8 | 63.8 | 0.76 | 0.1 |
| 775 | 4007.9 | 77.1 | 0.79 | 0.1 |
| 795 | 4113.8 | 94.5 | 0.72 | 0.1 |